

TECHNISCHE UNIVERSITÄT MÜNCHEN
Lehrstuhl für Biofunktionalität der Lebensmittel

Mitochondrial unfolded protein response in the epithelium: relevance to intestinal inflammation

Eva Brigitte Rath

Vollständiger Abdruck der von der Fakultät Wissenschaftszentrum Weihenstephan für Ernährung, Landnutzung und Umwelt der Technischen Universität München zur Erlangung des akademischen Grades eines

Doktors der Naturwissenschaften

genehmigten Dissertation.

Vorsitzende: Univ.-Prof. Dr. H. Daniel

Prüfer der Dissertation: 1. Univ.-Prof. Dr. D. Haller
2. Univ.-Prof. Dr. M. Klingenspor
3. Univ.-Prof. Dr. U. Protzer

Die Dissertation wurde am 28.07.2011 bei der Technischen Universität München eingereicht und durch die Fakultät Wissenschaftszentrum Weihenstephan für Ernährung, Landnutzung und Umwelt am 16.01.2012 angenommen.

Bibliographische Information der Deutschen Nationalbibliothek

Die Deutsche Nationalbibliothek verzeichnet diese Publikation in der Deutschen Nationalbibliografie;
Detaillierte bibliografische Daten sind im Internet über
<http://dnb.d-nb.de> abrufbar.

ISBN 978-3-8439-0346-2

© Verlag Dr. Hut, München 2012
Sternstr. 18, 80538 München
Tel.: 089/66060798
www.dr.hut-verlag.de

Die Informationen in diesem Buch wurden mit großer Sorgfalt erarbeitet. Dennoch können Fehler nicht vollständig ausgeschlossen werden. Verlag, Autoren und ggf. Übersetzer übernehmen keine juristische Verantwortung oder irgendeine Haftung für eventuell verbliebene fehlerhafte Angaben oder deren Folgen.

Alle Rechte, auch die des auszugsweisen Nachdrucks, der Vervielfältigung und Verbreitung in besonderen Verfahren wie fotomechanischer Nachdruck, Fotokopie, Mikrokopie, elektronische Datenaufzeichnung einschließlich Speicherung und Übertragung auf weitere Datenträger sowie Übersetzung in andere Sprachen, behält sich der Autor vor.

1. Auflage 2012

ZUSAMMENFASSUNG

Chronisch entzündliche Darmerkrankungen (CED) sind immunvermittelte, rezidivierende Erkrankungen des Gastrointestinaltrakts. Viele der Veränderungen, die bei CED auftreten, stehen im Zusammenhang mit dem intestinalen Epithel, das für die Aufrechterhaltung der Homöostase im Darm entscheidend ist. Intestinale Epithelzellen (IEZ) bilden die Grenzschicht zwischen der Mikrobiota und dem Immunsystem, und vermitteln damit zwischen den beiden Hauptfaktoren intestinaler Entzündung. Das Ziel dieser Arbeit war es, neue Zielproteine und zelluläre Signalwege, die an entzündlichen Vorgängen in IEZ beteiligt sind, zu identifizieren und zu beschreiben.

Mit Hilfe von 2D SDS-PAGE und Mikroarray Analysen wurden Veränderungen im Gen- und Proteinexpressionsmuster intestinaler Epithelzellen aus Mausmodellen für Kolitis bestimmt. Die Auswertung dieser Daten wies darauf hin, daß Zellorganellen, insbesondere das Endoplasmatische Retikulum (ER) und die Mitochondrien, durch die Entzündung beeinträchtigt werden. Unter anderem war Chaperonin (CPN) 60, ein Surrogatmarker der „mitochondrial unfolded protein response“ (mtUPR) deutlich erhöht. In Zusammenhang mit CED wurde bereits gezeigt, daß die ER UPR zur Entstehung von Entzündungen im Gastrointestinaltrakt beiträgt. Um die mtUPR genauer zu charakterisieren, wurde die murine IEZ-linie Mode-K mit einer Deletionsmutante der mitochondrialen Ornithin-transcarbamylase (OTCΔ) transfiziert. Durch selektives Auslösen der mtUPR konnte eine Phosphorylierung des „eukaryotic translation initiation factor (eIF2) α“ und von cJun beobachtet werden, zwei Signalproteinen, die ebenso an der ER UPR beteiligt sind. Durch pharmakologische Inhibition und siRNA-vermittelten Knockdown konnte eine Abhängigkeit der mtUPR Signalkaskade von der Aktivität der mitochondrialen Protease ClpP und der „double-stranded RNA-activated protein“ Kinase (PKR) gezeigt werden. Somit wurde PKR als ein neues, zytoplasmatisches Signalprotein der mtUPR identifiziert. Diese Ergebnisse wurden durch die Beobachtung bestätigt, daß es bei $Pkr^{-/-}$ Mäusen nach Dextran Natriumsulfat (DSS) Behandlung zu keiner Erhöhung der CPN60 Level in IEZ kam. Darüber hinaus waren $Pkr^{-/-}$ Mäuse widerstandsfähiger gegenüber einer DSS-induzierten Kolitis. Durch immunhistochemische Färbungen und Western blot Analysen konnten wir zudem zeigen, daß in IEZ von CED Patienten und den murinen Kolitismodellen die vermehrte Expression von CPN60 bei Entzündung mit einer Induktion von PKR einherging.

Zusammenfassend deuten unsere Ergebnisse darauf hin, daß sich die mtUPR über PKR in die krankheitsrelevante ER UPR Signalkaskade integriert und somit mitochondrialen Stress in das komplexe Entzündungsgeschehen einbindet. Unsere Daten sprechen daher für eine direkte Rolle der mtUPR in der Pathogenese der CED. Folglich könnten die mtUPR und speziell auch PKR Ziele für neue Therapienansätze darstellen.

ABSTRACT

Inflammatory bowel diseases (IBD) are immune-mediated chronic disorders of the gastrointestinal tract. Genetic risk factors as well as environmental triggers are implied in the pathogenesis of these multifactorial diseases. Many alterations characteristic for IBD cluster around intestinal epithelial cell (IEC) function; IEC are crucial for maintaining intestinal homeostasis, constituting an interface between the two major factors influencing intestinal inflammation, the microbiota and the immune system. The aim of this study was to identify and characterize novel target proteins/signaling pathways involved in inflammatory processes in IEC.

Applying 2D SDS-PAGE and microarray analysis, we screened for changes in gene and protein expression in primary IEC from murine models of T cell-mediated colitis under inflammatory conditions. Bibliometric analysis indicated cellular organelles including endoplasmic reticulum (ER) and mitochondria to be highly affected. In particular, protein expression profiling demonstrated marked changes in proteins assigned to the mitochondrial compartment, including induction of chaperonin (CPN) 60, the hallmark protein of mitochondrial unfolded protein response (mtUPR). UPR represent autoregulatory pathways adjusting organelle capacity to the cellular demand and ER UPR in IEC has been shown to contribute to the development of intestinal inflammation. Using the murine intestinal epithelial line Mode-K and a mutated protein prone to misfold in the mitochondrial matrix, truncated ornithine transcarbamylase (OTC Δ), we further characterized mtUPR-signaling. Selective mtUPR-induction by OTC Δ -transfection triggered the phosphorylation of eukaryotic translation initiation factor (eIF2) α and cJun, events also observed under ER stress conditions. Pharmacological inhibition and siRNA knockdown identified mtUPR-signaling to be dependent on the activity of the mitochondrial protease ClpP and the double-stranded RNA-activated protein kinase (PKR), adding a cytoplasmic mediator to the known mtUPR signaling components. Confirming our *in vitro* results, Pkr^{-/-} mice failed to upregulate CPN60 in IEC upon dextran sodium sulfate (DSS) treatment and showed almost complete resistance to DSS-induced colitis. Most importantly, immunohistochemistry and Western blot analysis demonstrated a strong induction of CPN60 associated with enhanced expression of PKR primary IEC from IBD patients and two murine models of colitis under inflammatory conditions.

In conclusion, we hypothesize that PKR integrates mtUPR- into the disease-relevant ER UPR-signaling cascade, thereby linking mitochondrial stress to intestinal inflammation. In addition, our results suggest a direct role for mtUPR in the pathogenesis of IBD and identify mtUPR-singaling and in particular PKR as new potential targets for disease-intervention.

TABLE OF CONTENTS

ZUSAMMENFASSUNG.....	3
ABSTRACT.....	5
TABLE OF CONTENTS	7
1 INTRODUCTION	11
1.1 Inflammatory bowel diseases.....	11
1.2 Unfolded protein responses	12
1.3 ER unfolded protein response.....	14
1.3.1. ER UPR and inflammation	17
1.3.2. ER UPR and autophagy.....	18
1.3.3. ER UPR and apoptosis	19
1.3.4. ER UPR and metabolism	20
1.3.5. ER UPR and IBD.....	22
1.4 Mitochondrial dynamics.....	23
1.4.1. Mitochondrial protein homeostasis	23
1.4.2. Mitochondrial unfolded protein response	24
1.4.3. Mitochondrial biogenesis and mitophagy.....	26
1.5 ER-mitochondrial network.....	28
2 AIMS OF THE WORK	31
3 MATERIAL AND METHODS.....	33
3.1 Animals.....	33
3.1.1. Adoptive CD4 ⁺ T cell transfer.....	33
3.1.2. Bacterial mono- and dual-association.....	34
3.1.3. DSS-induced colitis	34
3.1.4. Assessment of barrier function (Ussing chamber).....	35
3.1.5. Histological scoring	35
3.1.6. Isolation of primary mouse IEC	36
3.2 Patients.....	36
3.2.1. Isolation of primary human IEC.....	36
3.3 Immunohistochemical labeling and quantification.....	37
3.4 Protein expression profiling.....	37
3.4.1. 2D SDS-PAGE	37
3.4.2. Trypsin digestion of protein spots and MALDI-TOF-MS	38
3.5 Gene expression profiling.....	38
3.6 Bibliometric analysis.....	40

TABLE OF CONTENTS

3.7	Cell culture, transfection and stimulation	40
3.8	Mitochondrial Isolation.....	41
3.9	Western blot analysis	41
3.10	Co-immunoprecipitation	42
3.11	Chromatin Immunoprecipitation	42
3.12	DNA/RNA isolation, reverse transcription and real-time PCR	43
3.13	Statistical analysis	44
4	RESULTS	45
4.1	Markers of ER- and mitochondrial stress are induced in IEC under inflammatory conditions	45
4.1.1.	Protein expression profiling of IEC links ER- and mitochondrial stress in experimental colitis	45
4.1.2.	ER chaperone GRP78, mitochondrial CPN60 and PKR are induced in IEC in experimental colitis	49
4.1.3.	ER chaperone GRP78, mitochondrial CPN60 and PKR are induced in IEC from IBD patients	51
4.1.4.	Autophagy is induced in IEC in experimental colitis	53
4.2	Mitochondrial unfolded protein response in the IEC line Mode-K.....	54
4.2.1.	Truncated ornithine transcarbamylase induces mtUPR in IEC.....	54
4.2.2.	Mitochondrial UPR integrates into ER UPR-signaling	55
4.2.3.	Mitochondrial UPR-signaling employs PKR.....	56
4.2.4.	Mitochondrial UPR does not induce ATF4.....	58
4.2.5.	Mitochondrial UPR induces Akt phosphorylation.....	59
4.2.6.	Mitochondrial UPR-mediated PKR-induction is Ca ²⁺ and PACT independent	59
4.2.7.	Mitochondrial UPR signaling is dependent on PKR.....	60
4.2.8.	Mitochondrial UPR induces autophagy.....	62
4.3	Pkr ^{-/-} mice	63
4.3.1.	Pkr ^{-/-} mice display enhanced colonic barrier function and increased mitochondrial markers	63
4.3.2.	Pkr ^{-/-} mice show reduced sensitivity to DSS-induced colitis	64
4.3.3.	Mitochondrial abundance declines in Pkr ^{-/-} mice upon DSS-treatment	66
4.4	Gene expression profiling of IEC as tool to identify novel target proteins/signaling pathways in intestinal inflammation.....	69
4.4.1.	Most highly regulated genes in IEC in response to CD4 ⁺ T cell transfer.....	72
4.4.2.	Data analysis of regulated genes in IEC in response to CD4 ⁺ T cell transfer	79
4.4.3.	Genes best correlated to the histological score in IEC upon CD4 ⁺ T cell transfer	86
4.4.4.	Genes best correlated to the presence of IL-10 in IEC under non-inflammatory conditions .	93
5	DISCUSSION	95
5.1	PKR	95

5.2	Mitochondrial UPR signaling	96
5.3	Pkr ^{-/-} mice	98
5.4	Mitochondria as integrators of cellular danger signaling	99
5.5	ER UPR and mitochondrial dysfunction in IBD	100
5.6	Screening for potential new target genes and cellular pathways	102
5.7	Conclusion and perspective	104
6	APPENDIX	107
	LIST OF FIGURES	129
	LIST OF TABLES	131
	ABBREVIATIONS	133
	REFERENCES	135
	PUBLICATIONS AND PRESENTATIONS	145
	ACKNOWLEDGEMENTS	151
	CURRICULUM VITAE	153

1 INTRODUCTION

Chronic diseases comprise metabolically-driven pathologies such as obesity, insulin resistance, type 2 diabetes, and cardiovascular disease but also immunologically mediated disorders like allergies or inflammatory bowel diseases (IBD). The prevalence of chronic diseases has rapidly increased in the second half of the twentieth century [1-3], associated with the spread of the western lifestyle and now constitutes a global health problem [4]. Even though phenotypically different, these diseases share similarities at the molecular and cellular level [5]. In particular, inflammatory changes are characteristic not only for immunologically mediated disorders but also metabolically-driven pathologies exhibit strong inflammatory underpinnings [6]. Identifying common mechanisms underlying inflammation will increase the understanding of chronic diseases and should lead to new treatment approaches.

1.1 Inflammatory bowel diseases

IBD and its two main idiopathic pathologies ulcerative colitis (UC) and Crohn's disease (CD) are chronic remittent or progressive, immunologically mediated disorders that affect the colonic mucosa and entire gastrointestinal tract, respectively. UC as well as CD are multifactorial diseases and are characterized by alterations of the innate and adaptive immune system, luminal and mucosa associated microbiota as well as epithelial function [3]. The current paradigm for the pathogenesis of IBD is a dysregulated interaction between the intestinal microbiome and the mucosal immune system in genetically predisposed individuals, whereby onset and recurrence of disease are most likely triggered by unknown environmental agents [7]. Under normal conditions, it is a characteristic feature of the mucosal immune system that protective immune responses against enteropathogenic organisms are allowed to proceed while responses to microorganisms of the microbiota are prevented. The loss of this complex immune homeostasis in IBD might be due to insults generated by disease-associated alterations such as reduced epithelial barrier function, defective production of antimicrobial peptides, impaired intracellular handling of bacterial products and an inadequate regulation of innate and adaptive immune responses [7,8]. Intestinal epithelial cells (IEC) are crucial for maintaining intestinal homeostasis, constituting an interface between the two major factors influencing intestinal inflammation, the gut microbiota and the immune system [9]. Directly interacting with enteric luminal bacteria as well as with lamina propria immune cells and intraepithelial lymphocytes, IEC both sense and determine the composition of the luminal microbiota by producing antimicrobial substances [9,10] and on the mucosal side, modulate T cell responses within the lamina propria e.g. by

producing cytokines like thymic stromal lymphopoietin (TSLP) [11]. Thus, failure to control inflammatory processes at the IEC level may critically contribute to IBD pathogenesis (**Fig.1**).

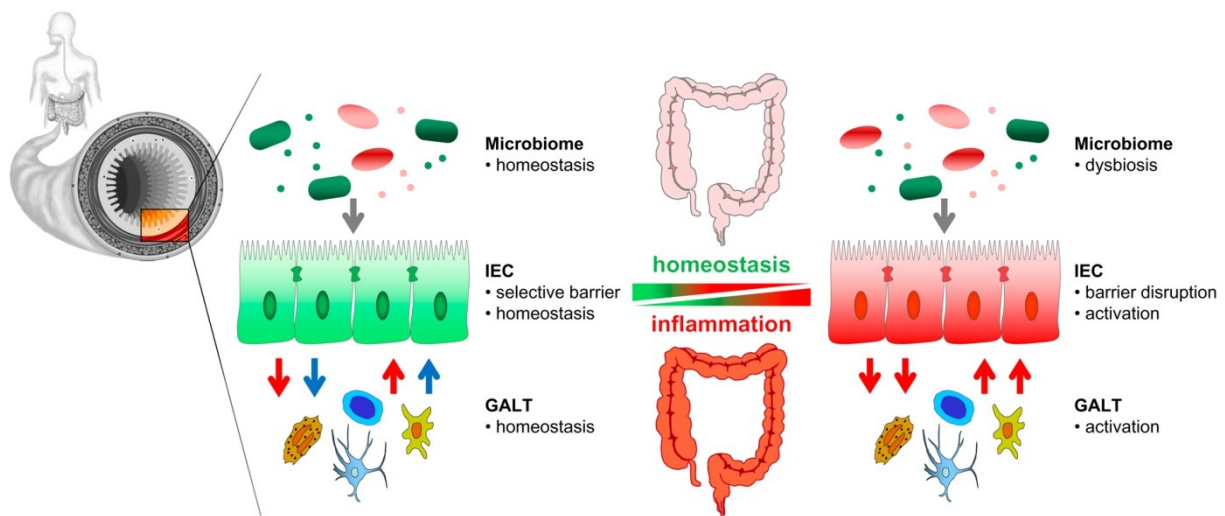


Figure 1. Intestinal alterations in IBD cluster around IEC.

Unknown environmental triggers lead to loss of intestinal homeostasis leading microbial dysbiosis, impaired IEC barrier function and activation of the gut-associated lymphoid tissue (GALT), finally resulting in intestinal inflammation/IBD in the genetically predisposed host.

1.2 Unfolded protein responses

A cellular condition present in various diseases including IBD is endoplasmic reticulum (ER) stress and the associated ER unfolded protein response (UPR) [12-14]. In eukaryotic cells, distinct cellular processes occur in specialized organelles such as the endoplasmic reticulum, mitochondria, peroxisomes and the Golgi apparatus. As a consequence, the abundance and/or capacity of each organelle have to be tightly regulated to meet fluctuating cellular demands. For example, this is reflected by enlarged mitochondria found in exercise-conditioned muscle cells and secretory cells containing large amounts of ER [15,16]. Autoregulatory mechanisms have been proposed to control organelle abundance, whereby sensor molecules monitor organelle function and, if the demand exceeds the capacity, elicit retrograde signaling enhancing biogenesis [16]. The so-called unfolded protein responses are a paradigm for this type of signaling (**Fig.2**). Maintaining protein homeostasis is essential to all cells and is dependent on chaperones, which promote protein folding and prevent protein aggregation [17]. Under normal conditions, chaperones of the heat shock protein (HSP) family, HSP70 in the cytosol and glucose-regulated protein (GRP) 78 in the ER, bind to stress-sensor proteins to repress their signaling [18,19]. Upon stress-induced accumulation of unfolded proteins, these chaperones dissociate from their binding partners, preferentially interacting with unfolded proteins.

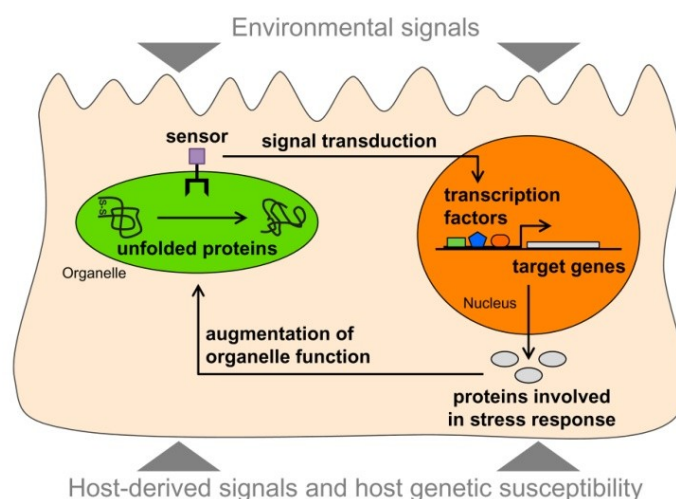


Figure 2. Schematic illustration of unfolded protein responses.

Accumulation of unfolded or misfolded proteins can be triggered by environmental factors like bacteria or nutrients as well as host-derived signals such as inflammatory cytokines. The insufficient protein folding capacity initiates a signaling cascade leading to the transcription of nuclear-encoded genes involved in the organelle-specific protein folding machinery and in cellular stress response. These signals result in augmentation of organelle capacity and lower the burden of unfolded proteins.

In the case of the HSP70, this leads to the release of the transcription factor HSF1 allowing its nuclear translocation and inducing genes involved in cytosolic protein folding [19]. Similarly, dissociation of GRP78 activates three ER transmembrane proteins, IRE1 (inositol requiring enzyme 1), ATF6 (activation transcription factor 6) and PERK (PKR-like ER kinase), initiating sophisticated downstream signaling to increase the ER folding capacity [18]. Additionally to the cytosolic and the ER UPR, a third, cognate signaling pathway responding to mitochondrial stress has been described, the mitochondrial UPR (mtUPR) [20-22]. Although the underlying molecular mechanisms of the mtUPR are less understood, studies in *Caenorhabditis elegans* suggested that the initial signal might be peptides generated from unfolded proteins of the mitochondrial matrix by the protease ClpP and their efflux into the cytosol [23]. As a result mtUPR responsive genes, mitochondrial proteases and chaperones such as chaperonin (CPN) 60 are activated, mainly through the transcription factor C/EBP homologous protein (CHOP) [21,24,25]. Cytosolic, ER and mitochondrial UPR are distinct signaling pathways targeting specific stress proteins of different cellular compartments, even though ER- and mtUPR share features like the transcription factors CHOP and activating protein (AP) 1 [18,21,24]. While cellular stress responses and mitochondrial dysfunction represent key regulators of metabolically-driven disorders, the role of mitochondria-related signaling in the pathogenesis of IBD is virtually unknown.

1.3 ER unfolded protein response

In mammalian cells, the endoplasmic reticulum is essential for cholesterol production, for calcium homeostasis, and for the transit of correctly folded proteins to the extracellular space, the plasma membrane, and the exo- and endocytic compartments. Among the conditions that challenge ER functions and elicit ER stress responses are changes in calcium homeostasis or redox status, elevated protein synthesis, accumulation of unfolded or misfolded proteins, energy deficiency and glucose deprivation, altered protein glycosylation, cholesterol depletion, and microbial infections [18].

Three ER membrane-associated sensors, IRE1, ATF6 and PERK, mediate distinct branches of the ER UPR. In unstressed cells, these transmembrane proteins are bound by GRP78 (also referred to as immunoglobulin heavy chain-binding protein, BIP) in their intraluminal domains and rendered inactive. Accumulation of mis- or unfolded proteins in the ER triggers recruitment of GRP78 away from these sensors. Liberation of PERK and IRE1 results in dimerization and activation of the two kinases and engages a complex downstream signaling pathway [18]. Activation of ATF6 requires release from the ER and migration to the Golgi apparatus where it is cleaved by site 1 protease (S1P) and site 2 protease (S2P) to generate an active transcription factor (nATF6) [26] (**Fig.3**). Together, the three branches of the ER UPR aim to restore ER homeostasis by (I) enhancing the degradation of misfolded proteins by ER-associated degradation (ERAD) (II) translational attenuation through phosphorylation of the α subunit of eukaryotic translation initiation factor (eIF) 2 and (III) expanding the protein folding capacity of the cell through upregulation of ER chaperones like GRP78. However, if the ER stress is prolonged or excessive, ER UPR can ultimately lead to cell death via mitochondria-dependent and mitochondria-independent apoptotic pathways [27,28].

IRE1

The most evolutionary conserved branch of the ER UPR is mediated by IRE1 [29], a Ser/Thr protein kinase and endoribonuclease. Upon activation of IRE1 α , a 26 nucleotide intron is spliced out of the mRNA encoding the transcription factor X-box binding protein (XBP) 1 [18]. This shift in the reading frame results in the translation of the active, spliced form of the transcription factor, XBP1s, that comprises an N-terminal DNA-binding domain and a potent transactivation domain at the C-terminus [30]. XBP1s, alone or as heterodimer in conjugation with ATF6 α , controls the upregulation of a broad spectrum of ER UPR-related genes such as chaperones (e.g. GRP78), and proteins involved in ERAD and protein quality control [31,32]. Since XBP1s also controls the expansion of secretory pathways by ER/Golgi biogenesis [33,34], it is crucial for survival and function of secretory cells which are

particularly susceptible to ER stress [10]. Recently, other mRNAs have been identified as substrates for IRE1 under stress conditions. IRE1 degrades these mRNAs to prevent their translation, a mechanism suggested to additionally alleviate ER stress [35]. Furthermore, the cytosolic domain of activated IRE1 can bind to the adaptor protein TNFR-associated factor (TRAF) 2 to activate the apoptosis signal-regulating kinase (ASK) 1 and cJun-N terminal kinase (JNK) [36,37].

ATF6

A second ER UPR pathway is initiated by the type II ER transmembrane proteins ATF6 α and ATF6 β , whose cytosolic domain encodes a bZIP transcription factor [18]. The active, cleaved form translocates to the nucleus, binds to promoters containing ER stress elements (ERSE), UPR elements (UPRE) and cAMP response elements (CRE) and enhances gene transcription of *xbp1* and many other ER UPR genes related to ERAD and protein folding [32,38,39]. In addition, ATF6 α may also modulate lipid biosynthesis and ER expansion under stress conditions [40]. A number of recently identified ATF6 homologues add complexity to this branch of the ER UPR. OASIS, CREBH, LUMAN/CREB3, CREB4 and BBF2H7 are ER-anchored bZIP transcription factors that are processed at the Golgi in a similar way as ATF6 [18]. All these factors respond to ER stress and can activate UPR target genes [41], however differences in activating stimuli, response element binding and distinct tissue distributions are proposed. For example, OASIS might play a role in osteoblast activity and bone formation [42], whereas CREBH is suggested to stimulate the acute phase response in the liver in response to lipopolysaccharide and cytokines [43]. Notably, ATF6 α - and ATF6 β -single knockout mice develop normally, in contrast to double-knockout mice which are embryonic lethal [32,44]. In summary, these data hint towards redundancies in the ER UPR as well as to a fine-tuned ER UPR in mammals that allows distinct responses depending on the affected tissue, the cause and duration of stress.

PERK

The third branch of ER UPR is mediated by PERK and results in the inhibition of global protein synthesis by phosphorylation of the eIF2 α [45]. Downstream, this leads to the induction of ATF4 through alternative translation. Target genes of ATF4 comprise genes involved in ER redox control (ER oxidoreductin (ERO) 1) and apoptosis (CHOP) as well as regulators of glucose metabolism [46,47].

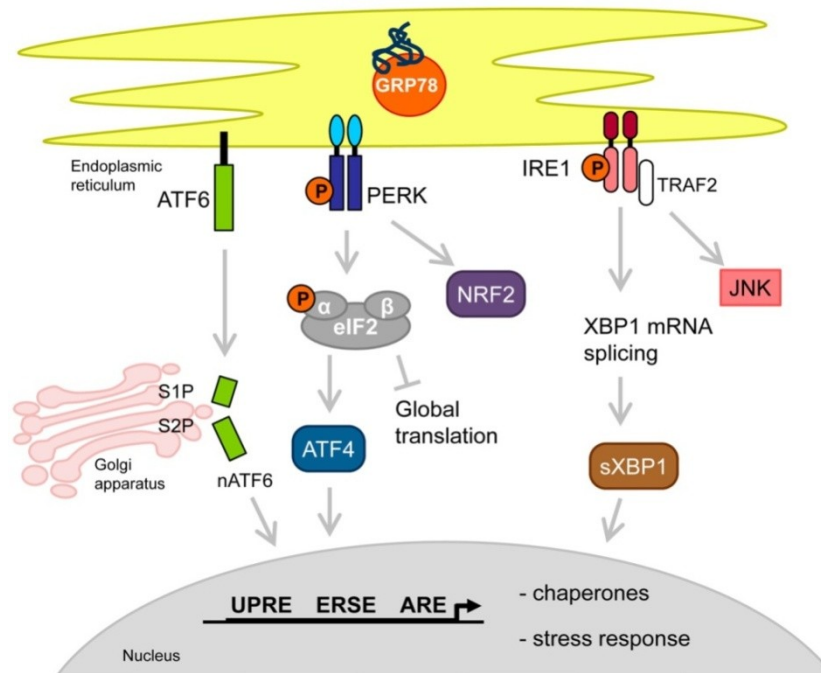


Figure 3. Endoplasmic reticulum unfolded protein response and associated signaling.

The recruitment of the chaperone GRP78 to mis- or unfolded proteins in the ER lumen induces signaling cascades mediated by the transmembrane proteins ATF6, PERK and IRE-1. Subsequently, this causes activation of kinases, attenuation of global protein translation and recruitment of transcription factors to UPRE, ERSE and ARE to evoke cellular stress responses.

In addition, ATF4 induces genes related to a negative feedback of eIF2 α phosphorylation, such as growth arrest and DNA-damage inducible protein (GADD) 34, which targets protein phosphatase (PP) 1 to the ER and promotes dephosphorylation of eIF2 α , thereby reversing the shut-off of protein synthesis and facilitating recovery of cells from stress [48,49]. PERK-dependent phosphorylation also triggers dissociation of Nrf2/Keap1 complexes, subsequent nuclear translocation of Nrf2 and transcription of genes harboring antioxidant response elements (ARE) in their promoters, a process thought to counteract oxidative stress evoked by ER stress [50,51]. Besides PERK, three other kinases are known to have eIF2 α as a substrate, double-stranded RNA-activated protein kinase (PKR), general control non-repressible kinase 2 (GCN2) and heme-regulated inhibitor kinase (HRI). Of those, only PKR is described to participate in ER stress signaling [52] whereas GCN2 and HRI might be activated under oxidative stress and amino acid starvation respectively.

1.3.1. ER UPR and inflammation

Inflammatory pathways and the ER UPR are tightly interrelated through all three branches of the ER UPR. IRE1 can activate JNK and thereby the transcription factor AP1 [53] and is able to modulate the inflammation-related MAP kinases p38 and ERK, possibly by binding of the adaptor protein Nck [54]. Moreover, IRE signaling might be interrelated to the inflammatory NF- κ B pathway through interaction with an inhibitor κ B kinase (IKK)/TRAF2 protein complex [55]. Downstream of IRE1, XBP1 and xbp1 splicing are required to elicit adequate antibody secretion in response to antigenic challenge in B cells [56,57] and are essential for the production of antimicrobial peptides in Paneth cells [10].

ATF6 itself, in addition to the suggested role of its homologue CREBH as regulator of acute phase proteins such as serum amyloid and C-reactive protein in the liver [43], was recently shown to activate the transcription factor NF- κ B via Akt phosphorylation [58]. In contrast, PERK-mediated translational suppression targets inhibitory kappa B (I κ B), the inhibitor of NF- κ B, thereby triggering NF- κ B nuclear translocation and expression of inflammatory cytokines like interleukin (IL)-6 and tumor necrosis factor (TNF) [59,60]. Other proinflammatory molecules including IL-8 and MCP-1 have been reported to be responsive to experimental induction of UPR *in vitro* as well [61]. Specific inflammatory triggers may activate different branches of the ER UPR, but there is evidence that not only ER UPR can induce inflammatory changes, but also that inflammation in terms of activated inhibitor of NF- κ B kinase (IKK)- β can induce ER UPR [62]. In addition to the mechanisms mentioned above, ER UPR and inflammatory pathways are interrelated by the generation of reactive oxygen species (ROS) and nitric oxide (NO) [50,63]. Increased protein folding due to ER UPR activation and formation of disulfide bonds results in the accumulation of ROS and oxidative stress [64], whereas ROS generated by inflammation could aggravate ER stress. Similarly, NO production triggered by inflammation can induce ER UPR through NO-induced inhibition of protein disulfide isomerase (PDI) and subsequent accumulation of polyubiquitinated proteins [63].

A prerequisite to effective immune responses is the sensing of danger signals such as microbial-associated molecular pattern (MAMP) motifs. Distinct families of pattern-recognition receptors, particularly cell- or endosomal membrane bound Toll-like receptors (TLR), cytoplasmic retinoic acid-inducible gene (RIG) I like receptors and cytoplasmic Nod-like receptors (NLR) carry out this function and activate transcriptional programs to orchestrate adaptive immune responses. Interestingly, recent data suggest that TLR-signaling can modulate ER UPR signaling and activate ER UPR-associated transcription factors [65-67]. Treatment of mice with low dose of the TLR4 ligand lipopolysaccharide (LPS) prior to induction of systemic ER stress prevented proapoptotic CHOP expression and tissue damage. This effect was shown to be mediated in a TRIF-dependant manner by selective

attenuation of ATF4 translation and its downstream target CHOP. The authors suggest that this mechanism protects TLR-expressing cells from prolonged ER stress evoked during host responses to pathogens [65]. Using TLR2 and TLR4-deficient mice, we could demonstrate TLR-signaling to modulate ER UPR in IEC [66] and another study showed that TLR2 and TLR4 specifically activated IRE1 and XBP1 in macrophages [67]. The latter study implies a distinct function for XBP1 in host defense, since TLR-mediated XBP1s induction did not induce ER UPR-associated target genes but was required for optimal and sustained production of proinflammatory cytokines in macrophages [67]. Regarding ROS, it is noteworthy that in a model of ischemia/reperfusion injury in which ROS participate, mice deficient in TLR2 showed increased levels of interferon (IFN) γ and IL-4 accompanied by aggravated tissue damage [68] hinting towards an additional protective, TLR-mediated mechanism in the context of ER UPR.

1.3.2. ER UPR and autophagy

Autophagy is a highly regulated lysosomal pathway involved in the turnover of long-lived proteins and organelles. It is involved in cellular homeostasis, maintenance of immunologic tolerance and host defense against pathogens [69-71]. Autophagy starts with the envelopment of cytosol and/or organelles in an isolating membrane, forming an autophagosome. Contrarily to phagosomes which possess a single membrane, autophagosomes feature double-membranes [70]. Undergoing progressive maturation by fusion with endolysosomal vesicles, an autolysosome is created in which the cargo is degraded [69,70]. Next to the autophagic-lysosomal pathway, the ubiquitin-proteasomal system is the second major degradation route in mammalian cells. During ER UPR and the associated degradation of mis- or unfolded proteins, the ER employs both proteasomal (ERAD) as well as autophagic pathways [53,72]. ER UPR-induced autophagy might represent an alternative mechanism to dispose misfolded proteins in the ER lumen that cannot be removed by ERAD, but is also implied in the degradation of damaged ER and the counterbalance of the ER expansion during ER UPR [73]. Several canonical ER UPR pathways have been implicated in the induction of autophagy [74] including conflicting data about the necessity of different signaling components. The PERK/eIF2 α pathway has been linked to the induction of autophagy [74,75] as well as the IRE1 pathway [72]. Using mouse embryonic fibroblasts (MEF) deficient in IRE1 or ATF6 as well as embryonic stem cells deficient in PERK, Ogata et al. presented evidence that accumulation of microtubule-associated protein 1 light chain (LC) 3-positive autophagic vesicles upon treatment with tunicamycin or thapsigargin, two chemical inducers of ER UPR, was dependent on IRE1, but not on PERK or ATF6 [72]. In accordance with these data, the thapsigargin-induced accumulation of LC3-positive vesicles was inhibited in MEF deficient in TRAF2, linking IRE1

to autophagy via JNK [37]. Subsequent pharmacological inhibition of JNK in this model system abrogated LC3 translocation suggesting the IRE1-TRAF2-JNK pathway to be essential for ER UPR-induced autophagy in MEF [69,72]. Independently of innate UPR-signaling, autophagy might also be triggered and/or amplified by ROS produced under stress conditions [76].

1.3.3. ER UPR and apoptosis

The purpose of ER UPR is to adapt the ER to cellular demands and to overcome the stress induced by mis- or unfolded proteins. However, the activation of ER UPR is not always sufficient to cope with ER stress and prolonged or excessive ER stress ultimately lead to cell death. Under ER stress, cell death is induced by apoptosis but the precise molecular mechanisms that mediate the switch from adaptive pathways to the induction apoptosis are still unclear. The first protease identified to mediate ER UPR-induced apoptosis was caspase-12. Although cells from mice deficient in caspase-12 undergo apoptosis in response to other death inducing signals, they show partially resistance to ER UPR induced apoptosis [77,78]. Consistent with the function of the ER in regulating cellular free calcium levels, caspase-12 is activated by calpains [77,79], cytoplasmic proteases that are activated by calcium. Subsequent to its activation at the ER, caspase-12 is thought to cleave procaspase-9, finally leading to the activation of caspase-3 via caspase-9 [80]. The ER stress induced activation of procaspase-9 seems to be independent of the mitochondrial cytochrome c/Apaf-1 pathway since the processing of procaspase-9 can occur in the absence of cytochrome c release [81]. In humans, caspase-4 is implicated in ER UPR induced cell death whereas the contribution of caspase-12 is arguable as the human gene contains several mutations impairing its function [82,83].

Activation of PERK and downstream ATF4-mediated CHOP expression plays a distinguished role in ER UPR-induced apoptosis [84-86], since the deletion of CHOP in mouse cells reduces apoptosis upon ER stress [87], whereas CHOP overexpression is sufficient to induce apoptosis in cell lines [88]. Several mechanisms by which CHOP elicits apoptosis are proposed. CHOP has been shown to sensitize cells to ER stress induced apoptosis through induction of Bim, a proapoptotic BH3-only member of the B cell lymphoma (Bcl) 2 family, and concurrent down-regulation of the anti-apoptotic factor Bcl2 [88,89]. Furthermore, CHOP-mediated upregulation of ERO1, a thiol oxidase required for disulfide bond formation during protein folding in the ER but also known to produce ROS as byproduct of its activity, might contribute to the induction of apoptosis. Supporting this hypothesis, reduced levels of ERO1 have been shown to strongly suppress ER UPR induced apoptosis [64,90]. In addition, the PERK/ATF4 pathway contributes to mitochondria-dependent apoptotic mechanisms under ER UPR. It induces a truncated form of the sarcoendoplasmic

reticulum Ca^{2+} -ATPase1 (S1T) that promotes transfer of calcium from the ER to mitochondria, mitochondrial calcium overload finally leading to activation of the mitochondrial apoptotic pathway [91].

IRE1 plays a dual role in ER UPR induced apoptosis. Splicing of xbp1 is supposed to mediate anti-apoptotic signals whereas the activation of JNK is assumed to be a rather pro-apoptotic event. At late stages of ER UPR when apoptosis is induced, xbp1 splicing seems to be attenuated and forced expression of XBP1s during these stages protects human cells from apoptosis [92]. Interestingly, the pro-apoptotic Bcl2 family members Bak and Bax, which are required for the induction of apoptosis under ER stress and regulate the release of pro-apoptotic factors from the mitochondria and calcium from the ER [93-95], also bind to IRE1. This interaction seems to be important for efficient xbp1 splicing during ER stress and is independent from the pro-apoptotic activity of Bak and Bax at the mitochondria [96].

It has been suggested that during mild and strong ER stress all UPR sensors are activated and evoke anti- as well as pro-apoptotic responses. The decision between adaptation vs apoptosis might primarily depend on the intensity of the signal which needs to overcome the low stability of pro-apoptotic mRNAs and proteins in order to prevail the activation of the apoptotic program [27].

1.3.4. ER UPR and metabolism

Protein folding and glycosylation in the ER are energy requiring processes and thus the ER is very sensitive to energy fluctuations and depends on glucose availability. During ER UPR, all three branches of ER UPR impact glucose metabolism as well as lipogenesis.

Pathways involved in glucose synthesis and breakdown are both transcriptionally regulated by ER UPR, for example by using genome wide approaches, XBP1 has been linked to glycolysis as well as glycogen synthesis [97]. Through interaction with CREB-regulated transcription coactivator (CRTC) 2, also ATF6 has been linked to the regulation of glucose synthesis in the liver [98]. Yet, the best characterized branch of the ER UPR in context of glucose metabolism is the PERK pathway. PERK-deficient mice and mice harboring a mutation that prevents phosphorylation of eIF2 α at serine 51 display defective gluconeogenesis in the liver [86,99], linked to pancreatic islet cell dysfunction and death triggered by ER failure [100]. Further addressing the role of eIF2 α phosphorylation, Oyadomari et al. showed that mice expressing a fragment of Gadd34 in the liver, resulting in forced eIF2 α dephosphorylation, encounter hypoglycemia during fasting due to impaired gluconeogenesis and low liver glycogen levels. However, on high fat diet these mice show improved glucose tolerance and diminished hepatosteatosis, probably as a result of reduced lipogenesis [101].

The family of sterol regulatory element-binding protein (SREBP) transcription factors is resident in the ER and is crucial for the regulation of genes involved in cholesterol metabolism or lipid synthesis [102]. SREBP transcription factors are classically activated in response to insulin or low sterol levels, but they might also integrate lipid metabolism into ER UPR. Indeed, lipid-lowering HMG-CoA reductase inhibitors (statins) have been shown to activate ER UPR [103]. The ER is the site of triglyceride formation in liver cells as well as adipocytes [104] and XBP1s regulates the transcription of genes involved in fatty acid synthesis [97]. Accordingly, XBP1 expression is required for normal fatty acid and cholesterol synthesis in the liver [105] and both XBP1 as well as eIF2 α have been shown to participate in basal and/or diet-induced regulation of lipid metabolism [101,105]. PERK has also been implicated in the regulation of fatty acid synthesis in mammary epithelial cells [106]. Moreover, using loss-of-function mouse models of multiple ER UPR proteins, all three branches of ER UPR have been shown to cooperate in protecting the organism from ER stress-induced deregulation of lipid metabolism [107]. Mice with genetic ablations of either ER stress-sensing pathways (ATF6 α , eIF2 α , IRE1 α) or of ER quality control (p58^{IPK}) have been shown to have a dysregulated response to tunicamycin-induced ER stress. This included the suppression of metabolic transcription factors regulating lipid homeostasis but at the same time development of hepatic steatosis, probably due to a loss of liver lipoprotein production. Liver tissue from these mice exhibited signs of unresolved ER stress, partially associated with perpetuated expression of CHOP. Underscoring the role of CHOP in this setup, livers from CHOP-deficient mice maintained metabolic gene expression under tunicamycin challenge [107]. CHOP can act as dominant-negative inhibitor of C/EBP family members including CEBP α , a key mediator of lipid homeostasis. Interestingly, mice with a postnatal, but not with a constitutive embryonic deletion of CEBP α also show a phenotype including fatty liver, hypoglycemia and changes in gene expression profiles [108-110]. Contrarily to the observations mentioned above, that tunicamycin challenge increased ectopic lipid accumulation in mice with a functional knockout of eIF2 α , Oyadomari et al. found reduced hepatic lipid accumulation in mice overexpressing Gadd34 in the liver (silencing eIF2 α phosphorylation) exposed to a high-fat diet [101,107]. These conflicting outcomes might be explained by the level of ER stress induced by the different stimuli. While a more physiological dietary stress might allow for gradual adaptation of eIF2 α -signaling depleted cells, a strong death-inducing UPR evoked by tunicamycin might not, significantly impacting the resultant phenotype. In summary, these findings suggest that ER UPR might be seen as an adaptive response to handle high metabolic loads [111] and raise the possibility that severe ER stress, by leading to profound metabolic disruption, is a contributing factor to the development of hepatic steatosis.

1.3.5. ER UPR and IBD

With respect to IBD, ER UPR at the epithelial cell level was implicated in promotion and perpetuation of intestinal inflammation [10,112,113]. Consistently, recent work using mice deficient in ER UPR-mediators (IRE1 β , XBP1, S1P) or mice with a mutation in the *Muc2* gene links ER stress in the highly secretory subtypes of IEC, anti-microbial peptides-producing Paneth cells and mucin-producing goblet cells, with antimicrobial defense and intestinal inflammation [10,113,114]. Moreover, we provided first evidence that ER UPR in IEC is relevant to patients with IBD [112], and Kaser et al. reported single-nucleotide polymorphisms within the *XBP1* locus in human IBD patients [10]. The commensal microbiota is one of the key drivers of intestinal inflammation in IBD and pathways crucial for sensing and controlling the composition of bacteria, like TLR signaling and autophagy interact with ER UPR. Genome wide association studies (GWAS) have identified multiple polymorphisms as disease susceptibility factors in CD such as the autophagy-related *ATG16L1* [115,116] and *IRGM* [117-119], and bacterial sensing-related *NOD2* [120,121], *TLR4* [122] genes. Interestingly, several of these polymorphisms affect Paneth cells. *NOD2*-as well as *XBP1*-deficient and *ATG16L1*-hypomorphic mice all display alterations in Paneth cell structure and function, consistently with CD patients harboring the *NOD2* or *ATG16L1* alleles [123-125]. Perpetuation of bacterial sensing and reduced ability to eliminate bacteria (via autophagy and antimicrobial peptides) might therefore be directly linked to ER UPR. Of note, also luminal iron was shown to impact the composition of the intestinal microbiota as well as epithelial ER UPR [126], and concomitant CREBH and CHOP have been implicated in iron metabolism through regulation of the peptide hormone hepcidin [127]. The central role of ER stress in intestinal inflammation is further emphasized by the suggestion that ER stress and particularly *XBP1* not only limit the antimicrobial activity of the epithelium but also determine the sensitivity of the epithelium towards cytokines and bacterial signals [9,10].

1.4 Mitochondrial dynamics

Due to the structure of mitochondria, mitochondrial protein homeostasis encounters unique challenges. More than 98% of the total mitochondrial protein is encoded by the nuclear genome, making it necessary to import cytosolically synthesized mitochondrial precursor proteins [128].

1.4.1. Mitochondrial protein homeostasis

Mitochondria are enclosed by two membranes and are well-known for the production of ATP from acetyl CoA in the tricarboxylic acid (TCA) cycle and the respiratory chain. Outer and inner membrane separate two compartments, the intermembrane space and the matrix, which is bound by the impermeable inner membrane that possess specific, gated channels for metabolite and protein exchange [128,129]. Furthermore, the inner membrane harbors five (in mammals) respiratory complexes involved in oxidative phosphorylation (OXPHOS) and ATP production [129]. Within the matrix, several copies of circular mitochondrial DNA are contained as well as the components required for its replication, transcription and subsequent translation of the encoded proteins. Additionally, various enzymes essential for metabolic processes such as TCA, fatty-acid oxidation, iron-sulfur cluster formation, and heme synthesis reside in the matrix [128]. Enclosing matrix and inner membrane, the intermembrane space forms cristae, long tubules or folds that project into the matrix as well as a narrow intermembrane boundary between the inner and outer membranes [130]. Cytochrome c which is involved in respiration in normal cells and apoptotic induction upon its release into the cytosol and other potential apoptotic inducers are present in this compartment [131,132].

Both in the outer and inner membrane, protein translocases enable precursor protein translocation and/or integration into membranes. Translocase of the outer mitochondrial membrane (TOM) acts as entry site and depending on targeting sequences, precursor proteins are subsequently directed to their destination by translocase of the mitochondrial inner membrane (TIM) family members [133]. Protein import into the matrix requires proteins to be unfolded, in order to transit the protein translocase channels [134,135]. Following import, signal sequences are cleaved and proteins are (re-)folded. The mitochondrial matrix contains its own set of molecular chaperones facilitating the folding of newly synthesized or imported proteins with the evolutionary conserved Hsp70 and Hsp60/10 (chaperonin60/10) as main players [21,128]. Additional chaperones and proteases essential for protein maturation and mitochondrial quality control residing in the matrix include ClpP, Lon, Yme1, DnaJ and Hsp78 [128,136,137].

Furthermore, expression of nuclear and mitochondrial DNA-encoded proteins has to be accurately coordinated since 13 out of 89 subunits of the respiratory chain are encoded by mitochondrial DNA in humans [128] and need to assemble into stoichiometric complexes with nuclear-encoded proteins.

Thus, cellular stress leading to increased mitochondrial biogenesis [20], generation of ROS [20,138] or metabolic alterations might impact mitochondrial protein homeostasis and evoke mtUPR.

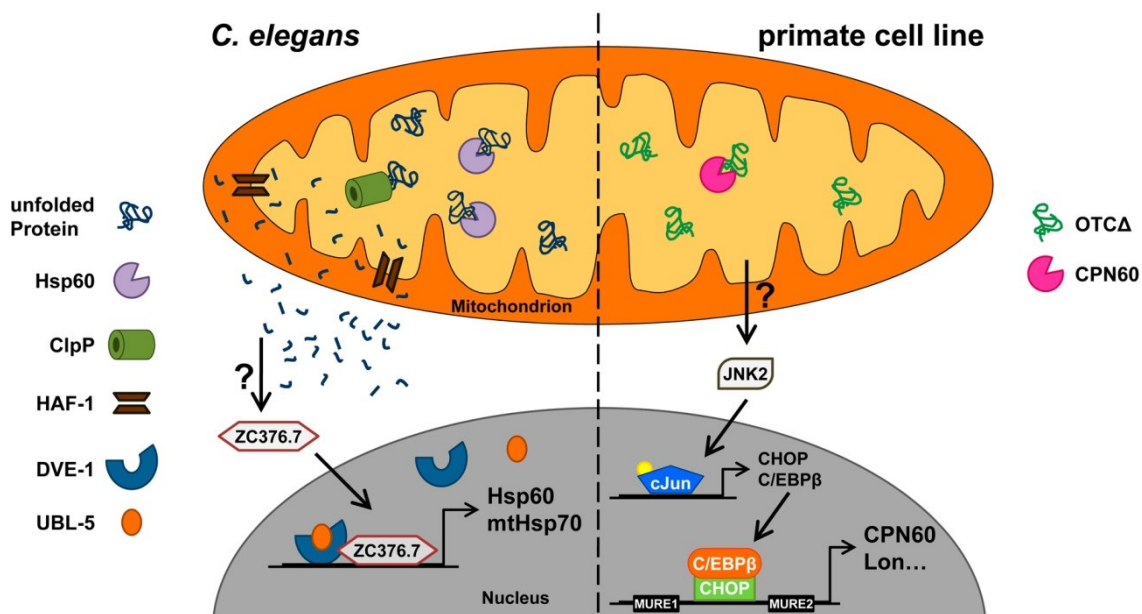


Figure 4. Mitochondrial unfolded protein response in *C. elegans* and primate cells.

The initial signal of mtUPR, peptides generated by ClpP and their translocation to the cytoplasm, has been identified in *C. elegans*; Also, downstream transcription factors are known for both, *C. elegans* as well as mammalian cells. However, cytoplasmic mediators of mtUPR-signaling are largely unknown.

1.4.2. Mitochondrial unfolded protein response

Like ER UPR, mtUPR senses insufficient protein-handling capacity, i.e. misfolded, misassembled or aggregated proteins and aims to restore protein homeostasis by expanding the folding capacity of the organelle and enhancing protein degradation [128,139].

Experiments using cells depleted of mitochondrial DNA through ethidium bromide provided first evidence for a mammalian mitochondrial-specific stress response [22]. Probably due to the disturbance of respiratory complex assembly and accumulation of orphaned nuclear-encoded subunits in the mitochondrial matrix, an induction of Cpn60 and Cpn10 was observed [22]. Consistently, overexpression of a truncated protein prone to aggregate in the mitochondrial matrix (truncated ornithine transcarbamylase, OTCA) increased the expression of Cpn60, Cpn10 and the mitochondrial protease ClpP in an organelle-specific manner since ER-associated chaperones were not induced [21].

Subsequent studies suggested a model in which protein aggregation in the mitochondrial matrix results in the transcriptional activation of the transcription factor CHOP and its cofactor C/EBP β via JNK2 and the transcription factor AP1 [21,24,25]. In turn, CHOP induces mtUPR-target genes containing a CHOP-C/EBP β element flanked by conserved sequences, so-called mtUPR elements (MURE), in their promoters [25] (**Fig.4**). CHOP is engaged both by ER- and mtUPR but deletion analysis of its promoter identified two adjacent but distinct elements for transcriptional activation, providing evidence for a separate induction of the *CHOP* gene in response to either UPR pathway [24,25]. Genetic approaches in *C. elegans* further characterized the mtUPR and lead to the identification of additional signaling components. In accordance with results obtained in mammalian cells [18,22], RNAi-mediated knockdown of mitochondrial chaperones and proteases as well as factors required for mitochondrial DNA expression activated mtUPR in worms that expressed green fluorescent protein (GFP) under the control of the *hsp-60* or *hsp-6* (a homologue of mitochondrial Hsp70) promoter [20].

A subsequent genome-wide RNAi screening identified additional nuclear genes involved in mtUPR signaling, *dve-1* encoding a putative homeobox-like transcription factor, *ubl-5* encoding a small ubiquitin-like protein and *clpp-1* encoding a mitochondrial matrix-localized homologue of the *E. coli* ClpP protease [23,140]. Furthermore, HAF-1, an ATP-binding cassette transporter similar to the yeast mitochondrial peptide transporter Mdl1p and the mammalian transporters associated with antigen presentation (TAP) as well as ZC376.7, a basic leucine zipper transcription factor were found to be essential for signaling mtUPR [141]. In summary, these results suggest a signaling cascade for mtUPR in which insufficient protein-handling capacity within the mitochondrial matrix leads to the accumulation of unfolded proteins and activation of mtUPR. The unfolded proteins are degraded by the matrix-localized ClpP protease to peptides that are transported through the mitochondrial inner membrane by HAF-1. Since small peptides like that generated by ClpP have been shown to be able to diffuse freely through the mitochondrial outer membrane into the cytoplasm [142] an additional transporter out of the mitochondria might not be needed [143]. Downstream, the transcription factor ZC376.7 translocates to the nucleus, UBL-5 and DVE-1 form a complex and DVE-1 redistributes within nuclei and binds to the *hsp-60* promoter. It is unclear whether ZC376.7 and the DVE-1/UBL-5 complex interact, but since the mammalian homologue of DVE-1, SATB2 functions as a global chromatin organizer, it has been suggested that DVE-1/UBL-5 complex-induced chromatin rearrangements might facilitate access of ZC376.7 to promoters of mtUPR target genes [143]. *Ubl-5* itself is a target gene of mtUPR probably representing an amplification circuit to enhance mtUPR signaling, and it has been speculated that ZC376.7 might fulfill similar functions to CHOP in *C. elegans*, as worms lack a conspicuous homologue of CHOP [143] (**Fig.4**). The importance of mtUPR-signaling in

protecting the mitochondrial protein homeostasis by transcriptional upregulation of mitochondrial chaperones has been demonstrated by knockdown or deletion of signaling components, all of which sensitized worms to mitochondrial stress resulting in altered mitochondrial morphology and decreased function, slowed development and shortened lifespan [23,140,141,143]. Highlighting the disease-relevance of mtUPR, mtUPR-associated signaling has recently been implicated as potential target in cancer therapy [144].

1.4.3. Mitochondrial biogenesis and mitophagy

MtUPR has been suggested to participate in the tightly and dynamically regulated mitochondrial biogenesis program to adjust mitochondrial abundance to cellular energy demands [15,145]. Mitochondria cannot be made *de novo*, but divide by a process that recruits lipids and new proteins leading to organelle growth and finally fission [128]. Defects in the respiratory chain and low cellular ATP levels have been shown to increase the number of mitochondria [146,147] as well as external factors such as nutrients, hormones, temperature, exercise, hypoxia, and aging impact mitochondrial biogenesis [128]. However, the underlying mechanisms are not completely understood. Mitochondrial calcium release has been implicated in mitochondrial retrograde signaling [148], NO [149,150], as well as reduced mitochondrial membrane potential ($\Delta\psi$), accumulation of NADH or reduced FAD [128] and the activation of AMP activated protein kinase (AMPK) by a high AMP:ATP ratio [151]. As a consequence of these initial signaling events, nuclear and mitochondrial genes encoding mitochondrial proteins as well as non-mitochondrial proteins involved in energy metabolism are transcriptionally induced [152,153]. Several transcription factors and coactivators involved in mitochondrial biogenesis have been identified in mammals [154]. These include Tfam, NRF1, NRF2, SP1, YY1, CREB, MEF2 and PGC-1 α [154] and through interaction with various binding partners they constitute a regulatory cascade controlling the expression of target genes in a tissue- and stimulus specific way. Recently, an additional factor regulating total mitochondrial mass was identified, mitochondrial DNA absence sensitive factor (MIDAS), a protein stimulating the synthesis of cardiolipin and total mitochondrial lipids [155].

Furthermore, the morphology of mitochondria seems to be directly related to mitochondrial function and respiratory activity. This was demonstrated by overexpression or knockdown of mitochondrial fusion-relevant proteins, mitofusin (Mfn) 2 and Optic atrophy protein (Opa) 1, resulting in altered mitochondrial structures and respiration [156,157]. Small, mobile mitochondria are needed for rapid distribution of ATP to subcellular sites with high energy demand [158,159], whereas larger mitochondria are more efficient in producing ATP [160]. In addition, mitochondrial fusion is important for maintaining mitochondrial DNA integrity [161]. Interestingly, fission has been described to produce metabolically different daughter units,

segregating dysfunctional mitochondria and targeting them for mitophagy [162]. Moreover, it has been suggested that serum withdrawal preferentially promotes mitophagic degradation of mitochondria carrying mtDNA mutations [163]. Mitophagy is a specialized form of autophagy degrading damaged, non-functional mitochondria thereby ensuring the maintenance of a functional mitochondrial population. Several factors have been implicated to selectively targeting mitochondria for autophagy such as the cargo adaptor protein Atg11 [164] and recently PINK1 has been shown to be a signal for the lack of mitochondrial fitness [165]. Expression of PINK1 on individual mitochondria is regulated by voltage-dependent proteolysis to maintain low levels of PINK1 on healthy, polarized mitochondria, while facilitating the rapid accumulation of PINK1 on mitochondria that sustain damage. In turn PINK1 provides the signal for selective recruited of Parkin to damaged mitochondria to trigger their mitophagy [165]. Remarkably, Parkin has been shown to be transcriptionally regulated by the ER UPR-associated transcription factor ATF4, strengthening the evidence for an interconnection between mitochondrial and ER stress [166]. Damaged, dysfunctional mitochondria display toxicity to cells possibly by enhanced ROS generation. Consequences of ROS-mediated damage due to lack of active autophagy have been demonstrated in mice with a liver-specific deficiency in Atg7 [167]. These mice show liver dysfunction associated with accumulation of ubiquitin-positive protein aggregates as well as enhanced expression of oxidative stress-inducible proteins demonstrating autophagy to be required to reduce oxidative stress, and hence cellular damage [167,168]. Additional evidence for a protective role of autophagy under inflammatory conditions came from a study suggesting that autophagy preserves mitochondrial integrity, thereby preventing mitochondrial DNA translocation to the cytosol [169]. In this model, depletion of autophagic proteins promoted the accumulation of dysfunctional mitochondria, mitochondrial ROS production and activation of the NALP3 inflammasome leading to the activation of caspase 1 and secretion of IL-1 β and IL-18 [169]. Consistently, Zhou et al. showed that mitophagy/autophagy blockade not only lead to the accumulation of dysfunctional mitochondria and activation of the NLRP3 inflammasome, but also that NLRP3 and its adaptor ASC redistribute from ER structures to ER/mitochondria organelle clusters upon inflammasome activation [170]. Thus, the authors suggest that the NLRP3 inflammasome senses mitochondrial dysfunction and that this might explain the frequent association of mitochondrial damage with inflammatory diseases [170].

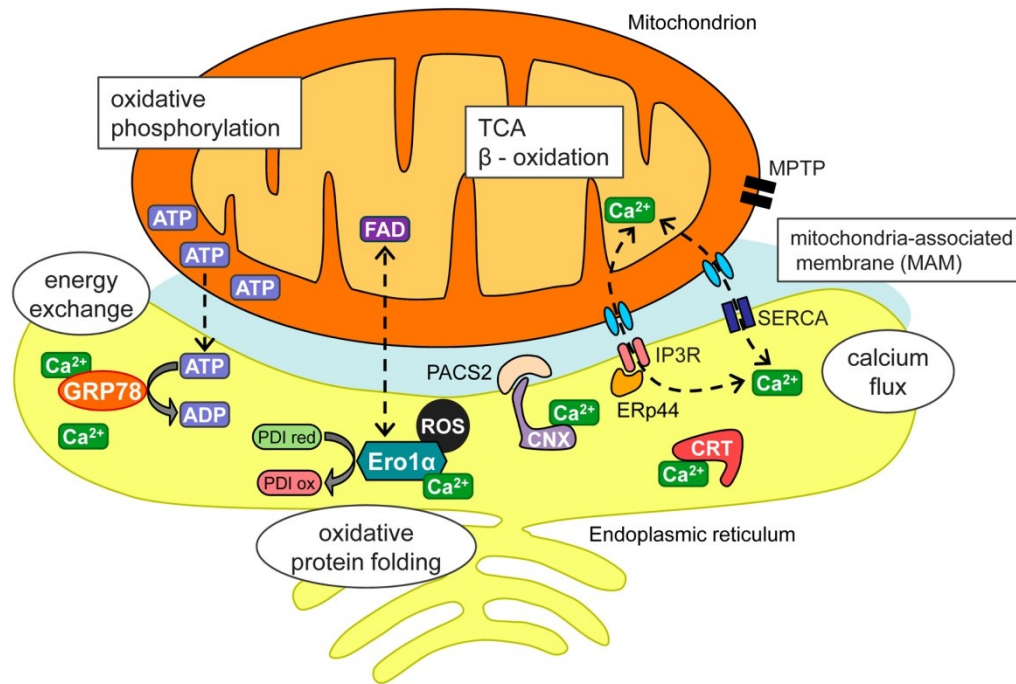


Figure 5. ER- mitochondrial network.

(Modified from Simmen et al.). On mitochondria-associated membranes (MAM), energy- and metabolite exchanges as well as calcium fluxes occur between ER and mitochondria. These processes directly impact ER protein folding since the ER chaperone system is dependent on ATP, calcium and FAD for disulfide bond formation. Reactive oxygen species generated as a byproduct during oxidative protein folding might affect the mitochondrial permeability transition pore and calcium fluxes via SERCA and IP3R. Calnexin localization to the MAM is dependent on PACS2, whereas ERp44 regulates calcium release via interaction with IP3R.

1.5 ER-mitochondrial network

In living cells, mitochondria form a dynamic network, constantly remodeled by fission and fusion events and should not be regarded as single organelles [128]. In fact, they are in close contact with the ER via mitochondria-associated membranes (MAM) [171,172]. These specialized ER domains are enriched in ER folding chaperones and oxidoreductases [173-175], and are sites of calcium- and lipid exchange. Furthermore, the proximity of ER and mitochondria might ensure the constant supply of the ER with ATP [176,177].

On the MAM, calcium release from the ER occurs at inositol 1,4,5-triphosphate receptors (IP3R). Mitochondria can take up these local high amounts of calcium in a quasi-synaptic manner [178] and upon mitochondrial calcium efflux sarcoplasmic/endoplasmic reticulum calcium ATPases (SERCA) mediate calcium re-uptake into the ER [179]. This calcium flux is regulated through calcium and redox-dependent interactions of IP3R and SERCA with ER chaperones such as calnexin (CNX) and calreticulin (CRT) and oxidoreductases such as ERp44, ERp57 and Ero1α [171,179]. ER-associated calcium signaling is not only important during apoptosis [180]. ER chaperones like GRP78 depend on calcium and ATP [181] and moreover, increased mitochondrial calcium levels promote the activity of ATP synthase [182].

Another link between mitochondrial and ER metabolism at MAM is provided by Ero1 α , a oxidoreductase that oxidizes PDI, which in turn catalyzes the formation of disulfide bonds within newly synthesized proteins in the ER [183-185]. Ero1 α requires FAD derived from the mitochondrial metabolism as cofactor and generates ROS as byproduct [183], probably directly impacting mitochondrial permeability transition pore (MPTP), SERCA and IP3R [171]. Interestingly, Ero1 α is induced under ER UPR [18] and at the same time riboflavin-deficiency and therefore FAD metabolism impairs oxidative folding in the ER [186] (**Fig.5**). An additional level of regulation of mitochondria-ER interaction is the regulation of MAM itself. Three proteins are implicated in MAM-regulation in mammalian cells, Mfn2 and the chaperones GRP75 and phosphofurin acidic cluster sorting protein (PACS) 2 [187-189]. Mfn2 is a GTPase localized at the mitochondrial outer membrane and plays a central role in mitochondrial fusion. Furthermore, it has been shown to mediate tethering of the ER to mitochondria and to affect ER morphology as well as calcium homeostasis [189]. In contrast, GRP75 bridges the mitochondrial voltage dependent anion channel (VDAC) to the regulatory domain of IP3R thereby enhancing MAM formation [171,188]. Of particular interest in the context of UPR is PACS2, since siRNA-mediated knockdown of this chaperone not only uncouples ER from mitochondria but also induces ER UPR [187]. In summary, MAM represent an interface linking protein folding in the ER to mitochondrial function via energy, calcium and metabolite exchange.

Consistently, changes in calcium homeostasis and redox status or energy deficiency trigger ER UPR and at the same time ER stress impacts mitochondrial gene expression [166,190] and *vice versa* mitochondria have been shown to modulate ER UPR [191-193]. Confirming the fact that this organelle interplay is not one-sided, the generation of ROS can be both, cause as well as consequence of ER UPR and mitochondrial dysfunction. Under cellular stress conditions, mitochondria and ER also interact on more sophisticated levels. Recent data present evidence that dysfunctional mitochondria contain endogenous high-affinity human TLR4 ligands and induce TLR4-mediated inflammatory reactions [194], suggesting a model in which mitochondria could impact TLR signaling and associated ER UPR. Furthermore, it has been reported that nuclear genes encoding mitochondrial proteins such as the mitochondrial matrix proteases Lon, mtHsp70, and Yme1 are induced by ER stress [190]. Likewise, the ER-mitochondria interconnection plays a prominent role in the caspase-mediated induction of neuronal cell death [192], and mitochondria modulate the ER UPR under glucose deprivation conditions [191]. Conversely, it has been suggested that mitochondria support ER function via adenylate kinase (AK) 2 [195] and mitochondrial dysfunction triggers the ER stress response and aggravates hepatic insulin resistance [193].

In summary, ER and mitochondria form a tight, interrelated network and interact with various cellular stress pathways.

2 AIMS OF THE WORK

IBD pathology features various alterations in cellular functions and immune functions in its complex etiology. Many of those cluster around IEC, which not only constitute a mechanistic barrier but mediate between the two major factors influencing intestinal inflammation, the microbiota and the immune system. Thus, failure to control inflammatory processes at the IEC level may critically contribute to IBD pathogenesis [10,112,113] and *vice versa*, IEC represent a promising target for disease-intervention. Therefore, the present work aimed to identify and characterize novel target proteins/signaling pathways involved in inflammatory processes in IEC.

To screen for changes in gene and protein expression in IEC, an adoptive T cell transfer model of colitis including IL-10 competent and IL-10 deficient T cell donor and recipient mice was used. Applying this model allowed to distinguish between different levels of IL-10 availability and provided different grades of inflammation as outcome. IL-10 mediates various anti-inflammatory and immunoregulatory functions and can be produced by subsets of T cells, B cells, dendritic cells and parenchymal cells as well as IEC [196,197]. Spontaneous enterocolitis in IL-10^{-/-} mice was one of the first models of intestinal inflammation [198], and the activation of ER UPR in IEC under inflammatory conditions was discovered in IL-10^{-/-} mice by a gel-based proteome approach [112].

Since analysis of microarray and proteome data indicated mitochondria to be highly affected under inflammation, we further characterized mtUPR-signaling *in vitro* and evaluated its disease-relevance in the context of intestinal inflammation *in vivo*.

3 MATERIAL AND METHODS

3.1 Animals

3.1.1. Adoptive CD4⁺ T cell transfer

CD4⁺ T cells were isolated from splenocytes of previously germfree 129 SvEv (Wt) and IL-10^{-/-} 129 SvEv donor mice moved to specific pathogen-free (SPF) conditions 4 weeks before splenectomy. Using the magnetic bead-based CD4⁺ T cell-isolation kit or the CD4⁺ CD25⁺-Regulatory T cell-isolation Kit (Miltenyi Biotec, Bergisch Gladbach, Germany), CD4⁺ T cells or CD4⁺ CD25⁺ and CD4⁺ CD25⁻ T cell subpopulations, respectively, were isolated according to the manufacturer's instructions. Briefly, splenocyte suspensions were prepared by cutting and gently grounding donor spleens. CD4⁺ T cells were enriched by negative selection using anti-biotin microbeads coated with lineage-specific biotin-conjugated antibodies against non-CD4⁺ T cells and columns designed for cell depletion (LD columns, Miltenyi Biotec). Unlabeled cells contained in the flow-through were collected. The purity of CD4⁺ T cell-isolation was determined by flow cytometric analysis and was >90% in all experiments. For purification of CD25⁺ and CD25⁻ T cell subpopulations, CD4⁺CD25⁺ T cells were positively selected using anti-CD25 PE-conjugated antibodies and anti-PE microbeads as well as columns designed for cell enrichment (MS columns, Miltenyi Biotec). Unlabeled cells representing the CD4⁺CD25⁺ T cell-depleted, CD4⁺CD25⁻ T cell enriched subpopulation were collected from the flow-through, and CD4⁺CD25⁺ T cells were obtained from the eluate. Purity of CD4⁺CD25⁺ T cells was >95% in all experiments as determined by flow cytometric analysis.

In the first experiment, lymphocyte-deficient SPF 129 SvEv recombination-activating gene (Rag) 2^{-/-} and SPF 129 SvEv Rag2^{-/-} x IL-10^{-/-} mice were reconstituted at 8 weeks of age by intraperitoneal injection of 3.5 x 10⁵ CD4⁺ T cells suspended in 300µl of PBS, derived from either Wt or IL-10^{-/-} mice. 1 and 4 weeks later, mice were killed by CO₂ anesthesia followed by cervical dislocation. Reconstitution of mice was determined by flow cytometric analysis of crude splenocyte suspensions and confirmed CD4⁺ T cell presence as well as absence of CD8⁺ T cells and B220⁺ B cells, respectively. Non-reconstituted Rag2^{-/-} and Rag2^{-/-} x IL-10^{-/-} mice served as controls. The number of mice was n≥5 in all groups.

In the second experiment (microarray), lymphocyte-deficient SPF 129 SvEv Rag2^{-/-} and SPF 129 SvEv Rag2^{-/-} x IL-10^{-/-} mice were reconstituted at 8 weeks of age by intraperitoneal injection of 5 x 10⁵ CD4⁺CD25⁻ or CD4⁺CD25⁺ T cells suspended in 300µl of PBS, derived from either Wt or IL-10^{-/-} mice. 4 weeks later, mice were killed by CO₂ anesthesia followed by cervical dislocation. Non-reconstituted Rag2^{-/-} and Rag2^{-/-} x IL-10^{-/-} mice served as controls. The number of mice was n≥5 in all groups. Animal-use protocols were approved by the

Institutional Animal Care and Use Committee (IACUC), University of North Carolina at Chapel Hill.

3.1.2. Bacterial mono- and dual-association

Germ-free 129 SvEvTAC mice (Wt) and germ-free IL-10^{-/-} 129 SvEvTAC mice were mono- or dual-associated at 12-14 weeks of age with the colitogenic human oral isolate *E.faecalis* strain OG1RF and/or *E.coli* NC101 (an endogenous isolate derived from an IL-10^{-/-} mouse) by gavage feeding and rectal swabbing with viable cultured bacteria, as previously described [199,200]. The mice were maintained in the National Gnotobiotic Rodent Resource Center at the University of North Carolina at Chapel Hill. Bacterial mono- or dual-association and absence of contamination by other bacterial species were confirmed by culturing samples from the small and large intestine at necropsy and culturing serial fecal samples, as previously described [199]. Mice were killed by CO₂ anesthesia followed by cervical dislocation 16 weeks later. Wt mice mono- or dual-associated with *E.faecalis* and/or *E.coli* served as controls. The number of mice was n≥5 in all groups. Animal-use protocols were approved by the Institutional Animal Care and Use Committee (IACUC), University of North Carolina at Chapel Hill.

3.1.3. DSS-induced colitis

Pkr^{-/-} mice (129/terSv x BALB/C) harboring a targeted disruption of the catalytic domain of PKR [201] were a generous gift from J.C. Bell (Ottawa Hospital Research Institute, Ontario, Canada). At 12 weeks of age, male Pkr^{-/-} and CTRL BALB/C mice received cycles of 1% DSS in the drinking water for 7 days followed by 7 days of water to induce chronic colitis [202]. Alternatively, 12 weeks old male Pkr^{-/-} and CTRL BALB/C mice received 1% DSS in the drinking water for 3 days. Mice were kept under conventional conditions and disease activity index (DAI) was scored daily (criteria for scoring see **Tab.1**). Mice receiving water served as controls. The number of mice was n≥5 in all groups. Mice were killed by cervical dislocation. Animal-use protocols were approved by the Bavarian Animal Care and Use Committee (AZ 55.2-1-54-2531-164-09).

Table 1. Criteria for scoring the disease activity index (DAI)¹ (adapted from Murphy et al., 1993)

Score	Weight loss (%)	Stool consistency ²	Rectal bleeding
0	None	Normal	Negative
1	1-5		
2	6-10	Loose	Gross bleeding
3	11-15		Gross bleeding >1d
4	>15	Diarrhea	Gross bleeding >2d

¹ Disease activity index (DAI) = combined score of weight loss, stool consistency, and bleeding/3.

² Normal stool = well formed pellets; loose = pasty stool that does not stick to the anus; diarrhea = liquid stool that sticks to the anus.

3.1.4. Assessment of barrier function (Ussing chamber)

For assessment of colonic barrier function in terms of transepithelial electrical resistance (TER) and colonic permeability, Ussing chamber systems (Easy mount chambers, Physiologic instruments, San Diego, USA) were used as previously described [203]. Briefly, distal colon segments of 12 weeks old untreated female *Pkr*^{-/-} and CTRL mice (n=5 in both groups) was prepared as whole and mounted into slider with a recording area of 0.25cm². Apical and basolateral sides were bathed separately in 3ml Krebs solution. During experimental procedures, the bath was maintained at 37°C and aerated continuously with Carbogen (95% O₂ and 5% CO₂). After an equilibration period of 45min, colonic TER was calculated from the short circuit current and the resulting voltage difference every hour.

Colonic permeability was determined by basolateral translocation of Sodium fluorescein (Sigma Aldrich, Saint Louis, USA). After an equilibration period of 30min apical/luminal Krebs buffer was replaced by Krebs buffer containing Sodium fluorescein (500µg/ml). 1h after changing buffers, 100µl of Krebs buffer from the basolateral chambers was sampled. The amount of translocated fluorescein was assessed by measuring fluorescence (Excitation: 485nm, emission: 515nm) using a fluorimeter (Thermo Scientific, Waltham, USA).

3.1.5. Histological scoring

Sections of the cecal tip and distal colon were fixed in 10% neutral buffered formalin (Sigma Aldrich). Fixed tissues were hematoxylin- and eosin-stained and embedded in paraffin.

Adoptive CD4⁺ T cell transfer and DSS-induced colitis: Histological scoring was performed by blindly assessing the degree of lamina propria mononuclear cell infiltration, crypt hyperplasia, goblet cell depletion and architectural distortion, resulting in a score from 0 (not inflamed) to 12 (massively inflamed), as previously described [204].

Bacterial mono- and dual-association: The histological score was assigned by blindly assessing the degree of lamina propria mononuclear cell infiltration, crypt hyperplasia, goblet

cell depletion, and architectural distortion resulting in a score from 0 (not inflamed) to 4 (inflamed), as previously described [205].

3.1.6. Isolation of primary mouse IEC

Primary IEC were purified as previously described [206]. Briefly, cecal and colonic tissue was cut into pieces and incubated (37°C, 15min) in Mode-K cell culture media supplemented with 1mM dithiothreitol (Roth, Karlsruhe, Germany). The tissue/IEC suspensions were filtered, centrifuged (7min, 300g, RT) and cell pellets were resuspended in DMEM containing 5% fetal calf serum. The remaining tissue was incubated in 30ml PBS (10min, 37°C) containing 1.5mmol/l EDTA (Roth, Karlsruhe, Germany). After filtration, the tissue was discarded and the cell suspension from this step was centrifuged as above. Finally, primary IEC were purified by centrifugation through a 20%/40% discontinuous Percoll gradient (GE Healthcare, Uppsala, Sweden) at 600g for 30min. Primary IEC were collected for subsequent protein and DNA/RNA isolation. Cell purity was assessed by determining the absence of CD3⁺ T cell contaminations and the presence of E-Cadherin, an epithelial cell marker, respectively by Western blot analysis (**Fig.1**).

3.2 Patients

Ileal and/or colonic tissue was obtained from patients with active CD or UC or from patients with colorectal carcinoma undergoing surgical resections, as previously described [112]. Whenever possible, non-inflamed and inflamed tissue regions of the same surgical specimens were included for further analysis. Resected inflamed tissue underwent histological evaluation and specimens were graded in respect to inflammation severity. Control tissue presented normal macroscopical and histological aspect and all samples were taken from bowel mucosa located at least 5cm from the tumor.

For immunohistochemical analysis samples were collected by Miquel Sans and Tiago Nunes at the Hospital Clínic i Provincial/IDIBAPS, Barcelona, Spain. Total number of patients included in the analysis were CTRL: n=5; UC: n=3; CD: n=5. For Western blot analysis samples were collected by Gerhard Rogler at the Regensburg University Medical Center, Regensburg, Germany. Total number of patients included in the analysis were CTRL: n=2; UC: n=4; CD: n=3. All studies were performed in accordance with the declaration of Helsinki.

3.2.1. Isolation of primary human IEC

Isolation of primary human IEC from resected ileal and colonic tissue sections was performed as previously described [207]. Briefly, the mucosa was stripped from the

submucosa within 30 minutes after intestinal resection and the mucus was removed by treatment with 1mM DTT for 15min. The mucosa was then incubated with 1.5mM EDTA in Hanks' balanced salt solution without calcium and magnesium and tumbled at 37°C for 10min. The supernatant containing debris and mainly villi cells was discarded. The mucosa was incubated again with EDTA at 37°C for 10min. The supernatant of this isolation step was collected. Subsequently, the remaining mucosa was vortexed and the supernatant was again collected containing complete crypts, some single cells and a small amount of debris. To separate IEC from contaminating non-epithelial cells, the suspension was allowed to sediment for 15min. The sediment containing mainly complete crypts was collected and washed twice with PBS. Primary IEC from the resected intestinal surgical specimens were combined and collected in sample buffer.

3.3 Immunohistochemical labeling and quantification

Paraffin embedded tissue was cut into 5µm sections using a Leica RM2255 and applied up onto polylysine coated slides, air dried at room temperature for 1h and dried at 37°C overnight. Samples were deparaffinized and antigens were unmasked by 10min incubation in boiling 10mmol/L sodium citrate buffer (pH 6.0) (Roth, Karlsruhe, Germany). Immunostaining was performed according to the protocol provided by Cell Signaling. Anti-GRP78 (Sigma-Aldrich, Saint Louis, MO), anti-CPN60, anti-PKR (M-515 for mouse and FJ-6 for human, all from Santa Cruz, Europe) and anti-E-Cadherin (Abcam, Cambridge, UK) were used in combination with Alexa Fluor 488 donkey anti-goat IgG, Alexa Fluor 488 goat anti-mouse and Alexa Fluor 488 goat anti-rabbit IgG and Alexa Fluor 594 goat anti-rabbit (all from Invitrogen Molecular Probes) to stain the respective immunoreactive protein. Rabbit IgG, mouse IgG and goat IgG (all from Santa Cruz, Europe) were used as isotype controls. The slides were counter stained with DAPI and mounted in vectashield (Vector laboratories). Sections were viewed on a Leica confocal microscope using LAS AF Version 2.3.0 (Leica Microsystems). Pictures were quantified using Volocity 5.4.1 Software (PerkinElmer). Epithelial cell regions were defined as region of interest (ROI) and the mean intensity of the fluorescence signal per µm² was measured.

3.4 Protein expression profiling

3.4.1. 2D SDS-PAGE

Protein from purified primary IEC was isolated and subjected to isoelectric focusing (IEF) in the first dimension and SDS-PAGE in the 2nd dimension as previously described [112]. Briefly, primary IEC were resuspended in lysis buffer containing 7mol/l urea, 2mol/l thiourea,

2% CHAPS, 1% DTT (all from Roth, Karlsruhe, Germany), protease inhibitor (Roche Diagnostics, Mannheim, Germany) and 2% Pharmalyte (Amersham Biosciences, Freiburg, Germany) and homogenized by ultrasonication. Total protein concentrations were determined using the BioRad protein assay (Munich, Germany) and used for further analysis or stored at -80°C. For IEF, 250µg of solubilized total protein was cup-loaded onto rehydrated immobilized pH gradient strips (IPG, pH 3-10, 18cm, Amersham Biosciences). Subsequent to the first dimension, IPG stripes were loaded onto 12.5% SDS-polyacrylamide gels and gel electrophoresis was performed. After fixation, proteins were stained using a Coomassie Brilliant Blue solution. For each individual mouse included in the experiments a separate gel was generated and analyzed ($n \geq 5$ for each group). All gels from each experimental setup were simultaneously submitted to all steps of 2-dimensional (2D)-gel electrophoresis including IEF, SDS-PAGE, Coomassie Brilliant Blue staining, and quantitative analysis to minimize variability between samples. Coomassie-stained gels were scanned (ImageScanner, Amersham Biosciences) and analyzed by ProteomWeaver software (Definiens), including background subtraction and volume normalization. For each experiment, gels from control- and treatment groups were compared. Spots picked for further matrix-assisted laser desorption/ionization time of flight (MALDI-TOF) MS analysis significantly differed at least 1.4-fold from the control group in protein intensity according to the Mann-Whitney-test ($P < 0.05$) and were present in at least 8 of 12 gels.

3.4.2. Trypsin digestion of protein spots and MALDI-TOF-MS

Coomassie stained spots were picked, washed, dried, and digested using sequencing grade modified trypsin (Promega) as previously described [112]. Mass analysis was performed according to the method of Bruker Daltonics using the Autoflex Control software and the mass spectrometer of Bruker Daltonics. Briefly, 2-3ml of the extracted protein sample together with 2ml of 0.1% Trifluoroacetic acid was spotted onto the target using the thin-layer affinity HCCA AnchorChip preparation by Bruker Daltonics. Proteins were identified by using the Mascot Server 1.9 (Bruker Daltonics) based on peptide mass searches within murine sequences only. The search parameters allowed the carboxyamidomethylation of cysteine and 1 missing cleavage. Mass accuracy was set to ± 100 ppm. A significant Mascot score obtained from protein spots derived from at least 4 different gels was selected as criteria for positive identification of proteins.

3.5 Gene expression profiling

Total RNA was isolated from primary large intestinal epithelial cells (derived from cecal and colonic tissue sections) using the column-based RNeasy Mini Kit (Qiagen, Hilden,

Germany) according to the manufacturer's instructions. RNA quality and concentration was determined by spectrophotometric analysis (ND-1000 spectrophotometer, NanoDrop and Agilent bioanalyzer) and the RNA integrity number (RIN) was >6 for all samples.

RNA preparation (starting with 200ng), RT, labeling, and hybridization were conducted using the kits provided in the 3'IVT Express Kit and Control Reagents package (Affymetrix) according to the Affymetrix Technical Manual. To assess efficiency and quality, RNA/DNA samples taken at several steps of the protocol and were applied on 2% agarose gels. All samples derived from either IL-10^{-/-} (n=20) or Rag2^{-/-} x IL-10^{-/-} recipient mice (n=20) were processed at the same time. Labeled RNA samples were hybridized to the murine genome array NuGO_Mm1a 520177 (Affymetrix). In principle, each gene on the chip is represented by 10 to 20 oligonucleotides, termed a "probe set." The level of expression of a particular gene is measured by hybridization of fluorescently labeled cDNA, synthesized from extracted mRNA, to these sets. These expression values are typically unitless and have meaning only in the context of a reference measurement [208]. The gene chips were washed and stained using the GeneChip® Hybridization, Wash, and Stain Kit and a GeneChip® Fluidics Station 450 (all from Affymetrix). Subsequently, gene chips were scanned with a GeneChip Scanner 3000 (Affymetrix) and were visually inspected for irregularities. Data were analyzed using Affymetrix GCOS Manager and the R- and Bioconductor-based [209,210] Management and Analysis Database for Multi-platform MicroArray eXperiments for quality control and statistical analysis (MADMAX, URL: <https://madmax.bioinformatics.nl>) or Genomatix ChipInspector.

MADMAX/Affymetrix statistical analysis pipeline: The used software and database version were: R: version 2.12.0, Bioconductor: version 2.7, AnnotationDbi: version 1.12. and Custom CDF library: nugomm1a520177mmentrezg.cdf with database version 13.0.1. gcRMA (slow) was selected as normalization strategy and genes displaying average intensities below 20 were excluded from the analysis. The Limma (log₂ based) Fold Change was calculated comparing the respective T cell reconstituted group vs the appropriate control group (n=5 for all groups). Changes were considered statistically significant according to the q-value of IBMT regularised t-test or according to the raw P-value of IBMT regularised t-test when comparing CD4⁺CD25⁺ T cell reconstituted mice to the control groups, respectively. Transcripts showing a fold change ≥1.74, corresponding to a log₂ fold change ≥0.8 and a q-value/P-value <0.05 were included in the subsequent analysis.

Heatmaps were generated using the MultiExperiment Viewer (TigrMEV) software [211].

Genomatix ChipInspector: the log₂ fold change for each sample and probe set vs each of the 5 control samples was calculated and the mean fold change of the T cell reconstituted group vs the control group was determined for each probe set. To test the significance of the difference in gene expression at the single probe level, a single-sided permutation t test

analysis was performed. The probes were then mapped onto the relevant transcripts using Genomatix proprietary genome annotation. A transcript was considered as differentially expressed if at least 3 associated probes showed a mean absolute log₂ fold change that was ≥ 0.8 and a P-value < 0.05 .

3.6 Bibliometric analysis

Bibliometric analysis for cocitation was performed using Bibliosphere Pathway Edition (Genomatix Software). Enrichment analysis of pathways and gene ontology (GO) terms was conducted using the Genomatix Pathways System (GePS, Genomatix Software).

3.7 Cell culture, transfection and stimulation

The small intestinal epithelial cell line Mode-K [212] (passage 10-25) was grown in a humidified 5% CO₂ atmosphere at 37°C to confluency in 12 well tissue culture plates (Cell Star, Greiner bio-one, Frickenhausen, Germany). The Mode-K cell culture media was Dulbecco's modified Eagle's medium (DMEM) containing 10% fetal calf serum (FCS), 1.0% Glutamine and 0.8% antibiotic antimycotic (Invitrogen, Carlsbad, USA). Cell culture media was changed prior to stimulation or transfection.

Mode-K cells (50% confluent) were transfected using FuGENE (Roche) for OTCA cDNA-transfection and Lipofectamine (Invitrogen) for siRNA-transfection according to the manufacturer's instructions. The OTCA-plasmid [21] was provided by N. Hoogenraad (La Trobe University, Melbourne, Australia). Synthetic *Pkr* (NM_011163)-specific and control siRNA was purchased from Qiagen. 2µg/ml cDNA and 10nmol/l siRNA respectively, were used for transfection. Whenever indicated, cells were stimulated with tunicamycin (500ng/ml) or incubated with PKR-inhibitor (1µmol/l), PD98059 (20µmol/l) (all from Calbiochem), TCS-JNK5a (20µmol/l) (Tocris), Z-LY-CMK (1µmol/l, Bachem), BABTA-AM (5µmol/l), KN-93 (20µmol/l) or AIP (20µmol/l) (all from Biomol, international). Cell media was changed 8h after transfection or prior the addition of the inhibitors or stimulation.

Murine embryonic fibroblasts (MEF) derived from mice harboring a targeted disruption of the catalytic domain of PKR (see 3.1.2 and [201]) and genetic background controls (BALB/C) were kindly provided by Nadine Waldschmitt (Chair for Biofunctionality, Technische Universität München, Freising). MEF with a disruption of the *Pact* gene resulting in complete ablation of protein expression [213] and genetic background controls (C57BL/6) were a generous gift from G.C. Sen (Cleveland Clinic Foundation, Cleveland, USA). MEF were grown in a humidified 5% CO₂ atmosphere at 37°C in 12 well tissue culture plates (Cell Star, Greiner bio-one, Frickenhausen, Germany). The MEF culture media was Dulbecco's modified Eagle's medium (DMEM) containing 10% fetal calf serum (FCS), 0.1mM non-

essential amino acids (NEAA), 2mM Glutamine, 1mM Pyruvate and 1% antibiotic antimycotic (Invitrogen, Carlsbad, USA). Cell culture media was changed prior to and 6h after transfection. Transfection with OTCA cDNA was performed according to the Moke-K cell protocol.

All cell culture experiments were performed at least three times, until otherwise stated.

3.8 Mitochondrial Isolation

36h after OTCA transfection or 2h after tunicamycin stimulation respectively, Mode-K cells were homogenized in STE buffer containing 250mmol/l saccharose, 5mmol/l Tris and 2mmol/l EGTA, pH 7.4 using a glass potter. Cells debris was removed by centrifugation (1000g, 4°C). Subsequently, mitochondria were pelleted by centrifugation (11600g, 4°C). The purified mitochondria were lysed in lysis buffer containing 7M urea, 2M thiourea, 2% CHAPS, 1% DTT (all from Roth, Karlsruhe, Germany) and protease inhibitor (Roche Diagnostics, Mannheim, Germany) and homogenized by ultrasonication.

3.9 Western blot analysis

Purified primary IEC, MEF or Mode-K cells were suspended in lysis buffer containing 7mol/l urea, 2mol/l thiourea, 2% CHAPS, 1% DTT (all from Roth, Karlsruhe, Germany) and protease inhibitor (Roche Diagnostics, Mannheim, Germany) and homogenized by ultrasonication. Total protein concentrations were determined using the BioRad protein assay (Munich, Germany). Samples were diluted with 5x SDS buffer and 25 / 50µg of protein were subjected to electrophoresis on 10% or 15% SDS-PAGE gels. Anti-E-Cadherin, anti-CHOP, anti-COXIV, anti-P-PERK, anti-PKR, anti-P-PKR, anti-P-PACT, anti-ATF4, (all from Santa Cruz, Europe), anti-CD3, anti-CPN60, anti-P-cJun, anti-P-eIF2 α , anti-LC3, mouse anti-rabbit IgG (light chain specific) (all from Cell signaling, Beverly MA), anti-GRP78, anti-OTC (Sigma-Aldrich, Saint Louis, MO) and anti- β -Actin (ICN, Costa Mesa, CA) were used with the appropriate HRP-conjugated secondary antibodies, goat anti-rabbit, goat anti-mouse and rabbit anti-goat (all from DIANOVA, Hamburg, Germany) to detect the respective immunoreactive protein, using an enhanced chemiluminescence light-detecting kit (GE, Arlington Heights, IL). Western blots representative of the respective experiment are shown.

3.10 Co-immunoprecipitation

Mode-K cells were transfected with OTCΔ for 34h. Co-immunoprecipitation was performed according to the protocol provided by Cell Signaling. Briefly, whole cells were lysed in lysis buffer (Cell Signaling, Beverly, MA) supplemented with PMSF (1mM). Cell debris were removed by centrifugation (1400g, 10min) and supernatants were incubated with anti-eIF2α (Cell signaling, Beverly MA) anti-PKR, or control IgG (rabbit or mouse) antibody (all from Santa Cruz, Europe) at 4°C for 3h in a shaker. Subsequently protein A/G-beads (Santa Cruz, Europe) were added and samples were incubated at 4°C over night in a shaker. Beads were collected by centrifugation (5min, 8000g), washed twice with 1x lysis buffer (Cell Signaling, Beverly, MA) and resuspended in lysis buffer containing 7M urea, 2M thiourea, 2% CHAPS, 1% DTT (all from Roth, Karlsruhe, Germany) and protease inhibitor (Roche Diagnostics, Mannheim, Germany) for subsequent Western blot analysis.

3.11 Chromatin Immunoprecipitation

36h after OTCΔ transfection respectively, Mode-K cells were fixed by incubation with serum free medium containing 1% formaldehyde for 10min. Nuclear extraction and chromatin immunoprecipitation were performed using the ChIP-IT Express Enzymatic kit (Active Motif; Carlsbad, CA) according to the manufacturer's instructions. Enzymatically sheared chromatin extracts were normalized according to their DNA content and immunoprecipitations were carried out at 4°C overnight using 2μg anti-p-cJun antibodies (Cell Signaling Beverly, MA). Immune complexes were collected with protein G-coated magnetic beads, washed and eluted from the beads. DNA was released from protein cross-links by chemical reversion, followed by proteinase K digestion at 37°C. DNA from chromatin which was not subjected to precipitation served as a loading control for the subsequent PCR (input control). PCR was performed with total DNA (6μl, input control) and immunoprecipitated DNA (6μl). The PCR products (10μL) were subjected to electrophoresis on 1% agarose gels. Primer sequences, amplicon size and predicted promoter binding site:

precipitation	Amplicon size	Forward Primer	Reverse Primer	Promoter binding site
P-cJUN at <i>Pkr</i>	104	5'-aattgtcacagacatagcttgctggac-3'	5'-ggaagcaactgggcacatggat-3'	agttactcag*

* according to Genomatix software

bold: positions with high degree of conservation within the matrix

3.12 DNA/RNA isolation, reverse transcription and real-time PCR

Total DNA and RNA was isolated using the column-based RNeasy Mini Kit or the DNA/RNA Isolation Kit, respectively (both from Qiagen, Hilden, Germany) according to the manufacturer's instructions. DNA and RNA concentrations and purity (A260/A280 ratio) was determined by spectrophotometric analysis (ND-1000 spectrophotometer, NanoDrop Technologies, Willigton, USA). Reverse transcription was performed using 1 µg total RNA. Real-time PCR was performed using 50ng crude DNA or 1 µl cDNA in a Light Cycler® 480 system (Roche Diagnostics, Mannheim, Germany) applying the Universal Probe Library system [214] according to the manufacturer's instructions. To determine the ratio of mitochondrial (mt) to nuclear DNA, primer specific for mitochondrial and nuclear sequences were designed and the ratio was calculated using the Ct values given by the Light Cycler® 480 software. Relative induction of gene mRNA expression was calculated using the Light Cycler® 480 software and 18S expression for normalization. Primer sequences are given in **Tab.2**. Data were expressed as fold change against untreated cells. The PCR products (10 µl) were subjected to electrophoresis on 2% agarose gels to determine amplicon specificity.

Table 2. Primer sequences for real-time PCR

	Forward primer	Reverse Primer	Probe#
<i>grp78</i> (NM_022310.2)	5'-ctgagggcgtatttgggaaag-3'	5'-tcatgacattcagtcagca-3'	105
<i>pkr</i> (NM_011163.3)	5'-gttggtgggagggagttgac-3'	5'-agaggcaccgggtttgtat-3'	99
<i>atf4</i> (NM_009716.2)	5'-atgatggcttgccagtg-3'	5'-ccatttctccaacatccaatc-3'	88
<i>atf3</i> (NM_007498.3)	5'-gctggagtcagttaccgtaa-3'	5'-cgcctcctttcctctcat-3'	80
<i>trib3</i> (NC_000068.6)	5'-gtcgcttgtcttcagcaact-3'	5'-tcatctgatccagtcacag-3'	67
<i>cpn60</i> (NM_010477.4)	5'-ggtgaaaaaaggatcattg-3'	5'-tcggctgtagtagcaaggag-3'	3
<i>coxI</i> (NP_904330.1)	5'-cagaccgcaacctaaacaca-3'	5'-ttctgggtgcccagaagaat-3'	25
<i>coxIV</i> (NM_009941.2)	5'-tactgcgctcgttctgat-3'	5'-cgatcgaaagatgagggatg-3'	7
<i>pgc-1α</i> (NM_008904.2)	5'-gagcgaaccttaagtgtgaa-3'	5'-tctggtggctttatgagga-3'	52
<i>18s</i> (NR_003278.1)	5'-aaatcagttatggtcctttggtc-3'	5'-gctctagaattaccacagttatccaa-3'	55
<i>nuclear DNA seq</i> (Chr8)	5'-tttacaggatctccaagattcaga-3'	5'-gatcaccatgtgaacaaa-3'	26
<i>mt DNA seq</i> (ChrM)	5'-caaattaccgctactcaactc-3'	5'-gctataatttctgattgtgttg-3'	101

3.13 Statistical analysis

All statistical computations were performed using SigmaStat software from Systat Software except Spearman's rank correlation coefficient, which was calculated using the WinSTAT add-in for MS Excel. Data comparing treatment vs corresponding control group were analyzed using unpaired t tests. Data comparing several treatments vs corresponding control group were analyzed using One-Way or Two-Way ANOVA followed by an appropriate multiple comparison procedure. If data were not normally distributed or comprised discontinuous data, non-parametrical tests (Mann-Whitney/Rank sum test, ANOVA on ranks) were used. Histopathology scores are expressed as means \pm SD of at least 5 mice per group. Real-time PCR data are expressed as mean fold of control group \pm SD, of 2 independent triplicates for the cell culture experiments. Differences between groups were considered significant if P-values were <0.05 .

4 RESULTS

4.1 Markers of ER- and mitochondrial stress are induced in IEC under inflammatory conditions

4.1.1. Protein expression profiling of IEC links ER- and mitochondrial stress in experimental colitis

To identify novel target proteins differentially regulated under inflammatory conditions in the intestinal epithelium, we performed protein expression profiling using total protein of isolated large IEC of a murine model of T cell-mediated colitis. IEC purity was assessed by determining the absence of CD3⁺ T cell contaminations and the presence of E-Cadherin, an epithelial marker, respectively by Western blot analysis (**Fig.6A**). Rag2^{-/-} mice as well as Rag2^{-/-} mice backcrossed to IL-10^{-/-} mice were reconstituted with CD4⁺ T cells from either Wt or IL-10^{-/-} donor mice. The CD4⁺ T cell population consists of colitogenic CD25⁻ as well as regulatory CD25⁺ T cells that mediate their protective function primarily by IL-10 [215]. Thus, the severity of colitis was associated with the ability of the host as well as the transferred T cells to produce IL-10 [215]. Histological analysis confirmed the presence of inflammatory changes in both recipient mouse strains, developing gradually mild to severe colitis over 4 weeks (**Fig.6B**, **Tab.3**). 2D SDS-PAGE and MALDI-TOF-MS analysis identified differentially regulated proteins comparing T cell-reconstituted mice with the appropriate control group. The numbers of differentially regulated proteins increased from the early (1 week) to the 4 weeks time point, associated with the development of chronic colitis. Yet, Rag2^{-/-} recipients seemed to be more sensitive towards T cell transfer at the early time point in terms of numbers of regulated proteins. Overall, T cells derived from IL-10^{-/-} donor mice seemed to be more efficient in inducing changes in IEC at the early time point, whereas after 4 weeks equal numbers of regulated proteins were found in both groups, mice reconstituted with T cells from Wt as well as IL-10^{-/-} donors (**Fig.7A**). Approximately one third of regulated proteins were identified in both recipient strains, indicating a subset of general target (stress-related) proteins with altered expression under inflammatory conditions. A total number of 132 unique proteins could be identified (see appendix, **Tab.A1**). On the basis of literature cocitation from NCBI PubMed, a bibliometric analysis was performed. The data-mining program BiblioSphere was used to generate a protein-protein network tree. Due to the restriction to co-cited proteins only 121 proteins were included in the network, clustering around mitochondrial CPN60 which is involved in the folding of polypeptides in the mitochondrial matrix [216] (**Fig.7B**).

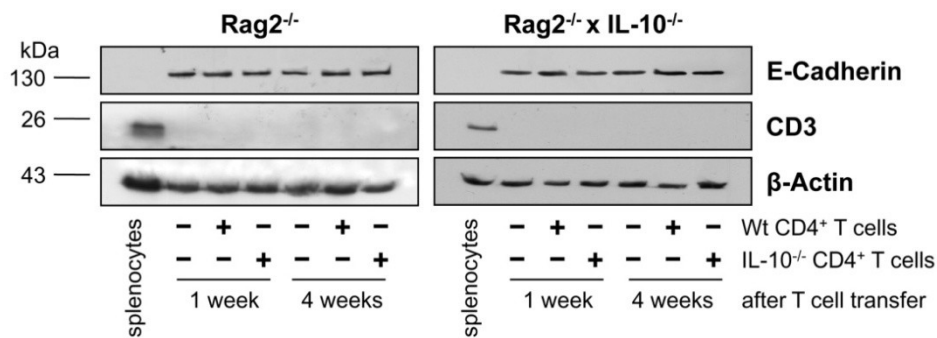
RESULTS

Table 3. Histological scores of Rag2^{-/-} and Rag2^{-/-} x IL-10^{-/-} recipients following adoptive T cell transfer.

Recipient mouse strain	Time after T cell transfer	Histological score (±SD)					
		Colon			Cecum		
		Wt CD4 ⁺ T cells	IL-10 ^{-/-} CD4 ⁺ T cells	Wt CD4 ⁺ T cells	IL-10 ^{-/-} CD4 ⁺ T cells		
Rag2 ^{-/-}	1 week	0.4 ± 0.22	0.5 ± 0.00	0.8 ± 0.27	0.5 ± 0.00	0.3 ± 0.27	1.2 ± 0.76**
Rag2 ^{-/-} x IL-10 ^{-/-}	1 week	0.4 ± 0.22	0.7 ± 0.27	0.4 ± 0.25	0.5 ± 0.00	2.1 ± 0.74*	1.8 ± 0.87
Rag2 ^{-/-}	4 weeks	0.7 ± 0.57	2.1 ± 1.48	4.1 ± 1.08*	0.3 ± 0.27	1.3 ± 0.57	2.1 ± 1.29*
Rag2 ^{-/-} x IL-10 ^{-/-}	4 weeks	0.6 ± 0.22	2.0 ± 1.84	3.8 ± 1.55*	0.9 ± 0.42	3.8 ± 1.60*	7.8 ± 0.96**

* different from CTRL group, ** different from Wt CD4⁺ T cell group, ANOVA on Ranks followed by Holm-Sidak test or Dunn's test P<0.05

6A



B

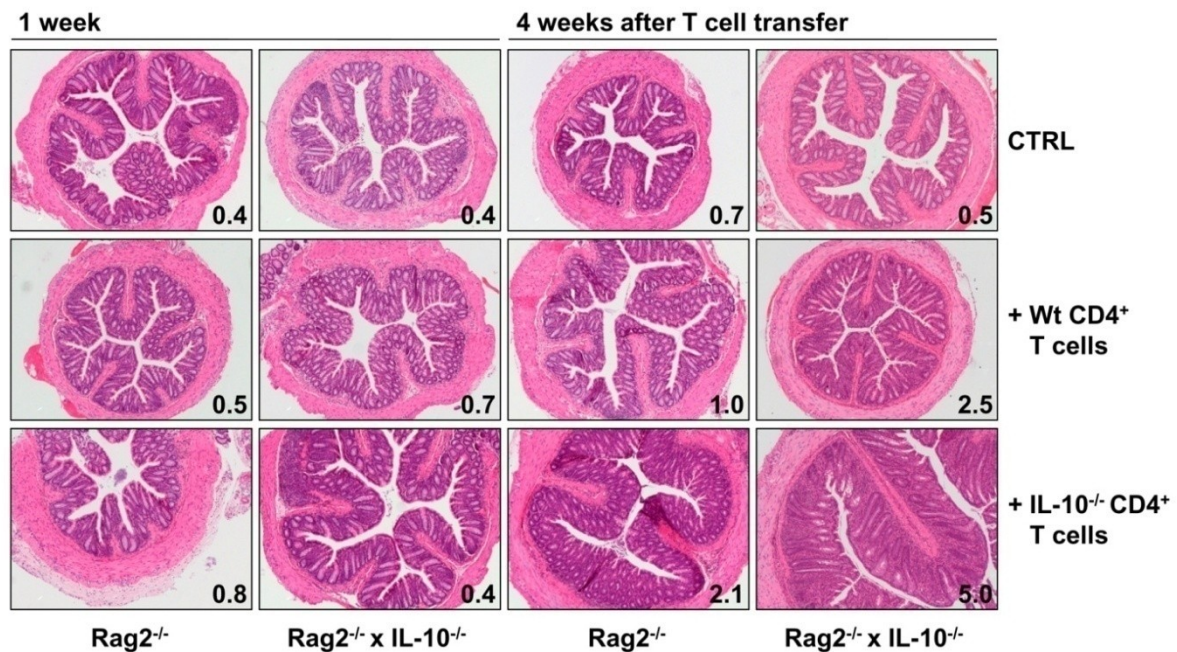


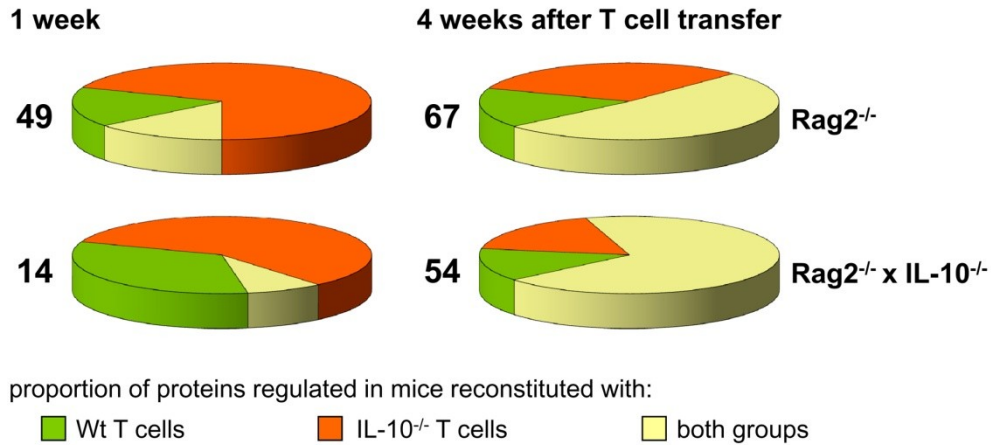
Figure 6. Inflammatory changes following CD4⁺ T cell transfer and purity of IEC isolation.

Rag2^{-/-} and Rag2^{-/-} x IL-10^{-/-} recipients were adoptively transferred with CD4⁺ T cells from Wt or IL-10^{-/-} mice (n=5 per group) and sacrificed 1 and 4 weeks later. (A) IEC of the large intestine were isolated and checked for their purity by Western blot analysis using specific antibodies for CD3 as lymphocyte- and E-Cadherin as IEC marker respectively. Protein was pooled for Western blot analysis. Total protein lysate of splenocytes served as positive control. (B) Representative H/E staining of distal colon sections of Rag2^{-/-} and Rag2^{-/-} x IL-10^{-/-} recipients with histological score indicated (100x magnification).

CPN60 is specifically upregulated by unfolded proteins in the mitochondrial matrix, and therefore has been considered as a mtUPR target gene and as surrogate marker for mtUPR [21]. Also included in the network was the endoplasmic reticulum chaperone GRP78, the surrogate marker of ER UPR, linking ER- and mtUPR under inflammatory conditions. By applying a GO-filter assigning genes to cellular components, overrepresented components were identified by calculating Z-scores. With a Z-score of 14.99 (a Z-score above 2 can be considered statistically significant, corresponding to a P-value of about 0.05) mitochondrial proteins were highly overrepresented.

In total, 46 out of the 132 proteins originally identified in our proteome approach were designated to the mitochondrial compartment. 37 of those were localized in the matrix and comprised enzymes of the TCA, fatty acid and amino acid metabolism as well as oxidative phosphorylation (**Tab.A1**). Interestingly, this pattern of proteins was also found in a study by Haynes et al., in which proteins degraded and exported from mitochondria under conditions that perturb mitochondrial protein folding were identified. The majority of these proteins were localized in the mitochondrial matrix and included proteins involved in various metabolic pathways like TCA and subunits of the ATP-synthase [141]. In summary, these results indicate that in addition to ER stress, also mitochondrial stress is present in IEC under inflammatory conditions.

7A



B

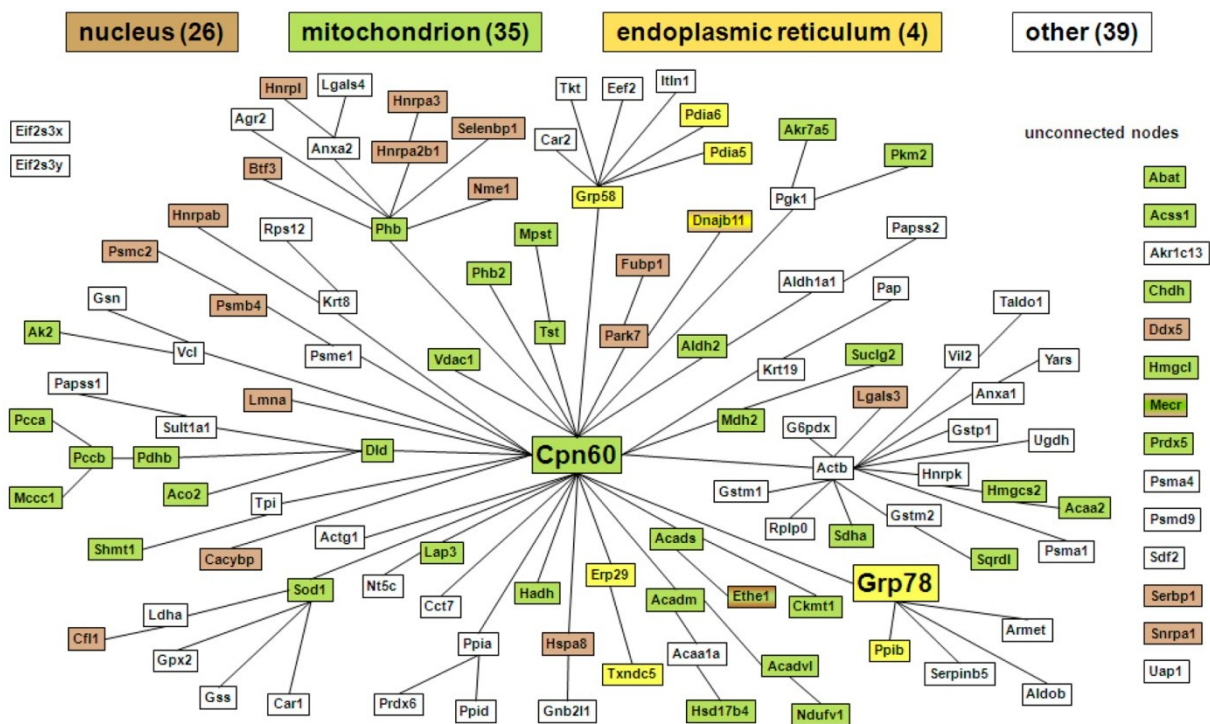


Figure 7. Protein expression profiling links ER- and mitochondrial stress in intestinal inflammation.

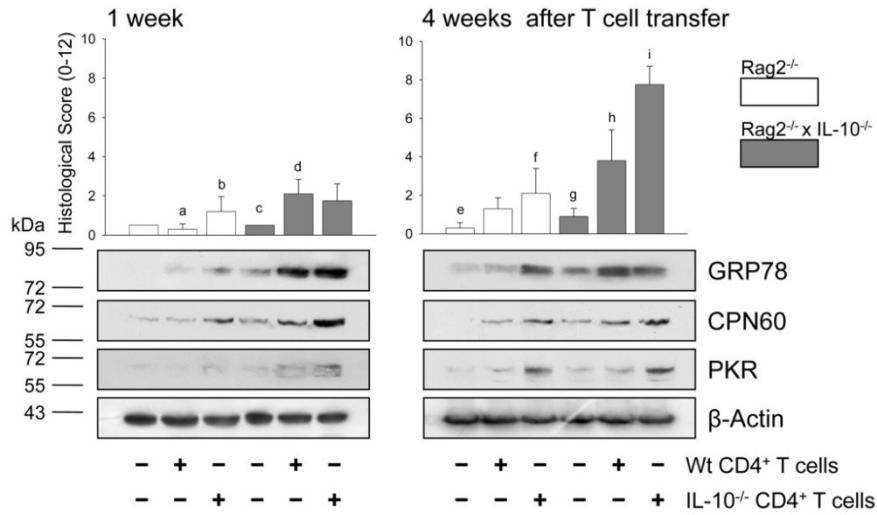
Rag2^{-/-} and Rag2^{-/-} x IL-10^{-/-} recipients were adoptively transferred with CD4⁺ T cells from Wt or IL-10^{-/-} mice (n=5). Mice were sacrificed 1 and 4 weeks later and primary IEC of the large intestine were isolated. 2D SDS-PAGE and MALDI-TOF mass spectrometry were used to identify proteins differentially regulated under inflammatory conditions. **(A)** Total number of differentially regulated proteins in both recipient strains at both time points. The color code indicates the proportion of proteins regulated in recipients reconstituted with T cells from Wt or IL-10^{-/-} mice or regulated proteins present in both groups. **(B)** Genomatix BiblioSphere software was used to generate a gene-gene network tree including all regulated proteins color-coded for the designated cellular compartment. With a Z-score of 14.99 mitochondrial proteins are highly overrepresented.

4.1.2. ER chaperone GRP78, mitochondrial CPN60 and PKR are induced in IEC in experimental colitis

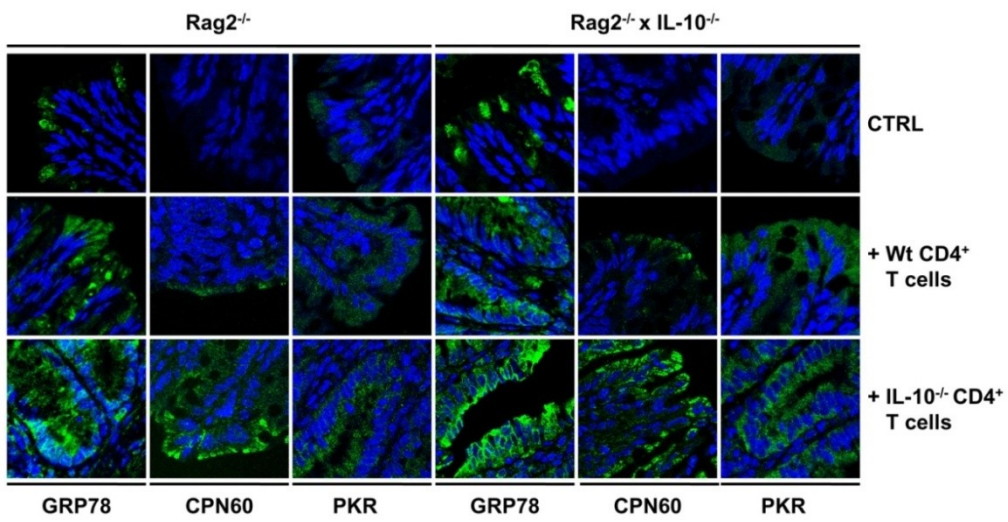
To confirm the results from the protein expression profiling, Western blot analysis was performed for the ER- and mtUPR hallmark proteins GRP78 and CPN60. Supporting previous results [112], GRP78 was induced in IEC under inflammatory conditions yet preceding histological changes. CPN60 followed the same pattern of expression. With regard to our *in vitro* observations suggesting a role for PKR in mtUPR signaling (described in 4.2), the expression levels of PKR were investigated. We did not identify PKR protein levels to be altered in our proteome approach but due to technical limitations only a subset of proteins can be identified using 2D SDS-PAGE and MALDI-TOF mass spectrometry [217]. Thus, we checked the protein levels of PKR by Western blot analysis and found PKR to be induced in IEC under inflammatory conditions accompanying histological changes (**Fig.8A**). Immunohistochemical (IHC) analysis and fluorescence intensity measurements in colonic tissue sections further verified the induction of GRP78, CPN60 and PKR in the intestinal epithelium after T cell transfer (**Fig.8B-D**). Notably, under non-inflammatory conditions, GRP78 seemed to be expressed predominantly in a restricted epithelial cell population, most likely mucin-producing goblet cells, whereas under inflammatory conditions GRP78-expressing cells could also be found in the lamina propria (**Fig.8B**). Immunohistochemical double-stainings of CPN60 with GRP78, PKR and E-Cadherin respectively confirmed the presence of the ER- and mtUPR hallmark proteins associated with the mtUPR signaling-relevant PKR in IEC under inflammatory conditions (**Fig.8D**).

To further validate our findings, another bacterial-driven model of colitis, germ-free IL-10^{-/-} mice mono- or dual-associated with non-pathogenic *Enterococcus faecalis* and/or *Escherichia coli* strains, was used. It was previously shown that these bacterial strains induce distinct disease phenotypes only in genetic susceptible hosts, namely IL-10^{-/-} mice [199]. Also in this model, inflammatory changes in the intestinal epithelium with concomitant induction of GRP78, CPN60 and PKR, is evident (**Fig.9**, data excluding PKR Western blot, have been published previously [218]). Taken together, these results strongly suggest that the induction of PKR was not due to viral infections, as the animals were maintained under specific pathogen-free environment or germ-free conditions ensuring the mono-/dual-association, respectively.

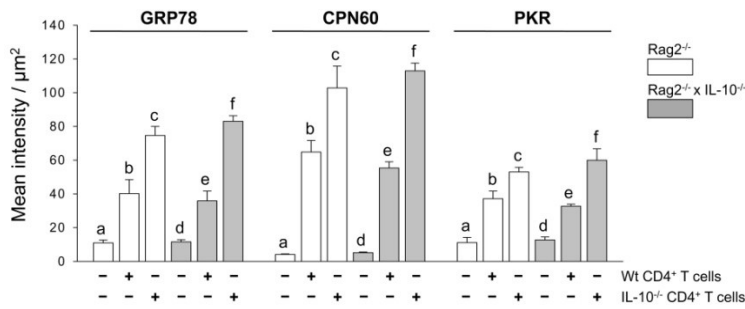
8A



B



C



D

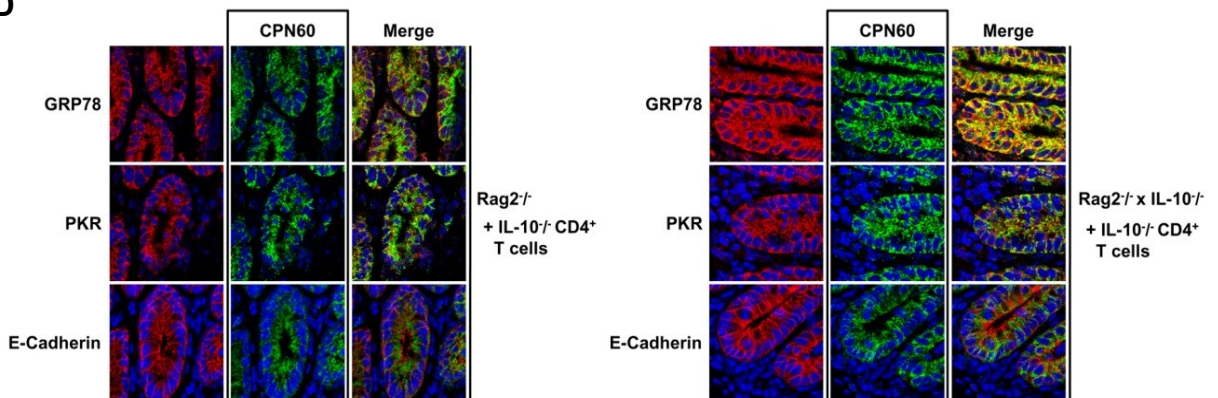


Figure 8. ER chaperone GRP78, mitochondrial CPN60 and PKR are induced in primary IEC in response to colitogenic T cell transfer.

Rag2^{-/-} and Rag2^{-/-} x IL-10^{-/-} recipients were adoptively transferred with CD4⁺ T cells from Wt or IL-10^{-/-} mice (n=5 per group). Mice were sacrificed 1 and 4 weeks later and histopathological scoring was performed. (A) The bar charts show the mean histopathologic score \pm SD. b different from a, f different from e, h different from g and i, ANOVA on Ranks followed by Holm-Sidak test P<0.01; d different from c, ANOVA on Ranks followed by Dunn's test P<0.05. Pooled isolated large IEC were analyzed for GRP78, CPN60 and PKR expression by Western blot. (B) Representative immunohistochemical staining of GRP78, CPN60 and PKR in colonic tissue sections 4 weeks after T cell transfer (GRP78, CPN60; PKR (green), DAPI (blue), 1,800x). (C) The bar charts show the mean intensity/ μm^2 \pm SD of the fluorescence signal of each group. b different from a and c, e different from d and f, One-Way-ANOVA followed by Holm-Sidak test, P<0.001. (D) Immunohistochemical double-staining of CPN60 and GRP78, PKR and E-Cadherin respectively in colonic tissue sections 4 weeks after IL-10^{-/-} T cell transfer (GRP78, PKR, E-Cadherin (red), CPN60 (green), DAPI (blue), 1,800x).

9

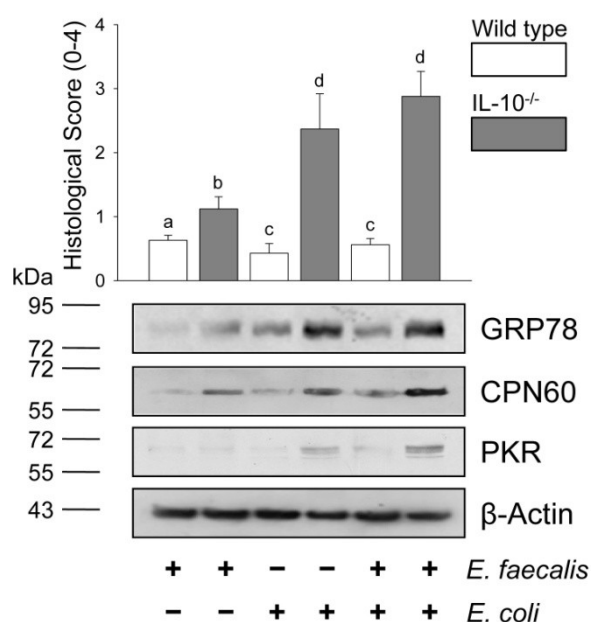


Figure 9. ER chaperone GRP78, mitochondrial CPN60 and PKR are induced in primary IEC in bacteria-induced colitis.

Germ-free Wt and IL-10^{-/-} mice were mono-or dual-associated with *E. faecalis* and/or *E. coli*. Mice were sacrificed 6 weeks later and histopathological scoring was performed. The bar charts show the mean histopathologic score \pm SD, b different from c and d, d different from a and c, ANOVA on Ranks followed by Holm-Sidak test P<0.01. Isolated large IEC were analyzed for GRP78, CPN60 and PKR expression by Western blot. Data, excluding PKR Western blot, have been published previously [218].

4.1.3. ER chaperone GRP78, mitochondrial CPN60 and PKR are induced in IEC from IBD patients

Most importantly, determining the relevance of our findings for human intestinal inflammation, the induction of CPN60 and GRP78 associated with elevated PKR protein levels was also observed in IEC from human IBD patients. This was not only true for patients

RESULTS

with ulcerative colitis, but also for Crohn's disease patients suffering from ileitis as shown by Western blot (**Fig.10A**, data, excluding PKR Western blot, have been published previously [218]) and immunohistochemical analysis (**Fig.10B-D**). Total number of patients included in the analysis: UC: WB: n=4, IHC: n=3; CD: WB: n=3, IHC: n=5; CTRL (colorectal cancer): WB: n=2, IHC: n=5. Together, these results indicate that, in addition to the recently established role of ER UPR in IEC during onset and course of intestinal inflammation [219], the involvement of mitochondrial UPR also seems to be a general disease feature.

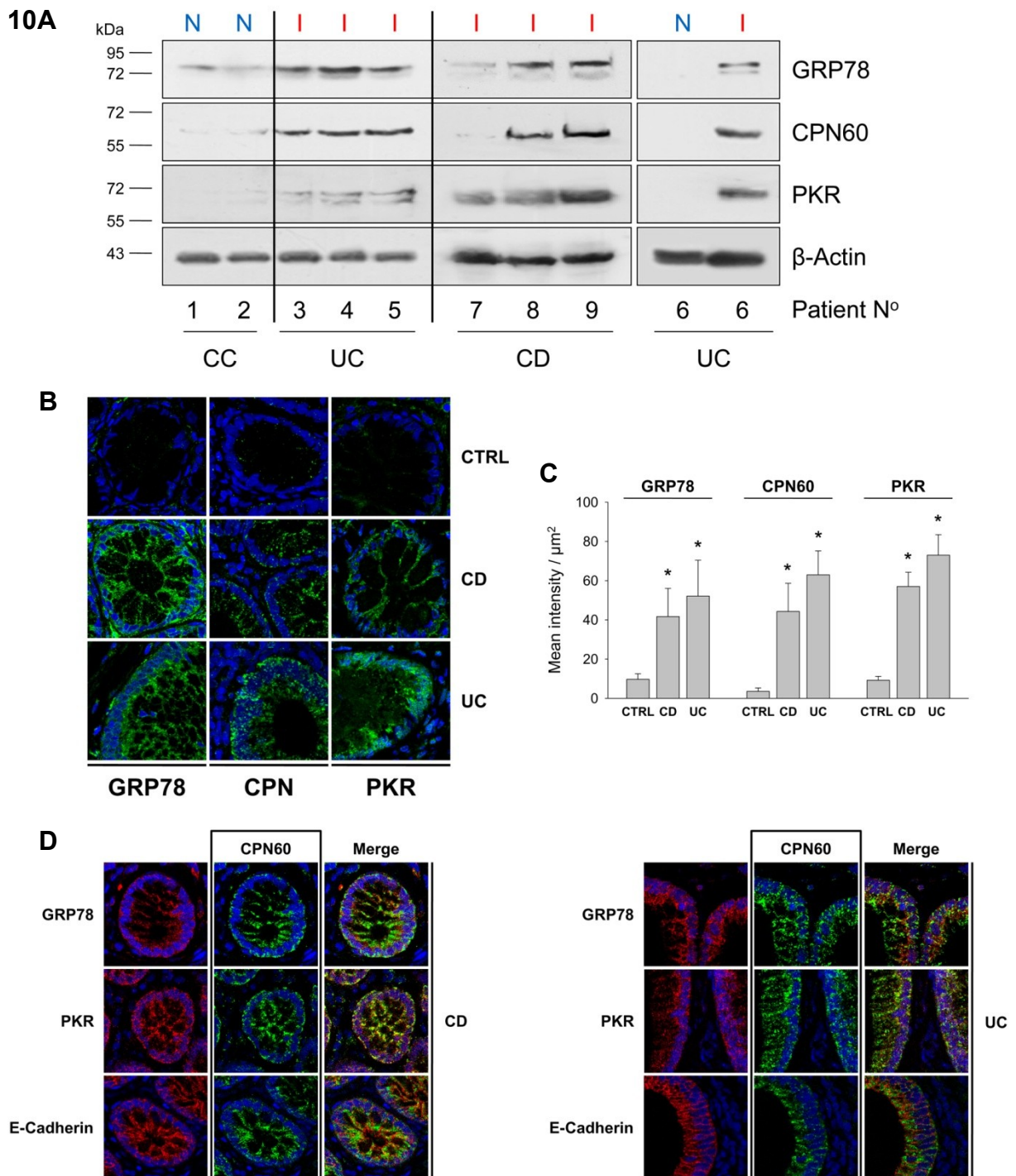


Figure 10. ER chaperone GRP78, mitochondrial CPN60 and PKR are induced in primary IEC from IBD patients.

(A) Primary IEC were isolated from surgical specimen of patients with colorectal cancer (CC, non-inflammatory control), active Crohn's disease (CD) and ulcerative colitis (UC). UC patient 6: IEC of non-inflamed (N) and inflamed (I) tissue regions. GRP78, CPN60 and PKR expression was analyzed by Western blot. Patient 1-5 and 7-9 were analyzed on the same Western blot. Data, excluding PKR Western blot, have been published previously [218] (B) Immunohistochemical staining of GRP78, CPN60 and PKR in surgical specimen of patients with colorectal cancer (control), active CD or UC (note: not the same patients as in A). (C) The bar charts show the mean intensity/ $\mu\text{m}^2 \pm \text{SD}$ of the fluorescence signal of each group (n=5 for CTRL and CD, n=3 for UC; 10 IEC regions per patient). *different from CTRL, ANOVA on Ranks followed by Dunn's test $P < 0.05$. (D) Immunohistochemical double-staining of CPN60 and GRP78, PKR and E-Cadherin respectively in surgical specimen of patients with UC and CD (GRP78, PKR, E-Cadherin (red), CPN60 (green), DAPI (blue), 1,800x).

4.1.4. Autophagy is induced in IEC in experimental colitis

Autophagy is a highly regulated lysosomal pathway involved in the turnover of long-lived proteins and organelles. It is involved in cellular homeostasis, maintenance of immunologic tolerance and host defense against pathogens [69-71]. A specialized form of autophagy, mitophagy, degrades damaged, non-functional mitochondria, ensuring the maintenance of a functional mitochondrial population. During ER UPR and the associated degradation of mis- or unfolded proteins, the ER employs both proteasomal (ERAD) as well as autophagic pathways [53,72]. ER UPR-induced autophagy might represent an alternative mechanism to dispose misfolded proteins in the ER lumen that cannot be removed by ERAD, but is also implied in the degradation of damaged ER and the counterbalance of the ER expansion during ER UPR [73]. Independently of innate UPR signaling, autophagy might also be triggered and/or amplified by ROS produced under stress conditions [76].

Under inflammatory conditions, autophagy was induced in IEC in the adoptive T cell transfer model as determined by LC3 Western blot analysis (**Fig.11**). Conversion of LC3-I to LC3-II is indicative of autophagic activity and the amount of LC3-II correlates with the number of autophagosomes [220]. Even though autophagy represents a cellular pathway commonly activated under stress conditions, induction of autophagy in IEC might partially reflect ER- and/or mitochondrial UPR-signaling.

11

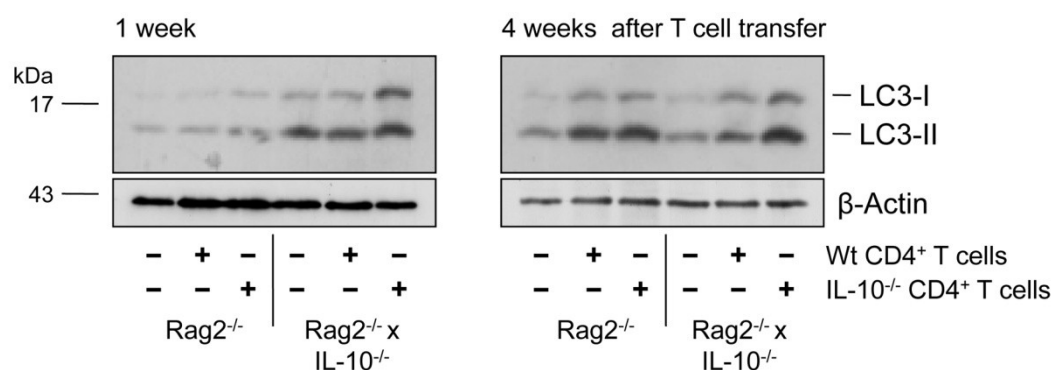


Figure 11. Autophagy is induced in primary IEC following T cell transfer.

Rag2^{-/-} and Rag2^{-/-} x IL-10^{-/-} recipients were adoptively transferred with CD4⁺ T cells from Wt or IL-10^{-/-} mice (n=5 per group) and sacrificed 1 and 4 weeks later. Pooled isolated large IEC were analyzed for LC3-I and LC3-II presence by Western blot.

4.2 Mitochondrial unfolded protein response in the IEC line Mode-K

4.2.1. Truncated ornithine transcarbamylase induces mtUPR in IEC

To further study the role of mitochondrial UPR in the context of intestinal inflammation, we transfected the murine intestinal epithelial cell line Mode-K with a truncated variant of the mitochondrial matrix protein OTC Δ . The deletion prevents the imported protein from folding properly in the mitochondrial matrix and produces a mitochondrial specific UPR [21]. To show expression and mitochondrial translocation of OTC Δ and induction of mitochondrial UPR by OTC Δ in Mode-K cells, Western blot analysis was performed with whole cell- and mitochondrial lysates using an antibody recognizing both the truncated as well as the Wt variant of OTC and one specific for CPN60 (**Fig.12**). The presence of OTC Δ in the mitochondria and the associated induction of mitochondrial CPN60 demonstrate mitochondrial UPR-induction and -signaling in transfected Mode-K cells, confirming previous results [218]. Induction of CPN60 in whole cell lysates was only detectable at late time points (>56h) (data not shown, published previously in [218]).

12

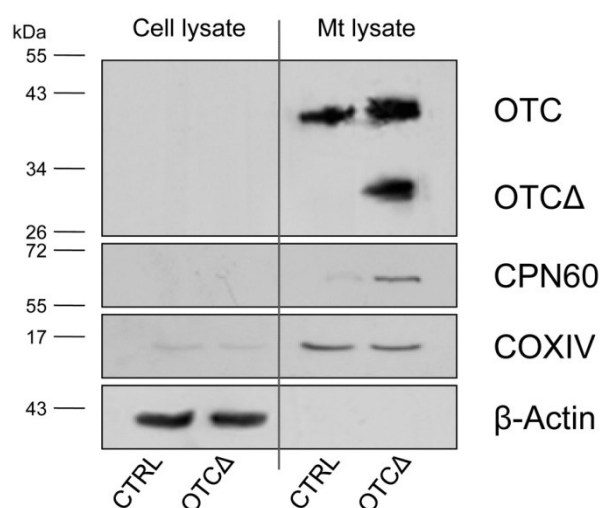


Figure 12. Truncated OTC induces mtUPR in Mode-K cells.

Mode-K cells were transfected with OTCΔ cDNA for 36h. Mitochondrial- and whole-cell protein lysates were used to analyze OTCΔ expression and translocation to the mitochondria as well as CPN60 recruitment to the mitochondria by Western blot. Cytochrome C Oxidase (COX) IV was used as mitochondrial loading control.

4.2.2. Mitochondrial UPR integrates into ER UPR-signaling

In addition to OTCΔ transfection, Mode-K cells were stimulated with the ER UPR-inducer tunicamycin (Tm), an inhibitor of protein glycosylation in the ER. Consistent with published results, both treatments induced the transcription factor CHOP and the phosphorylation of cJun, a component of the transcription factor AP1 [24,53] (**Fig.13A**). ER UPR is supposed to employ the ER membrane-associated protein kinase IRE1 to activate JNK and downstream AP1 [53], and to induce transcription of CHOP through an ERSE [25] or a C/EBP-ATF composite site [47] in its promoter. In the case of mtUPR, it is suggested that the MEK/JNK2 pathway is utilized to activate AP1 [24] and that transcriptional activation of CHOP is mediated via AP1 binding sites [25] in its promoter. CHOP-binding to the *Cpn60* promoter is required for CPN60 induction under mtUPR [24,25] and was also confirmed in Mode-K cells [218].

In contrast, only tunicamycin-mediated ER UPR induced transcriptional activation of the *grp78* gene as shown by elevated mRNA levels and protein induction (**Fig.13A**), confirming the finding that mtUPR does not affect expression levels of ER resident chaperones such as GRP78 [21]. Surprisingly, both ER- and mtUPR led to phosphorylation of eIF2α (**Fig.13A**). It is established that this event efficiently inhibits translation, thereby protecting the cell from further accumulation of unfolded proteins under ER stress [53], but this process has not been previously described as a consequence of mtUPR. In the case of tunicamycin-induced ER UPR, the ER membrane-associated PERK seems to be largely responsible for eIF2α

phosphorylation [53]. Also in Mode-K cells phosphorylation and thereby activation of PERK was demonstrated by Western blot analysis following tunicamycin but not OTCA stimulation (**Fig.13B**).

These data indicate that ER and mtUPR signaling converge at the level of eIF2 α phosphorylation as well as at the activation of transcription factors AP1 and CHOP, although probably utilizing different signaling cascades. The time point of maximal eIF2 α phosphorylation following tunicamycin treatment or OTCA transfection respectively was chosen for further analysis.

4.2.3. Mitochondrial UPR-signaling employs PKR

To identify the kinase responsible for eIF2 α phosphorylation upon mitochondrial UPR, we screened for the recruitment of the four known mammalian eIF2 α kinases (HRI, GCN2, PKR and PERK) following OTCA transfection. In response to mtUPR, we found PKR to be selectively activated. PKR was first described for its role in antiviral defense [221] but has since been shown to be involved in a broad variety of cellular stress responses [52]. It is a serine/threonine kinase displaying two distinct kinase activities: autophosphorylation leading to activation and the phosphorylation of eIF2 α [52]. Although it has been described previously that PKR participates in ER UPR signaling [222,223], we found PKR only to be induced under mtUPR (**Fig.13B**). This was demonstrated at the level of mRNA and total protein as well as on the basis of the activation status represented by phosphorylated PKR (**Fig.13B**). To rule out the possibility that PKR phosphorylation/induction was due to a non-specific response toward transfection, Mode-K cells were transfected with GFP as well as OTC and OTCA. PKR phosphorylation was only detectable in cells following OTCA transfection (data not shown). In order to verify that the phosphorylation of eIF2 α is directly mediated by PKR, we showed association of PKR with eIF2 α using co-immunoprecipitation analysis (**Fig.13C**). The time point of maximal eIF2 α phosphorylation following tunicamycin treatment or OTCA transfection respectively was chosen for co-immunoprecipitation.

Applying Genomatix Gene2Promotor software, we screened for putative transcription factor binding sites in the *Pkr* promoter and found an AP1 binding-site predicted. Considering the fact that we found the AP1 component cJun to be phosphorylated under mtUPR (**Fig.13A**) and mtUPR employs AP1 to activate transcription of *Chop* [25] (which was confirmed in Mode-K cells, data not shown), we performed chromatin immunoprecipitation (ChIP) analysis to determine AP1-binding to the *Pkr* promoter. Indeed, phosphorylated cJun and thus AP1-binding to the *Pkr* promoter was detected after mtUPR induction (**Fig.13D**).

Taken together, these results clearly show that PKR is selectively activated and induced under mtUPR, and that the induction is mediated, at least in part, by the transcription factor

AP1. Furthermore, PKR directly phosphorylates eIF2 α , thereby integrating mtUPR- into the disease-relevant ER UPR-signaling cascade.

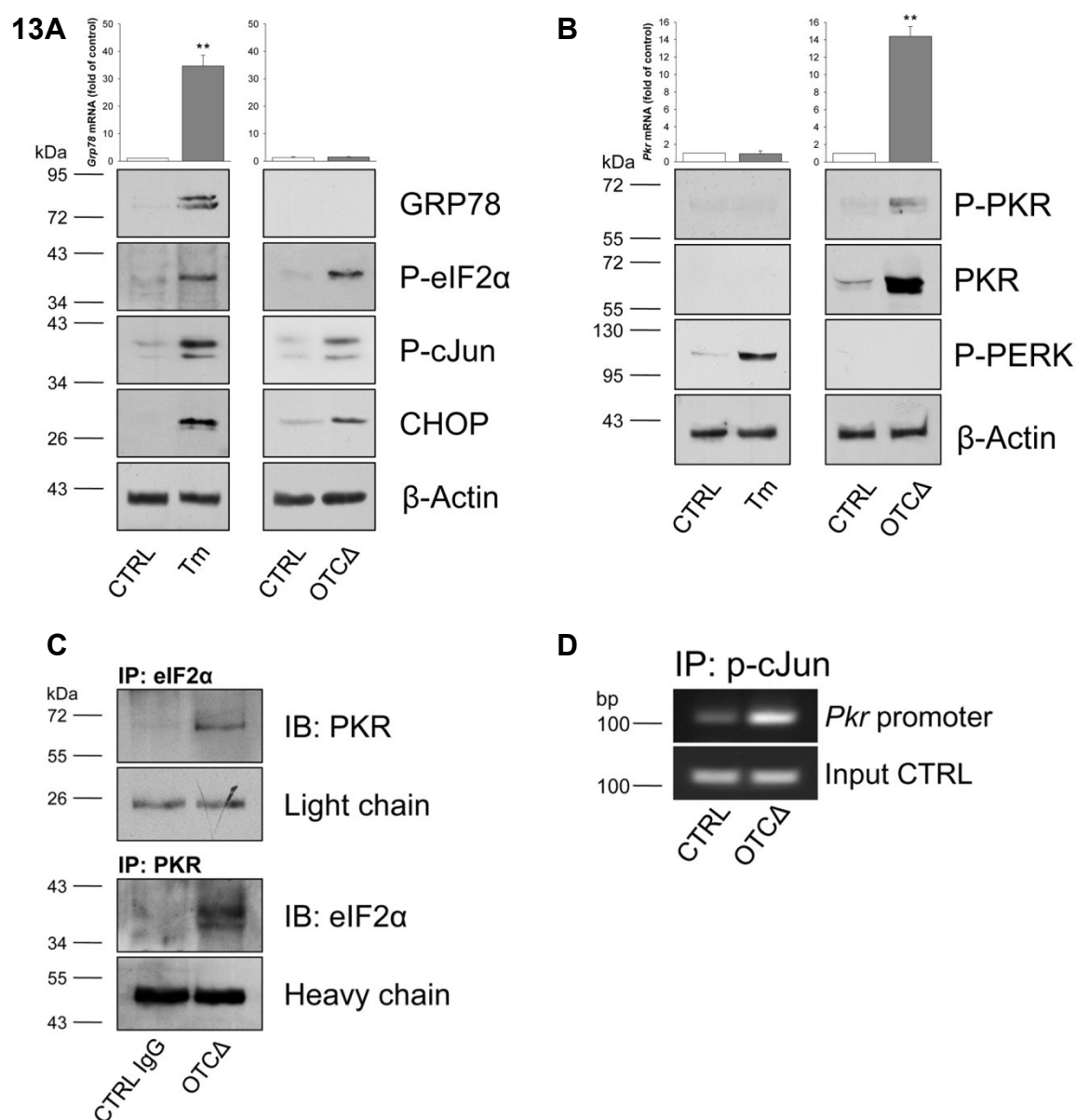


Figure 13. Mitochondrial UPR integrates into ER UPR-signaling via PKR and AP1.

Mode-K cells were stimulated with tunicamycin (Tm) or transfected with OTCA Δ cDNA. **(A)** Bar charts: relative *Grp78* gene expression 6h after Tm stimulation or 36h after OTCA Δ transfection. Data are shown as mean \pm SD, **P<0.01, t test. Phosphorylation of eIF2 α and cJun 3h after Tm stimulation or 30h after OTCA Δ transfection, as well as GRP78 and CHOP expression 6h after Tm stimulation or 36h after OTCA Δ transfection analyzed by Western blot. **(B)** Bar charts: relative *Pkr* gene expression 6h after Tm stimulation or 36h after OTCA Δ transfection. Data are shown as mean \pm SD, **P<0.01 t test. PKR- and PERK phosphorylation 30h after OTCA Δ transfection/ 3h after Tm treatment and PKR expression 36h after OTCA Δ transfection/ 6h after Tm treatment analyzed by Western blot. **(C)** Cell lysates were prepared 30h after OTCA Δ transfection followed by immunoprecipitation (IP) with anti-eIF2 α or anti-PKR antibody and Western blot analysis for PKR or eIF2 α . **(D)** AP1 recruitment to the *Pkr* promoter 30h after OTCA Δ transfection was analyzed by ChIP using an anti-p-cJun antibody and subsequent PCR analysis. **(C+D)** Data are representative of two independent experiments.

4.2.4. Mitochondrial UPR does not induce ATF4

Phosphorylation of eIF2 α not only results in the inhibition of global protein synthesis, but also enhances the translation of several mRNAs encoding short upstream open reading frames (uORF) [53], including the transcription factor ATF4. Under ER UPR, ATF4 is the major activator of CHOP [99] and mediates its transcriptional activation via a C/EBP-ATF composite site (a part of AARE1 (amino acid response element)) [25,224]. In Mode-K cells, ATF4 was induced in response to tunicamycin treatment (**Fig.14A**) and also ATF4-binding to the *Chop* promoter was detected by ChIP [218]. However, even though eIF2 α was phosphorylated under mtUPR, neither elevated ATF4 protein- nor mRNA levels could be detected (**Fig.14A**). A selective attenuation of translational activation of ATF4 has been described before [65]. Yet, in the case of OTCA-induced mtUPR, Western blot analysis might not be sensitive enough to detect ATF4 upregulation, since mRNA levels of two ATF4 target genes, ATF3 and TRIB3, were significantly induced (**Fig.14B,C**).

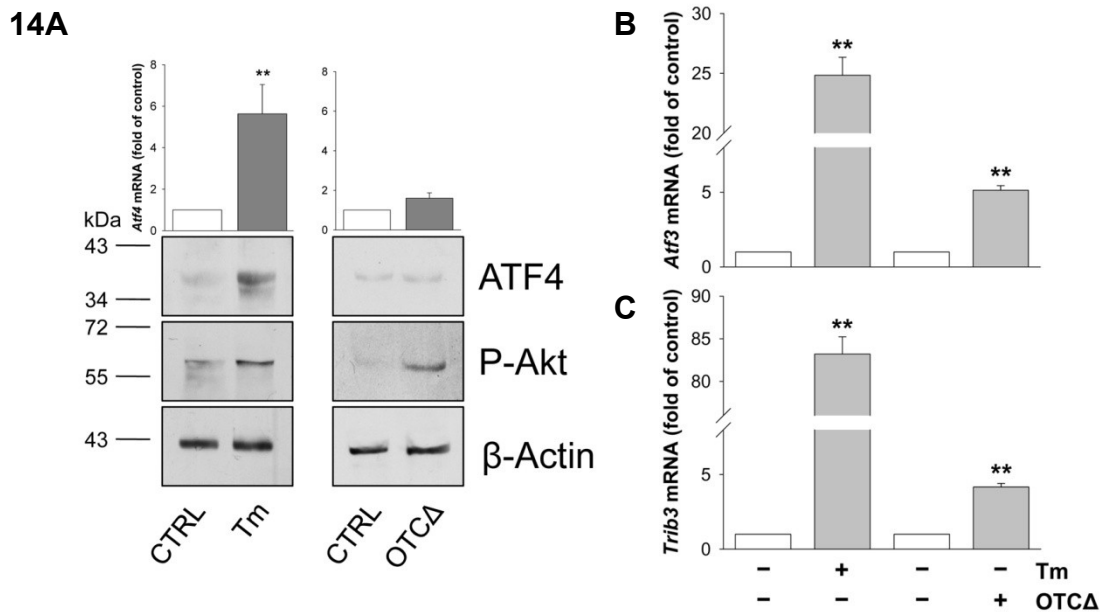


Figure 14. Mitochondrial UPR does not induce ATF4 but Akt phosphorylation

Mode-K cells were stimulated with tunicamycin (Tm) or transfected with OTCA cDNA. **(A)** Bar charts: relative *Atf4* gene expression 6h after Tm stimulation or 36h after OTCA transfection. Data are shown as mean \pm SD, **P<0.01, t test. Phosphorylation of Akt 3h after Tm stimulation or 30h after OTCA transfection, as well as ATF4 expression 6h after Tm stimulation or 36h after OTCA transfection analyzed by Western blot. Relative gene expression levels of **(B)** *Atf3* and **(C)** *Trib3* mRNA 6h after Tm stimulation or 36h after OTCA transfection. Data are shown as mean \pm SD, **P<0.01, t test.

4.2.5. Mitochondrial UPR induces Akt phosphorylation

ER and mitochondria are in close contact via MAM [171,172], sites of calcium- and lipid exchange [176,177]. On the MAM, calcium fluxes between ER and mitochondria occur at IP3R and the associated signaling is not only important during apoptosis [180] but ER chaperones like GRP78 are dependent on calcium [181]. MAM themselves are regulated by Mtn2 and the chaperones GRP75 and PACS2 [187-189]. IP3R, in particular IP3R3, as well as PACS2 can be phosphorylated by the kinase Akt to regulate the ER- mitochondrial network, and phosphorylation of these proteins is thought to mediate anti-apoptotic signals [225,226]. Therefore we determined activation of Akt, as indicated by Akt phosphorylation, in response to tunicamycin-induced ER UPR as well as OTCA-induced mtUPR and found Akt activated upon both treatments (**Fig.14A**).

4.2.6. Mitochondrial UPR-mediated PKR-induction is Ca²⁺ and PACT independent

Mitochondria to nucleus signaling, the so-called retrograde signaling, has mostly been studied either by treating cells with ethidium bromide to deplete mtDNA content (p0 cells) or with uncouplers of OXPHOS such as CCCP, treatments that alter the mitochondrial membrane potential. These treatments result in the elevation of cytosolic free Ca²⁺ and activation of calcium/calmodulin-dependent protein kinase (CaMK) and calcineurin responsive genes [154]. Furthermore, CaMK is involved in AMPK-mediated mitochondrial biogenesis in skeletal muscle cells in response to chronic energy deficits [151]. Interestingly, it has been suggested that Ca²⁺ release from the ER activates PKR via CaMKII and PACT [227]. PACT (the murine orthologue is also called RAX) is a cellular activator of PKR and can activate PKR in the absence of infection [52]. Different stresses trigger PACT phosphorylation [228], and only then does PACT bind and activate PKR [229].

Nevertheless, neither the calcium chelator BAPTA-AM, nor inhibitors of CaMK (KN-93) and CaMKII (AIP) were able to interfere with OTCA-induced mtUPR signaling (**Fig.15A**). Furthermore, we were not able to detect phosphorylation of PACT at any time after the transfection of cells with OTCA using Western blot analysis (data not shown) and more importantly, *Pact*^{-/-} MEF did not display altered mtUPR-signaling in terms of PKR induction and eIF2 α phosphorylation (**Fig.15B**).

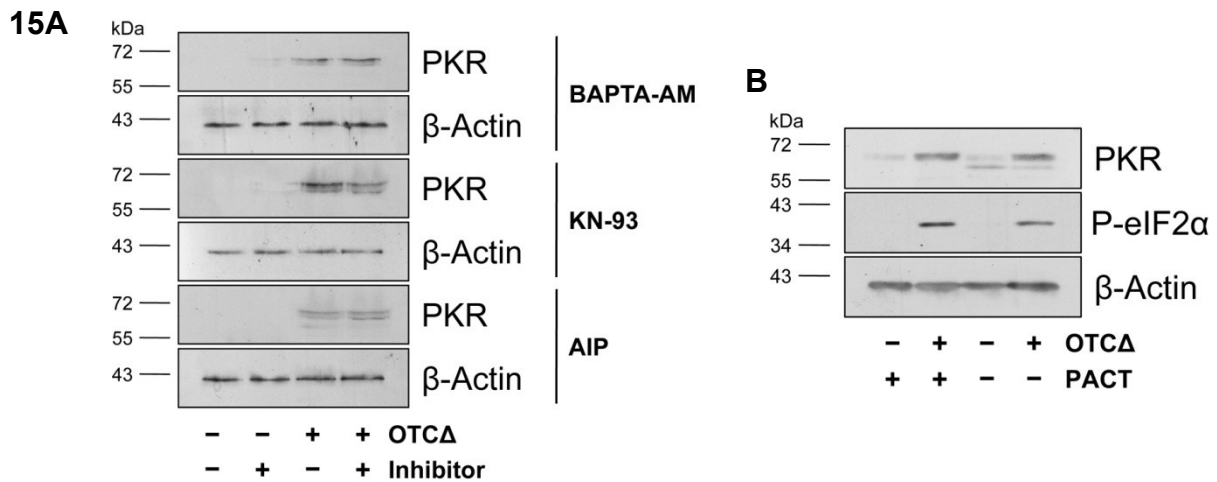


Figure 15. Mitochondrial UPR-mediated PKR-induction is Ca^{2+} and PACT independent.

Cells were transfected with OTC Δ cDNA. **(A)** Mode-K cells: 10h after transfection media were changed and calcium chelator BAPTA-AM, CaMK inhibitor KN-93 or specific CaMKII inhibitor AIP were added. 36h after OTC Δ transfection PKR expression was determined by Western blot. Data are representative of two independent experiments **(B)** Wt and PACT^{-/-} MEF were analyzed for PKR expression and eIF2 α phosphorylation 32h after OTC Δ transfection by Western blot.

4.2.7. Mitochondrial UPR signaling is dependent on PKR

As PKR is not only known to phosphorylate eIF2 α but also to be an activator for signaling cascades regulating stress-activated protein kinases such as JNK [52,230], we next investigated the role of PKR in mtUPR signaling in more detail. Using specific siRNA to knock down PKR and a PKR inhibitor, we examined the dependency of mtUPR on PKR-mediated signaling. SiRNA knock down of PKR prior to OTC Δ transfection-induced mtUPR completely abrogated eIF2 α and c-Jun phosphorylation as well as CHOP induction (**Fig.16A**). By applying an imidazolo-oxindole derivative that acts as an ATP-binding site-directed inhibitor of PKR, we were able to demonstrate that the mtUPR-mediated induction of PKR itself was dependent on PKR activity as were the downstream events, eIF2 α and c-Jun phosphorylation and CHOP induction (**Fig.16B**). The impairment of mtUPR-signaling was additionally confirmed in Pkr^{-/-} MEF (**Fig.16C**).

Autoregulation of PKR expression upon its activation has been described before [231]. In line with our results indicating tunicamycin-induced ER UPR-signaling not involving PKR in Mode-K cells (**Fig.13A,B**), neither the siRNA-mediated knockdown of PKR nor the PKR inhibitor had an impact on tunicamycin-induced ER UPR as measured by phosphorylation of eIF2 α , cJun and CHOP (**Fig.17A,B**). Since previous results indicated that mitochondrial to nuclear signaling in mtUPR utilizes a JNK pathway including MEK and JNK2 [24], we determined the effect of the specific MEK inhibitor PD98059 and the JNK2/3-specific inhibitor TCS JNK 5a on PKR-mediated signaling in mtUPR.

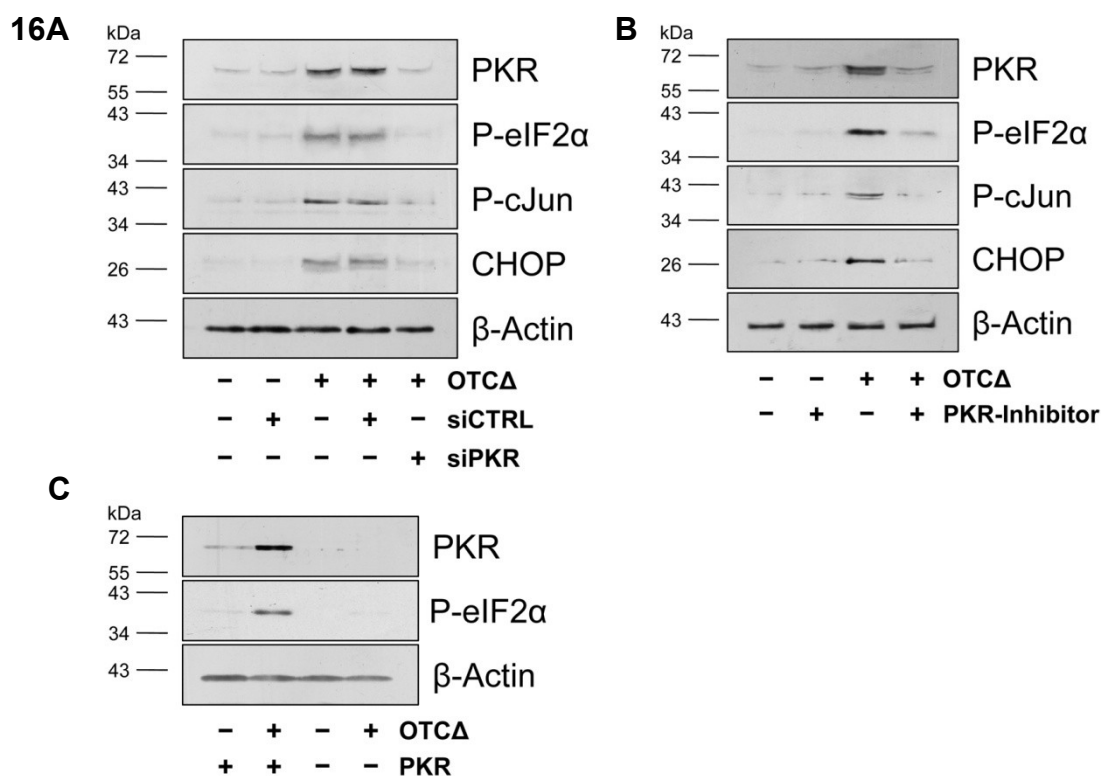


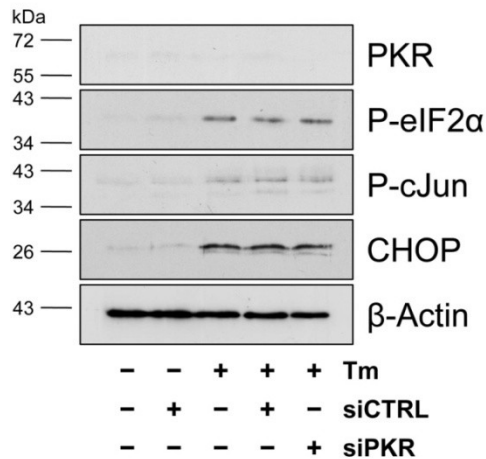
Figure 16. Mitochondrial UPR signaling is dependent on PKR.

(A) Mode-K cells were transfected with siRNA specific for *Pkr* or control siRNA for 12h and subsequently transfected with OTCA cDNA for 30h or 36h to determine protein phosphorylation (eIF2, cJun) and expression (PKR, CHOP), respectively. (B) Mode-K cells were pretreated with PKR-inhibitor for 10h and subsequently transfected with OTCA for 30h or 36h to determine protein phosphorylation (eIF2, cJun) and expression (PKR, CHOP), respectively. (C) Wt and *Pkr*^{-/-} MEF were analyzed for PKR expression and eIF2α phosphorylation 32h after OTCA transfection by Western blot.

Inhibition of MEK (Fig.18A) as well as inhibition of JNK2/3 (Fig.18B) was sufficient to mimic the effects of the PKR inhibitor on mtUPR-mediated signaling. In *C. elegans*, it has been shown that mtUPR is dependent on peptides generated by the mitochondrial protease ClpP [23,141] and furthermore, OTCA has been shown to co-immunoprecipitate with ClpP [21]. Therefore, we used the ClpP inhibitor Z-LY-CMK and could demonstrate for the first time, to our knowledge, also the mammalian mtUPR to be dependent on ClpP activity (Fig.18C).

Taken together, these data suggest that mtUPR is dependent on the mitochondrial protease ClpP, which provides the initial signal for PKR activation. PKR in turn induces its own transcription via MEK, JNK2 and AP1. Enhanced PKR-signaling then amplifies eIF2α and cJun phosphorylation thereby inducing CHOP, acting as transcription factor for the *Cpn60* gene. It is appealing to speculate that CPN60 thereafter translocates to the mitochondria helping to abrogate the stress induced by unfolded proteins (Fig.35).

17A



B

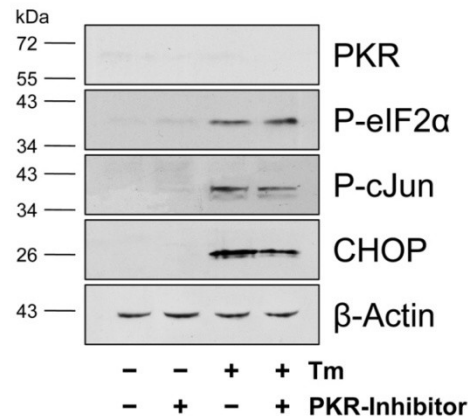
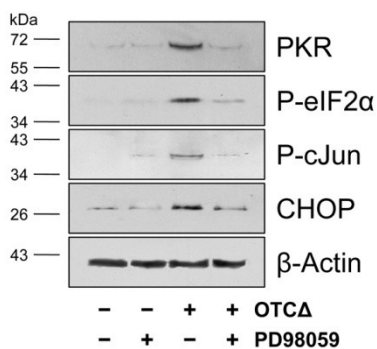


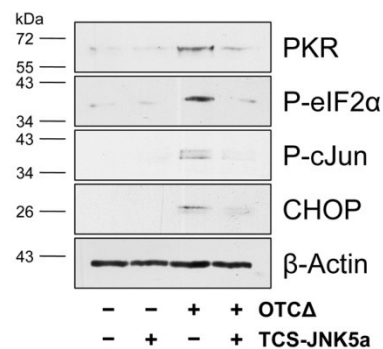
Figure 17. Tunicamycin-induced ER UPR signaling is not dependent on PKR

(A) Mode-K cells were transfected with siRNA specific for PKR or control siRNA for 36h or (B) pretreated with PKR inhibitor for 10h. Subsequently, cells were stimulated with tunicamycin (Tm) for 3h or 6h to determine protein phosphorylation (eIF2, cJun) and expression (PKR, CHOP), respectively. Data are representative of two independent experiments.

18A



B



C

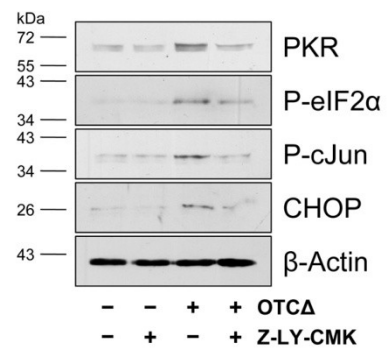


Figure 18. Mitochondrial UPR-signaling employs MEK and JNK2/3 and is dependent on ClpP

Mode-K cells were pretreated with (A) MEK-inhibitor PD98059, (B) JNK2/3-inhibitor TCS-JNK5a or (C) ClpP-inhibitor Z-LY-CMK for 10h. Subsequently, cells were transfected with OTCA cDNA for 30h or 36h to determine protein phosphorylation (eIF2, cJun) and expression (PKR, CHOP), respectively.

4.2.8. Mitochondrial UPR induces autophagy

Previous reports showed that the persistence of the mutated protein in OTCA-transfected cells was short lived, probably due to protease-mediated degradation [21], a hypothesis supported by our results. Autophagy/mitophagy represents another major cellular degradation route that can deal with damaged organelles as well as misfolded, insoluble proteins which cannot be removed otherwise, and consistent with enhanced protease-mediated degradation, also autophagy was induced under OTCA-induced mtUPR (Fig.19).

19

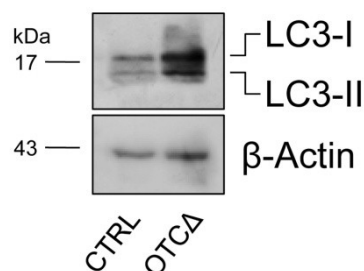


Figure 19. Mitochondrial UPR induces autophagy

Mode-K cells were transfected with OTCA cDNA for 48h. Presence of LC3-I and LC3-II analyzed by Western blot.

4.3 $Pkr^{-/-}$ mice

4.3.1. $Pkr^{-/-}$ mice display enhanced colonic barrier function and increased mitochondrial markers

To evaluate the disease-relevance of PKR-mediated mitochondrial stress-signaling *in vivo*, we subjected $Pkr^{-/-}$ mice with a deletion in the catalytic subunit of the *Pkr* gene [201] to a DSS-feeding protocol to induce chronic colitis [202]. These mice do not have an obvious phenotype showing no impairment in tumor suppression, anti-viral response, TNF-induced apoptosis or eIF2 α phosphorylation [201]. In the context of intestinal inflammation, the epithelial barrier plays a crucial role, since barrier dysfunction can permit luminal antigens to enter the subepithelial tissues, resulting in the recruitment and activation of leukocytes [232]. Interestingly, Ussing chamber experiments indicated enhanced colonic barrier function in untreated $Pkr^{-/-}$ mice as measured by reduced sodium fluorescein (NaF) translocation associated with increased transepithelial electrical resistance (TER) (**Fig.20A,B**). In addition, comparing colonic IEC from untreated $Pkr^{-/-}$ and control mice, $Pkr^{-/-}$ mice exhibited elevated CPN60 and COX4 baseline levels (**Fig.20C, Fig.22A,C**), associated with an increased ratio of mitochondrial to nuclear DNA (**Fig.22B**), suggesting PKR-independent regulation of CPN60 and mitochondrial biogenesis under normal conditions.

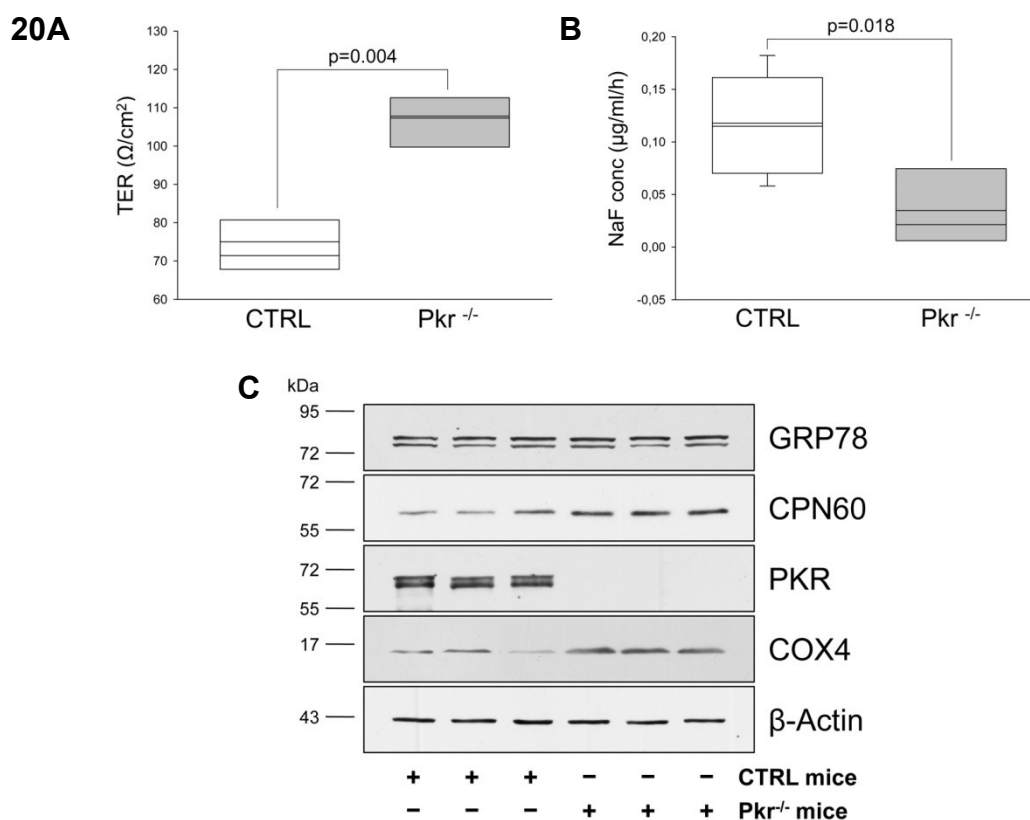


Figure 20. Pkr^{-/-} mice display enhanced colonic barrier function and increased mitochondrial markers

Distal colon segments from 12 weeks old Pkr^{-/-} and CTRL mice (n=5 per group) were mounted into Ussing chamber systems and equilibrated with Krebs buffer (A) TER was calculated from the short circuit current and the resulting voltage difference (B) amount of Sodium fluorescein translocated to the basolateral compartment after 1h. Lines in the box plots represent the median and 25th/75th percentile. P values were calculated using unpaired t tests. (C) Baseline expression of GRP78, CPN60, PKR and COX4 in colonic IEC from untreated individual mice analyzed by Western blot.

4.3.2. Pkr^{-/-} mice show reduced sensitivity to DSS-induced colitis

After a second cycle of 1%DSS, control mice showed a significantly increased disease activity index, including severe weight loss compared to Pkr^{-/-} mice (Tab.4, Fig.21A). Macroscopically, colons were thickened and shortened, indicating severe edema as well as inflammation and consistently, H&E staining of distal colon sections displayed leukocyte infiltration into the mucosa as well as IEC and crypt loss (Tab.4, Fig.21A). Immunohistochemical staining and fluorescence intensity measurements of IEC regions revealed increased expression levels of GRP78, CPN60 and PKR in DSS-treated control animals, confirming the relevance of ER- and mtUPR as well as associated PKR-signaling also in the DSS-induced model of colitis. Contrarily, Pkr^{-/-} mice showed a selective loss of CPN60 expression upon DSS-treatment whereas GRP78 expression remained unaltered (Fig.21B,C). Additionally, the elevated CPN60 baseline protein levels in colonic IEC from

$Pkr^{-/-}$ mice detected by Western blot (**Fig.20C**) could be confirmed by the immunohistochemical analysis.

Table 4. $Pkr^{-/-}$ mice show reduced sensitivity to DSS-induced colitis. $Pkr^{-/-}$ and CTRL mice received cycles of 1%DSS for 7 days followed by 7 days of water. The criteria for scoring the disease activity index (DAI) are given in **Tab.1**.

Group	Treatment	Weight loss	Stool consistency	Rectal bleeding	DAI	Colon length (cm)	Histological score (0-12)
CTRL	Water	0 ± 0	0 ± 0	0 ± 0	0 ± 0	8.83 ± 0.58	0.00 ± 0.00
	DSS	2.8 ± 1.47 ^a	3.6 ± 0.80 ^{ab}	2.6 ± 1.36 ^{ab}	3.0 ± 1.19 ^{ab}	6.04 ± 0.30 ^{cd}	6.20 ± 2.02 ^{de}
$Pkr^{-/-}$	Water	0 ± 0	0 ± 0	0 ± 0	0 ± 0	9.00 ± 0.73	0.58 ± 0.25
	DSS	0.2 ± 0.40	0 ± 0 ^b	0 ± 0	0.07 ± 0.13 ^b	7.42 ± 0.56 ^{cd}	2.30 ± 3.25 ^e

^a statistically different from Water control group; ANOVA on Ranks followed by Dunn's test, $P < 0.05$.

^b statistically different from treatment control group; ANOVA on Ranks followed by Dunn's test, $P < 0.05$.

^c statistically different from treatment control group; Two-Way-ANOVA followed by Tukey test, $P < 0.001$.

^d statistically different from Water control group; Two-Way-ANOVA followed by Tukey test, $P < 0.001$.

^e statistically different from treatment control group; Two-Way-ANOVA followed by Tukey test, $P = 0.010$.

21A

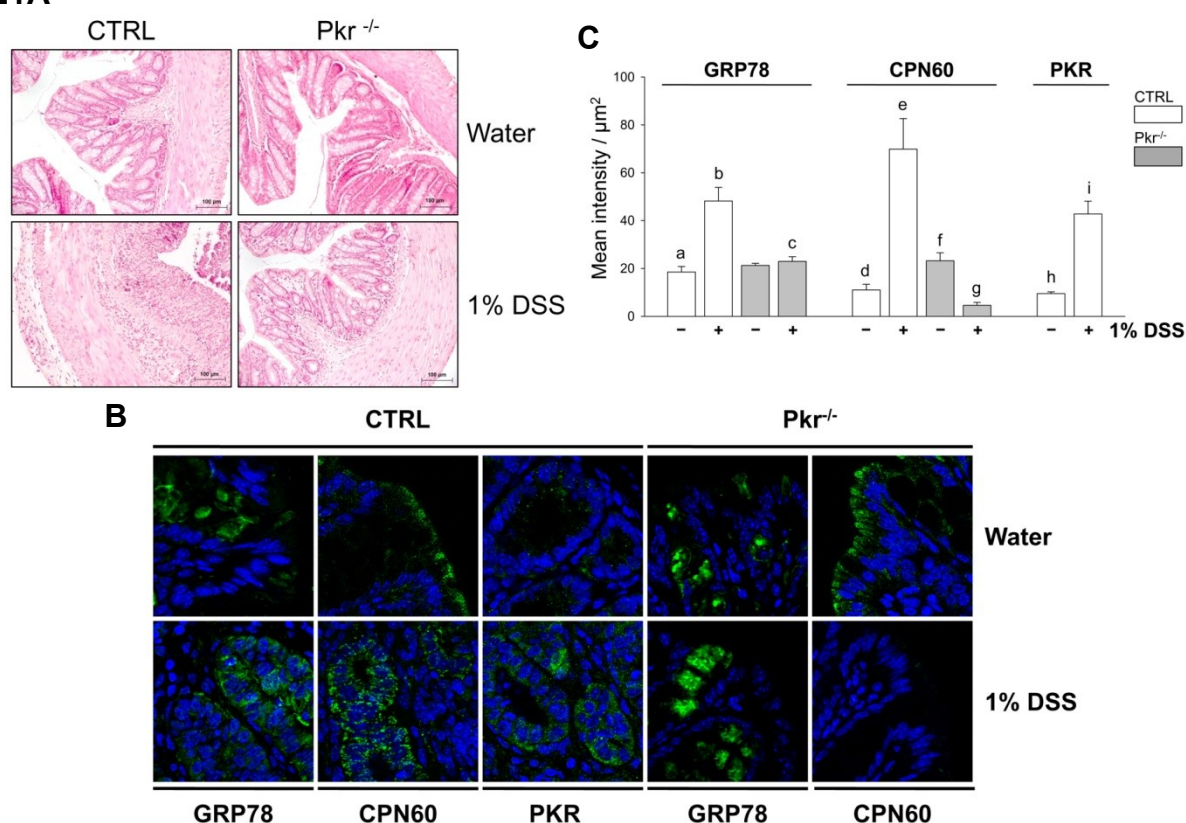


Figure 21. $Pkr^{-/-}$ mice show reduced sensitivity to DSS-induced colitis.

$Pkr^{-/-}$ and CTRL mice received cycles of 1%DSS for 7 days followed by 7 days of water. (A) Representative H/E staining of the distal colon of $Pkr^{-/-}$ and CTRL mice receiving DSS or water. (B) Immunohistochemical staining of GRP78, CPN60 and PKR in colonic tissue sections of $Pkr^{-/-}$ and CTRL mice receiving water or DSS (GRP78, CPN60, PKR (green), DAPI (blue), 1,800x). (C) The bar charts show the mean intensity/ $\mu m^2 \pm SD$ of the fluorescence signal of each group ($n=5$ per group). b different from a and c, e different from d and g; d different from f, Two-Way-ANOVA followed by Tukey test, $P < 0.01$, h different from i, $P < 0.001$, t test.

22A

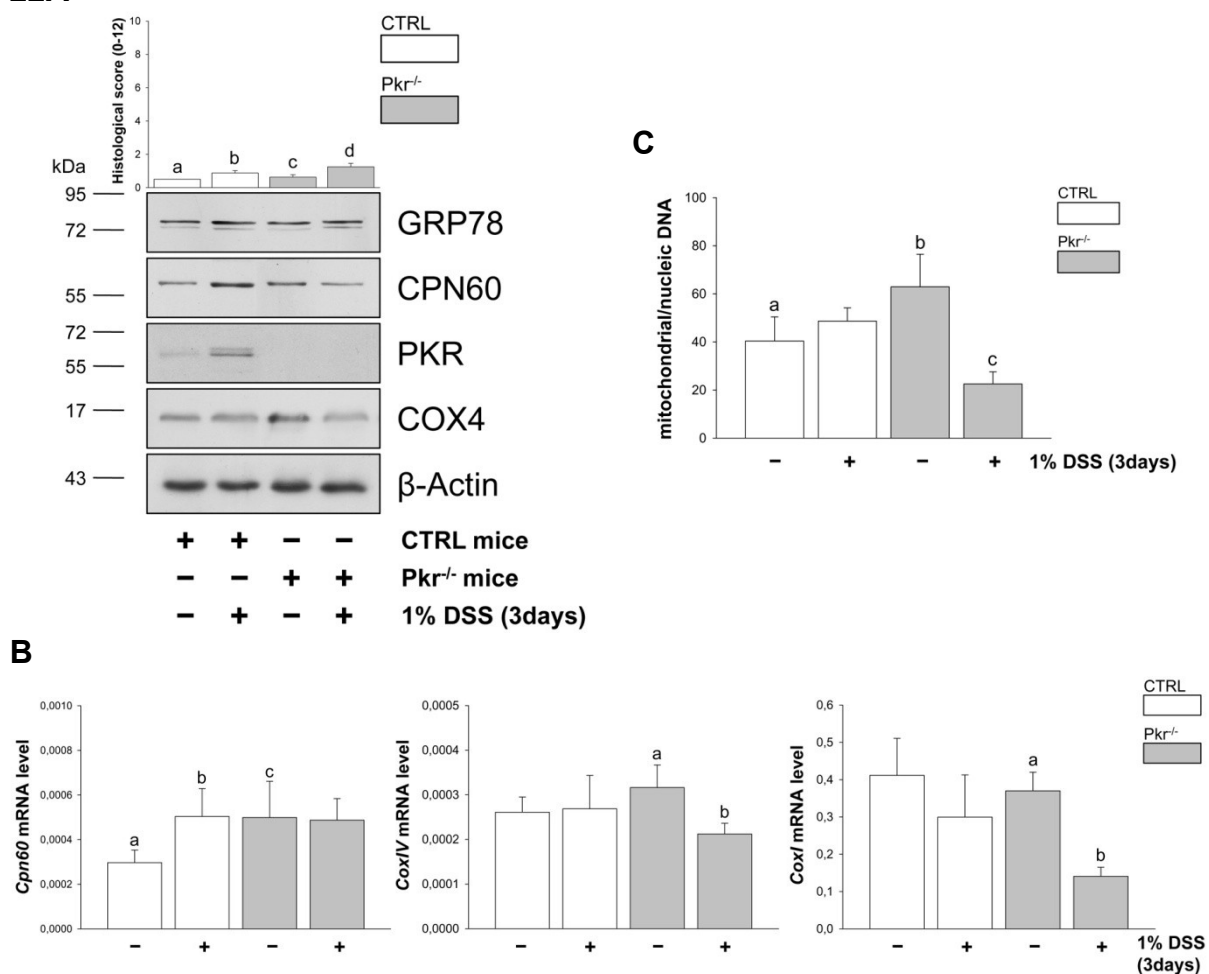


Figure 22. Mitochondrial abundance declines in Pkr^{-/-} mice upon DSS-treatment.

Pkr^{-/-} and CTRL mice received 1%DSS for 3 day (n=5 per group). Histological scoring (0-12) was performed and colonic IEC were isolated. **(A)** The bar charts show the mean histological score \pm SD. a different from b, c different from d, Two-Way-ANOVA followed by Tukey test, P<0.05. Expression of GRP78, CPN60, PKR and COX4 in colonic IEC analyzed by Western blot. **(B)** mRNA expression level of *cpn60*, nuclear encoded *coxIV* and mtDNA encoded *coxI* normalized to *18s* expression in colonic IEC determined by real-time PCR. a different from b and c, Two-Way-ANOVA followed by Tukey test, P<0.05. **(C)** Ratio of mitochondrial- to nuclear DNA in colonic IEC. b different from a and c, Two-Way-ANOVA followed by Tukey test P<0.022.

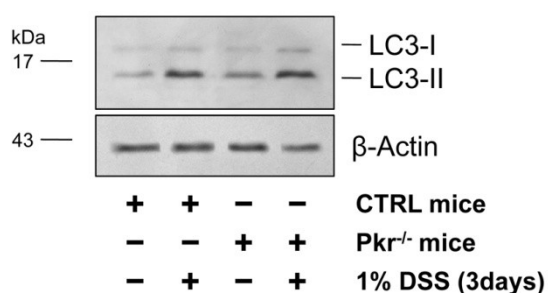
4.3.3. Mitochondrial abundance declines in Pkr^{-/-} mice upon DSS-treatment

To investigate early events during DSS-induced colitis, mice were administered 1%DSS for 3 days and colonic IEC were isolated. Control as well as Pkr^{-/-} mice remained healthy in terms of DAI and weight during DSS-feeding, but showed a slight but significant increase in the histological score in the distal colon, due to leukocyte infiltration into the mucosa and submucosa (**Fig.22A**). GRP78 levels were not induced in IEC at this time point upon DSS treatment, whereas CPN60 was increased in control mice, but showed a tendency to decrease in Pkr^{-/-} mice. At the same time, the mitochondrial marker COX4 remained

unaltered in control mice and was diminished in $Pkr^{-/-}$ mice (**Fig.22A,B**). The induction of CPN60 and PKR without augmented COX4 expression suggests mtUPR to be activated in control animals, while the concomitant decrease of *cpn60*, nuclear DNA-encoded *coxIV* and mtDNA-encoded *coxI* seen in $Pkr^{-/-}$ mice indicates a decline in mitochondrial abundance. Determining the ratio of mitochondrial to nuclear DNA, these assumptions were confirmed as the ratio remained stable in the control mice but decreased in $Pkr^{-/-}$ mice upon DSS treatment (**Fig.22C**). Since the reduction of mitochondria could be either a result of increased mitophagy or impaired mitochondrial biogenesis (or both), autophagy as well as gene expression levels of PGC-1 α , the main transcription factor involved in mitochondrial biogenesis, were determined. While autophagy was induced in IEC of control and $Pkr^{-/-}$ mice upon DSS treatment (**Fig.23A**), only in $Pkr^{-/-}$ mice a drop in PGC-1 α mRNA levels was observed (**Fig.23B**).

These data implicate PKR to be essential for CPN60 induction under inflammatory conditions thereby conferring protection on mitochondria. Yet, reduced mitochondrial abundance was associated with augmented resistance to DSS-induced colitis.

23A



B

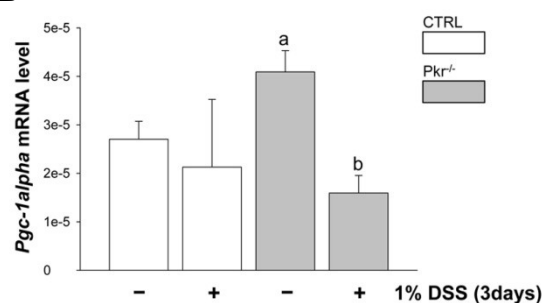


Figure 23. Mitochondrial biogenesis is impaired in $Pkr^{-/-}$ mice upon DSS-treatment.

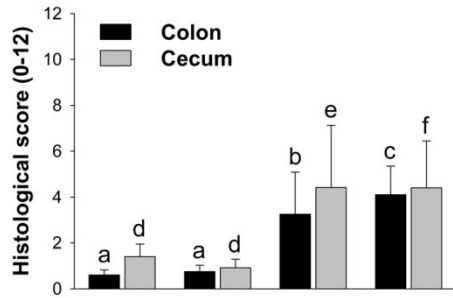
$Pkr^{-/-}$ and CTRL mice received 1%DSS for 3 day (n=5 per group) and colonic IEC were isolated. (A) Presence of LC3-I and LC3-II analyzed by Western blot. (B) *Pgc-1 α* mRNA expression normalized to 18s expression in colonic IEC determined by real-time PCR. a different from b, Two-Way-ANOVA followed by Tukey test, P=0.007.

4.4 Gene expression profiling of IEC as tool to identify novel target proteins/signaling pathways in intestinal inflammation

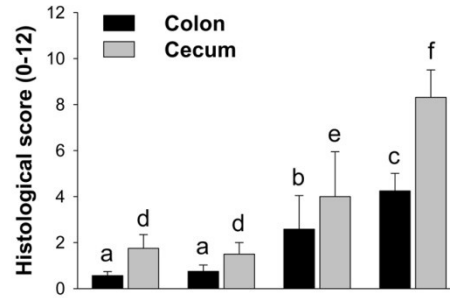
Gene- as well as protein expression profiling can be used as a screening method to identify novel target proteins/signaling pathways involved in inflammatory processes. For example, GRP78 was initially found to be induced in IEC from IL-10^{-/-} mice under inflammatory conditions by a gel-based proteome approach [112]. Subsequently, this drew the attention towards ER stress and helped identifying ER UPR as a disease-relevant pathway in IBD. Previous studies using mRNA and protein from the same samples to perform gene- as well as protein expression profiling showed that most proteins found to be regulated by SDS-PAGE and MALDI-TOF mass spectrometry could be recovered in the microarray analysis [233]. However, due to technical limitations of the gel-based proteome approach [217], many changes such as induction of secretory proteins could only be detected on mRNA level [233]. To get a more global impression of inflammation associated changes in IEC, we performed microarray analysis of isolated large intestinal epithelial cells (colon and cecum pooled). Rag2^{-/-} and Rag2^{-/-} x IL-10^{-/-} recipient mice were reconstituted for 4 weeks with either CD4⁺ CD25⁺ (regulatory) T cells from Wt donors or CD4⁺ CD25⁻ (colitogenic) T cells from Wt or IL-10^{-/-} donor mice. This model allowed us to distinguish between different levels of IL-10 availability and provided different grades of inflammation as outcome (**Fig.24**). The importance of adaptive immune signals including IL-10 for the onset and regulation of chronic intestinal inflammation has been shown in various animal models. In particular, IL-10 has been shown to inhibited ER stress responses in the intestinal epithelium [112], thereby directly conferring protection to IEC.

For microarray data analysis, two different strategies/software packages were applied. First, the ChipInspector software from Genomatix, which calculates gene regulation based on single probes instead of probe sets. This approach circumvents the problem that sequence information can be outdated and genes can be translated into alternative transcripts, i.e. probes cannot be assigned uniquely to different gene variants and the probes in a probe set are often distributed among different transcripts of the same gene locus. As a consequence, calculating signals from probe sets might not reflect the expression value of the gene properly. For annotation, ChipInspector uses the Genomatix genome annotation based on EIDorado [234,235]. A drawback of this software is that only ratios between treatment- and control group arrays are calculated and crude intensity values of gene expression are not available.

24A



B



C

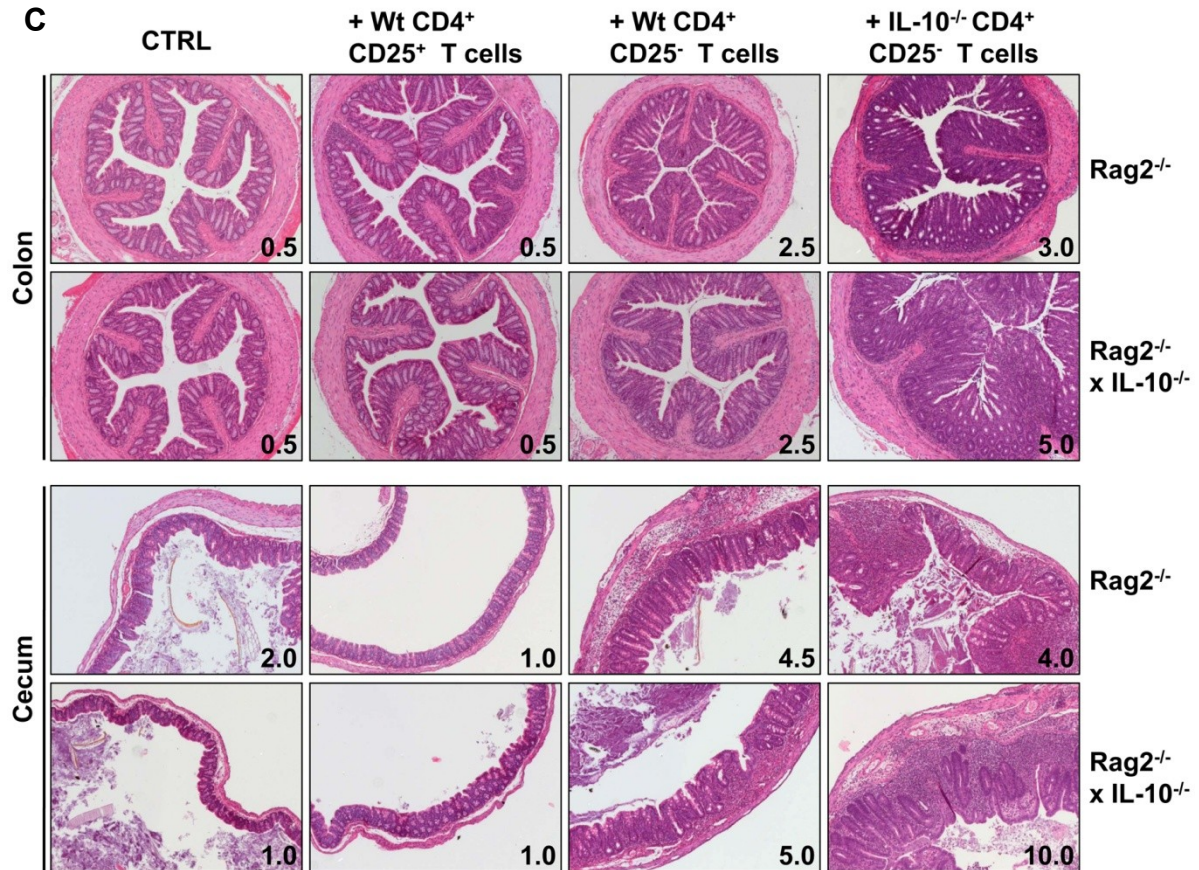


Figure 24. Histological changes in the large intestine of Rag2^{-/-} and Rag2^{-/-} x IL-10^{-/-} recipients in response to regulatory or colitogenic T cell transfer.

Rag2^{-/-} and Rag2^{-/-} x IL-10^{-/-} recipients were adoptively transferred with either CD4⁺ CD25⁺ T cells from Wt- or CD4⁺ CD25⁻ T cells from Wt or IL-10^{-/-} mice (n=5 per group). Mice were sacrificed 4 weeks later and histopathological scoring was performed. (A) The bar charts show the mean histopathologic score \pm SD in Rag2^{-/-} recipients. a different from b and c, $P < 0.01$, d different from e and f, $P \leq 0.014$, One Way ANOVA followed by Holm-Sidak test (B) The bar charts show the mean histopathologic score \pm SD in Rag2^{-/-} x IL-10^{-/-} recipients. a different from b and c, b different from c, $P < 0.01$, d different from e and f, e different from f, $P < 0.01$, One Way ANOVA followed by Holm-Sidak test. Representative H/E staining of (C) distal colon and cecum sections of Rag2^{-/-} and Rag2^{-/-} x IL-10^{-/-} recipients with histological scores indicated (100x magnification).

Thus, we chose to analyse the data in parallel with the Management and Analysis Database for Multi-platform MicroArray eXperiments (MADMAX). This software package

uses probe sets to calculate gene expression levels and uses custom CDFs for annotation [236]. Gene intensity values of single samples can be obtained in this analysis, allowing to generate heatmaps and calculating correlations between gene expression levels and histological scores. The number of significantly regulated genes identified by either ChipInspector or MADMAX and of genes detected by both softwares can be found in **figure 25** and **table 5**.

25

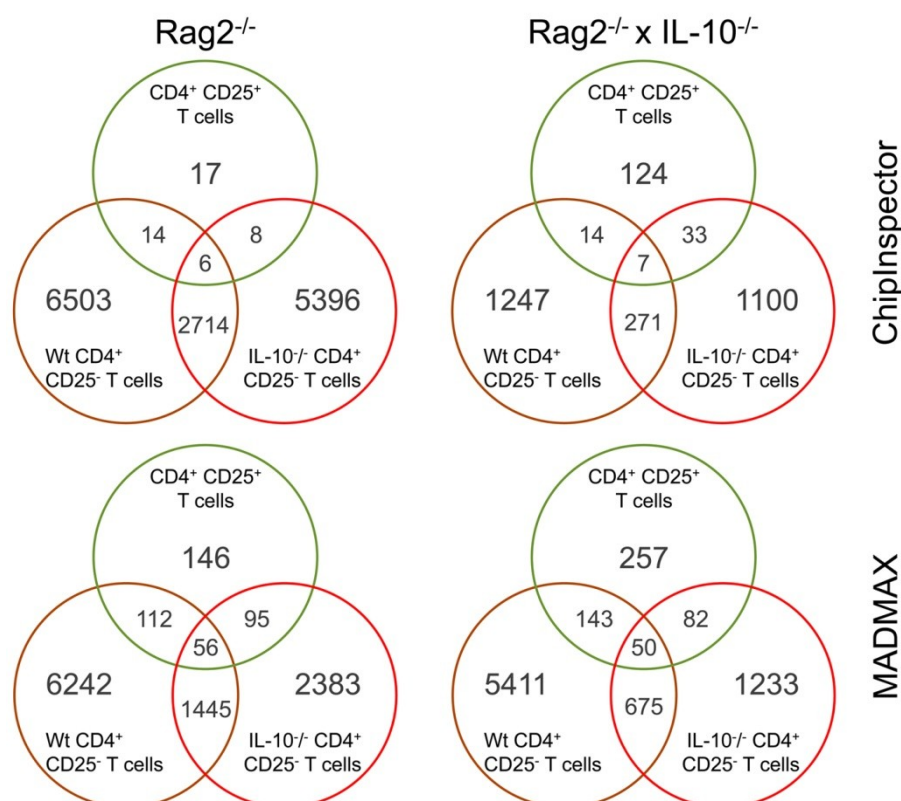


Figure 25. Number and overlap of regulated genes in IEC of $Rag2^{-/-}$ and $Rag2^{-/-} \times IL-10^{-/-}$ recipients in response to $CD4^{+}$ T cell transfer.

$Rag2^{-/-}$ and $Rag2^{-/-} \times IL-10^{-/-}$ recipients were adoptively transferred with either $CD4^{+}$ $CD25^{+}$ T cells from Wt- or $CD4^{+}$ $CD25^{-}$ T cells from Wt or $IL-10^{-/-}$ mice (n=5 per group). 4 weeks later mice were sacrificed, large intestinal epithelial cells were isolated and microarray analysis was performed. Data were analyzed using Genomatix ChipInspector or MADMAX software, respectively.

Table 5. Number of regulated genes in IEC of $Rag2^{-/-}$ and $Rag2^{-/-} \times IL-10^{-/-}$ recipients according to Genomatix ChipInspector or MADMAX software and number of genes found in both analyses.

$Rag2^{-/-}$ recipients			$Rag2^{-/-} \times IL-10^{-/-}$ recipients			
CD4 ⁺ CD25 ⁺ T cells	Wt CD4 ⁺ CD25 ⁻ T cells	IL-10 ^{-/-} CD4 ⁺ CD25 ⁻ T cells	CD4 ⁺ CD25 ⁺ T cells	Wt CD4 ⁺ CD25 ⁻ T cells	IL-10 ^{-/-} CD4 ⁺ CD25 ⁻ T cells	
17	6503	5396	124	1247	1100	ChipInspector
146	6242	2382	257	5411	1233	MADMAX
7	2482	922	31	861	624	Overlap

4.4.1. Most highly regulated genes in IEC in response to CD4⁺ T cell transfer

Most highly regulated genes for all comparisons and both recipient mouse strains identified by ChipInspector and MADMAX software are given in **tables 6-17**. In general, the recovery rate of regulated genes was fairly high within both analyses. Following Wt CD4⁺ CD25⁻ T cell transfer, more genes were significantly regulated than after IL-10^{-/-} CD4⁺ CD25⁻ T cell transfer, even in Rag2^{-/-} recipients developing comparable tissue pathology upon reconstitution with colitogenic T cells from both genotypes. Additionally, there was a tendency for more regulated genes in IEC from moderately inflamed Rag2^{-/-} recipients compared to severely inflamed Rag2^{-/-} x IL-10^{-/-} recipients. Of note, under non-inflammatory conditions, transfer of regulatory T cells into Rag2^{-/-} x IL-10^{-/-} recipients triggered substantially more gene expression changes compared to Rag2^{-/-} recipients. These data suggest that T cell-derived IL-10 is (I) necessary to efficiently evoke counterregulation to inflammatory signals and is (II) sufficient to induce homeostatic changes in IEC from Rag2^{-/-} x IL-10^{-/-} recipients.

Among the most highly regulated genes were cytokines such as *Cxcl2* (MIP-2) or *S100a8* and *S100a9* which form complexes also known as calprotectin [237] as well as genes involved in the inflammatory response (e.g. *Ido1*) [238] and arachidonic acid metabolism (*Cyp2c55*) [239]. Furthermore, regulated genes were subjected to a transcription factor analysis using Genomatix Bibliosphere. Differentially expressed genes clustered around IL-10 signaling-, inflammation-, enterocyte differentiation- and colorectal cancer-associated transcription factors SP1, AP1, HNF4 α , ATF3, KLF5 and KLF6 [240-244], respectively.

Table 6. Most highly regulated genes in IEC of Rag2^{-/-} recipients 4 weeks after CD4⁺ CD25⁺ T cell transfer according to Genomatix ChiplInspector software. Genes also identified by MADMAX software as highly regulated are in bold type.

Rag2 ^{-/-} +Wt CD4 ⁺ CD25 ⁺ T cells vs CTRL							
TOP10 upregulated				TOP10 downregulated			
gene ID	gene name	description	fold change	gene ID	gene name	description	fold change
15511	Hspa1b	Heat shock 70 kDa protein 1B	2.04	13170	Dbp	D site-binding protein	-1.83
56338	Txnip	Thioredoxin-interacting protein	1.78	192113	Atp12a	Potassium-transporting ATPase alpha chain 2	-1.73
72082	Cyp2c55	Cytochrome P450 2C55	1.77	21685	Tef	Thyrotroph embryonic factor	-1.71
68585	Rtn4	Reticulon-4	1.75	67038	2010109 I03Rik	RIKEN cDNA 2010109I03 gene	-1.71
104158	Ces3	Carboxylesterase 3	1.71				
18703	Pigr	Polymeric immunoglobulin receptor	1.71				
70045	2610528 A11Rik	RIKEN cDNA 2610528A11 gene	1.69				
12623	Ces1	Liver carboxylesterase 1	1.67				
19122	Prnp	Major prion protein	1.67				
16600	Klf4	Krueppel-like factor 4	1.65				

Table 7. Most highly regulated genes in IEC of Rag2^{-/-} recipients 4 weeks after CD4⁺ CD25⁺ T cell transfer according to MADMAX software. Genes also identified by Genomatix ChiplInspector software as highly regulated are in bold type.

Rag2 ^{-/-} +Wt CD4 ⁺ CD25 ⁺ T cells vs CTRL							
TOP10 upregulated				TOP10 downregulated			
gene ID	gene name	description	fold change	gene ID	gene name	description	fold change
70335	Reep6	receptor accessory protein 6	2.77	13170	Dbp	D site-binding protein	-5.17
16859	Lgals9	lectin, galactose binding, soluble 9	2.60	67038	2010109 I03Rik	RIKEN cDNA 2010109I03 gene	-3.67
29858	Pmm1	phosphomannomutase 1	2.53	21685	Tef	Thyrotroph embryonic factor	-3.34
66912	Bzw2	basic leucine zipper and W2 domains 2	2.43	192113	Atp12a	Potassium-transporting ATPase alpha chain 2	-2.55
15958	Ifit2	interferon-induced protein with tetratricopeptide repeats 2	2.42	108154	Adamts6	a disintegrin-like metallo peptidase with thrombospondin type 1 motif, 6	-2.48
665146	Gm7517	predicted gene 7517	2.37	546644	Ly6g	lymphocyte antigen 6 complex, locus G	-2.25
20454	St3gal5	ST3 beta-galactoside alpha-2,3-sialyltransferase 5	2.36	381280	Hjurp	Holliday junction recognition protein	-2.17
67266	Fam69a	family with sequence similarity 69, member A	2.32	53376	Usp2	ubiquitin specific peptidase 2	-2.13
104158	Ces3	Carboxylesterase 3	2.31	17752	Mt4	metallothionein 4	-2.02
11732	Ank	progressive ankylosis	2.30	103964	Try5	trypsin 5	-2.00

RESULTS

Table 8. Most highly regulated genes in IEC of Rag2^{-/-} x IL-10^{-/-} recipients 4 weeks after CD4⁺ CD25⁺ T cell transfer according to Genomatix ChiplInspector software. Genes also identified by MADMAX software as highly regulated are in bold type.

Rag2 ^{-/-} x IL-10 ^{-/-} +Wt CD4 ⁺ CD25 ⁺ T cells vs CTRL							
TOP10 upregulated				TOP10 downregulated			
gene ID	gene name	description	fold change	gene ID	gene name	description	fold change
109901	Ela1	elastase 1, pancreatic	2.91	57262	Retnla	resistin like alpha	-2.36
71578	Sval1	seminal vesicle antigen-like 1	2.83	231591	Vmn2r14	vomeronasal 2, receptor 14	-2.01
68891	Cd177	CD177 antigen	2.66	381917	Dnahc3	dynein, axonemal, heavy chain 3	-1.93
26366	Ceacam10	carcinoembryonic antigen-related cell adhesion 10	2.64	67896	Ccdc80	coiled-coil domain containing 80	-1.91
11522	Adh1	alcohol dehydrogenase 1 (class I)	2.62	12652	Chga	chromogranin A	-1.87
68416	Sycn	syncollin	2.48	237310	Il22ra2	interleukin 22 receptor, alpha 2	-1.86
76113	Lpo	lactoperoxidase	2.45	237979	Sdk2	sidekick homolog 2 (chicken)	-1.85
67701	Wfdc2	WAP four-disulfide core domain 2	2.30	12309	S100g	S100 calcium binding protein G	-1.84
219033	Ang4	angiogenin, ribonuclease A family, member 4	2.22	69564	Itgb1bp3	integrin beta 1 binding protein 3	-1.84
66289	Mptx	Mucosal pentraxin	2.20	208936	Adams18	a disintegrin-like metallo-peptidase with thrombospondin type 1 motif, 18	-1.83

Table 9. Most highly regulated genes in IEC of Rag2^{-/-} x IL-10^{-/-} recipients 4 weeks after CD4⁺ CD25⁺ T cell transfer according to MADMAX software. Genes also identified by Genomatix ChiplInspector software as highly regulated are in bold type.

Rag2 ^{-/-} x IL-10 ^{-/-} +Wt CD4 ⁺ CD25 ⁺ T cells vs CTRL							
TOP10 upregulated				TOP10 downregulated			
gene ID	gene name	description	fold change	gene ID	gene name	description	fold change
21828	Thbs4	thrombospondin 4	5.44	17105	Lyz2	lysozyme 2	-5.26
23919	Insl5	insulin-like 5	4.44	93721	Cpn1	carboxypeptidase N, polypeptide 1	-4.04
68891	Cd177	CD177 antigen	4.28	231591	Vmn2r14	vomeronasal 2, receptor 14	-3.98
13615	Edn2	endothelin 2	3.85	14598	Ggt1	gamma-glutamyltransferase 1	-3.93
108017	Fxyd4	FXDY domain-containing ion transport regulator 4	3.78	13809	Enpep	glutamyl aminopeptidase	-3.49
108105	B3gnt5	UDP-GlcNAc:betaGal beta-1,3-N-acetylglucosaminyl-transferase 5	3.64	16792	Laptm5	lysosomal-associated protein transmembrane 5	-3.24
15433	Hoxd13	homeobox D13	3.63	14938	Gzma	granzyme A	-3.05
26366	Ceacam10	carcinoembryonic antigen-related cell adhesion 10	3.47	19073	Srgn	serglycin	-2.81
13034	Ctse	cathepsin E	3.32	12309	S100g	S100 calcium binding protein G	-2.70
21825	Thbs1	thrombospondin 1	3.04	11854	Rhod	ras homolog gene family, member D	-2.60

Table 10. Most highly regulated genes in IEC of Rag2^{-/-} recipients 4 weeks after Wt CD4⁺ CD25⁻ T cell transfer according to Genomatix ChipInspector software. Genes also identified by MADMAX software as highly regulated are in bold type.

Rag2 ^{-/-} +Wt CD4 ⁺ CD25 ⁻ T cells vs CTRL							
TOP10 upregulated				TOP10 downregulated			
gene ID	gene name	description	fold change	gene ID	gene name	description	fold change
16149	Cd74	CD74 antigen	2.81	72082	Cyp2c55	Cytochrome P450 2C55	-12.47
67402	Txndc8	thioredoxin domain containing 8	2.53	17831	Muc2	mucin 2	-10.78
51842	D2Ert93e	DNA segment, Chr 2, ERATO Doi 93, expressed	2.43	666339	Muc3	mucin 3, intestinal	-9.65
16869	Lhx1	LIM homeobox protein 1	2.41	16612	Klk1	kallikrein 1	-9.32
101113	Snx21	sorting nexin family member 21	2.39	68416	Sycn	syncollin	-9.32
100044236	Copg2as2	coatamer protein complex, subunit gamma 2, antisense 2	2.31	20341	Selenbp1	selenium binding protein 1	-9.19
20310	Cxcl2	chemokine (C-X-C motif) ligand 2	2.31	13730	Emp1	epithelial membrane protein 1	-8.75
327954	Dnahc2	dynein, axonemal, heavy chain 2	2.31	14915	Guca2a	guanylate cyclase activator 2a	-8.57
81014	V1rd4	vomeronal 1 receptor 58	2.31	22236	Ugt1a2	UDP glucuronosyltransferase 1 family, polypeptide A2	-8.28
20202	S100a9	S100 calcium binding protein A9	2.28	20501	Slc16a1	solute carrier family 16, member 1	-8.17

Table 11. Most highly regulated genes in IEC of Rag2^{-/-} recipients 4 weeks after Wt CD4⁺ CD25⁻ T cell transfer according to MADMAX software. Genes also identified by Genomatix ChipInspector software as highly regulated are in bold type.

Rag2 ^{-/-} +Wt CD4 ⁺ CD25 ⁻ T cells vs CTRL							
TOP10 upregulated				TOP10 downregulated			
gene ID	gene name	description	fold change	gene ID	gene name	description	fold change
320383	B230317F23Rik	RIKEN cDNA B230317F23 gene	30.28	14282	Fosb	FBJ osteosarcoma oncogene B	-45.06
211232	Cpne9	copine family member IX	25.98	27979	Eif3b	eukaryotic translation initiation factor 3, subunit B	-41.40
16792	Laptm5	lysosomal-associated protein transmembrane 5	16.16	108705	Pttg1ip	pituitary tumor-transforming 1 interacting protein	-35.19
20310	Cxcl2	chemokine (C-X-C motif) ligand 2	14.29	11502	Adam9	a disintegrin and metalloproteinase domain 9	-34.42
80515	A030009H04Rik	RIKEN cDNA A030009H04 gene	14.05	231070	Insig1	insulin induced gene 1	-32.48
20202	S100a9	S100 calcium binding protein A9	13.89	14590	Ggh	gamma-glutamyl hydrolase	-30.28
14131	Fcgr3	Fc receptor, IgG, low affinity III	13.86	14248	Flii	flightless I homolog (Drosophila)	-29.62
54352	Irx5	Iroquois related homeobox 5	13.74	76459	Car12	carbonic anhydrase 12	-28.93
668544	Gm9232	predicted gene 9232	12.46	55980	Impa1	inositol (myo)-1(or 4)-monophosphatase 1	-28.36
16149	Cd74	CD74 antigen	11.95	12724	Clcn2	chloride channel 2	-27.42

RESULTS

Table 12. Most highly regulated genes in IEC of Rag2^{-/-} x IL-10^{-/-} recipients 4 weeks after Wt CD4⁺ CD25⁻ T cell transfer according to Genomatix ChipInspector software. Genes also identified by MADMAX software as highly regulated are in bold type.

Rag2 ^{-/-} x IL-10 ^{-/-} +Wt CD4 ⁺ CD25 ⁻ T cells vs CTRL							
TOP10 upregulated				TOP10 downregulated			
gene ID	gene name	description	fold change	gene ID	gene name	description	fold change
76509	Plet1	placenta expressed transcript 1	4.56	72082	Cyp2c55	Cytochrome P450 2C55	-21.86
76905	Lrg1	leucine-rich alpha-2-glycoprotein 1	4.50	14079	Fabp2	fatty acid binding protein 2, intestinal	-9.58
20201	S100a8	S100 calcium binding protein A8	4.26	99663	Clca6	chloride channel calcium activated 6	-7.94
16149	Cd74	CD74 antigen	4.23	56857	Slc37a2	solute carrier family 37, member 2	-7.78
60440	Iigp1	interferon inducible GTPase 1	3.92	15360	Hmgcs2	3-hydroxy-3-methylglutaryl-Coenzyme A synthase 2	-7.67
18393	Orc2l	origin recognition complex, subunit 2	3.78	11833	Aqp8	aquaporin 8	-7.11
14969	H2-Eb1	histocompatibility 2, class II antigen E beta	3.63	14915	Guca2a	guanylate cyclase activator 2a	-6.73
20762	Sprp2h	small proline-rich protein 2H	3.51	17153	Mal	myelin and lymphocyte protein	-6.63
234378	Klhl26	kelch-like 26	3.34	12925	Crip1	cysteine-rich protein 1 (intestinal)	-6.59
12628	Cfh	complement component factor h	3.32	13730	Emp1	epithelial membrane protein 1	-6.59

Table 13. Most highly regulated genes in IEC of Rag2^{-/-} x IL-10^{-/-} recipients 4 weeks after Wt CD4⁺ CD25⁻ T cell transfer according to MADMAX software. Genes also identified by Genomatix ChipInspector software as highly regulated are in bold type.

Rag2 ^{-/-} x IL-10 ^{-/-} +Wt CD4 ⁺ CD25 ⁻ T cells vs CTRL							
TOP10 upregulated				TOP10 downregulated			
gene ID	gene name	description	fold change	gene ID	gene name	description	fold change
215654	Cdh12	cadherin 12	20.81	72082	Cyp2c55	Cytochrome P450 2C55	-41.26
22061	Trp63	transformation related protein 63	16.60	104158	Ces3	Carboxylesterase 3	-35.07
22775	Zik1	zinc finger protein interacting with K protein 1	16.18	13120	Cyp4b1	cytochrome P450, family 4, subfamily b, polypeptide 1	-32.31
15930	Ido1	indoleamine 2,3-dioxygenase 1	14.85	235674	Acaa1b	acetyl-Coenzyme A acyltransferase 1B	-27.28
77908	9230113 P08Rik	RIKEN cDNA 9230113P08 gene	14.56	72269	Cda	cytidine deaminase	-24.62
258543	Olfir810	olfactory receptor 810	14.33	12623	Ces1	Liver carboxylesterase 1	-24.02
74946	4930472 D16Rik	RIKEN cDNA 4930472D16 gene	14.14	15486	Hsd17b2	hydroxysteroid (17-beta) dehydrogenase 2	-20.90
17700	Mstn	myostatin	13.86	55950	Bri3	brain protein I3	-19.64
65255	Asb4	ankyrin repeat and SOCS box-containing 4	13.59	170460	Stard5	StAR-related lipid transfer (START) domain containing 5	-17.62
14969	H2-Eb1	histocompatibility 2, class II antigen E beta	12.63	69083	Sult1c2	sulfotransferase family, cytosolic, 1C, member 2	-16.36

Table 14. Most highly regulated genes in IEC of Rag2^{-/-} recipients 4 weeks after IL-10^{-/-} CD4⁺ CD25⁻ T cell transfer according to Genomatix ChipInspector software. Genes also identified by MADMAX software as highly regulated are in bold type.

Rag2 ^{-/-} +IL-10 ^{-/-} CD4 ⁺ CD25 ⁻ T cells vs CTRL							
TOP10 upregulated				TOP10 downregulated			
gene ID	gene name	description	fold change	gene ID	gene name	description	fold change
15930	Ido1	indoleamine 2,3-dioxygenase 1	19.97	72082	Cyp2c55	Cytochrome P450 2C55	-7.11
20202	S100a9	S100 calcium binding protein A9	14.12	68416	Sycn	syncollin	-7.11
20201	S100a8	S100 calcium binding protein A8	13.74	56857	Slc37a2	solute carrier family 37, member 2	-6.28
76509	Plet1	placenta expressed transcript 1	12.55	18671	Abcb1a	ATP-binding cassette, subfamily B, member 1A	-3.76
16149	Cd74	CD74 antigen	12.30	12623	Ces1	Liver carboxylesterase 1	-3.61
14969	H2-Eb1	histocompatibility 2, class II antigen E beta	12.21	21818	Tgm3	transglutaminase 3, E polypeptide	-3.39
76905	Lrg1	leucine-rich alpha-2-glycoprotein 1	11.71	13120	Cyp4b1	cytochrome P450, family 4, subfamily b, polypeptide 1	-3.36
14961	H2-Ab1	histocompatibility 2, class II antigen A, beta 1	11.63	69083	Sult1c2	sulfotransferase family, cytosolic, 1C, member 2	-3.32
60440	ligp1	interferon inducible GTPase 1	9.92	225997	Trpm6	transient receptor potential cation channel, M6	-3.25
22271	Upp1	uridine phosphorylase 1	9.78	235674	Acaa1b	acetyl-Coenzyme A acyltransferase 1B	-3.16

Table 15. Most highly regulated genes in IEC of Rag2^{-/-} recipients 4 weeks after IL-10^{-/-} CD4⁺ CD25⁻ T cell transfer according to MADMAX software. Genes also identified by Genomatix ChipInspector software as highly regulated are in bold type.

Rag2 ^{-/-} +IL-10 ^{-/-} CD4 ⁺ CD25 ⁻ T cells vs CTRL							
TOP10 upregulated				TOP10 downregulated			
gene ID	gene name	description	fold change	gene ID	gene name	description	fold change
15930	Ido1	indoleamine 2,3-dioxygenase 1	306.02	68416	Sycn	syncollin	-19.46
20201	S100a8	S100 calcium binding protein A8	216.55	56857	Slc37a2	solute carrier family 37, member 2	-16.38
20202	S100a9	S100 calcium binding protein A9	188.70	69083	Sult1c2	sulfotransferase family, cytosolic, 1C, member 2	-16.05
76905	Lrg1	leucine-rich alpha-2-glycoprotein 1	142.76	21818	Tgm3	transglutaminase 3, E polypeptide	-13.93
17329	Cxcl9	chemokine (C-X-C motif) ligand 9	99.05	72082	Cyp2c55	Cytochrome P450 2C55	-13.63
14961	H2-Ab1	histocompatibility 2, class II antigen A, beta 1	80.90	13120	Cyp4b1	cytochrome P450, family 4, subfamily b, polypeptide 1	-13.60
60440	ligp1	interferon inducible GTPase 1	79.20	235674	Acaa1b	acetyl-Coenzyme A acyltransferase 1B	-13.08
20310	Cxcl2	chemokine (C-X-C motif) ligand 2	78.98	100039	Gm2357	predicted gene 2357	-13.01
20311	Cxcl5	chemokine (C-X-C motif) ligand 5	67.39	66859	Slc16a9	solute carrier family 16, member 9	-12.57
17224	Mcpt1	mast cell protease 1	62.10	225997	Trpm6	transient receptor potential cation channel, M6	-11.19

RESULTS

Table 16. Most highly regulated genes in IEC of Rag2^{-/-} x IL-10^{-/-} recipients 4 weeks after IL-10^{-/-} CD4⁺ CD25⁻ T cell transfer according to Genomatix ChipInspector software. Genes also identified by MADMAX software as highly regulated are in bold type.

Rag2 ^{-/-} x IL-10 ^{-/-} +IL-10 ^{-/-} CD4 ⁺ CD25 ⁻ T cells vs CTRL							
TOP10 upregulated				TOP10 downregulated			
gene ID	gene name	description	fold change	gene ID	gene name	description	fold change
76509	Plet1	placenta expressed transcript 1	13.93	72082	Cyp2c55	Cytochrome P450 2C55	-41.93
20311	Cxcl5	chemokine (C-X-C motif) ligand 5	11.16	12623	Ces1	Liver carboxylesterase 1	-7.89
76905	Lrg1	leucine-rich alpha-2-glycoprotein 1	11.16	15360	Hmgcs2	3-hydroxy-3-methylglutaryl-Coenzyme A synthase 2	-7.73
15930	Ido1	indoleamine 2,3-dioxygenase 1	10.56	14079	Fabp2	fatty acid binding protein 2, intestinal	-7.52
14969	H2-Eb1	histocompatibility 2, class II antigen E beta	9.51	56857	Slc37a2	solute carrier family 37, member 2	-7.26
20202	S100a9	S100 calcium binding protein A9	9.06	18671	Abcb1a	ATP-binding cassette, subfamily B (MDR/TAP), member 1A	-6.06
20310	Cxcl2	chemokine (C-X-C motif) ligand 2	8.88	68416	Sycn	syncollin	-6.06
192113	Atp12a	ATPase, H+/K+ transporting, nongastric, alpha polypeptide	8.82	102022	Ces6	carboxylesterase 2A	-5.82
20201	S100a8	S100 calcium binding protein A8	8.82	20887	Sult1a1	sulfotransferase family 1A, member 1	-5.74
20762	Sprp2h	small proline-rich protein 2H	8.28	14915	Guca2a	guanylate cyclase activator 2a	-5.43

Table 17. Most highly regulated genes in IEC of Rag2^{-/-} x IL-10^{-/-} recipients 4 weeks after IL-10^{-/-} CD4⁺ CD25⁻ T cell transfer according to MADMAX software. Genes also identified by Genomatix ChipInspector software as highly regulated are in bold type.

Rag2 ^{-/-} x IL-10 ^{-/-} +IL-10 ^{-/-} CD4 ⁺ CD25 ⁻ T cells vs CTRL							
TOP10 upregulated				TOP10 downregulated			
gene ID	gene name	description	fold change	gene ID	gene name	description	fold change
20201	S100a8	S100 calcium binding protein A8	121.58	72082	Cyp2c55	Cytochrome P450 2C55	-184.08
76905	Lrg1	leucine-rich alpha-2-glycoprotein 1	119.75	104158	Ces3	Carboxylesterase 3	-62.28
20202	S100a9	S100 calcium binding protein A9	119.73	13120	Cyp4b1	cytochrome P450, family 4, subfamily b, polypeptide 1	-46.03
20311	Cxcl5	chemokine (C-X-C motif) ligand 5	112.45	12623	Ces1	Liver carboxylesterase 1	-34.44
15930	Ido1	indoleamine 2,3-dioxygenase 1	94.31	69083	Sult1c2	sulfotransferase family, cytosolic, 1C, member 2	-26.57
20762	Sprp2h	small proline-rich protein 2H	89.98	72269	Cda	cytidine deaminase	-26.43
17329	Cxcl9	chemokine (C-X-C motif) ligand 9	74.33	235674	Acaa1b	acetyl-Coenzyme A acyltransferase 1B	-24.80
20310	Cxcl2	chemokine (C-X-C motif) ligand 2	55.57	68416	Sycn	syncollin	-18.16
16819	Lcn2	lipocalin 2	51.95	16956	Lpl	lipoprotein lipase	-15.68
20307	Ccl8	chemokine (C-C motif) ligand 8	50.18	56857	Slc37a2	solute carrier family 37, member 2	-14.76

4.4.2. Data analysis of regulated genes in IEC in response to CD4⁺ T cell transfer

To characterize the sets of regulated genes and to get an overview of the extensive data, data analysis was performed to obtain biological terms and signal transduction pathways with a significant enrichment of regulated genes. The Genomatix Pathway System (GePS) was applied for these analysis. Since previous studies indicated changes in cellular organelles under inflammatory conditions, Z-scores of selected gene ontology (GO) terms from the domain “cellular components” are comprised in **table 18** and **table 19**. Accordingly, selected GO terms from the domain “biological process” are comprised in **table 20** and **table 21**. Taken together, these data confirm ER and mitochondria to be highly affected by inflammatory processes in IEC and indicate cellular stress pathways to be activated. Of note, inflammation also seems to have a profound impact on metabolic pathways including OXPHOS. In mice reconstituted with CD4⁺ CD25⁺ T cells, no signal transduction pathways with significant enrichment within the regulated genes were detected. Yet, several significant pathways were found in the other groups (**tables 22-25**). Regarding the pathways observed, rather the T cells transferred than the genotype of the recipient mice seemed to be the crucial factor determining similarity between groups. In general, most significant pathways can be assigned to inflammation such as pathways involved in apoptosis, cell cycle and immune responses. Signal transduction pathways with the highest significance found in both recipients mouse strains are shown in **figure 26** for Wt CD4⁺ CD25⁻ T cell-reconstituted mice and in **figure 27** for IL-10^{-/-} CD4⁺ CD25⁻ T cell- reconstituted mice. The pathways displayed are the P21-activated kinase pathway and the IL-6 pathway for mice reconstituted with Wt and IL-10^{-/-} CD4⁺ CD25⁻ T cells, respectively.

RESULTS

Table 18. Z-scores of selected GO terms from the domain “cellular components”. A Z-score above 2 can be considered statistically significant, corresponding to a P-value of 0.05. The gene sets used for this analysis were regulated genes in IEC following T cell transfer according to ChIPInspector software.

term	ID	Z-scores					
		Rag2 ^{-/-} recipients reconstituted with			Rag2 ^{-/-} x IL-10 ^{-/-} recipients reconstituted with		
		CD25 ⁺ T cells	Wt CD25 ⁻ T cells	IL-10 ^{-/-} CD25 ⁻ T cells	CD25 ⁺ T cells	Wt CD25 ⁻ T cells	IL-10 ^{-/-} CD25 ⁻ T cells
organelle	GO:0043226	3.72	20.77	14.23	1.10	12.32	10.41
nucleus	GO:0005634	2.49	7.52	9.24	-2.42	-0.04	5.66
cytoplasm	GO:0005737	2.69	23.52	13.94	2.09	16.33	11.78
mitochondrion	GO:0005739	-	15.40	1.85	0.17	16.46	4.08
endoplasmic reticulum	GO:0005783	6.75	9.56	8.94	4.25	4.55	9.53
Golgi apparatus	GO:0005794	-	8.40	4.60	2.11	3.32	0.80

Table 19. Z-scores of selected GO terms from the domain “cellular components”. A Z-score above 2 can be considered statistically significant, corresponding to a P-value of 0.05. The gene sets used for this analysis were regulated genes in IEC following T cell transfer according to MADMAX software.

term	ID	Z-scores					
		Rag2 ^{-/-} recipients reconstituted with			Rag2 ^{-/-} x IL-10 ^{-/-} recipients reconstituted with		
		CD25 ⁺ T cells	Wt CD25 ⁻ T cells	IL-10 ^{-/-} CD25 ⁻ T cells	CD25 ⁺ T cells	Wt CD25 ⁻ T cells	IL-10 ^{-/-} CD25 ⁻ T cells
organelle	GO:0043226	2.39	23.72	16.51	3.40	22.92	9.81
nucleus	GO:0005634	2.79	12.22	14.04	0.33	10.97	4.98
cytoplasm	GO:0005737	1.53	25.20	14.65	4.13	24.63	11.90
mitochondrion	GO:0005739	1.23	16.36	2.50	0.67	16.69	4.04
endoplasmic reticulum	GO:0005783	0.60	10.10	10.89	5.38	9.77	7.07
Golgi apparatus	GO:0005794	-	7.09	3.72	0.84	6.35	1.97

Table 20. Z-scores of selected GO terms from the domain “biological process”. A Z-score above 2 can be considered statistically significant, corresponding to a P-value of 0.05. The gene sets used for this analysis were regulated genes in IEC following T cell transfer according to ChipInspector software.

term	ID	Z-scores					
		Rag2 ^{-/-} recipients reconstituted with			Rag2 ^{-/-} x IL-10 ^{-/-} recipients reconstituted with		
		CD25 ⁺ T cells	Wt CD25 ⁻ T cells	IL-10 ^{-/-} CD25 ⁻ T cells	CD25 ⁺ T cells	Wt CD25 ⁻ T cells	IL-10 ^{-/-} CD25 ⁻ T cells
apoptosis	GO:0006915	3.83	5.22	5.20	0.28	4.19	5.79
autophagy	GO:0006914	-	0.95	-0.19	-	-	-
cellular component biogenesis	GO:0044085	-	4.37	7.41	0.89	3.39	6.10
cellular component organization	GO:0016043	1.87	5.59	8.64	-	1.75	4.45
cellular metabolic process	GO:0044237	3.01	16.21	11.88	0.90	8.45	10.03
oxidative phosphorylation	GO:0006119	-	7.79	3.84	-	7.99	-
cellular response to oxidative stress	GO:0034599	-	3.77	2.91	-	-	5.04
ER unfolded protein response	GO:0030968	-	2.75	4.22	-	-	8.20
ER-nucleus signaling pathway	GO:0006984	-	2.89	4.63	-	-	8.79
inflammatory response	GO:0006954	-	2.62	6.79	-	0.70	6.32
response to stress	GO:0006950	2.97	4.74	6.52	1.17	1.55	8.62
response to wounding	GO:0009611	-	2.21	5.72	1.35	0.37	6.17

Table 21. Z-scores of selected GO terms from the domain “biological process”. A Z-score above 2 can be considered statistically significant, corresponding to a P-value of 0.05. The gene sets used for this analysis were regulated genes in IEC following T cell transfer according to MADMAX software.

term	ID	Z-scores					
		Rag2 ^{-/-} recipients reconstituted with			Rag2 ^{-/-} x IL-10 ^{-/-} recipients reconstituted with		
		CD25 ⁺ T cells	Wt CD25 ⁻ T cells	IL-10 ^{-/-} CD25 ⁻ T cells	CD25 ⁺ T cells	Wt CD25 ⁻ T cells	IL-10 ^{-/-} CD25 ⁻ T cells
apoptosis	GO:0006915	1.57	5.87	7.70	2.59	4.23	5.93
autophagy	GO:0006914	-	2.97	0.97	-	3.76	3.96
cellular component biogenesis	GO:0044085	0.92	6.70	6.59	0.71	5.78	4.36
cellular component organization	GO:0016043	-1.00	6.82	8.13	-0.48	5.49	3.56
cellular metabolic process	GO:0044237	4.13	19.61	12.77	3.37	16.8	7.83
oxidative phosphorylation	GO:0006119	-	4.05	-0.53	-	2.66	-
cellular response to oxidative stress	GO:0034599	-	1.08	1.37	-	1.09	2.06
ER unfolded protein response	GO:0030968	-	0.93	4.26	-	-	4.35
ER-nucleus signaling pathway	GO:0006984	-	0.72	4.01	-	-0.23	2.99
inflammatory response	GO:0006954	-	3.74	7.62	1.90	3.61	6.70
response to stress	GO:0006950	-0.23	6.02	10.14	1.72	5.77	8.55
response to wounding	GO:0009611	-	2.99	7.36	1.76	3.01	6.61

RESULTS

Table 22. Signal transduction pathways with a significant enrichment of regulated genes. The gene sets used for this analysis were regulated genes in IEC from Rag2^{-/-} recipients reconstituted with Wt CD4⁺ CD25⁻ T cells according to ChiplInspector (CI) or MADMAX (MM) software. Pathways also identified in Rag2^{-/-} x IL-10^{-/-} recipients are in bold type.

pathway	pathway ID	analysis	genes observed	genes expected	P-value
Phosphatidylinositol	PW_PI_M._MUSC.	CI	116	90.94	9.34E-04
Angiotensin	PW_AGT_M._MUSC.	CI	40	26.36	1.44E-03
FBJ Murine Osteosarcoma Viral Oncogene Homolog B	PW_FOSB_M._MUSC.	CI	7	2.67	3.91E-03
Protein Kinase G	PW_PKG_M._MUSC.	CI	27	17.48	6.06E-03
Wiskott Aldrich Syndrome Like	PW_WASL_M._MUSC.	CI	10	4.74	6.35E-03
Epidermal Growth Factor Receptor Family Member ERBB3	PW_EGF_M._MUSC.	CI	94	75.83	7.24E-03
		MM	87	67.27	3.04E-03
Serum/Glucocorticoid Regulated Kinase	PW_SGK_M._MUSC.	CI	24	15.40	8.28E-03
Mitogen Activated Protein Kinase	PW_MAPK_M._MUSC.	CI	191	166.47	9.77E-03
P21(CDKN1A) Activated Kinase	PW_PAK_M._MUSC.	MM	31	16.82	1.08E-04
Apoptosis Inducing Factor, Mitochondrion Associated, 1	PW_AIFM1_M._MUSC.	MM	10	4.20	2.43E-03
Integrin	PW_INTEGRIN_M._MUS	MM	53	38.63	5.09E-03
ATP Binding Cassette, Subfamily C (CFTR/MRP)	PW_ABCC_M._MUSC.	MM	11	5.52	9.42E-03
Apoptotic Peptidase Activating Factor 1	PW_APAF1_M._MUSC.	MM	11	5.52	9.42E-03
Nuclear Factor (Erythroid Derived 2) Like 2	PW_NFE2L2_M._MUSC.	MM	15	8.41	9.49E-03

Table 23. Signal transduction pathways with a significant enrichment of regulated genes. The gene sets used for this analysis were regulated genes in IEC from Rag2^{-/-} x IL-10^{-/-} recipients reconstituted with Wt CD4⁺ CD25⁻ T cells according to ChiplInspector (CI) or MADMAX (MM) software. Pathways also identified in Rag2^{-/-} recipients are in bold type.

pathway	pathway ID	analysis	genes observed	genes expected	P-value
ATP Binding Cassette, Subfamily C (CFTR/MRP)	PW_ABCC_M._MUSC.	CI	7	1.22	1.16E-04
Epidermal Growth Factor Receptor Family Member ERBB3	PW_EGF_M._MUSC.	CI	26	14.82	3.22E-03
Cystic Fibrosis Transmembrane Conductance Regulator (ATP Binding Cassette Subfamily C, Member 7)	PW_CFTR_M._MUSC.	CI	6	1.56	3.76E-03
Caveolin 1	PW_CAVEOLIN_M._MUS C.	CI	9	3.24	4.39E-03
Parathroid Hormone	PW_PTH_M._MUSC.	CI	9	3.59	8.68E-03
Nuclear Factor (Erythroid Derived 2) Like 2	PW_NFE2L2_M._MUSC.	CI	6	1.85	9.02E-03
Platelet Derived Growth Factor	PW_PDGF_M._MUSC.	CI	11	4.92	9.29E-03
Cyclin G2	PW_CCNG2_M._MUSC.	CI	2	0.17	9.44E-03
Integrin	PW_INTEGRIN_M._MUS C.	MM	55	37.30	7.08E-04
P21(CDKN1A) Activated Kinase	PW_PAK_M._MUSC.	MM	28	16.24	9.78E-04
Tumor Necrosis Factor (TNF Superfamily, Member 2)	PW_TNF_M._MUSC.	MM	78	57.86	1.45E-03
Leukemia Inhibitory Factor Receptor	PW_LIF_M._MUSC.	MM	12	6.09	8.01E-03
Hepatocyte Growth Factor Receptor	PW_HGF_M._MUSC.	MM	30	20.05	8.62E-03
LIM Domain Kinase	PW_LIMK_M._MUSC.	MM	14	7.61	9.18E-03

Table 24. Signal transduction pathways with a significant enrichment of regulated genes. The gene sets used for this analysis were regulated genes in IEC from Rag2^{-/-} recipients reconstituted with IL-10^{-/-} CD4⁺ CD25⁻ T cells according to ChiplInspector (CI) or MADMAX (MM) software. Pathways also identified in Rag2^{-/-} x IL-10^{-/-} recipients are in bold type.

pathway	pathway ID	analysis	genes observed	genes expected	P-value
Aurora Kinase	PW_AURORA_M._MUSC.	CI	20	10.11	7.54E-04
		MM	17	6.33	5.81E-05
Minichromosome Maintenance Complex	PW_MCM_M._MUSC.	CI	12	4.94	9.20E-04
		MM	12	3.09	7.75E-06
Interleukin 6 (Interferon, Beta 2)	PW_IL6_M._MUSC.	CI	43	28.69	2.04E-03
		MM	37	17.96	6.60E-06
Phosphatidylinositol	PW_PI_M._MUSC.	CI	93	72.18	2.91E-03
Interleukin 1	PW_IL1_M._MUSC.	CI	45	32.21	7.43E-03
		MM	33	20.17	2.23E-03
S Phase Kinase Associated Protein 2 (P45)	PW_SKP2_M._MUSC.	CI	11	5.41	9.10E-03
Polo Like Kinase 1	PW_PLK1_M._MUSC.	MM	26	9.57	5.01E-07
Cell Division Cycle 2, G1 To S And G2 To M	PW_CDC2_M._MUSC.	MM	34	15.02	1.49E-06
NF Kappa B	PW_NFKB_M._MUSC.	MM	81	49.61	1.88E-06
CHK1 Checkpoint Homolog	PW_CHEK1_M._MUSC.	MM	23	8.83	5.43E-06
Toll Like Receptor	PW_TOLL_M._MUSC.	MM	35	18.55	9.09E-05
Cell Division Cycle 25C	PW_CDC25_M._MUSC.	MM	13	4.27	9.46E-05
Tumor Necrosis Factor (TNF Superfamily, Member 2)	PW_TNF_M._MUSC.	MM	54	33.56	1.61E-04
Receptor Interacting Serine Threonine Kinase	PW_RIPK_M._MUSC.	MM	15	5.74	2.27E-04
Tumor Necrosis Factor Receptor Superfamily (FAS, RANK, ETC.)	PW_TNFRSF_M._MUSC.	MM	45	27.53	3.89E-04
Cyclin D1	PW_CCND1_M._MUSC.	MM	27	14.57	7.77E-04
BH3 Interacting Domain Death Agonist	PW_BID_M._MUSC.	MM	9	2.94	1.13E-03
Myeloid Differentiation Primary Response Gene (88)	PW_MYD88_M._MUSC.	MM	26	14.43	1.50E-03
Cyclin E	PW_CCNE_M._MUSC.	MM	13	5.45	1.59E-03
Ataxia Teleangiectasia And RAD3 Related	PW_ATR_M._MUSC.	MM	17	8.10	1.67E-03
Interleukin 12	PW_IL12_M._MUSC.	MM	21	10.89	1.69E-03
Interleukin 18 (Interferon Gamma Inducing Factor)	PW_IL18_M._MUSC.	MM	15	6.77	1.70E-03
ATP Binding Cassette, Subfamily B (MDR/TAP)	PW_ABCB_M._MUSC.	MM	7	2.06	1.94E-03
Granzyme A	PW_GZMA_M._MUSC.	MM	4	0.74	1.99E-03
Cyclin A2	PW_CCNA2_M._MUSC.	MM	13	5.59	2.10E-03
Caspase	PW_CASPASE_M._MUSC.	MM	36	22.52	2.22E-03
Signal Transducer And Activator Of Transcription	PW_STAT_M._MUSC.	MM	52	36.36	3.70E-03
Granzyme B	PW_GZMB_M._MUSC.	MM	6	1.77	4.16E-03
Janus Kinase	PW_JAK_M._MUSC.	MM	35	22.52	4.16E-03
Baculoviral IAP Repeat Containing Protein, Apoptosis Inhibitor	PW_BIRC_M._MUSC.	MM	16	8.10	4.45E-03
Interleukin 4	PW_IL4_M._MUSC.	MM	22	12.51	4.68E-03
Ataxia Telangiectasia Mutated	PW_ATM_M._MUSC.	MM	18	9.57	4.71E-03
Lymphotoxin Alpha (TNF Superfamily, Member 1)	PW_LTA_M._MUSC.	MM	7	2.36	4.94E-03
Leukemia Inhibitory Factor Receptor	PW_LIF_M._MUSC.	MM	9	3.53	5.06E-03
Interleukin 10	PW_IL10_M._MUSC.	MM	23	13.40	5.32E-03
TNF Receptor Associated Factor	PW_TRAF_M._MUSC.	MM	28	17.52	6.58E-03
TNFRSF1A Associated Via Death Domain	PW_TRADD_M._MUSC.	MM	8	3.09	7.29E-03
Interleukin 1 Receptor	PW_IL1R_M._MUSC.	MM	10	4.42	8.27E-03
Interleukin 6 Singnal Transducer (GP130, Oncostatin M Receptor)	PW_IL6ST_M._MUSC.	MM	10	4.42	8.27E-03
Hepatocyte Growth Factor Receptor	PW_HGF_M._MUSC.	MM	20	11.63	8.85E-03
Nucleotide Oligomerization Domain/Caspase Recruitment Domain Protein Family	PW_NOD_M._MUSC.	MM	14	7.21	9.00E-03

RESULTS

Table 25. Signal transduction pathways with a significant enrichment of regulated genes. The gene sets used for this analysis were regulated genes in IEC from Rag2^{-/-} x IL-10^{-/-} recipients reconstituted with IL-10^{-/-} CD4⁺ CD25⁻ T cells according to ChipInspector (CI) or MADMAX (MM) software. Pathways also identified in Rag2^{-/-} recipients are in bold type.

pathway	pathway ID	analysis	genes observed	genes expected	P-value
Interleukin 6 (Interferon, Beta 2)	PW_IL6_M._MUSC.	CI	26	9.82	2.81E-06
		MM	31	11.07	6.46E-08
ATP Binding Cassette, Subfamily B (MDR/TAP)	PW_ABCB_M._MUSC.	CI	8	1.13	3.21E-06
		MM	7	1.27	9.43E-05
Interleukin 1	PW_IL1_M._MUSC.	CI	26	11.03	2.57E-05
		MM	29	12.43	9.69E-06
NF Kappa B	PW_NFKB_M._MUSC.	CI	47	27.13	9.79E-05
		MM	59	30.58	2.93E-07
Protein Kinase C	PW_PKC_M._MUSC.	CI	52	31.96	2.14E-04
Tumor Necrosis Factor (TNF Superfamily, Member 2)	PW_TNF_M._MUSC.	CI	34	18.36	2.68E-04
		MM	37	20.69	2.83E-04
Toll Like Receptor	PW_TOLL_M._MUSC.	CI	22	10.14	3.78E-04
		MM	30	11.43	4.96E-07
Signal Transducer And Activator Of Transcription	PW_STAT_M._MUSC.	CI	35	19.89	5.86E-04
		MM	43	22.41	1.58E-05
Macrophage Stimulating 1 Receptor (C MET Related Tyrosine Kinase) (RON)	PW_MST1R_M._MUSC.	CI	5	0.81	5.92E-04
Lymphotoxin Alpha (TNF Superfamily, Member 1)	PW_LTA_M._MUSC.	CI	6	1.29	1.05E-03
		MM	6	1.45	1.96E-03
Myeloid Differentiation Primary Response Gene (88)	PW_MYD88_M._MUSC.	CI	17	7.89	1.85E-03
		MM	23	8.89	1.42E-05
Cyclin E	PW_CCNE_M._MUSC.	CI	9	2.98	2.11E-03
Interleukin 10	PW_IL10_M._MUSC.	CI	16	7.33	2.16E-03
		MM	17	8.26	2.91E-03
Interleukin 18 (Interferon Gamma Inducing Factor)	PW_IL18_M._MUSC.	CI	10	3.70	2.99E-03
		MM	12	4.17	5.95E-04
Parathyroid Hormone	PW_PTH_M._MUSC.	CI	12	4.99	3.35E-03
Cystic Fibrosis Transmembrane Conductance Regulator (ATP Binding Cassette Subfamily C, Member 7)	PW_CFTR_M._MUSC.	CI	7	2.17	4.48E-03
Minichromosome Maintenance Complex	PW_MCM_M._MUSC.	CI	6	1.69	5.01E-03
Interleukin 12	PW_IL12_M._MUSC.	CI	13	5.96	5.52E-03
		MM	17	6.71	2.47E-04
B Cell CLL/Lymphoma 2	PW_BCL2_M._MUSC.	CI	18	9.66	6.95E-03
Interleukin 1 Receptor	PW_IL1R_M._MUSC.	CI	7	2.42	8.32E-03
Hepatocyte Growth Factor Receptor	PW_HGF_M._MUSC.	CI	13	6.36	9.64E-03
		MM	15	7.17	4.29E-03
Leukemia Inhibitory Factor Receptor	PW_LIF_M._MUSC.	MM	8	2.18	8.58E-04
Tyrosine Kinase 2	PW_TYK2_M._MUSC.	MM	10	3.63	2.39E-03
Interleukin 6 Signal Transducer (GP130, Oncostatin M Receptor)	PW_IL6ST_M._MUSC.	MM	8	2.72	4.20E-03
Tumor Necrosis Factor Receptor Superfamily (FAS, RANK, ETC.)	PW_TNFRSF_M._MUSC.	MM	28	16.97	5.12E-03

26

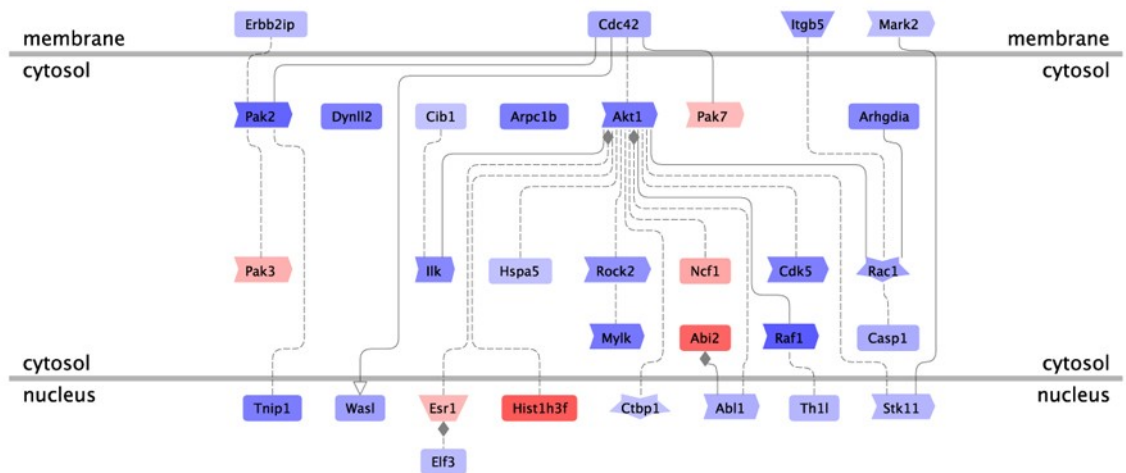


Figure 26. P21-activated kinase pathway.

Signal transduction pathway with the highest significance found in both Rag2^{-/-} and Rag2^{-/-} x IL-10^{-/-} recipients following Wt CD4⁺ CD25⁻ T cells transfer. Genes upregulated are displayed in blue, genes downregulated in red. Adopted from GePS.

27

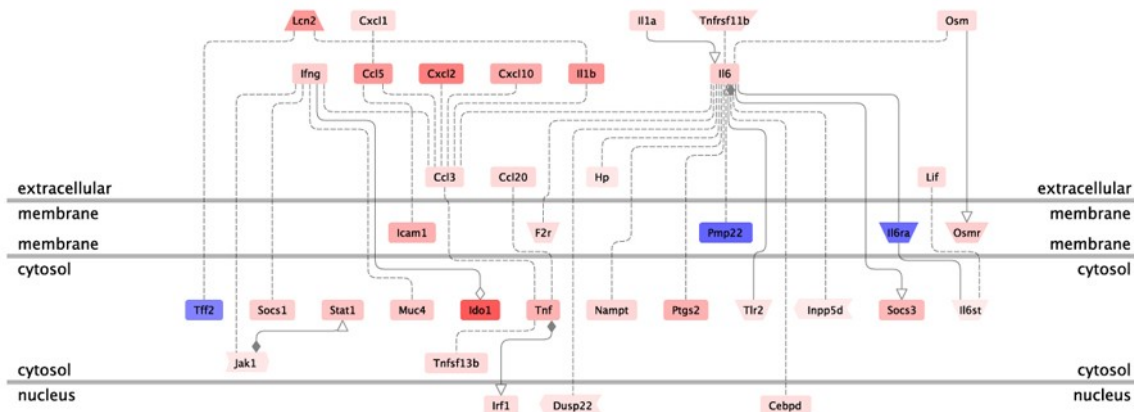


Figure 27. Interleukin 6 pathway.

Signal transduction pathway with the highest significance found in both Rag2^{-/-} and Rag2^{-/-} x IL-10^{-/-} recipients following IL-10^{-/-} CD4⁺ CD25⁻ T cells transfer. Genes upregulated are displayed in blue, genes downregulated in red. Adopted from GePS.

4.4.3. Genes best correlated to the histological score in IEC upon CD4⁺ T cell transfer

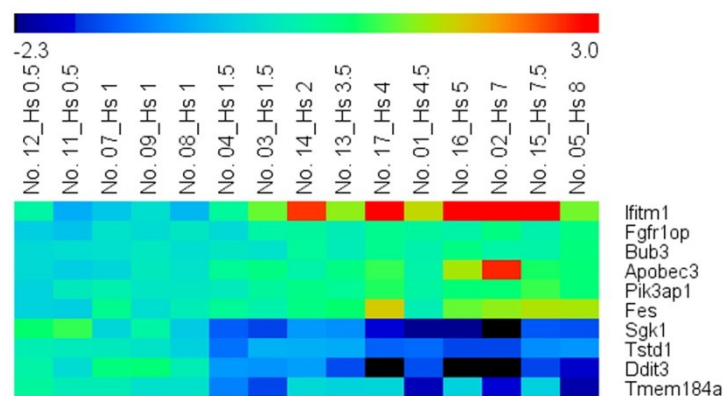
Correlations between gene expression levels and histological scores were calculated using the Spearman's rank correlation coefficient (r_s), a non-parametric measure of statistical dependence. Genes best correlated to the histological score of the cecum, colon or the cumulative score are given in **tables 26-31** for both recipient mouse strains. All genes with expression levels displaying a correlation $r_s > 0.8$, generally considered as strong correlation, are comprised in **table A2** for Rag2^{-/-} recipients and **table A3** for Rag2^{-/-} x IL-10^{-/-} recipients. Complementary heatmaps and graphs plotting gene intensity (according to MADMAX software) vs histological score of best correlated genes can be found in **figures 28-33**. Several of the most highly regulated genes also appeared among the genes which were best correlated to tissue pathology, including *Ido1* and *Cyp2c55*. Other genes showing a strong correlation are involved in immune responses (e.g. *Lbp*, *Ccl3*), response to hypoxia (e.g. *Edu1*, *Nox*) and epithelial to mesenchymal transisiton (*Nfatc1*) which is linked to fibrosis/fistulae in IBD [245,246], but also genes assigned to metabolic pathways (e.g. *Nceh*, *Aadac*).

Table 26. Genes best correlated to the histological score (cecum) in IEC of Rag2^{-/-} recipients 4 weeks after CD4⁺ T cell transfer according to Spearman's rank correlation (r_s) and using gene intensities obtained by MADMAX software. The one-sided significance for r_s was $P < 0.001$ for all genes.

TOP10 genes best correlated (r_s) to histological score (cecum) in Rag2^{-/-} recipients

gene ID	gene name	description	(r_s)	GO-BP descriptions	GO-MF descriptions	GO-CC descriptions
68713	Ifitm1	interferon induced transmembrane protein 1	0.88	anterior/posterior pattern formation	molecular_function	integral to membrane
75296	Fgfr1op	Fgfr1 oncogene partner	0.87	biological process	molecular function	cellular component
12237	Bub3	budding uninhibited by benzimidazoles 3 homolog	0.86	cell cycle /// mitosis	NA	kinetochore /// nucleus
80287	Apobec3	apolipoprotein B mRNA editing enzyme, catalytic polypeptide 3	0.85	NA	catalytic activity	nucleus /// cytoplasm
83490	Pik3ap1	phosphoinositide-3-kinase adaptor protein 1	0.85	signal transduction	protein binding	membrane /// nucleus
14159	Fes	feline sarcoma oncogene	0.85	protein phosphorylation	nucleotide/protein binding	cytosol
20393	Sgk1	serum/glucocorticoid regulated kinase 1	-0.84	apoptosis	protein serine/threonine kinase	endoplasmic reticulum /// cytoplasm
226654	Tstd1	thiosulfate sulfurtransferase -like domain containing 1	-0.85	biological process	molecular function	mitochondrion
13198	Ddit3	DNA-damage inducible transcript 3	-0.85	ER overload response	transcription factor activity	nucleus /// cytoplasm
231832	Tmem184a	transmembrane protein 184a	-0.85	NA	NA	integral to membrane

28A



B

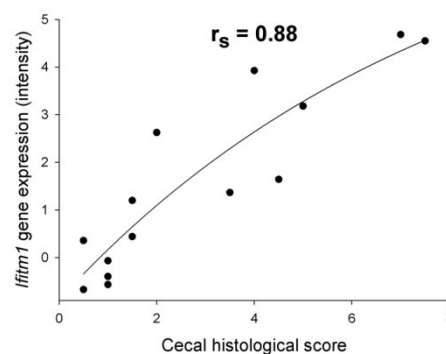


Figure 28. Genes best correlated to the histological score (cecum) in IEC of Rag2^{-/-} recipients 4 weeks after CD4⁺ T cell transfer according to r_s and using gene intensities obtained by MADMAX software.

(A) Heatmap (B) Best correlated gene: interferon induced transmembrane protein 1 (*Ifitm1*); intensity vs histological score.

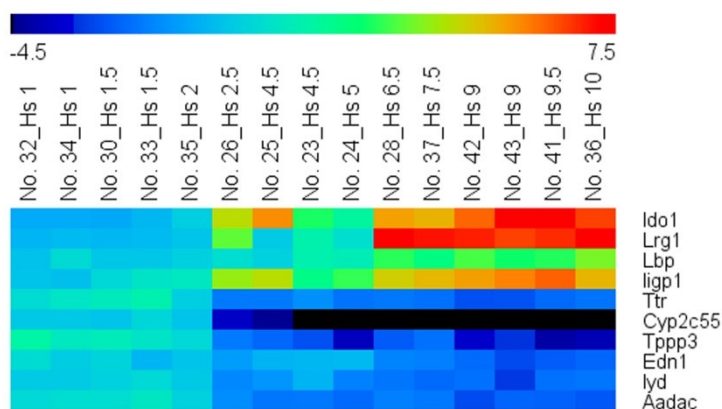
RESULTS

Table 27. Genes best correlated to the histological score (cecum) in IEC of Rag2^{-/-} x IL-10^{-/-} recipients 4 weeks after CD4⁺ T cell transfer according to Spearman's rank correlation (r_s) and using gene intensities obtained by MADMAX software. The one-sided significance for r_s was $P < 0.001$ for all genes.

TOP10 genes best correlated (r_s) to histological score (cecum) in Rag2^{-/-} x IL-10^{-/-} recipients

gene ID	gene name	description	(r_s)	GO-BP descriptions	GO-MF descriptions	GO-CC descriptions
15930	Ido1	indoleamine 2,3-dioxygenase 1	0.92	involved in inflammatory response	tryptophan 2,3-dioxygenase activity	cytosol /// cytoplasm
76905	Lrg1	leucine-rich alpha-2-glycoprotein 1	0.92	brown fat cell differentiation	molecular function	cellular component
16803	Lbp	lipopolysaccharide binding protein	0.90	innate immune response	lipoteichoic acid binding	extracellular region
60440	ligp1	interferon inducible GTPase 1	0.90	GTP catabolic process	GTPase activity	cellular component
22139	Ttr	transthyretin	-0.89	transport	hormone activity	extracellular region
72082	Cyp2c55	cytochrome P450, family 2, subfamily c, polypeptide 55	-0.89	oxidation reduction	electron carrier activity	endoplasmic reticulum
67971	Tppp3	tubulin polymerization-promoting protein family member 3	-0.89	biological process	molecular function	cytoplasm /// cytoskeleton
13614	Edn1	endothelin 1	-0.89	response to hypoxia	protein binding /// receptor binding	extracellular space
70337	lyd	iodotyrosine deiodinase	-0.90	oxidation reduction	iodide peroxidase activity	integral to membrane
67758	Aadac	arylacetamide deacetylase (esterase)	-0.91	regulation of triglyceride catabolic process	carboxylesterase activity	endoplasmic reticulum

29A



B

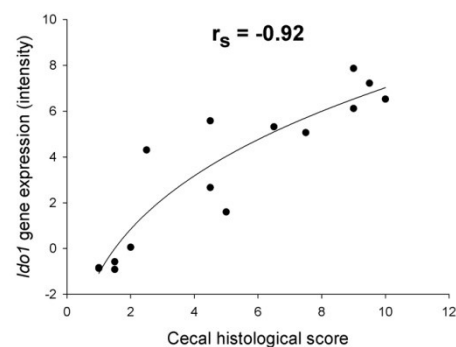


Figure 29. Genes best correlated to the histological score (cecum) in IEC of Rag2^{-/-} x IL-10^{-/-} recipients 4 weeks after CD4⁺ T cell transfer according to r_s and using gene intensities obtained by MADMAX software.

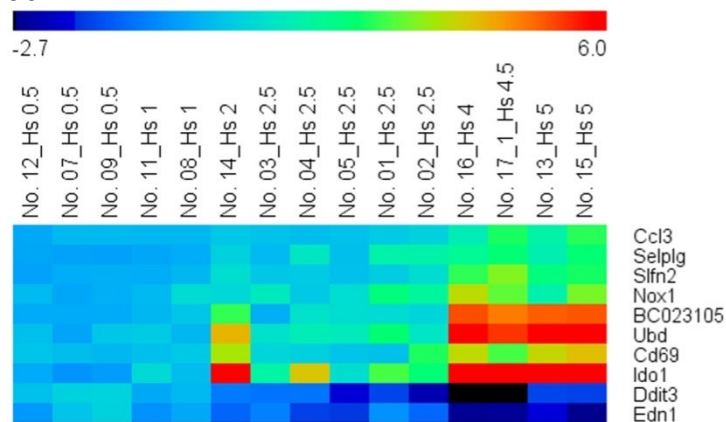
(A) Heatmap (B) Best correlated gene: indoleamine 2,3-dioxygenase 1 (*Ido1*); intensity vs histological score.

Table 28. Genes best correlated to the histological score (colon) in IEC of Rag2^{-/-} recipients 4 weeks after CD4⁺ T cell transfer according to Spearman's rank correlation (r_s) and using gene intensities obtained by MADMAX software. The one-sided significance for r_s was $P < 0.001$ for all genes.

TOP10 genes best correlated (r_s) to histological score (colon) in Rag2^{-/-} recipients

gene ID	gene name	description	(r_s)	GO-BP descriptions	GO-MF descriptions	GO-CC descriptions
20302	Ccl3	chemokine (C-C motif) ligand 3	0.91	inflammatory response	cytokine/chemokine activity	extracellular space
20345	Selplg	selectin, platelet (p-selectin) ligand	0.91	cell adhesion	protein binding /// sugar binding	plasma membrane
20556	Sfn2	schlafen 2	0.90	regulation of cell proliferation	NA	NA
237038	Nox1	NADPH oxidase 1	0.90	response to ROS	electron carrier activity	integral to membrane
667597	BC023105	cDNA sequence BC023105	0.90	NA	NA	NA
24108	Ubd	ubiquitin D	0.88	protein ubiquitination	protein binding	nucleus /// cytoplasm
12515	Cd69	CD69 antigen	0.88	NA	calcium binding /// sugar binding	integral to membrane
15930	Ido1	indoleamine 2,3-dioxygenase 1	0.88	involved in inflammatory response	tryptophan 2,3-dioxygenase activity	cytosol /// cytoplasm
13198	Ddit3	DNA-damage inducible transcript 3	-0.87	ER overload response	transcription factor activity	nucleus /// cytoplasm
13614	Edn1	endothelin 1	-0.89	response to hypoxia	protein binding /// receptor binding	extracellular space

30A



B

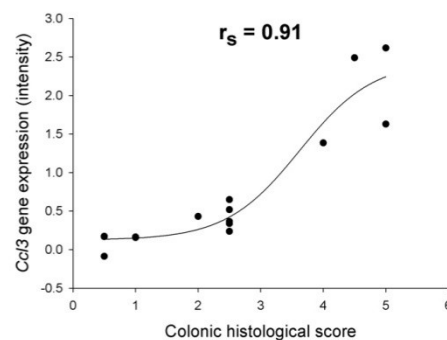


Figure 30. Genes best correlated to the histological score (colon) in IEC of Rag2^{-/-} recipients 4 weeks after CD4⁺ T cell transfer according to r_s and using gene intensities obtained by MADMAX software.

(A) Heatmap (B) Best correlated gene: chemokine (C-C motif) ligand 3 (*Ccl3*); intensity vs histological score.

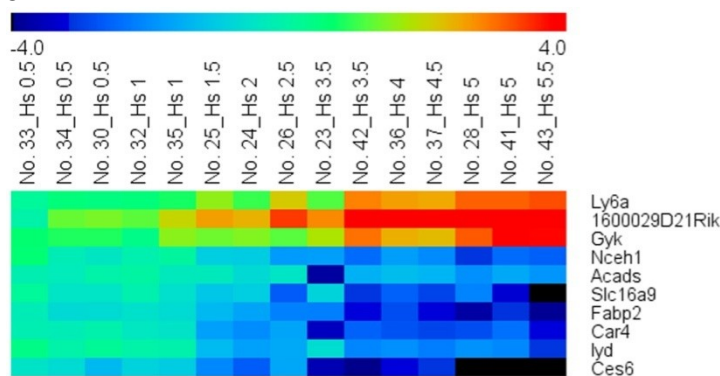
RESULTS

Table 29. Genes best correlated to the histological score (colon) in IEC of Rag2^{-/-} x IL-10^{-/-} recipients 4 weeks after CD4⁺ T cell transfer according to Spearman's rank correlation (r_s) and using gene intensities obtained by MADMAX software. The one-sided significance for r_s was $P < 0.001$ for all genes.

TOP10 genes best correlated (r_s) to histological score (colon) in Rag2^{-/-} x IL-10^{-/-} recipients

gene ID	gene name	description	(r_s)	GO-BP descriptions	GO-MF descriptions	GO-CC descriptions
110454	Ly6a	lymphocyte antigen 6 complex, locus A	0.96	NA	NA	anchored to membrane
76509	Plet	Placenta-expressed transcript 1 1600029D21Rik	0.93	wound healing	NA	integral to membrane
14933	Gyk	glycerol kinase	0.92	carbohydrate metabolic process	nucleotide binding /// histone binding	nucleus /// cytoplasm /// mitochondrion
320024	Nceh1	arylacetamide deacetylase-like 1	-0.91	lipid catabolic process	carboxylesterase activity	endoplasmic reticulum
11409	Acads	acyl-Coenzyme A dehydrogenase, short chain	-0.91	oxidation reduction	oxidoreductase activity	mitochondrion
66859	Slc16a9	solute carrier family 16, member 9	-0.91	transmembrane transport	symporter activity	integral to membran
14079	Fabp2	fatty acid binding protein 2, intestinal	-0.92	long-chain fatty acid transport	fatty acid binding /// lipid binding	membrane /// microvillus ///
12351	Car4	carbonic anhydrase 4	-0.92	one-carbon metabolic process	metal ion binding /// lyase activity	anchored to membrane
70337	lyd	iodotyrosine deiodinase	-0.92	oxidation reduction	iodide peroxidase activity	integral to membrane
102022	Ces6	carboxylesterase 6	-0.92	protein amino acid glycosylation	hydrolase activity	microsome

31A



B

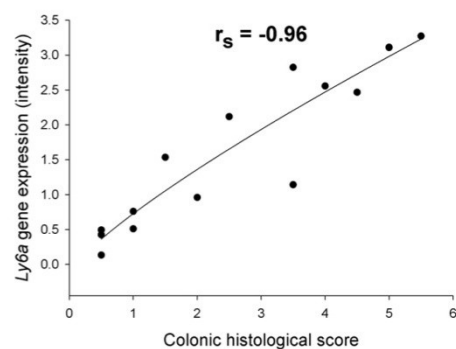


Figure 31. Genes best correlated to the histological score (colon) in IEC of Rag2^{-/-} x IL-10^{-/-} recipients 4 weeks after CD4⁺ T cell transfer according to r_s and using gene intensities obtained by MADMAX software.

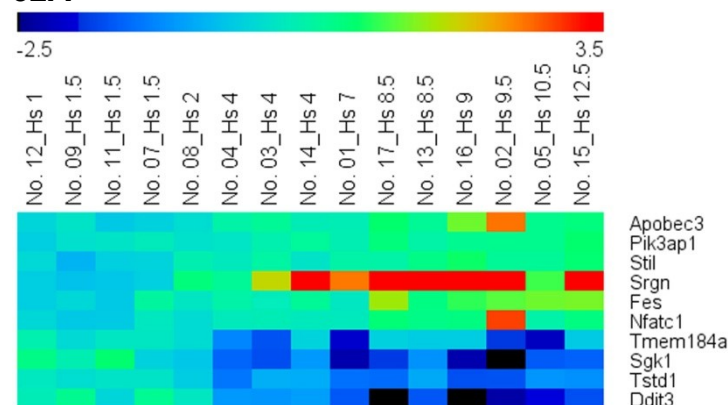
(A) Heatmap (B) Best correlated gene: lymphocyte antigen 6 complex, locus A (*Ly6a*); intensity vs histological score.

Table 30. Genes best correlated to the histological score (cumulative) in IEC of Rag2^{-/-} recipients 4 weeks after CD4⁺ T cell transfer according to Spearman's rank correlation (r_s) and using gene intensities obtained by MADMAX software. The one-sided significance for r_s was $P < 0.001$ for all genes.

TOP10 genes best correlated (r_s) to histological score (cumulative) in Rag2^{-/-} recipients

gene ID	gene name	description	(r_s)	GO-BP descriptions	GO-MF descriptions	GO-CC descriptions
80287	Apobec3	apolipoprotein B mRNA editing enzyme, catalytic polypeptide 3	0.90	NA	catalytic activity	nucleus /// cytoplasm
83490	Pik3ap1	phosphoinositide-3-kinase adaptor protein 1	0.90	signal transduction	protein binding	membrane /// nucleus
20460	Stil	Scl/Tal1 interrupting locus	0.89	negative regulation of apoptosis	NA	cytoplasm
19073	Srgn	serglycin	0.88	regulation of cytokine secretion	protein binding	Golgi membrane /// zymogen granule
14159	Fes	feline sarcoma oncogene	0.87	protein phosphorylation	nucleotide/ protein binding	cytosol
18018	Nfatc1	nuclear factor of activated T-cells, cytoplasmic, calcineurin-dependent 1	0.87	epithelial to mesenchymal transition	transcription activator activity	nucleus /// cytoplasm
231832	Tmem184a	transmembrane protein 184a	-0.87	NA	NA	integral to membrane
20393	Sgk1	serum/glucocorticoid regulated kinase 1	-0.88	apoptosis	protein serine/threonine kinase	endoplasmic reticulum /// cytoplasm
226654	Tstd1	thiosulfate sulfurtransferase -like domain containing 1	-0.89	biological process	molecular function	mitochondrion
13198	Ddit3	DNA-damage inducible transcript 3	-0.91	ER overload response	transcription factor activity	nucleus /// cytoplasm

32A



B

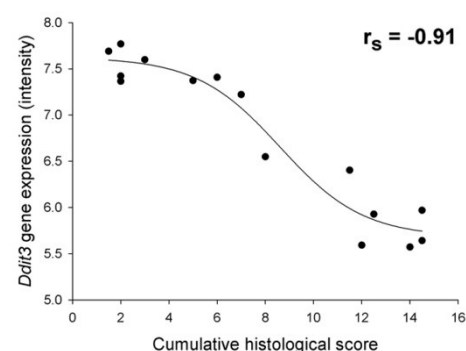


Figure 32. Genes best correlated to the histological score (cumulative) in IEC of Rag2^{-/-} recipients 4 weeks after CD4⁺ T cell transfer according to r_s and using gene intensities obtained by MADMAX software.

(A) Heatmap (B) Best correlated gene: DNA-damage inducible transcript 3 (*Ddit3*); intensity vs histological score.

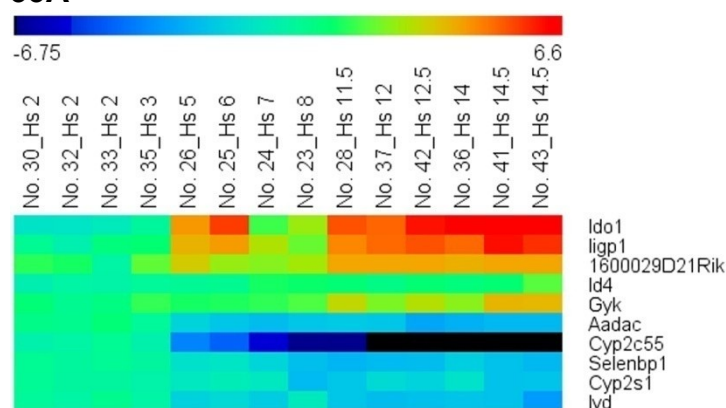
RESULTS

Table 31. Genes best correlated to the histological score (cumulative) in IEC of Rag2^{-/-} x IL-10^{-/-} recipients 4 weeks after CD4⁺ T cell transfer according to Spearman's rank correlation (r_s) and using gene intensities obtained by MADMAX software. The one-sided significance for r_s was P<0.001 for all genes.

TOP10 genes best correlated (r_s) to histological score (cumulative) in Rag2^{-/-} x IL-10^{-/-} recipients

gene ID	gene name	description	(r_s)	GO-BP descriptions	GO-MF descriptions	GO-CC descriptions
15930	Ido1	indoleamine 2,3-dioxygenase 1	0.93	involved in inflammatory response	tryptophan 2,3-dioxygenase activity	cytosol /// cytoplasm
60440	ligp1	interferon inducible GTPase 1	0.92	GTP catabolic process	GTPase activity	cellular component
76509	Plet	Placenta-expressed transcript 1 1600029D21Rik	0.91	wound healing	NA	integral to membrane
15904	Id4	inhibitor of DNA binding 4	0.91	regulation of transcription process	transcription regulator activity	nucleus
14933	Gyk	glycerol kinase	0.90	carbohydrate metabolic process	nucleotide binding /// histone binding	nucleus /// cytoplasm /// mitochondrion
67758	Aadac	arylacetamide deacetylase (esterase)	-0.90	regulation of triglyceride catabolic process	carboxylesterase activity	endoplasmic reticulum
72082	Cyp2c55	cytochrome P450, family 2, subfamily c, polypeptide 55	-0.91	oxidation reduction	electron carrier activity	endoplasmic reticulum
20341	Selenbp1	selenium binding protein 1	-0.91	protein transport	selenium binding	nucleus /// cytoplasm
74134	Cyp2s1	cytochrome P450, family 2, subfamily s, polypeptide 1	-0.91	oxidation reduction	monooxygenase activity	endoplasmic reticulum
70337	lyd	iodotyrosine deiodinase	-0.93	oxidation reduction	iodide peroxidase activity	integral to membrane

33A



B

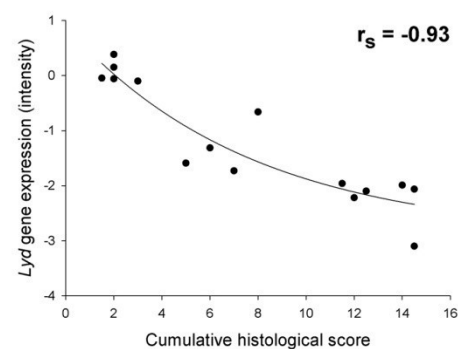


Figure 33. Genes best correlated to histological score (cumulative) in IEC of Rag2^{-/-} x IL-10^{-/-} recipients 4 weeks after CD4⁺ T cell transfer according to r_s and using gene intensities obtained by MADMAX software.

(A) Heatmap (B) Best correlated gene: iodotyrosine deiodinase (*Lyd*); intensity vs histological score.

4.4.4. Genes best correlated to the presence of IL-10 in IEC under non-inflammatory conditions

The Spearman's rank correlation test can assess the dependence also of ordinaly scaled data, in this case enabling the assignment of values to IL-10 presence under non-inflammatory conditions and calculating correlations between IL-10 presence and gene expression levels. For assigning these values, the best distinguishable situations were chosen. The values were set to 0 for unreconstituted Rag2^{-/-} x IL-10^{-/-} mice; to 1 for unreconstituted Rag2^{-/-} mice and to 2 for Rag2^{-/-} x IL-10^{-/-} mice reconstituted with Wt CD4⁺ CD25⁺ T cells. All genes displaying a correlation $r_s > 0.8$ are comprised in **table A4**, best correlated genes, the respective heatmap and dot plot can be found in **table 32** and **figure 34**. Of note, the gene best correlated as well as the gene best negatively correlated to IL-10 presence, *Clic6* and *Pth* respectively, are both involved in cellular calcium homeostasis. Furthermore, several genes participating in metabolic processes (*Soc2b*, *Ggt1*, *Gbgt1*), associated with MAP kinase signaling (*Gadd45γ*, *Mapkapk3*) and transcription factors (*Hoxd13*, *Rnf14*) were found to be highly correlated to IL-10 presence.

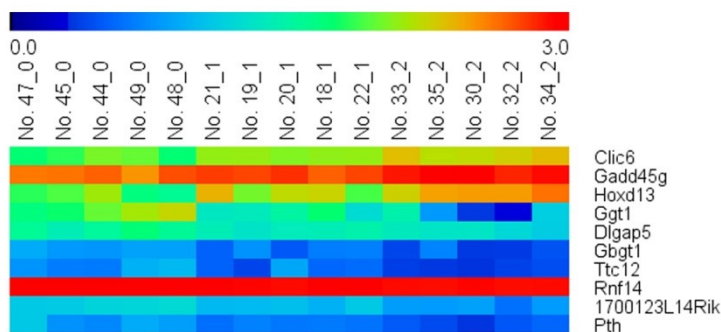
RESULTS

Table 32. Genes best correlated to the presence of non-T cell-/ T cell-derived IL-10 in IEC of recipients 4 weeks after non-colitogenic CD4⁺ CD25⁺ T cell transfer according to Spearman's rank correlation (r_s) and using gene intensities obtained by MADMAX software. The values assigned to the presence of IL-10 were: 0 for unreconstituted Rag2^{-/-} x IL-10^{-/-} mice; 1 for unreconstituted Rag2^{-/-} mice and 2 for Rag2^{-/-} x IL-10^{-/-} mice reconstituted with Wt CD4⁺ CD25⁺ T cells. The one-sided significance for r_s was P<0.001 for all genes.

TOP10 genes best correlated (r_s) to the presence of IL-10^{-/-}

gene ID	gene name	description	(r_s)	GO-BP descriptions	GO-MF descriptions	GO-CC descriptions
209195	Clic6	chloride intracellular channel 6	0.94	ion transport	voltage-gated ion channel activity	integral to membrane
23882	Gadd45g	growth arrest and DNA-damage-inducible 45 gamma	0.91	activation of MAPKK activity	protein binding	nucleus
15433	Hoxd13	homeobox D13	0.87	regulation of transcription	transcription regulator activity	nucleus
14598	Ggt1	gamma-glutamyltransferase 1	-0.87	glutathione biosynthesis	gamma-glutamyl-transferase	integral to membrane
56736	Rnf14	ring finger protein 14	-0.87	regulation of transcription	small conjugating protein ligase	nucleus /// cytoplasm
218977	Dlgap5	discs, large (Drosophila) homolog-associated protein 5	-0.87	cell cycle /// cell-cell signaling	NA	nucleus /// cytoskeleton
227671	Gbgt1	globoside alpha-1,3-N-acetylgalactosaminyl-transferase 1	-0.87	carbohydrate metabolic process	metal ion binding /// transferase activity	integral to membrane /// Golgi apparatus
235330	Ttc12	tetratricopeptide repeat domain 12	-0.87	biological process	molecular function	cellular component
78482	1700123L14Rik	nucleoporin 50 pseudogene	-0.93	intracellular transport	molecular function	cellular component
19226	Pth	parathyroid hormone	-0.94	cellular calcium ion homeostasis	hormone activity	extracellular space

34A



B

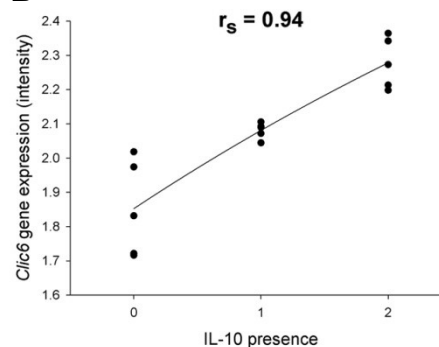


Figure 34. Genes best correlated to the presence of non-T cell-/ T cell-derived IL-10 in IEC of recipients 4 weeks after non-colitogenic CD4⁺ CD25⁺ T cell transfer according to r_s and using gene intensities obtained by MADMAX software.

The values assigned to the presence of IL-10 were: 0 for unreconstituted Rag2^{-/-} x IL-10^{-/-} mice; 1 for unreconstituted Rag2^{-/-} mice and 2 for Rag2^{-/-} x IL-10^{-/-} mice reconstituted with Wt CD4⁺ CD25⁺ T cells. (A) Heatmap (B) Best correlated gene: chloride intracellular channel 6 (*Clic6*); intensity vs histological score.

5 DISCUSSION

Although ER stress has been identified to participate during the onset and the course of neoplasia, metabolic diseases and inflammation [12-14], and functional alterations of the mitochondria and energy metabolism in general have been implicated in these diseases [191,193,247], little is known regarding the cooperation of ER and mitochondria in the development of these pathological conditions.. Considering our finding that PKR is specifically induced under mitochondrial stress and the recent finding that PKR integrates inflammatory signaling and metabolic homeostasis [248], leads to the suggestion that PKR represents a possible link between metabolic and intestinal diseases. Moreover, mtUPR has been implicated in cancer cell survival, demonstrating the disease-relevance of this pathway [144]. Mitochondria and ER interact physically and functionally [172]; consistently, ER stress impacts mitochondrial gene expression [166,190] and *vice versa* mitochondria have been shown to modulate ER UPR [191-193].

5.1 PKR

Interestingly, we found that the highly selective mitochondrial UPR pathway employs PKR to recruit ER UPR-associated signaling molecules, namely eIF2 α , cJun (AP1) and CHOP (**Fig.35**). Although we did not find evidence for a contribution of PKR to ER UPR in our experimental settings, it has been reported that PKR participates in thapsigargin-induced ER stress and apoptosis [223] and contributes to GRP94 induction under ER stress [222] and is involved in ER stress-induced neuronal cell death [249]. Moreover, PKR-mediated eIF2 α phosphorylation has been shown to be responsible, at least in part, for the translational inhibition of cytoprotective inducible heat shock proteins in colonic IEC under inflammatory conditions [250]. Significantly, Nakamura et al. suggest that PKR-coordinated sensing and signaling may represent a central mechanism for the integration of innate immunity with metabolic pathways that are critical in metabolic diseases [248]. PKR can be activated by various triggers including dsRNA, TLRs, growth receptor signaling, cytokines, palmitic acid, metabolic stress and in response to cell stress [52,248]. In turn, it is able to modulate tumor necrosis factor (TNF)-induced signaling [230], cJun N-terminal kinase (JNK) and I κ B kinase (IKK) [52,230] activity and can induce insulin receptor substrate (IRS) phosphorylation at serine 307 thereby blocking insulin action [248]. These broad functions of PKR are reflected by the observation that *Pkr*^{-/-} mice, in response to high fat diet, exhibit significantly reduced levels of several inflammatory cytokines such as TNF, IL-6, and IL-1 β , and the anti-inflammatory cytokine IL-10, a potential target of PKR-signaling [248,251].

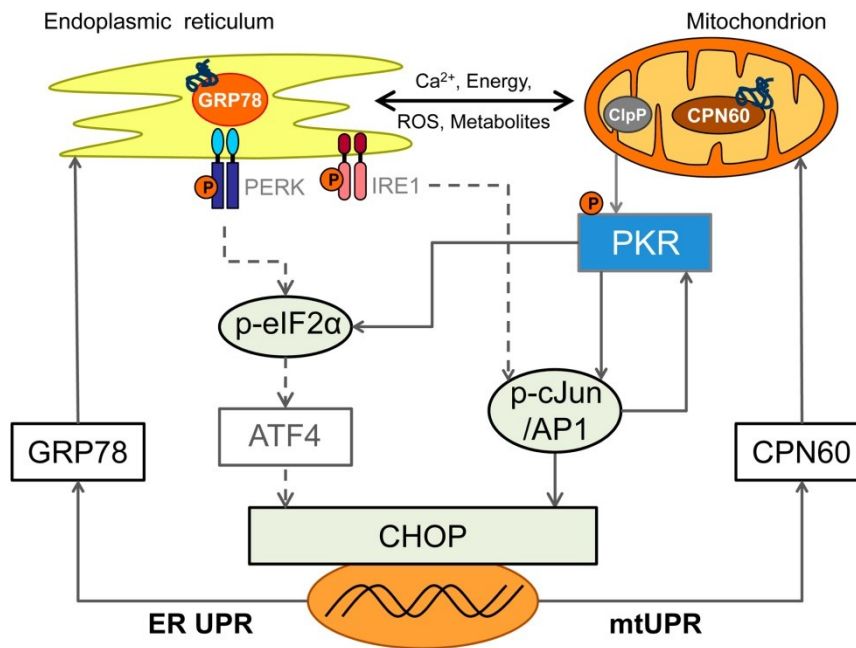


Figure 35. Schematic illustration of mitochondrial- and ER UPR integration.

PKR is activated by ClpP-dependent mtUPR-signaling and in turn induces its own transcription via MEK, JNK2/3 and AP1. Enhanced PKR signaling then amplifies eIF2 α - and cJun phosphorylation thereby inducing CHOP expression, leading to transcriptional activation of the *Cpn60* gene. ER- and mtUPR signaling converge at the level of eIF2 α phosphorylation and the activation of transcription factors AP1 and CHOP. As a consequence of ER- and mtUPR, nuclear encoded compartment specific chaperones such as GRP78 and CPN60 are induced.

Regarding the diverse properties of PKR, one cannot exclude the possibility that the induction of PKR seen in both animal models and in the human patients is not, or not solely, due to mitochondrial signaling. However, our finding that PKR is selectively induced during mtUPR and acts in concert with ER UPR-derived signals, implicates that PKR is a central player in mitochondrial-nuclear communication.

5.2 Mitochondrial UPR signaling

Our data indicate that in mammalian cells, like in *C.elegans*, the efflux of peptides resulting from the activity of ClpP may provide the initial signal for mtUPR [23]. Several possibilities have been suggested how ClpP-generated peptides might activate downstream-signaling [141,143]. Since peptides released from mitochondria in a HAF-1-dependent manner originate from a broad spectrum of mainly matrix-localized proteins and differ in amino acid composition and length [141], rather the rate of efflux than the peptides themselves might provide a specific signal. Yet, the presence of a peptide-specific receptor cannot be ruled out [141]. Alternatively, ClpP-mediated proteolysis might release a non-peptide ligand which is subsequently transported by HAF-1 [141]. Of note, the related

mammalian ABC transporter ABCB10 has been implicated in heme transport across the mitochondrial inner membrane [252].

Alongside, it has been supposed that a mechanism analogous to the ER UPR, where sensing of stress appears via binding of GRP78 to unfolded proteins [53], may exist in mitochondria through the association of CPN60 with mutant proteins [128], targeting them for proper reassembly or degradation (**Fig.36**). In this context, it is noteworthy that OTCA has already been shown to co-immunoprecipitate with CPN60 as well as ClpP [21].

Free cytosolic Ca^{2+} is a key player in mitochondria-to-nucleus signaling, the so-called retrograde signaling [128]. Furthermore, it has been suggested that Ca^{2+} release from the ER activates PKR via CaMKII and that PACT is involved in this activation [227]. Nevertheless, we did neither find evidence for a contribution of Ca^{2+} and CaMKII nor PACT in our experimental setup. To specify the cytosolic signal leading to PKR activation under mtUPR, further investigations are needed.

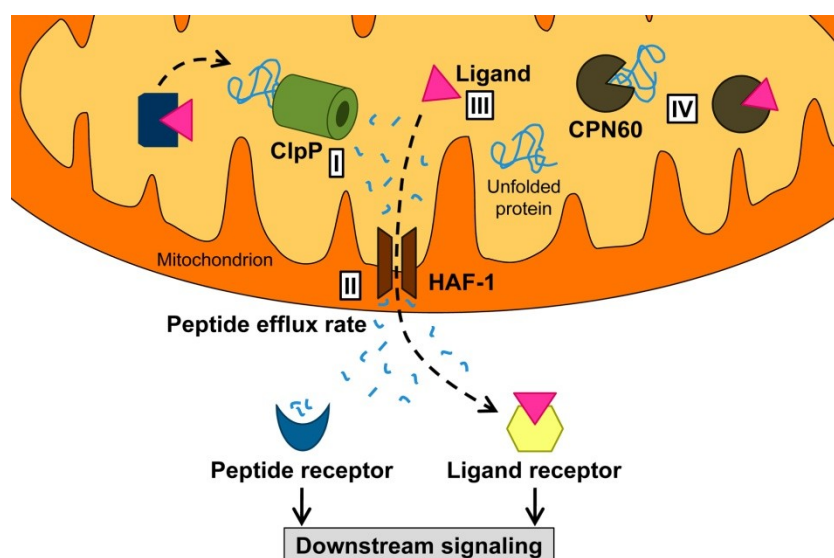


Figure 36. Proposed mechanisms of mtUPR-induction.

(Modified from Kirstein-Miles et al., and Haynes et al.) Under mitochondrial stress, ClpP degrades unfolded proteins which are released from mitochondria in a HAF-1-dependent manner. The resulting peptides (I) might activate a cytosolic peptide receptor or the efflux rate of peptides might provide a signal (II). Alternatively, ClpP-activity might release a specific ligand (III) with a cytosolic receptor. The association of CPN60 with unfolded proteins represents another possibility for mtUPR-induction (IV).

5.3 $Pkr^{-/-}$ mice

Strikingly, $Pkr^{-/-}$ mice showed almost complete resistance to DSS-induced colitis associated with loss of CPN60 expression and decreased mitochondrial abundance in IEC upon DSS treatment. Although it cannot be ruled out that the reduced sensitivity to DSS-induced colitis seen in our experimental setup is due to other functions of PKR, the early induction of PKR and CPN60 in control mice while CPN60 level remain unaltered in $Pkr^{-/-}$ mice, provide strong evidence for a role of PKR in stress-induced CPN60 expression. Concomitantly, DSS administration induced autophagy in IEC from treated mice, but diminished the expression of the mitochondrial biogenesis-associated transcription factor *Pgc-1 α* exclusively in $Pkr^{-/-}$ mice. Yet, baseline CPN60 protein levels were elevated in $Pkr^{-/-}$ mice as well as the mitochondrial to nucleic DNA ratio.

This implies (I) that PKR is only relevant to CPN60-induction and mitochondrial biogenesis under stress conditions and (II) that the potential beneficial absence of a stress signal amplifying ER UPR-signaling, might outweigh for the negative effects of a partial loss of mitochondria (**Fig.37**). Along this line, it might be possible that mitochondria-protective effect mediated by PKR might contribute to enhanced generation of ROS by damaged or dysfunctional mitochondria. Similarly, increased mitochondrial biogenesis as well as impaired fission and degradation of mitochondria, accompanying mitochondrial dysfunction and aggravating ROS production, has been implicated in ageing [253].

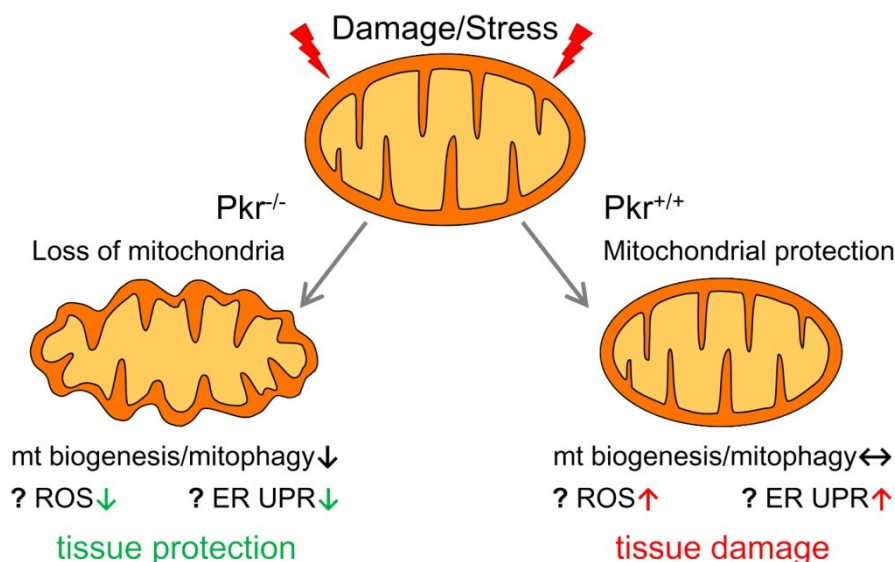


Figure 37. Possible consequences of PKR-signaling under stress conditions.

Genetic ablation of PKR leads to loss of mitochondrial abundance in IEC under DSS-treatment probably due to decreased mitochondrial biogenesis. The mitochondria-protective effect mediated by PKR might promote accumulation of dysfunctional mitochondria resulting in enhanced ROS production and in addition, ER UPR-signaling might be amplified.

5.4 Mitochondria as integrators of cellular danger signaling

Next to the well-established functions of mitochondria in cell metabolism and during apoptosis accumulating data have placed mitochondria at the center of diverse cellular functions and suggest mitochondria as integrators of various signaling pathways (**Fig.38**). As mentioned above, mitochondria participate in cellular calcium homeostasis and constitute a major source of cellular ROS [128,132], thereby affecting processes such as autophagy and inflammation [254-256]. Under conditions of nutrient deficiencies mitochondria have evolved mechanisms to regulate the cell cycle [257]. Additionally, they have been suggested to serve as a signaling platform by providing microdomains for molecule activation in their unique membrane environment [258]. Moreover, since the description of a protein located in the mitochondrial outer membrane, mitochondrial antiviral signaling (MAVS), required for the production of type I interferon in response to viral infection in 2005 [259], mitochondria are thought to modulate innate immune signaling. During viral infection, RIG-I binds single- or double-stranded RNA and is recruited to the mitochondrial outer membrane to bind MAVS, subsequently leading to activation of interferon-regulatory factors (IRF) and NF- κ B, and downstream to the production of IFN as well as proinflammatory cytokines [259,260]. Notably, with regard to mtUPR-induced PKR activation, PKR has also been shown to act in concert with mitochondria-dependent RIG-I/MAVS-signaling to mount an efficient IFN- β -secretion in response to rotavirus infection [261]. Recent work has confirmed the role of mitochondria in immune responses by linking mitochondrial ROS production and autophagy to the activation of the NLRP3 inflammasome [169,170] a multiprotein complex involved in proteolytic maturation and release of IL-1 β and IL-18 [262]. Notably, polymorphisms in *NLRP3* have been associated with CD in a candidate-gene study [263] and a SNP within the IL-18 receptor accessory protein gene (*IL18RAP*) has been identified as risk factor for both, CD as well as UC [264]. Consistently, IL-1 β as well as IL-18 expression is enhanced in IBD, particularly in the epithelium [265-267]. In line with these data, neutralization of IL-18 as well as genetic ablation of caspase-1, a downstream effector of the NALP3 inflammasome involved in IL-1 β and IL-18 processing [268], has been shown to ameliorated DSS colitis. Moreover, administration of anti-IL-1 β was effective in experimental rabbit complex colitis [269,270]. Therefore, it might be possible that the protective effect towards DSS-induced colitis seen in *Pkr*^{-/-} mice is related to inflammasome activation and IL-1 β and IL-18 production, respectively. Hence, future experiments should address this question. Interestingly, also ATG16L1, encoded by the CD-associated gene, has been demonstrated to regulate inflammasome activation [271].

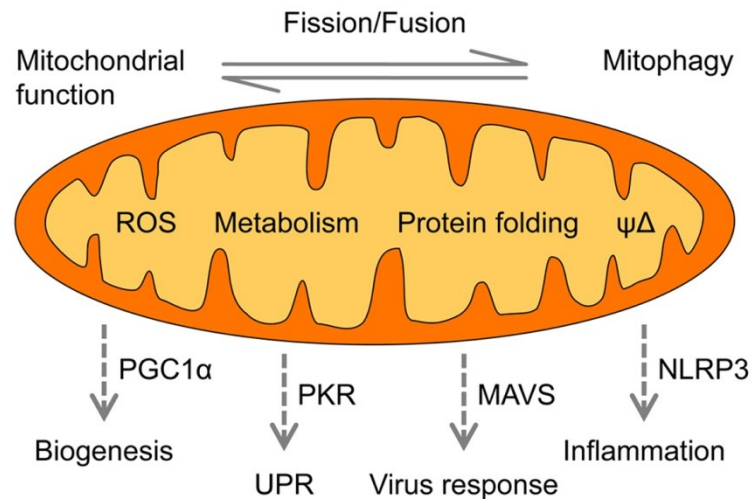


Figure 38. Mitochondria as integrators of cellular danger signaling.

Several cellular signaling pathways converge on mitochondria. Mitochondrial function is reflected by the protein folding environment in the matrix, metabolic rates, mitochondrial membrane potential ($\psi\Delta$) and generation of ROS. Whereas mitochondrial biogenesis-related pathways as well as mtUPR might serve to sustain a functional mitochondrial population, mitochondria additionally represent a signaling platform for inflammation-related signals.

5.5 ER UPR and mitochondrial dysfunction in IBD

During the last years, accumulating evidence implicated ER UPR at the epithelial cell level in promotion and perpetuation of intestinal inflammation [10,112,113] and at the same time, it has been sporadically suggested that chronic intestinal inflammation represents an energy-deficiency disease involving mitochondria and featuring alterations in epithelial cell oxidative metabolism [247,272]. Considering our findings, it is likely that mitochondrial and ER stress cannot be regarded separately and that mitochondrial stress, as well as ER stress, participates in the pathology of IBD.

Pathways including TLR signaling and autophagy, crucial for sensing and controlling the composition of the commensal microbiota, the key driver of intestinal inflammation in IBD, interact with ER UPR as well as mitochondrial signaling. Besides IBD-associated polymorphisms in autophagy- and bacterial sensing-related genes [115-118,122] a polymorphism leading to lower expression levels in the promoter of the gene encoding the mitochondrial carrier protein uncoupling protein (UCP) 2 was associated with CD as well as UC [273]. Consistently with CD patients harboring the *NOD2* or *ATG16L1* alleles [123-125], *NOD2*- as well as *XBP1*-deficient and *ATG16L1*-hypomorphic mice display alterations in Paneth cell structure and function, but in addition, *NOD1* and *NOD2* have been demonstrated to be critical for the autophagic response to invasive bacteria by recruiting *ATG16L1* to the bacterial entry site. Cells homozygous for the CD-associated frameshift mutation of *NOD2* failed to recruit *ATG16L1* and displayed impaired bacterial autophagy,

providing a functional link between the proteins encoded by the two most prominent CD-associated genes [274]. In contrast, IRGM as well as UCP2 directly impact mitochondrial function. By affecting mitochondrial fission, IRGM was shown to induce autophagy of intracellular mycobacteria but also to influence mitochondrial membrane polarization and cause Bax/Bak-dependent cell death, suggesting IRGM to be a double-edged sword in the context of intestinal inflammation [275]. On the other hand, UCP2 is thought to promote a metabolic shift from glucose oxidation to fatty acid oxidation and by controlling the speed of the Krebs cycle, decrease the production of mitochondrial ROS [276-278]. Macrophages stimulated with LPS have been shown to quickly down-regulate UCP2 in a TLR4- and MAP kinase-dependent manner to increase mitochondrial ROS production, thereby linking UCP2 and immune cell activation [279].

It has been suggested that chronic intestinal inflammation might represent an energy-deficiency disease involving the mitochondria and featuring alterations in epithelial cell oxidative metabolism [247,272]. In particular, β -oxidation is implicated in CD pathogenesis and a polymorphism in *SLC22A5* [280,281], encoding the carnitine transporter OCTN2, has been described as risk factor in IBD. Carnitine is essential to the energy metabolism of IEC by transporting long-chain fatty acids into mitochondria for β -oxidation [282]. Consequently, genetic ablation of OCTN2 as well as pharmacological inhibition of intestinal fatty acid β -oxidation also results in experimental colitis [283,284]. Sustaining β -oxidation and thereby energy supply might be particularly important in IEC metabolically challenged by alterations in the microbiota and/or in the context of energy-consuming inflammatory processes [8]. Furthermore, several pathogens and their toxins specifically target mitochondria to disrupt their function [285] and proinflammatory cytokine-evoked ROS generation is associated with a drop in mitochondrial membrane potential [286]. Contrarily, treating epithelial cells with the oxidative phosphorylation-uncoupler dinitrophenol (DNP) to induce mitochondrial stress, caused a decrease in TER and increased translocation of *E. coli* [287]. Supporting the relevance of these data, enterocytes of IBD patients have been reported to display swollen mitochondria with irregular cristae indicative of impaired function [288,289]. In accordance, reduced ATP levels have been found in the colon of some CD patients [290] and biopsies from patients with IBD can be more susceptible to uncouplers of oxidative phosphorylation [289].

Our results, demonstrating ER UPR as well as mtUPR to be activated in two murine models of chronic, immune-mediated colitis as well as human patients with IBD, further emphasizes the importance of mitochondrial signaling in intestinal inflammation. Moreover, identifying PKR as mtUPR-mediator as well as integrator of ER UPR- and mtUPR-signaling, strengthens the hypothesis of interrelated, disease-relevant organelle signaling.

5.6 Screening for potential new target genes and cellular pathways

Mouse models of IBD have provided important insights into mechanisms that control intestinal homeostasis and regulation of intestinal inflammation. For example, an early finding in a T cell transfer models of colitis was the proinflammatory activity of TNF [291] and an anti-TNF therapy has since been successfully implemented in IBD treatment [292]. Functional and genetic studies have highlighted the importance of IL-10 and IL-10-associated signaling in mouse models of intestinal inflammation as well as in IBD [8]. Previous studies suggested that IL-10 may directly confer protective mechanisms to the intestinal epithelium by affecting ER UPR [112]. The identification of new target genes is essential to elucidate the molecular mechanisms employed by IL-10 to confer protection to IEC. *Vice versa*, screening for alterations associated with tissue pathology might offer new strategies to interfere with disease progression.

In addition to the proteomic approach, we used microarray analysis to get a global impression of inflammation associated changes in IEC. Gene expression profiling can detect changes missed by gel-based proteome approaches due to the technical limitations of these methods [217]. However, changes in mRNA level do not necessarily translate into altered protein expression or functional changes and therefore the relevance needs to be confirmed on additional levels. Another challenge is the analysis of the extensive data obtained by this method. We applied two strategies/software packages, ChipInspector as well as MADMAX software, to profit from the different strengths and focuses of each. Looking at selected GO terms from different domains in a hypothesis-driven way confirmed ER and mitochondria to be highly affected by inflammatory processes in IEC and indicated cellular stress pathways to be activated. In contrast, identifying the most highly regulated or best correlated genes can help generating new hypotheses or showing new aspects of already known mechanisms.

Among the genes identified in our approaches to be highly regulated or associated with tissue pathology or IL-10-signaling respectively, several are assigned to pathways/functions relevant to metabolism and host-microbe interaction. IEC as well as innate and adaptive immune system cooperate in maintaining a balanced composition of the microbiome, crucial for intestinal homeostasis. Interestingly, transfer of regulatory T cells induced expression levels of carcinoembryonic antigen-related cell adhesion molecule (CEACAM) 10. CEACAM10 can interact with other members of the family, whereby CEACAM1 and CEACAM6 have been shown to be responsible for altered colonization patterns seen in IBD by serving as ligand for bacteria [293,294]. Another striking finding is the decline of *Cyp2c55* expression under inflammatory conditions. This enzyme contributes to the detoxification of the intestinal-derived, hepatotoxic secondary bile acid lithocholic acid (LCA) [239,295] and moreover, metabolizes arachidonic acid, primarily to 19-hydroxyeicosatetraenoic acid [296], thus interacting with a metabolic pathway playing a prominent role in inflammation.

Arachidonic acid gives rise to the eicosanoid family of inflammatory mediators, including prostaglandin PGD₂ and PGE₂. Cyclooxygenase (COX1 and COX2) catalyze the production of prostanoids from arachidonic acid, and nonsteroidal anti-inflammatory drugs (NSAID), which share COX inhibition as a common feature, have been associated with relapses in IBD [297]. Accordingly, mice deficient in COX1 and COX2 show increased susceptibility of to DSS-induced colitis [298]. Furthermore, lipoxins derived from arachidonic acid are actively involved in the resolution of inflammation [299,300] by inhibiting neutrophil and eosinophil recruitment as well as stimulation of phagocytosis involved clearance of microorganisms and apoptotic cells [300]. In addition, Cyp2c55 as well as Ido1 are involved in tryptophan metabolism, participating in the generation of 6-hydroxymelatonin and formyl-N-acetyl-5-methoxykynurenamine respectively, from melatonin (**Fig.39**). Recently, melatonin has been shown to possess powerful anti-inflammatory and antioxidant activities, protecting against radiation-induced intestinal injury [301], improving intestinal permeability via regulation of mitochondrial function in mice [302], and improving acetic-acid-induced colitis in rats [303]. The virtual shut down of *Cyp2c55* gene expression under inflammatory conditions indicated by our microarray analysis suggests this gene as a promising candidate to follow up in additional animal models of intestinal inflammation and IBD.

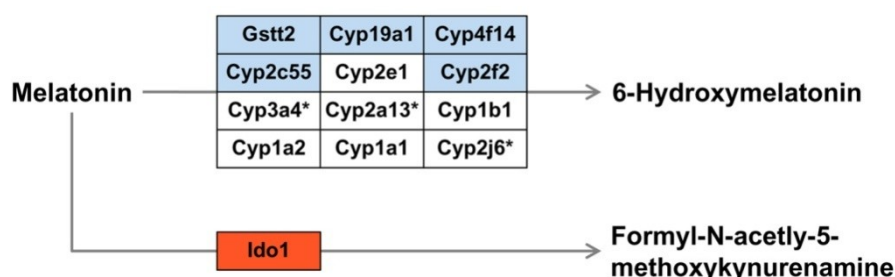


Figure 39. Involvement of Cyp2c55 and Ido1 in melatonin metabolism.

(Adapted from Wikipathways) *Cypc55* and *Ido1*, two highly regulated genes under inflammation participate in melatonin metabolism. Blue: genes downregulated, red: genes induced under inflammation according to MADMAX software. * gene not included on the microarray.

5.7 Conclusion and perspective

Cellular stress responses including metabolic, inflammatory, mitochondrial and ER UPR pathways are common features of many diseases. These signaling pathways have been extensively investigated regarding their contributions to numerous pathologies, leading to improved characterization of specific cellular responses. Yet, accumulating evidence suggest that these pathways cannot be regarded separately but are tightly interrelated (**Fig.40**). Especially in multifactorial disorders like IBD, where several triggers may be needed for the onset of pathology, it is indispensable to take various cellular processes such as protein folding, secretion, organelle biosynthesis, bacterial sensing, autophagy, apoptosis and their interaction into account for a better understanding of disease pathogenesis. Furthermore, recent data highlight how a specific microbe can determine the phenotype of a host carrying the autophagy-related *ATG16L1* risk allele for inflammatory disease [304]. These complex interactions underscore the necessity to identify cellular check points at which different signals converge and which may thus be promising targets for therapeutical interventions.

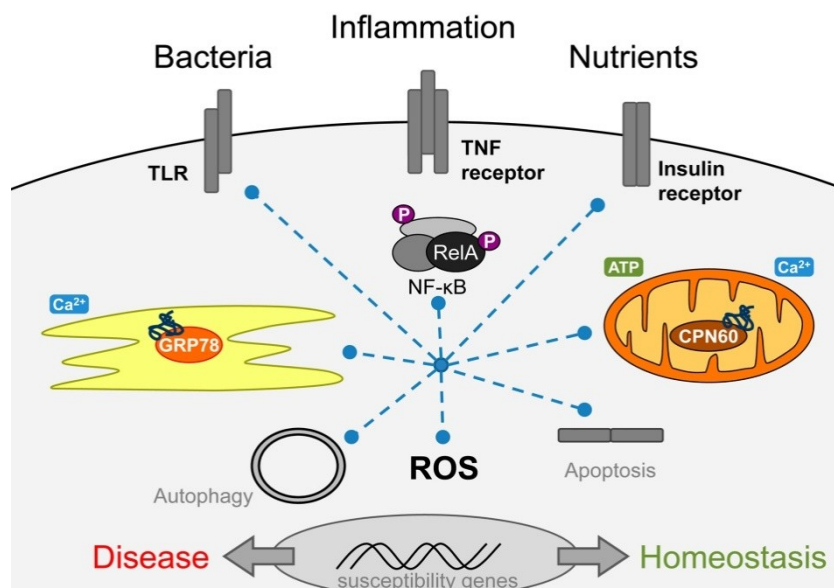


Figure 40. Cellular stress responses form a tightly interrelated network.

Stress responses including metabolic, inflammatory, mitochondrial and ER UPR pathways are interrelated and connected to bacterial and nutrient sensing. Polymorphisms in genes associated with these cellular processes have been identified as disease susceptibility factors and underlie several chronic diseases.

Mitochondrial signaling as well as ER UPR might represent those check points, integrating disease-relevant functions such as energy supply, ROS generation and cytokine production. Therapeutic approaches to improve mitochondrial- and ER function could have beneficial outcomes on various (cellular and organ) levels. Notably, several chemicals already used to

treat type 2 diabetes like PPAR agonists or salicylates have been shown to affect ER UPR-associated pathways [305,306]. Moreover, studies with chemical chaperones, phenyl butyric acid (PBA) and tauro-ursodeoxycholic acid (TUDCA), confirmed that the ER can be chemically targeted to enhance its functional capacity and that multiple diseases could be tackled by such strategies. In murine models of obesity and diabetes, administration of these chaperones increased systemic insulin sensitivity, established normoglycemia, reduced fatty liver disease and suppressed inflammatory signaling [307]. PBA and TUDCA were furthermore shown to prevent ER stress-induced inhibition of apoB100 secretion, a feature contributing to hepatic steatosis [308] and to ameliorate atherosclerosis in mouse models [309]. Alongside, specific molecules of the ER UPR could be directly targeted. For example, Salubrinal, a small molecule that prevents dephosphorylation of eIF2 α [310] has been shown to confer protection against ER stress-induced cell death both *in vitro* and *in vivo* [311]. Likewise, specifically increasing the activity of XBP1s (e.g. by p85) could improve the outcome of metabolically-driven as well as inflammatory diseases. The use of mitochondria-specific antioxidants such as acetyl-L-carnitine and R-alpha-lipoic acid could complement such strategies by additionally diminishing causes/consequences of ER stress [312]. Whether the data obtained from animal models can be translated into treatments for human diseases is currently unknown, but they provide promising evidence for new therapeutic approaches.

6 APPENDIX

Table A1. Differentially regulated proteins in primary large IEC identified by 2D SDS-PAGE and MALDI-TOF-MS analysis comparing recipients reconstituted with CD4⁺ T cells derived from Wt or IL-10^{-/-} mice with non-reconstituted mice.

gene ID	gene name	description	compartment	Rag2 ^{-/-}		Rag2 ^{-/-} xIL-10 ^{-/-}	
				1 week Wt/IL10 ^{-/-}	4 weeks Wt/IL10 ^{-/-}	1 week Wt/IL10 ^{-/-}	4 weeks Wt/IL10 ^{-/-}
11364	Acadm	acyl-Coenzyme A dehydrogenase, medium chain	mitochondrion		↓/↓		↓/↓
11370	Acadvl	acyl-Coenzyme A dehydrogenase, very long chain	mitochondrion		↓/-		↓/↓
11409	Acads	acyl-Coenzyme A dehydrogenase, short chain	mitochondrion		↓/↓		
11429	Aco2	aconitase 2, mitochondrial	mitochondrion	-/↑	↓/↓		↓/-
11637	Ak2	adenylate kinase 2	mitochondrion		-/↓		↓/↓
11669	Aldh2	aldehyde dehydrogenase 2, mitochondrial	mitochondrion		↓/↓		↓/↓
12716	Ckmt1	creatine kinase, mitochondrial 1, ubiquitous	mitochondrion	↓/-		↓/↓	↓/↓
13382	Dld	dihydrolipoamide dehydrogenase	mitochondrion			-/↑	
15107	Hadh	hydroxyacyl-Coenzyme A dehydrogenase	mitochondrion	-/↑			↓/-
15356	Hmgcl	3-hydroxy-3-methylglutaryl-Coenzyme A lyase	mitochondrion	-/↑			
15360	Hmgcs2	3-hydroxy-3-methylglutaryl-Coenzyme A synthase 2	mitochondrion	-/↓	↓/↓		↓/↓
15488	Hsd17b4	hydroxysteroid (17-beta) dehydrogenase 4	mitochondrion		-/↑		
15510	Hspd1	heat shock protein 1 (chaperonin)	mitochondrion	-/↑	↑/↑	-/↑	-/↑
15929	Idh3g	isocitrate dehydrogenase 3 (NAD ⁺), gamma	mitochondrion				-/↑
17448	Mdh2	malate dehydrogenase 2, NAD (mitochondrial)	mitochondrion		-/↓		
17995	Ndufv1	NADH dehydrogenase (ubiquinone) flavoprotein 1	mitochondrion	-/↓			
18673	Phb	prohibitin	mitochondrion	-/↑			
18746	Pkm2	pyruvate kinase, muscle	mitochondrion	↑/-			↑/↑
20425	Shmt1	serine hydroxymethyltransferase 1 (soluble)	mitochondrion	-/↓			
20655	Sod1	superoxide dismutase 1, soluble	mitochondrion				-/↓
20917	Sucg2	succinate-Coenzyme A ligase, GDP-forming, beta subunit	mitochondrion		-/↓		
22117	Tst	thiosulfate sulfurtransferase, mitochondrial	mitochondrion	-/↓	↓/↓		↓/↓

APPENDIX

gene ID	gene name	description	compartment	Rag2 ^{-/-}		Rag2 ^{-/-} xIL-10 ^{-/-}	
				1 week	4 weeks	1 week	4 weeks
				Wt/IL10 ^{-/-}	Wt/IL10 ^{-/-}	Wt/IL10 ^{-/-}	Wt/IL10 ^{-/-}
22333	Vdac1	voltage-dependent anion channel 1	mitochondrion		-/↓		
52538	Acaa2	acetyl-Coenzyme A acyltransferase 2 (mitochondrial 3-oxoacyl-Coenzyme A thiolase)	mitochondrion				↓/↓
54683	Prdx5	peroxiredoxin 5	mitochondrion		↓/-		↓/↓
59010	Sqrdl	sulfide quinone reductase-like (yeast)	mitochondrion			-/↑	
66904	Pccb	propionyl Coenzyme A carboxylase, beta polypeptide	mitochondrion		↓/↓		
66945	Sdha	succinate dehydrogenase complex, subunit A, flavoprotein (Fp)	mitochondrion	↓/-			
66988	Lap3	leucine aminopeptidase 3	mitochondrion	↑/↑			
68263	Pdhb	pyruvate dehydrogenase (lipoamide) beta	mitochondrion	-/↑			
68738	Acss1	acyl-CoA synthetase short-chain family member 1	mitochondrion			-/↑	
71679	Atp5h	ATP synthase, H ⁺ transporting, mitochondrial F0 complex, subunit d	mitochondrion	↓/-			
72039	Mccc1	methylcrotonoyl-Coenzyme A carboxylase 1 (alpha)	mitochondrion	-/↓		↑/-	
94279	Sfxn2	sideroflexin 2	mitochondrion	-/↑			
107029	Me2	malic enzyme 2, NAD(+)-dependent, mitochondrial	mitochondrion	-/↓	↓/↓		
107271	Yars2	tyrosyl-tRNA synthetase, mitochondrial	mitochondrion				-/↓
110198	Akr7a5	aldo-keto reductase family 7, member A5 (aflatoxin aldehyde reductase)	mitochondrion		↓/↓		
110821	Pcca	propionyl-Coenzyme A carboxylase, alpha polypeptide	mitochondrion		↓/↓	↑/-	
218865	Chdh	choline dehydrogenase	mitochondrion	-/↓	-/↑		
233870	Tufm	Tu translation elongation factor, mitochondrial	mitochondrion	-/↓			
246221	Mpst	mercaptopyruvate sulfurtransferase	mitochondrion		↓/↓		
268860	Abat	4-aminobutyrate aminotransferase	mitochondrion				↓/↓
12034	Phb2	prohibitin 2	mitochondrion, nucleus				↑/↑
26922	Mecr	mitochondrial trans-2-enoyl-CoA reductase	mitochondrion, nucleus		-/↑		
66071	Ethe1	ethylmalonic encephalopathy 1	mitochondrion, nucleus	-/↑	-/↓		-/↓
51179	HAO2	hydroxyacid oxidase 2 (long chain)	mitochondrion, other	-/↓	↓/↓		↓/↓
14827	Pdia3	protein disulfide isomerase associated 3	endoplasmic reticulum		↑/↑		↑/↑

gene ID	gene name	description	compartment	Rag2 ^{-/-}		Rag2 ^{-/-} xIL-10 ^{-/-}	
				1 week	4 weeks	1 week	4 weeks
				Wt/IL10 ^{-/-}	Wt/IL10 ^{-/-}	Wt/IL10 ^{-/-}	Wt/IL10 ^{-/-}
14828	Hspa5	heat shock 70kD protein 5 (glucose-regulated protein)	endoplasmic reticulum		-/↑	↑/↑	↑/↑
19035	Ppib	peptidylprolyl isomerase B	endoplasmic reticulum		↑/-		
67397	Erp29	endoplasmic reticulum protein 29	endoplasmic reticulum	-/↑			
71853	Pdia6	protein disulfide isomerase associated 6	endoplasmic reticulum			↑/-	
72599	Pdia5	protein disulfide isomerase associated 5	endoplasmic reticulum	-/↓			
105245	Txndc5	thioredoxin domain containing 5	endoplasmic reticulum		-/↑		
67838	Dnajb11	DnaJ (Hsp40) homolog, subfamily B, member 11	endoplasmic reticulum, nucleus		-/↑		
12301	Cacybp	calcyclin binding protein	nucleus		-/↑		
12631	Cfl1	cofilin 1, non-muscle	nucleus				↑/↑
13207	Ddx5	DEAD (Asp-Glu-Ala-Asp) box polypeptide 5	nucleus		-/↑		
15384	Hnrpab	heterogeneous nuclear ribonucleoprotein A/B	nucleus				↑/↑
15388	Hnrpl	heterogeneous nuclear ribonucleoprotein L	nucleus	↓/↓	↓/↓		
15481	Hspa8	heat shock protein 8	nucleus		-/↑		
16854	Lgals3	lectin, galactose binding, soluble 3	nucleus		↑/-		
16905	Lmna	lamin A	nucleus	-/↓			
18102	Nme1	expressed in non-metastatic cells 1, protein	nucleus		↑/-		
19172	Psmb4	proteasome (prosome, macropain) subunit, beta type 4	nucleus			↑/↑	
19181	Psmc2	proteasome (prosome, macropain) 26S subunit, ATPase 2	nucleus				-/↑
20341	Selenbp1	selenium binding protein 1	nucleus	↓/↓			
51886	Fubp1	far upstream element (FUSE) binding protein 1	nucleus			↑/↑	
53379	Hnrpa2b1	heterogeneous nuclear ribonucleoprotein A2/B1	nucleus			↑/-	
57320	Park7	Parkinson disease (autosomal recessive, early onset) 7	nucleus		-/↑		
66870	Serbp1	Serpine1 mRNA binding protein 1	nucleus		-/↑		↑/↑
68981	Snrpa1	small nuclear ribonucleoprotein polypeptide A'	nucleus		-/↑		
70984	4931406C07Rik	Ester hydrolase C11orf54 homolog	nucleus		-/↓		
76936	Hnrpm	heterogeneous nuclear ribonucleoprotein M	nucleus		-/↑		
218490	Btf3	basic transcription factor 3	nucleus	↑/-	↑/↑		↑/-

APPENDIX

gene ID	gene name	description	compartment	Rag2 ^{-/-}		Rag2 ^{-/-} xIL-10 ^{-/-}	
				1 week	4 weeks	1 week	4 weeks
				Wt/IL10 ^{-/-}	Wt/IL10 ^{-/-}	Wt/IL10 ^{-/-}	Wt/IL10 ^{-/-}
76491	Abhd14b	abhydrolase domain containing 14b	other, nucleus				-/↑
11461	Actb	actin, beta, cytoplasmic	other				-/↑
11465	Actg1	actin, gamma, cytoplasmic 1	other				-/↑
11668	Aldh1a1	aldehyde dehydrogenase family 1, subfamily A1	other	-/↓			
11758	Prdx6	peroxiredoxin 6	other		↓/↓	↓/-	↓/↓
12306	Anxa2	annexin A2	other	↓/↓	↓/↓		↓/↓
12346	Car1	carbonic anhydrase 1	other	-/↓	↓/↓		↓/↓
12349	Car2	carbonic anhydrase 2	other		↓/↓		↓/↓
12468	Cct7	chaperonin subunit 7 (eta)	other	↓/↓			↑/-
13629	Eef2	eukaryotic translation elongation factor 2	other		-/↑		↑/-
14381	G6pdx	glucose-6-phosphate dehydrogenase X-linked	other				-/↑
14694	Gnb211	guanine nucleotide binding protein (G protein), beta polypeptide 2 like 1	other				↑/↑
14776	Gpx2	glutathione peroxidase 2	other	↓/-			
14854	Gss	glutathione synthetase	other		-/↑		
14862	Gstm1	glutathione S-transferase, mu 1	other		↓/↓		
14863	Gstm2	glutathione S-transferase, mu 2	other		↓/-		-/↓
14870	Gstp1	glutathione S-transferase, pi 1	other		-/↓		
15387	Hnrpk	heterogeneous nuclear ribonucleoprotein K	other		-/↑		
16429	Itln1	intelectin 1 (galactofuranose binding)	other		↑/-	↑/-	
16669	Krt19	keratin 19	other	↓/-			↓/-
16691	Krt8	keratin 8	other	↓/-			↓/↓
16828	Ldha	lactate dehydrogenase A	other	↓/↓			
16855	Lgals4	lectin, galactose binding, soluble 4	other		-/↑		
16952	Anxa1	annexin A1	other				-/↑
18489	Pap	pancreatitis-associated protein	other	-/↑	↑/↑		
18655	Pgk1	phosphoglycerate kinase 1	other				↑/↑
19186	Psme1	proteasome (prosome, macropain) 28 subunit, alpha	other		↑/-		
20042	Rps12	ribosomal protein S12	other	-/↑			
20316	Sdf2	stromal cell derived factor 2	other		↑/↑		
20724	Serpinb5	serine (or cysteine) peptidase inhibitor, clade B, member 5	other		↑/-		
20887	Sult1a1	sulfotransferase family 1A, phenol-preferring, member 1	other		-/↓		↓/↓
21351	Taldo1	transaldolase 1	other		-/↓		-/↑
21881	Tkt	transketolase	other	-/↓			
21991	Tpi1	triosephosphate isomerase 1	other		-/↓		
22235	Ugdh	UDP-glucose dehydrogenase	other				↓/↓

gene ID	gene name	description	compartment	Rag2 ^{-/-}		Rag2 ^{-/-} xIL-10 ^{-/-}	
				1 week	4 weeks	1 week	4 weeks
				Wt/IL10 ^{-/-}	Wt/IL10 ^{-/-}	Wt/IL10 ^{-/-}	Wt/IL10 ^{-/-}
22330	Vcl	vinculin	other	-/↑			
22350	Vil2	villin 2	other	-/↓			
23795	Agr2	anterior gradient 2 (Xenopus laevis)	other				↑/↑
23971	Papss1	3'-phosphoadenosine 5'-phosphosulfate synthase 1	other	-/↓		-/↑	
23972	Papss2	3'-phosphoadenosine 5'-phosphosulfate synthase 2	other	-/↓	↓/↓		↓/↓
26440	Psma1	proteasome (prosome, macropain) subunit, alpha type 1	other	↑/-			
26441	Psma4	proteasome (prosome, macropain) subunit, alpha type 4	other				-/↑
26905	Eif2s3x	eukaryotic translation initiation factor 2, subunit 3, structural gene X-linked	other		-/↑		
26908	Eif2s3y	eukaryotic translation initiation factor 2, subunit 3, structural gene Y-linked	other		-/↑		
27384	Akr1c13	aldo-keto reductase family 1, member C13	other		↓/↓		
50773	Nt5c	5',3'-nucleotidase, cytosolic	other	-/↑			
64336	Rplp0	ribosomal protein, large, P0	other			-/↑	
67089	Psmc6	proteasome (prosome, macropain) 26S subunit, ATPase, 6	other		↓/↓		
67151	Psmc9	proteasome (prosome, macropain) 26S subunit, non-ATPase, 9	other	-/↑			
67738	Ppid	peptidylprolyl isomerase D (cyclophilin D)	other	-/↑			
74246	Gale	galactose-4-epimerase, UDP	other	-/↓			-/↑
74840	Armet	arginine-rich, mutated in early stage tumors	other		-/↑		
107652	Uap1	UDP-N-acetylglucosamine pyrophosphorylase 1	other		↑/-		
113868	Acaa1a	acetyl-Coenzyme A acyltransferase 1A	other				↑/↑
227753	Gsn	gelsolin	other		↑/-		
229279	Hnrpa3	heterogeneous nuclear ribonucleoprotein A3	other		↑/-		↑/↑
230163	Aldob	aldolase 2, B isoform	other		-/↓		
268373	Ppia	peptidylprolyl isomerase A	other				↑/↑

Table A2. Genes best correlated (according to Spearman correlation coefficient, $r_s > 0.8$) to histological scores in Rag2^{-/-} recipients and fold changes in gene expression of the different CD4⁺ T cell reconstituted groups vs non-reconstituted controls. The one-sided significance for r_s was $P < 0.001$ for all genes with $r_s > 0.8$.

Genes best correlated ($r_s > 0.8$) to histological score in Rag2^{-/-} recipients

gene ID	gene name	description	gene expression (fold change of CTRL)			r_s : gene expression vs histo. score		
			CD25 ⁺ T cells	Wt CD25 ⁻ T cells	IL-10 ⁺ CD25 ⁻ T cells	Cecum	Colon	Cumulative
80287	Apobec 3	apolipoprotein B mRNA editing enzyme, catalytic polypeptide 3	-1.07	1.96	1.80	0.85	0.83	0.90
83490	Pik3ap 1	phosphoinositide-3-kinase adaptor protein 1	1.04	1.38	1.65	0.85	0.84	0.90
20460	Stil	Scf/Tal1 interrupting locus	-1.09	1.41	1.59	0.82	0.85	0.89
19073	Srgn	serglycin	-1.04	4.75	53.52	0.81	0.87	0.88
14159	Fes	feline sarcoma oncogene	1.02	1.70	2.26	0.85	0.75	0.87
18018	Nfatc1	nuclear factor of activated T-cells, cytoplasmic, calcineurin-dependent 1	-1.07	1.81	1.63	0.79	0.87	0.87
20302	Ccl3	chemokine (C-C motif) ligand 3	1.08	1.34	3.27	0.77	0.91	0.86
68713	Ifitm1	interferon induced transmembrane protein 1	-1.21	3.58	8.76	0.88	0.78	0.86
20345	Selplg	selectin, platelet (p-selectin) ligand	-1.09	1.95	3.28	0.78	0.91	0.86
268880	AI4806 53	expressed sequence AI480653	-1.03	1.33	1.18	0.81	0.78	0.86
100340	Smpdl3 b	sphingomyelin phosphodiesterase, acid-like 3B	1.08	1.81	6.67	0.81	0.86	0.85
17225	Mcpt2	mast cell protease 2	-1.14	2.59	40.17	0.82	0.80	0.85
20556	Slnf2	schlafen 2	-1.00	1.47	4.88	0.75	0.90	0.85
60361	Ms4a4b	membrane-spanning 4-domains, subfamily A, member 4B	-1.15	9.80	6.25	0.81	0.79	0.85
80885	Niacr1	niacin receptor 1	1.02	1.64	3.87	0.78	0.86	0.85
71920	Epgn	epithelial mitogen	-1.08	2.47	2.86	0.79	0.84	0.85
65221	Slc15a3	solute carrier family 15, member 3	-1.04	1.59	2.12	0.79	0.81	0.84
237038	Nox1	NADPH oxidase 1	1.17	2.53	5.42	0.75	0.90	0.84
72512	Tmem1 73	transmembrane protein 173	-1.37	1.61	4.27	0.81	0.81	0.84
54354	Rassf5	Ras association (RalGDS/AF-6) domain family member 5	-1.11	1.69	2.22	0.81	0.83	0.84
17068	Ly6d	lymphocyte antigen 6 complex, locus D	-1.23	2.19	31.74	0.79	0.85	0.84
245195	Retnlg	resistin like gamma	-1.19	2.46	14.25	0.80	0.83	0.84
226652	Arhgap 30	Rho GTPase activating protein 30	-1.09	1.76	2.12	0.79	0.83	0.84
75296	Fgfr1op	Fgfr1 oncogene partner	-1.11	1.30	1.27	0.87	0.65	0.83
170755	Sgk3	serum/glucocorticoid regulated-kinase 3	-1.01	1.23	1.89	0.76	0.86	0.83
238377	Gpr68	G protein-coupled receptor 68	-1.08	1.46	1.15	0.77	0.74	0.83
12477	Ctla4	cytotoxic T-lymphocyte-associated protein 4	-1.58	1.36	2.09	0.79	0.81	0.83
18392	Orc1l	origin recognition complex, subunit 1-like (S.cereviaiae)	1.04	1.37	1.75	0.76	0.80	0.83
19200	Pstpip1	proline-serine-threonine phosphatase-interacting protein 1	-1.07	1.42	1.91	0.80	0.80	0.83
12237	Bub3	budding uninhibited by benzimidazoles 3 homolog	-1.04	1.21	1.34	0.86	0.68	0.83

Genes best correlated ($r_s > 0.8$) to histological score in Rag2^{-/-} recipients

gene ID	gene name	description	gene expression (fold change of CTRL)			r _s : gene expression vs histo. score		
			CD25 ⁺ T cells	Wt CD25 ⁻ T cells	IL-10 ⁺ CD25 ⁻ T cells	Cecum	Colon	Cumulative
237400	Mex3d	mex3 homolog D (C. elegans)	1.04	1.78	1.50	0.74	0.82	0.83
234915	29341	cDNA sequence AK129341	1.12	1.57	1.82	0.78	0.83	0.83
14360	Fyn	Fyn proto-oncogene	1.02	4.95	2.12	0.71	0.80	0.83
76509	Plet	RIKEN cDNA 1600029D21 gene	-1.23	3.69	12.70	0.73	0.85	0.82
16994	Ltb	lymphotoxin B	-1.09	1.97	3.59	0.77	0.83	0.82
16797	Lat	linker for activation of T cells	-1.17	1.90	1.64	0.79	0.75	0.82
14127	Fcer1g	Fc receptor, IgE, high affinity I, gamma polypeptide	1.07	1.78	3.69	0.71	0.87	0.82
218820	Zfp503	zinc finger protein 503	-1.33	2.37	1.47	0.76	0.78	0.82
71398	5430427O19	RIKEN cDNA 5430427O19 gene	-1.16	1.32	1.35	0.84	0.71	0.82
70435	Inf2	inverted formin, FH2 and WH2 domain containing	-1.07	1.45	1.61	0.82	0.74	0.82
208084	Pif1	PIF1 5'-to-3' DNA helicase homolog	-1.15	1.96	1.53	0.83	0.73	0.82
20750	Spp1	secreted phosphoprotein 1	-1.07	2.11	4.85	0.76	0.85	0.82
246707	Emilin2	elastin microfibril interfacier 2	-1.08	1.31	3.93	0.79	0.76	0.82
22352	Vim	vimentin	1.14	1.71	5.21	0.75	0.84	0.82
67052	Ndc80	NDC80 homolog, kinetochore complex component (S. cerevisiae)	-1.25	1.48	1.86	0.75	0.73	0.82
19659	Rbp1	retinol binding protein 1, cellular	-1.01	1.43	1.47	0.79	0.73	0.82
54199	Ccr12	chemokine (C-C motif) receptor-like 2	-1.01	1.22	2.46	0.71	0.86	0.81
13845	Ephb3	Eph receptor B3	-1.15	1.63	1.57	0.77	0.77	0.81
76589	Unc5cl	unc-5 homolog C (C. elegans)-like	1.06	1.29	1.98	0.79	0.75	0.81
12258	Serping1	serine (or cysteine) peptidase inhibitor, clade G, member 1	-1.07	1.45	3.75	0.73	0.87	0.81
16365	Irg1	immunoresponsive gene 1	-1.18	5.59	11.56	0.78	0.79	0.81
12265	Ciita	class II transactivator	-1.12	2.80	2.83	0.73	0.85	0.81
18080	Nin	ninein	-1.08	1.45	1.66	0.75	0.81	0.81
20202	S100a9	S100 calcium binding protein A9 (calgranulin B)	-1.25	13.89	188.70	0.73	0.85	0.81
22780	Ikzf3	IKAROS family zinc finger 3	-1.01	1.66	1.83	0.72	0.77	0.81
15439	Hp	haptoglobin	-1.09	1.64	2.14	0.78	0.76	0.81
667597	BC023105	cDNA sequence BC023105	1.06	1.66	23.76	0.70	0.90	0.81
70461	Crtc3	CREB regulated transcription coactivator 3	-1.04	1.64	1.43	0.71	0.78	0.81
12516	Cd7	CD7 antigen	-1.21	1.60	2.79	0.77	0.78	0.81
21832	Thpo	thrombopoietin	-1.14	1.33	1.27	0.82	0.71	0.81
193217	BC018473	cDNA sequence BC018473	1.36	6.63	3.28	0.71	0.78	0.81
20762	Spr2h	small proline-rich protein 2H	1.03	2.80	29.54	0.71	0.87	0.80
17105	Lyz2	lysozyme 2	-1.23	1.72	6.52	0.81	0.76	0.80
20723	Serpinb9	serine (or cysteine) peptidase inhibitor, clade B, member 9	-1.07	1.44	2.07	0.74	0.82	0.80
12266	C3	complement component 3	1.18	2.86	27.22	0.76	0.80	0.80
16331	Inpp5d	inositol polyphosphate-5-phosphatase D	-1.05	1.44	1.90	0.73	0.82	0.80
19260	Ptpn22	protein tyrosine phosphatase, non-receptor type 22 (lymphoid)	-1.32	1.93	4.24	0.80	0.70	0.80

Genes best correlated ($r_s > 0.8$) to histological sore in Rag2^{-/-} recipients

gene ID	gene name	description	gene expression (fold change of CTRL)			r_s : gene expression vs histo. score		
			CD25 ⁺ T cells	Wt CD25 ⁺ T cells	IL-10 ^{-/-} CD25 ⁻ T cells	Cecum	Colon	Cumulative
22177	Tyrbp	TYRO protein tyrosine kinase binding protein	1.06	1.93	14.94	0.70	0.84	0.80
108011	Ap4e1	adaptor-related protein complex AP-4, epsilon 1	-1.04	2.50	1.36	0.80	0.72	0.80
14938	Gzma	granzyme A	1.01	3.79	46.82	0.71	0.83	0.80
234779	Plcg2	phospholipase C, gamma 2	-1.20	2.06	1.23	0.83	0.67	0.79
16803	Lbp	lipopolysaccharide binding protein	-1.06	1.52	7.82	0.72	0.81	0.79
12282	Hyou1	hypoxia up-regulated 1	1.17	1.55	2.24	0.66	0.84	0.79
71982	Snx10	sorting nexin 10	-1.06	2.10	8.18	0.70	0.85	0.79
102084	NA	NA	-1.16	2.06	18.23	0.73	0.84	0.79
210992	Lpcat1	lysophosphatidylcholine acyltransferase 1	1.14	2.26	2.19	0.71	0.83	0.78
56644	Clec7a	C-type lectin domain family 7, member a	-1.24	4.52	7.53	0.74	0.81	0.78
20310	Cxcl2	chemokine (C-X-C motif) ligand 2	1.00	14.29	78.98	0.71	0.81	0.78
66439	2010012005	RIKEN cDNA 2010012005 gene	-1.08	1.33	1.38	0.66	0.80	0.78
20307	Ccl8	chemokine (C-C motif) ligand 8	-1.18	1.56	35.64	0.73	0.81	0.78
16193	Il6	interleukin 6	-1.04	2.70	5.21	0.71	0.82	0.78
67198	Spats2l	spermatogenesis associated, serine-rich 2-like	-1.04	1.40	1.86	0.68	0.84	0.77
170625	Snx18	sorting nexin 18	-1.07	1.82	2.11	0.70	0.81	0.77
15490	Hsd17b7	hydroxysteroid (17-beta) dehydrogenase 7	1.10	1.52	2.01	0.66	0.82	0.77
328561	Apol10b	apolipoprotein L 10b	-1.01	6.17	20.95	0.69	0.82	0.77
76905	Lrg1	leucine-rich alpha-2-glycoprotein 1	-1.11	2.24	142.76	0.68	0.81	0.77
100034251	Gm11428	predicted gene 11428	-1.07	1.97	12.83	0.71	0.83	0.77
56619	Clec4e	C-type lectin domain family 4, member e	-1.06	1.61	4.16	0.71	0.81	0.77
60440	ligp1	interferon inducible GTPase 1	1.72	9.44	79.20	0.67	0.85	0.76
110033	Kif22	kinesin family member 22	-1.06	2.18	2.85	0.63	0.84	0.76
16186	Il2rg	interleukin 2 receptor, gamma chain	1.09	1.22	1.75	0.69	0.81	0.75
229900	Gbp6	guanylate binding protein 6	1.06	3.51	7.03	0.68	0.83	0.75
24108	Ubd	ubiquitin D	1.19	2.71	58.61	0.63	0.88	0.75
18301	Fxyd5	FXVD domain-containing ion transport regulator 5	-1.11	1.74	2.97	0.69	0.82	0.75
14969	H2-Eb1	histocompatibility 2, class II antigen E beta	-1.08	9.79	55.31	0.65	0.82	0.74
12515	Cd69	CD69 antigen	1.25	1.91	12.02	0.57	0.88	0.74
17329	Cxcl9	chemokine (C-X-C motif) ligand 9	-1.01	1.44	99.05	0.64	0.81	0.73
257632	Nod2	nucleotide-binding oligomerization domain containing 2	1.06	1.21	1.75	0.57	0.84	0.73
16822	Lcp2	lymphocyte cytosolic protein 2	-1.06	1.59	2.50	0.68	0.81	0.73
16543	Mdfic	MyoD family inhibitor domain containing	1.02	1.49	2.13	0.63	0.81	0.73
20304	Ccl5	chemokine (C-C motif) ligand 5	1.20	1.98	32.18	0.59	0.82	0.72
15930	Ido1	indoleamine 2,3-dioxygenase 1	1.04	5.09	306.02	0.58	0.88	0.72
18780	Pla2g2a	phospholipase A2, group IIA	1.10	2.45	6.15	0.62	0.82	0.71
19271	Ptprj	protein tyrosine phosphatase, receptor type, J	1.07	1.71	1.43	0.58	0.81	0.71

Genes best correlated ($r_s > 0.8$) to histological sore in Rag2^{-/-} recipients

gene ID	gene name	description	gene expression (fold change of CTRL)			r_s : gene expression vs histo. score		
			CD25 ⁺ T cells	Wt CD25 ⁺ T cells	IL-10 ^{-/-} CD25 ⁺ T cells	Cecum	Colon	Cumulative
16149	Cd74	CD74 antigen	1.59	11.95	34.26	0.61	0.83	0.70
244882	Tnfaip8l3	tumor necrosis factor, alpha-induced protein 8-like 3	1.13	1.37	2.38	0.59	0.82	0.70
15951	Ifi204	interferon activated gene 204	1.03	1.40	2.47	0.62	0.80	0.69
24051	Sgcb	sarcoglycan, beta (dystrophin-associated glycoprotein)	1.07	1.36	2.90	0.52	0.81	0.69
14961	H2-Ab1	histocompatibility 2, class II antigen A, beta 1	1.82	4.19	80.90	0.56	0.81	0.67
12654	Chi3l1	chitinase 3-like 1	1.11	1.26	2.09	0.54	0.82	0.66
67556	Pigm	phosphatidylinositol glycan anchor biosynthesis, class M	1.42	1.82	2.31	0.46	0.81	0.61
53376	Usp2	ubiquitin specific peptidase 2	-2.13	-2.90	-3.82	-0.48	-0.82	-0.65
224019	Tmem191c	transmembrane protein 191C	1.07	-1.22	-1.45	-0.56	-0.81	-0.70
14199	Fhl1	four and a half LIM domains 1	-1.15	-4.63	-5.01	-0.61	-0.83	-0.70
12953	Cry2	cryptochrome 2 (photolyase-like)	-1.81	-2.31	-3.23	-0.59	-0.82	-0.71
28135	Cep63	centrosomal protein 63	-1.16	-2.95	-1.87	-0.58	-0.82	-0.72
170716	Cyp4f13	cytochrome P450, family 4, subfamily f, polypeptide 13	1.30	-2.76	-2.69	-0.67	-0.81	-0.75
67426	Cabc1	chaperone, ABC1 activity of bc1 complex like (S. pombe)	1.16	-1.63	-3.92	-0.66	-0.85	-0.75
12651	Chkb	choline kinase beta	-1.06	-6.57	-3.14	-0.63	-0.82	-0.75
20535	Slc4a2	solute carrier family 4 (anion exchanger), member 2	-1.15	-3.70	-2.00	-0.64	-0.82	-0.75
56643	Slc15a1	solute carrier family 15 (oligopeptide transporter), member 1	-1.55	-3.43	-5.28	-0.67	-0.83	-0.75
231717	Fam109a	family with sequence similarity 109, member A	1.01	-1.39	-2.08	-0.68	-0.85	-0.75
28027	NA	NA	-1.11	-2.53	-1.62	-0.64	-0.80	-0.75
226781	Slc30a10	solute carrier family 30, member 10	1.13	-1.48	-2.16	-0.69	-0.81	-0.76
11997	Akr1b7	aldo-keto reductase family 1, member B7	-1.45	-2.41	-3.91	-0.65	-0.86	-0.76
69581	Rhou	ras homolog gene family, member U	1.16	-1.41	-1.87	-0.70	-0.81	-0.76
70337	Iyd	iodotyrosine deiodinase	1.60	-1.63	-2.14	-0.73	-0.82	-0.76
66090	Ypel3	yippee-like 3 (Drosophila)	1.36	-1.84	-2.09	-0.73	-0.80	-0.76
13107	Cyp2f2	cytochrome P450, family 2, subfamily f, polypeptide 2	1.61	-2.33	-3.39	-0.69	-0.83	-0.76
78887	Sfi1	Sfi1 homolog, spindle assembly associated (yeast)	-1.37	-3.42	-4.67	-0.66	-0.83	-0.76
69149	Kbtbd3	kelch repeat and BTB (POZ) domain containing 3	-1.20	-2.77	-1.78	-0.64	-0.82	-0.76
319176	Hist2h2ac	histone cluster 2, H2ac	-1.04	-3.31	-3.20	-0.66	-0.85	-0.77
67441	Isoc2b	isochorismatase domaincontaining 2b	-1.08	-2.20	-1.89	-0.64	-0.82	-0.77
14979	H2-Ke6	H2-K region expressed gene 6	-1.03	-2.66	-2.50	-0.68	-0.81	-0.77
225997	Trpm6	transient receptor potential cation channel, subfamily M, member 6	-1.06	-12.81	-11.19	-0.67	-0.81	-0.77
13614	Edn1	endothelin 1	1.02	-2.15	-4.41	-0.63	-0.89	-0.77
238023	Hexdc	hexosaminidase (glycosyl hydrolase family 20) containing	-1.11	-3.37	-2.58	-0.70	-0.83	-0.78
107227	MacroD	MACRO domain containing 1	1.24	-3.94	-5.28	-0.72	-0.84	-0.78

Genes best correlated ($r_s > 0.8$) to histological sore in Rag2^{-/-} recipients

gene ID	gene name	description	gene expression (fold change of CTRL)			r_s : gene expression vs histo. score		
			CD25 ⁺ T cells	Wt CD25 ⁺ T cells	IL-10 ^{-/-} CD25 ⁺ T cells	Cecum	Colon	Cumulative
75568	Capsl	calcyphosine-like	1.70	-1.48	-1.79	-0.80	-0.67	-0.78
67023	Use1	unconventional SNARE in the ER 1 homolog (<i>S. cerevisiae</i>)	1.32	-3.24	-1.73	-0.81	-0.71	-0.79
66469	2810405K02	RIKEN cDNA 2810405K02 gene	1.55	-3.13	-1.66	-0.78	-0.76	-0.80
16971	Lrp1	low density lipoprotein receptor-related protein 1	-1.13	-5.70	-2.77	-0.72	-0.77	-0.80
228730	Plk1s1	polo-like kinase 1 substrate 1	1.46	-2.95	-1.81	-0.80	-0.71	-0.80
67013	Oma1	OMA1 homolog, zinc metallopeptidase (<i>S. cerevisiae</i>)	1.04	-5.72	-2.29	-0.72	-0.76	-0.80
217138	Prr15l	proline rich 15-like	-1.06	-1.83	-1.80	-0.74	-0.79	-0.80
228765	Sdcbp2	syndecan binding protein (syntenin) 2	1.14	-2.30	-1.44	-0.81	-0.68	-0.80
70984	4931406C07	RIKEN cDNA 4931406C07 gene	1.34	-6.39	-1.78	-0.78	-0.70	-0.80
432720	Akr1c19	aldo-keto reductase family 1, member C19	1.00	-11.66	-8.11	-0.75	-0.76	-0.80
11774	Ap3b1	adaptor-related protein complex 3, beta 1 subunit	1.51	-4.18	-1.53	-0.77	-0.72	-0.80
68347	0610011F06	RIKEN cDNA 0610011F06 gene	1.07	-3.30	-2.39	-0.78	-0.73	-0.80
14871	Gstt1	glutathione S-transferase, theta 1	1.73	-3.78	-3.77	-0.82	-0.73	-0.80
104816	Aspg	asparaginase homolog (<i>S. cerevisiae</i>)	1.00	-1.82	-1.78	-0.67	-0.86	-0.81
268663	Cdhr2	cadherin-related family member 2	1.03	-9.70	-2.42	-0.75	-0.72	-0.81
66601	Tmigd1	transmembrane and immunoglobulin domain containing 1	-1.10	-2.24	-2.72	-0.76	-0.76	-0.81
11551	Adra2a	adrenergic receptor, alpha 2a	-1.16	-12.73	-5.03	-0.75	-0.72	-0.81
70152	Mettl7a1	methyltransferase like 7A1	1.46	-3.74	-3.26	-0.79	-0.74	-0.81
56517	Slc22a21	solute carrier family 22 (organic cation transporter), member 21	1.22	-2.04	-1.59	-0.77	-0.78	-0.81
14794	Spsb2	splA/ryanodine receptor domain and SOCS box containing 2	1.15	-1.23	-1.42	-0.80	-0.76	-0.81
320234	Ccdc66	coiled-coil domain containing 66	1.28	-1.52	-1.96	-0.81	-0.70	-0.81
20918	Eif1	eukaryotic translation initiation factor 1	1.04	-1.67	-1.15	-0.71	-0.79	-0.81
18671	Abcb1a	ATP-binding cassette, sub-family B (MDR/TAP), member 1A	1.27	-9.21	-8.10	-0.80	-0.76	-0.81
67665	Dctn4	dynactin 4	-1.11	-2.03	-1.72	-0.75	-0.79	-0.81
56362	Sult1b1	sulfotransferase family 1B, member 1	1.11	-2.91	-1.68	-0.81	-0.70	-0.81
72948	Tppp	tubulin polymerization promoting protein	1.49	-6.08	-3.11	-0.81	-0.72	-0.81
110826	Etfb	electron transferring flavoprotein, beta polypeptide	1.12	-5.00	-1.69	-0.76	-0.78	-0.81
433023	Gm5485	predicted gene 5485	1.18	-5.10	-2.16	-0.82	-0.72	-0.81
72082	Cyp2c55	cytochrome P450, family 2, subfamily c, polypeptide 55	1.41	-19.58	-13.63	-0.78	-0.74	-0.81
232087	Mat2a	methionine adenosyltransferase II, alpha	1.05	-25.22	-1.81	-0.75	-0.74	-0.81
66847	Hint3	histidine triad nucleotide binding protein 3	-1.05	-2.26	-1.70	-0.78	-0.76	-0.81
68024	Hist1h2bc	histone cluster 1, H2bc	-1.06	-2.05	-2.04	-0.75	-0.81	-0.81
14263	Fmo5	flavin containing monooxygenase 5	1.23	-1.78	-1.89	-0.82	-0.66	-0.82
13370	Dio1	deiodinase, iodothyronine, type I	1.05	-7.45	-5.10	-0.75	-0.76	-0.82

Genes best correlated ($r_s > 0.8$) to histological sore in Rag2^{-/-} recipients

gene ID	gene name	description	gene expression (fold change of CTRL)			r_s : gene expression vs histo. score		
			CD25 ⁺ T cells	Wt CD25 ⁺ T cells	IL-10 ^{-/-} CD25 ⁻ T cells	Cecum	Colon	Cumulative
15370	Nr4a1	nuclear receptor subfamily 4, group A, member 1	1.23	-5.39	-3.39	-0.78	-0.81	-0.82
27375	Tjp3	tight junction protein 3	1.05	-2.72	-1.11	-0.79	-0.73	-0.82
66353	2310007A19	RIKEN cDNA 2310007A19Rik	1.52	-1.30	-1.32	-0.78	-0.77	-0.82
66162	Bola2	bolA-like 2 (E. coli)	1.12	-19.87	-1.60	-0.74	-0.78	-0.82
15184	Hdac5	histone deacetylase 5	1.57	-1.64	-2.01	-0.79	-0.81	-0.82
231999	Plekha8	pleckstrin homology domain containing, family A member 8	1.37	-11.44	-2.24	-0.77	-0.72	-0.82
17161	Maoa	monoamine oxidase A	1.28	-3.20	-2.32	-0.77	-0.74	-0.82
224807	Tmem63b	transmembrane protein 63b	1.03	-1.91	-2.11	-0.75	-0.84	-0.82
53315	Sult1d1	sulfotransferase family 1D, member 1	1.09	-2.47	-2.55	-0.80	-0.74	-0.82
234673	Ces5	carboxylesterase 5	1.10	-3.92	-2.14	-0.76	-0.75	-0.82
56857	Slc37a2	solute carrier family 37 (glycerol-3-phosphate transporter), member 2	1.18	-10.06	-16.38	-0.80	-0.80	-0.82
23970	Pacsin2	protein kinase C and casein kinase substrate in neurons 2	-1.10	-5.12	-1.51	-0.74	-0.77	-0.82
57276	Vsig2	V-set and immunoglobulin domain containing 2	2.03	-4.53	-3.87	-0.83	-0.71	-0.82
102022	Ces6	carboxylesterase 6	-1.17	-6.45	-7.22	-0.76	-0.81	-0.82
14312	Brd2	bromodomain containing 2	-1.06	-9.57	-1.37	-0.76	-0.75	-0.83
72269	Cda	cytidine deaminase	1.63	-4.79	-7.79	-0.78	-0.79	-0.83
22239	Ugt8a	UDP galactosyltransferase 8A	1.28	-2.75	-9.87	-0.78	-0.80	-0.83
19714	Rev3l	REV3-like, catalytic subunit of DNA polymerase zeta RAD54 like	1.03	-2.01	-1.40	-0.75	-0.79	-0.83
14149	Fdxr	ferredoxin reductase	1.38	-2.42	-2.11	-0.80	-0.74	-0.83
20501	Slc16a1	solute carrier family 16 (monocarboxylic acid transporter), member 1	1.08	-6.07	-2.00	-0.79	-0.72	-0.83
234669	BC015286	cDNA sequence BC015286	-1.07	-2.96	-4.05	-0.78	-0.79	-0.83
58210	Sectm1	secreted and transmembrane 1B	1.12	-3.60	-2.03	-0.82	-0.72	-0.84
11833	Aqp8	aquaporin 8	-1.02	-5.78	-5.73	-0.81	-0.76	-0.84
67971	Tppp3	tubulin polymerization-promoting protein family member 3	1.26	-4.41	-6.62	-0.78	-0.87	-0.84
18741	Pitx2	paired-like homeodomain transcription factor 2	1.08	-3.20	-2.79	-0.82	-0.74	-0.84
211798	Mfsd9	major facilitator superfamily domain containing 9	1.04	-4.98	-1.58	-0.83	-0.74	-0.85
231832	Tmem184a	transmembrane protein 184a	1.10	-3.30	-1.16	-0.85	-0.76	-0.87
20393	Sgk1	serum/glucocorticoid regulated kinase 1	1.25	-4.11	-2.75	-0.84	-0.80	-0.88
226654	Tstd1	thiosulfate sulfurtransferase (rhodanese)-like domain containing 1	1.03	-2.18	-2.07	-0.85	-0.82	-0.89
13198	Ddit3	DNA-damage inducible transcript 3	1.28	-2.83	-3.69	-0.85	-0.87	-0.91

Table A3. Genes best correlated (according to Spearman correlation coefficient, $r_s > 0.8$) to histological scores in Rag2^{-/-} x IL-10^{-/-} recipients and fold changes in gene expression of the different CD4⁺ T cell reconstituted groups vs non-reconstituted controls. The one-sided significance for r_s was $P < 0.001$ for all genes with $r_s > 0.8$.

Genes best correlated ($r_s > 0.8$) to histological score in Rag2^{-/-} x IL-10^{-/-} recipients

gene ID	gene name	description	gene expression (fold change of CTRL)			r_s : gene expression vs histo. score		
			CD25 ⁺ T cells	Wt CD25 ⁻ T cells	IL-10 ^{-/-} CD25 ⁻ T cells	Cecum	Colon	Cumulative
15930	Ido1	indoleamine 2,3-dioxygenase 1	-1.54	14.85	94.31	0.92	0.85	0.93
60440	ligp1	interferon inducible GTPase 1	1.20	11.73	43.65	0.90	0.89	0.92
76509	Plet	RIKEN cDNA 1600029D21 gene	2.21	8.26	16.97	0.86	0.93	0.91
15904	Id4	inhibitor of DNA binding 4	-1.06	1.66	1.99	0.87	0.87	0.91
14933	Gyk	glycerol kinase	1.76	3.42	8.36	0.87	0.92	0.90
110454	Ly6a	lymphocyte antigen 6 complex, locus A	1.38	3.42	7.19	0.85	0.96	0.90
76905	Lrg1	leucine-rich alpha-2-glycoprotein 1	-1.38	6.00	119.75	0.92	0.84	0.90
16803	Lbp	lipopolysaccharide binding protein	-1.03	2.25	7.11	0.90	0.85	0.89
226844	Mfsd7b	major facilitator superfamily domain containing 7B	-1.20	1.59	2.34	0.87	0.84	0.89
24108	Ubd	ubiquitin D	-1.65	5.93	26.05	0.85	0.84	0.87
78611	Btbd19	BTB (POZ) domain containing 19	-1.15	1.15	1.56	0.87	0.75	0.87
109019	Obfc2a	oligonucleotide/oligosaccharide-binding fold containing 2A	1.06	1.45	2.26	0.81	0.85	0.87
21832	Thpo	thrombopoietin	-1.05	1.27	1.58	0.87	0.82	0.87
60533	Cd274	CD274 antigen	-1.40	1.48	3.16	0.86	0.80	0.87
237436	Gas2l3	growth arrest-specific 2 like 3	-1.05	1.47	2.83	0.82	0.88	0.86
100340	Smpd3b	sphingomyelin phosphodiesterase, acid-like 3B	1.28	1.99	6.26	0.84	0.85	0.86
73112	3110003A17	RIKEN cDNA 3110003A17 gene	-1.01	1.18	1.59	0.83	0.87	0.86
15894	Icam1	intercellular adhesion molecule 1	1.16	2.09	8.95	0.82	0.85	0.86
68713	Ifitm1	interferon induced transmembrane protein 1	-1.36	3.48	7.40	0.87	0.79	0.86
16365	Irg1	immunoresponsive gene 1	-1.23	2.45	11.35	0.86	0.83	0.86
102084	NA	NA	1.06	3.48	16.19	0.82	0.87	0.85
12768	Ccr1	chemokine (C-C motif) receptor 1	-1.12	1.32	2.54	0.86	0.77	0.85
74107	Cep55	centrosomal protein 55	-1.09	1.54	2.94	0.80	0.87	0.85
20306	Ccl7	chemokine (C-C motif) ligand 7	-1.04	1.45	4.55	0.82	0.84	0.85
69736	Nup37	nucleoporin 37	1.22	2.06	2.51	0.83	0.85	0.85
218973	Wdhd1	WD repeat and HMG-box DNA binding protein 1	1.16	1.46	2.17	0.83	0.84	0.85
11687	Alox15	arachidonate 15-lipoxygenase	-1.09	1.36	1.58	0.80	0.84	0.85
243753	2010107G12	RIKEN cDNA 2010107G12 gene	1.12	1.44	2.70	0.85	0.79	0.85
14969	H2-Eb1	histocompatibility 2, class II antigen E β	-1.32	12.63	35.84	0.83	0.83	0.85
16688	Krt6b	keratin 6B	-1.08	1.32	1.80	0.83	0.82	0.84
22271	Upp1	uridine phosphorylase 1	1.07	8.75	19.29	0.82	0.85	0.84
15945	Cxcl10	chemokine (C-X-C motif) ligand 10	-1.25	2.53	15.46	0.83	0.82	0.84
21938	Tnfrsf1b	tumor necrosis factor receptor superfamily, member 1b	-1.38	2.59	10.30	0.83	0.84	0.84
14609	Gja1	gap junction protein, alpha 1	1.19	2.24	3.53	0.78	0.85	0.83

Genes best correlated ($r_s > 0.8$) to histological sore in Rag2^{-/-} x IL-10^{-/-} recipients

gene ID	gene name	description	gene expression (fold change of CTRL)			r_s : gene expression vs histo. score		
			CD25 ⁺ T cells	Wt CD25 ⁻ T cells	IL-10 ^{-/-} CD25 ⁻ T cells	Cecum	Colon	Cumulative
100034251	Gm11428	predicted gene 11428	-1.08	2.30	6.46	0.84	0.80	0.83
20201	S100a8	S100 calcium binding protein A8 (calgranulin A)	-1.36	10.65	121.58	0.83	0.84	0.83
84652	Fam126a	family with sequence similarity 126, member A	-1.01	1.33	2.13	0.84	0.71	0.83
76974	1190003J15	RIKEN cDNA 1190003J15 gene	-1.02	1.51	2.22	0.80	0.88	0.83
60530	Fignl1	fidgetin-like 1	-1.18	1.84	2.39	0.82	0.81	0.83
217847	Serpina10	serine (or cysteine) peptidase inhibitor, clade A, member 10	1.04	1.95	15.19	0.79	0.84	0.83
56619	Clec4e	C-type lectin domain family 4, member e	-1.04	1.47	2.86	0.82	0.82	0.83
17975	Ncl	nucleolin	-1.02	1.86	2.02	0.81	0.82	0.83
12508	Cd53	CD53 antigen	-1.37	1.83	2.88	0.82	0.80	0.83
12263	C2	complement component 2	1.12	1.48	3.04	0.75	0.87	0.82
16176	Il1b	interleukin 1 beta	-1.56	3.92	18.18	0.82	0.81	0.82
21950	Tnfsf9	tumor necrosis factor (ligand) superfamily, member 9	-1.04	1.49	1.45	0.77	0.84	0.82
14841	Gsg2	germ cell-specific gene 2	-1.03	1.54	2.22	0.80	0.77	0.82
328561	Apol10b	apolipoprotein L 10b	-1.26	7.27	39.11	0.81	0.84	0.82
20307	Ccl8	chemokine (C-C motif) ligand 8	-1.01	3.97	50.18	0.78	0.86	0.82
15186	Hdc	histidine decarboxylase	-1.14	1.26	5.97	0.83	0.76	0.82
72415	Sgol1	shugoshin-like 1 (S. pombe)	-1.17	1.02	1.99	0.79	0.77	0.82
16153	Il10	interleukin 10	-1.07	1.26	2.37	0.79	0.84	0.82
14289	Fpr2	formyl peptide receptor 2	-1.20	1.76	6.48	0.81	0.80	0.81
20202	S100a9	S100 calcium binding protein A9 (calgranulin B)	-1.23	10.78	119.73	0.79	0.87	0.81
16878	Lif	leukemia inhibitory factor	1.17	2.29	6.15	0.78	0.80	0.81
54369	Nme6	non-metastatic cells 6, (nucleoside-diphosphate kinase)	-1.05	1.16	1.49	0.80	0.79	0.81
98415	Nucks1	nuclear casein kinase and cyclin-dependent kinase substrate 1	1.05	1.98	1.95	0.79	0.72	0.81
234463	Tmem184c	transmembrane protein 184C	1.03	2.47	3.94	0.80	0.81	0.81
12364	Casp12	caspase 12	-1.12	1.65	2.99	0.81	0.66	0.81
18414	Osmr	oncostatin M receptor	-1.15	2.51	4.22	0.81	0.75	0.81
66811	Duoxa2	dual oxidase maturation factor 2	1.05	2.01	5.12	0.78	0.82	0.80
71982	Snx10	sorting nexin 10	1.31	3.34	6.47	0.77	0.87	0.80
14114	Fbln1	fibulin 1	-1.11	1.14	1.91	0.83	0.70	0.80
76574	Mfsd2a	major facilitator superfamily domain containing 2A	1.15	3.55	36.56	0.74	0.90	0.80
71920	Ep gn	epithelial mitogen	-1.20	2.12	2.13	0.76	0.85	0.80
56644	Clec7a	C-type lectin domain family 7, member a	-1.55	2.45	16.90	0.79	0.81	0.80
101602	467606	expressed sequence AI467606	-1.17	1.23	1.78	0.78	0.79	0.80
80879	Slc16a3	solute carrier family 16 (monocarboxylic acid transporters), member 3	-1.13	1.52	1.91	0.80	0.81	0.80
22042	Tfrc	transferrin receptor	-1.02	1.15	1.40	0.78	0.84	0.80
14961	H2-Ab1	histocompatibility 2, class II antigen A, beta 1	1.44	7.53	23.41	0.78	0.81	0.80
65221	Slc15a3	solute carrier family 15, member 3	-1.10	1.22	1.83	0.77	0.80	0.80
17329	Cxcl9	chemokine (C-X-C motif) ligand 9	-1.08	2.88	74.33	0.77	0.82	0.80

Genes best correlated ($r_s > 0.8$) to histological score in Rag2^{-/-} x IL-10^{-/-} recipients

gene ID	gene name	description	gene expression (fold change of CTRL)			r _s : gene expression vs histo. score		
			CD25 ⁺ T cells	Wt CD25 ⁺ T cells	IL-10 ^{-/-} CD25 ⁺ T cells	Cecum	Colon	Cumulative
14373	G0s2	G0/G1 switch gene 2	-1.11	1.67	5.38	0.78	0.82	0.79
330122	Cxcl3	chemokine (C-X-C motif) ligand 3	-1.08	2.66	12.61	0.81	0.78	0.79
20762	Sprr2h	small proline-rich protein 2H	1.46	6.68	89.98	0.73	0.90	0.79
16149	Cd74	CD74 antigen	1.17	12.05	18.25	0.77	0.81	0.79
13017	Ctbp2	C-terminal binding protein 2	-1.15	1.64	1.71	0.76	0.83	0.79
229900	Gbp6	guanylate binding protein 6	1.04	6.35	8.27	0.76	0.81	0.78
17002	Ltf	lactotransferrin	1.06	4.53	9.36	0.73	0.86	0.77
68545	Ecsr	endothelial cell-specific chemotaxis regulator	1.22	2.16	11.44	0.74	0.83	0.77
11307	Abcg1	ATP-binding cassette, sub-family G (WHITE), member 1	-1.22	1.08	1.58	0.80	0.68	0.77
76074	Gbp8	guanylate-binding protein 8	-1.07	2.26	3.26	0.71	0.85	0.76
20556	Slnf2	schlafen 2	-1.06	2.37	5.85	0.74	0.82	0.75
19260	Ptpn22	protein tyrosine phosphatase, non-receptor type 22 (lymphoid)	-1.00	1.44	2.02	0.70	0.81	0.75
15958	Ifit2	interferon-induced protein with tetratricopeptide repeats 2	1.30	3.07	9.17	0.67	0.82	0.75
21333	Tac1	tachykinin 1	1.87	5.86	33.53	0.72	0.83	0.74
114304	Slc28a3	solute carrier family 28 (sodium-coupled nucleoside transporter), member 3	1.07	1.41	2.10	0.66	0.80	0.73
11641	Akap2	A kinase (PRKA) anchor protein 2	1.27	1.53	1.61	0.66	0.80	0.71
20701	Serpina1b	serine (or cysteine) peptidase inhibitor, clade A, member 1B	1.05	1.25	1.24	0.63	0.81	0.70
277089	Gm5068	predicted gene 5068	1.22	1.65	2.32	0.63	0.81	0.69
16768	Lag3	lymphocyte-activation gene 3	1.01	1.38	1.31	0.57	0.82	0.66
215748	Cnksr3	Cnksr family member 3	-1.24	-4.24	-2.72	-0.61	-0.81	-0.67
11668	Aldh1a1	aldehyde dehydrogenase family 1, subfamily A1	-1.04	-4.54	-4.67	-0.64	-0.82	-0.69
66530	Ubxn6	UBX domain protein 6	-1.10	-4.33	-1.64	-0.64	-0.81	-0.70
217732	2310044G17	RIKEN cDNA 2310044G17 gene	1.25	-3.35	-2.86	-0.66	-0.81	-0.71
76768	Alpi	alkaline phosphatase, intestinal	-2.37	-14.65	-13.14	-0.63	-0.81	-0.71
16168	Il15	interleukin 15	-1.06	-5.69	-5.85	-0.69	-0.82	-0.71
56448	Cyp2d2	cytochrome P450, family 2, subfamily 2, polypeptide 22	-1.24	-3.64	-3.26	-0.66	-0.83	-0.72
59038	Pxmp4	peroxisomal membrane protein 4	-1.35	-4.81	-4.66	-0.66	-0.84	-0.72
14786	Grb7	growth factor receptor bound protein 7	-1.11	-7.71	-2.80	-0.67	-0.81	-0.72
66990	Tmem134	transmembrane protein 134	1.02	-1.60	-1.63	-0.71	-0.81	-0.72
56807	Scamp5	secretory carrier membrane protein 5	-1.22	-2.78	-2.17	-0.69	-0.81	-0.73
70510	Rnf167	ring finger protein 167	1.19	-5.00	-3.10	-0.68	-0.80	-0.73
77219	Ptgr2	prostaglandin reductase 2	-1.10	-2.53	-1.72	-0.67	-0.82	-0.73
68338	Golt1a	golgi transport 1 homolog A	-1.21	-9.30	-2.74	-0.69	-0.82	-0.73
17161	Maoa	monoamine oxidase A	-1.11	-2.50	-2.22	-0.70	-0.82	-0.73
74901	Kbtbd11	kelch repeat and BTB (POZ) domain containing 11	-1.07	-5.35	-6.13	-0.69	-0.83	-0.74
14979	H2-Ke6	H2-K region expressed gene 6	1.08	-2.59	-2.43	-0.69	-0.84	-0.74
114664	Hsd17b11	hydroxysteroid (17-beta) dehydrogenase 11	-1.09	-1.98	-1.46	-0.70	-0.80	-0.74
11826	Aqp1	aquaporin 1	1.22	-6.79	-4.71	-0.70	-0.81	-0.74

Genes best correlated ($r_s > 0.8$) to histological score in Rag2^{-/-} x IL-10^{-/-} recipients

gene ID	gene name	description	gene expression (fold change of CTRL)			r _s : gene expression vs histo. score		
			CD25 ⁺ T cells	Wt CD25 ⁺ T cells	IL-10 ^{-/-} CD25 ⁺ T cells	Cecum	Colon	Cumulative
231396	Ugt2b3 6	UDP glucuronosyltransferase 2 family, polypeptide B36	-1.18	-3.27	-4.83	-0.70	-0.86	-0.74
13897	Es22	esterase 22	1.07	-3.15	-2.40	-0.72	-0.84	-0.75
11551	Adra2a	adrenergic receptor, alpha 2a	-1.23	-7.69	-7.08	-0.70	-0.85	-0.75
14605	Tsc22d3	TSC22 domain family, member 3	1.29	-6.37	-2.22	-0.71	-0.81	-0.75
12577	Cdkn1c	cyclin-dependent kinase inhibitor 1C	-1.77	-2.59	-3.71	-0.71	-0.85	-0.75
68616	Gdpd3	glycerophosphodiester phosphodiesterase domain containing 3	-1.30	-3.29	-1.60	-0.72	-0.83	-0.75
223646	Naprt1	nicotinate phosphoribosyltransferase domain containing 1	1.06	-4.94	-3.10	-0.71	-0.81	-0.75
103551	E13001 2A19	RIKEN cDNA E130012A19 gene	-1.51	-3.50	-4.21	-0.73	-0.81	-0.76
13487	Slc26a3	solute carrier family 26, member 3	-1.03	-3.93	-5.28	-0.74	-0.81	-0.76
328330	D13003 7M23	RIKEN cDNA D130037M23 gene	1.05	-1.81	-1.67	-0.70	-0.85	-0.76
17287	Mep1a	mepriin 1 alpha	1.15	-9.23	-10.42	-0.73	-0.83	-0.76
50776	Polg2	polymerase (DNA directed), gamma 2, accessory subunit	1.23	-3.06	-1.92	-0.73	-0.81	-0.76
17181	Matn2	matrilin 2	-1.78	-3.34	-8.94	-0.69	-0.83	-0.76
235674	Acaa1b	acetyl-CoA acyltransferase 1B	-1.77	-27.28	-24.80	-0.72	-0.83	-0.76
66822	Fbxo25	F-box protein 25	-1.06	-5.89	-3.17	-0.71	-0.83	-0.76
14149	Fdxr	ferredoxin reductase	-1.04	-3.08	-3.16	-0.73	-0.82	-0.76
114654	Ly6g6d	lymphocyte antigen 6 complex, locus G6D	1.01	-1.60	-1.71	-0.72	-0.84	-0.76
16854	Lgals3	lectin, galactose binding, soluble 3	-1.04	-1.78	-1.61	-0.75	-0.80	-0.76
93721	Cpn1	carboxypeptidase N, polypeptide 1	-4.04	-10.81	-12.27	-0.76	-0.82	-0.76
227801	Dennd1 a	DENN/MADD domain containing 1A	1.04	-1.42	-1.56	-0.73	-0.82	-0.77
94282	Sfxn5	sideroflexin 5	1.21	-1.41	-1.47	-0.72	-0.85	-0.77
66273	181002 0D17	RIKEN cDNA 1810020D17 gene	-1.05	-8.92	-2.52	-0.73	-0.80	-0.77
99663	Clca6	chloride channel calcium activated 6	-1.53	-10.48	-8.58	-0.73	-0.81	-0.77
225997	Trpm6	transient receptor potential cation channel, subfamily M, member 6	-1.47	-12.08	-8.07	-0.73	-0.84	-0.77
12651	Chkb	choline kinase beta	-1.21	-3.54	-2.73	-0.71	-0.81	-0.77
14672	Gna11	guanine nucleotide binding protein, alpha 11	-1.04	-2.53	-1.58	-0.73	-0.84	-0.77
13730	Emp1	epithelial membrane protein 1	-1.16	-3.15	-4.64	-0.76	-0.83	-0.77
217138	Prr15l	proline rich 15-like	-1.21	-1.64	-1.79	-0.73	-0.81	-0.77
238055	Apob	apolipoprotein B	-1.03	-1.43	-2.04	-0.75	-0.81	-0.77
99586	Dpyd	dihydropyrimidine dehydrogenase	1.42	-2.06	-3.50	-0.74	-0.82	-0.77
26357	Abcg2	ATP-binding cassette, sub-family G (WHITE), member 2	-1.12	-5.92	-4.29	-0.76	-0.83	-0.77
68024	Hist1h2 bc	histone cluster 1, H2bc	-1.19	-2.79	-3.04	-0.75	-0.84	-0.77
20501	Slc16a 1	solute carrier family 16 (monocarboxylic acid transporters), member 1	-1.01	-4.18	-3.57	-0.75	-0.82	-0.78
380629	Heca	headcase homolog (Drosophila)	1.04	-2.00	-2.07	-0.75	-0.83	-0.78
69083	Sult1c2	sulfotransferase family, cytosolic, 1C, member 2	1.09	-16.36	-26.57	-0.76	-0.84	-0.78
319604	Fam16 8a	family with sequence similarity 168, member A	1.13	-1.50	-1.80	-0.81	-0.72	-0.78
381409	Cdh26	cadherin-like 26	1.07	-1.44	-1.74	-0.72	-0.88	-0.78
20887	Sult1a1	sulfotransferase family 1A, phenol-preferring, member 1	1.28	-8.65	-9.05	-0.75	-0.81	-0.78

Genes best correlated ($r_s > 0.8$) to histological score in Rag2^{-/-} x IL-10^{-/-} recipients

gene ID	gene name	description	gene expression (fold change of CTRL)			r_s : gene expression vs histo. score		
			CD25 ⁺ T cells	Wt CD25 ⁺ T cells	IL-10 ^{-/-} CD25 ⁺ T cells	Cecum	Colon	Cumulative
72948	Tppp	tubulin polymerization promoting protein	1.45	-9.26	-11.07	-0.76	-0.80	-0.78
104271	Tex15	testis expressed gene 15	1.30	-1.79	-4.08	-0.75	-0.83	-0.78
228765	Sdcbp2	syndecan binding protein (syntenin) 2	-1.23	-2.69	-2.73	-0.78	-0.80	-0.78
68738	Acss1	acyl-CoA synthetase short-chain family member 1	1.10	-4.61	-3.05	-0.76	-0.81	-0.78
12346	Car1	carbonic anhydrase 1	1.01	-2.73	-3.26	-0.76	-0.85	-0.78
68347	0610011F06	RIKEN cDNA 0610011F06 gene	-1.04	-3.87	-2.87	-0.75	-0.83	-0.78
14794	Spsb2	splA/ryanodine receptor domain and SOCS box containing 2	-1.16	-1.98	-2.03	-0.75	-0.82	-0.79
53315	Sult1d1	sulfotransferase family 1D, member 1	-1.07	-3.04	-5.08	-0.77	-0.86	-0.79
66601	Tmigd1	transmembrane and immunoglobulin domain containing 1	-1.42	-4.21	-5.07	-0.73	-0.90	-0.79
234564	AU018778	expressed sequence AU018778	-1.08	-5.79	-3.98	-0.73	-0.88	-0.79
103711	Pnpo	pyridoxine 5'-phosphate oxidase	-1.14	-8.18	-5.03	-0.75	-0.85	-0.79
13850	Ephx2	epoxide hydrolase 2, cytoplasmic	-1.12	-15.37	-11.56	-0.75	-0.86	-0.79
20517	Slc22a1	solute carrier family 22 (organic cation transporter), member 1	-1.05	-4.35	-2.94	-0.75	-0.82	-0.79
67763	Prpsap1	phosphoribosyl pyrophosphate synthetase-associated protein 1	-1.03	-2.10	-1.76	-0.74	-0.89	-0.79
21818	Tgm3	transglutaminase 3, E polypeptide	2.34	-5.31	-5.18	-0.82	-0.73	-0.79
107227	MacroD	MACRO domain containing 1	1.12	-6.79	-4.61	-0.78	-0.80	-0.79
268663	Cdhr2	cadherin-related family member 2	-1.16	-3.30	-3.20	-0.75	-0.85	-0.79
30794	Pdlim4	PDZ and LIM domain 4	1.10	-4.57	-5.02	-0.81	-0.80	-0.79
231717	Fam109a	family with sequence similarity 109, member A	1.07	-1.22	-1.78	-0.77	-0.82	-0.79
18671	Abcb1a	ATP-binding cassette, sub-family B (MDR/TAP), member 1A	-1.11	-10.49	-14.68	-0.75	-0.87	-0.79
16956	Lpl	lipoprotein lipase	1.02	-2.58	-15.68	-0.79	-0.80	-0.79
70152	Mettl	methyltransferase like 7A1	1.11	-5.56	-6.57	-0.79	-0.83	-0.79
66071	Ethe1	ethylmalonic encephalopathy 1	-1.04	-3.20	-2.86	-0.76	-0.84	-0.79
20535	Slc4a2	solute carrier family 4 (anion exchanger), member 2	-1.09	-2.35	-1.77	-0.75	-0.86	-0.79
213522	Plekhg6	pleckstrin homology domain containing, family G member 6	-1.34	-1.94	-2.99	-0.77	-0.83	-0.80
72040	Cdhr5	cadherin-related family member 5	1.08	-2.40	-2.32	-0.80	-0.76	-0.80
22785	Slc30a4	solute carrier family 30 (zinc transporter), member 4	-1.28	-1.74	-2.23	-0.74	-0.90	-0.80
14635	Galk1	galactokinase 1	1.13	-2.52	-1.97	-0.79	-0.82	-0.80
114679	Selm	selenoprotein M	1.37	-3.42	-3.33	-0.80	-0.78	-0.80
71597	Isx	intestine specific homeobox	-1.41	-3.87	-3.95	-0.75	-0.87	-0.80
11735	Ank3	ankyrin 3, epithelial	1.23	-1.39	-1.54	-0.81	-0.75	-0.80
13808	Eno3	enolase 3, beta muscle	1.13	-3.63	-2.21	-0.81	-0.77	-0.80
52521	Zfp622	zinc finger protein 622	1.05	-4.52	-2.95	-0.78	-0.79	-0.80
11732	Ank	progressive ankylosis	1.50	-5.40	-7.79	-0.78	-0.83	-0.80
56857	Slc37a2	solute carrier family 37 (glycerol-3-phosphate transporter), member 2	1.34	-13.20	-14.76	-0.75	-0.87	-0.80
66734	Map1lc3a	microtubule-associated protein 1 light chain 3 alpha	-1.04	-2.96	-2.66	-0.80	-0.75	-0.80
433023	Gm5485	predicted gene 5485	1.02	-5.88	-4.62	-0.77	-0.82	-0.80
67013	Oma1	OMA1 homolog, zinc metallopeptidase (<i>S. cerevisiae</i>)	-1.04	-3.13	-2.53	-0.77	-0.86	-0.80

Genes best correlated ($r_s > 0.8$) to histological score in Rag2^{-/-} x IL-10^{-/-} recipients

gene ID	gene name	description	gene expression (fold change of CTRL)			r_s : gene expression vs histo. score		
			CD25 ⁺ T cells	Wt CD25 ⁺ T cells	IL-10 ^{-/-} CD25 ⁺ T cells	Cecum	Colon	Cumulative
67445	C1qtnf4	C1q and tumor necrosis factor related protein 4	1.32	-1.46	-1.49	-0.80	-0.79	-0.81
67709	Reg4	regenerating islet-derived family, member 4	1.23	-1.77	-2.63	-0.81	-0.76	-0.81
15360	Hmgcs2	3-hydroxy-3-methylglutaryl-Coenzyme A synthase 2	1.15	-9.13	-12.37	-0.78	-0.82	-0.81
74548	Gsdmc4	gasdermin C4	1.40	-1.56	-2.39	-0.82	-0.79	-0.81
54120	Gipc2	GIPC PDZ domain containing family, member 2	-1.05	-4.15	-3.40	-0.79	-0.81	-0.81
70113	Odf3b	outer dense fiber of sperm tails 3B	-1.21	-1.79	-2.68	-0.79	-0.83	-0.81
18534	Pck1	phosphoenolpyruvate carboxykinase 1, cytosolic	1.28	-6.11	-10.80	-0.77	-0.85	-0.81
432720	Akr1c19	aldo-keto reductase family 1, member C19	1.13	-8.44	-9.61	-0.78	-0.88	-0.81
54391	Rfk	riboflavin kinase	-1.19	-2.40	-3.06	-0.76	-0.88	-0.81
20148	Dhrs3	dehydrogenase/reductase (SDR family) member 3	1.03	-3.04	-2.70	-0.76	-0.81	-0.81
12623	Ces1	carboxylesterase 1	1.20	-24.02	-34.44	-0.80	-0.81	-0.81
20363	Sepp1	selenoprotein P, plasma, 1	-1.38	-4.23	-5.41	-0.76	-0.89	-0.81
67564	Tmem35	transmembrane protein 35	-1.04	-1.36	-1.92	-0.82	-0.74	-0.81
1E+08	Gm16418	ubiquinol-cytochrome c reductase subunit pseudogene	1.14	-2.30	-1.47	-0.82	-0.74	-0.81
12411	Cbs	cystathionine beta-synthase	1.35	-2.60	-3.85	-0.81	-0.77	-0.81
69726	Smyd3	SET and MYND domain containing 3	1.08	-1.39	-1.40	-0.80	-0.83	-0.81
20655	Sod1	superoxide dismutase 1, soluble	1.15	-2.26	-1.49	-0.80	-0.79	-0.81
20287	Sct	secretin	-1.36	-2.96	-2.96	-0.76	-0.88	-0.81
226654	Tstd1	thiosulfate sulfurtransferase (rhodanese)-like domain containing 1	1.01	-1.95	-2.54	-0.79	-0.83	-0.81
56327	Arl2	ADP-ribosylation factor-like 2	1.20	-2.10	-2.12	-0.82	-0.80	-0.82
67405	Nts	neurotensin	-1.01	-2.62	-2.99	-0.77	-0.87	-0.82
73072	BC068157	cDNA sequence BC068157	1.14	-1.22	-1.33	-0.79	-0.78	-0.82
13823	Epb4.1l3	erythrocyte protein band 4.1-like 3	-1.01	-1.65	-2.10	-0.77	-0.87	-0.82
14263	Fmo5	flavin containing monooxygenase 5	-1.24	-2.96	-3.41	-0.78	-0.83	-0.82
13120	Cyp4b1	cytochrome P450, family 4, subfamily b, polypeptide 1	-1.30	-32.31	-46.03	-0.79	-0.84	-0.82
14963	H2-BI	histocompatibility 2, blastocyst	-1.69	-3.82	-3.60	-0.76	-0.88	-0.82
73822	F630110N24	RIKEN cDNA F630110N24 gene	-1.04	-1.85	-2.04	-0.81	-0.83	-0.82
170716	Cyp4f13	cytochrome P450, family 4, subfamily f, polypeptide 13	1.33	-3.26	-3.11	-0.79	-0.85	-0.82
71664	Mettl7b	methyltransferase like 7B	1.01	-4.71	-5.58	-0.78	-0.88	-0.82
102566	Ano10	anoctamin 10	1.12	-3.24	-3.25	-0.85	-0.77	-0.82
67307	3110049J23	RIKEN cDNA 3110049J23 gene	1.16	-2.15	-4.07	-0.83	-0.78	-0.82
232227	Iqsec1	IQ motif and Sec7 domain 1	1.01	-1.90	-1.98	-0.84	-0.79	-0.82
225010	Lclat1	lysocardiolipin acyltransferase 1	1.17	-1.28	-1.24	-0.82	-0.79	-0.82
72269	Cda	cytidine deaminase	-1.35	-24.62	-26.43	-0.79	-0.86	-0.82
69864	1810065E05	RIKEN cDNA 1810065E05 gene	1.03	-2.11	-3.07	-0.82	-0.83	-0.83
14533	Bloc1s1	biogenesis of lysosome-related organelles complex-1, subunit 1	-1.02	-2.20	-1.60	-0.80	-0.83	-0.83
67426	Cabc1	chaperone, ABC1 activity of bc1 complex like (S. pombe)	1.44	-2.99	-4.66	-0.80	-0.84	-0.83

Genes best correlated ($r_s > 0.8$) to histological sore in Rag2^{-/-} x IL-10^{-/-} recipients

gene ID	gene name	description	gene expression (fold change of CTRL)			r_s : gene expression vs histo. score		
			CD25 ⁺ T cells	Wt CD25 ⁺ T cells	IL-10 ^{-/-} CD25 ⁻ T cells	Cecum	Colon	Cumulative
13370	Dio1	deiodinase, iodothyronine, type I	-1.21	-10.65	-9.79	-0.79	-0.87	-0.83
22238	Ugt2b5	UDP glucuronosyltransferase 2 family, polypeptide B5	-1.08	-6.09	-4.94	-0.77	-0.88	-0.83
13107	Cyp2f2	cytochrome P450, family 2, subfamily f, polypeptide 2	2.17	-2.14	-4.16	-0.86	-0.75	-0.83
110075	Bmp3	bone morphogenetic protein 3	1.44	-2.57	-3.23	-0.81	-0.81	-0.83
225791	Zadh2	zinc binding alcohol dehydrogenase, domain containing 2	1.03	-1.91	-1.42	-0.80	-0.83	-0.83
20441	St3gal3	ST3 beta-galactoside alpha-2,3-sialyltransferase 3	1.37	-3.07	-2.59	-0.83	-0.79	-0.83
192654	Pla2g15	phospholipase A2, group XV	-1.17	-2.39	-2.42	-0.83	-0.83	-0.83
12460	Ccs	copper chaperone for superoxide dismutase	1.18	-3.77	-4.76	-0.83	-0.84	-0.83
15184	Hdac5	histone deacetylase 5	1.30	-1.49	-2.07	-0.83	-0.83	-0.83
66090	Ypel3	yippee-like 3 (Drosophila)	-1.02	-3.20	-3.69	-0.82	-0.90	-0.83
16548	Khk	ketohexokinase	1.32	-1.88	-2.61	-0.85	-0.81	-0.84
66066	Gng11	guanine nucleotide binding protein (G protein), gamma 11	-1.04	-2.37	-2.07	-0.79	-0.87	-0.84
22235	Ugdh	UDP-glucose dehydrogenase	-1.06	-2.86	-3.12	-0.79	-0.88	-0.84
68416	Sycn	syncollin	2.21	-5.11	-18.16	-0.82	-0.81	-0.84
12953	Cry2	cryptochrome 2 (photolyase-like)	1.20	-2.08	-2.87	-0.84	-0.85	-0.84
11997	Akr1b7	aldo-keto reductase family 1, member B7	-1.99	-4.27	-6.54	-0.79	-0.89	-0.84
14079	Fabp2	fatty acid binding protein 2, intestinal	-1.50	-4.69	-9.49	-0.80	-0.92	-0.84
12351	Car4	carbonic anhydrase 4	-1.22	-5.08	-6.80	-0.78	-0.92	-0.84
11833	Aqp8	aquaporin 8	-1.40	-5.69	-8.23	-0.83	-0.87	-0.84
320024	Nceh1	arylacetamide deacetylase-like 1	-1.02	-3.32	-4.79	-0.81	-0.91	-0.84
13047	Cux1	cut-like homeobox 1	1.27	-1.42	-1.84	-0.85	-0.80	-0.85
67460	Decr1	2,4-dienoyl CoA reductase 1, mitochondrial	1.12	-3.63	-1.52	-0.82	-0.82	-0.85
216019	Hkdc1	hexokinase domain containing 1	-1.09	-3.52	-6.27	-0.80	-0.89	-0.85
57276	Vsig2	V-set and immunoglobulin domain containing 2	-1.03	-7.17	-10.45	-0.81	-0.89	-0.85
622404	Ccdc107	coiled-coil domain containing 107	1.20	-3.89	-3.07	-0.83	-0.86	-0.86
212398	Frat2	frequently rearranged in advanced T-cell lymphomas 2	1.13	-2.27	-4.08	-0.83	-0.86	-0.86
217214	Nags	N-acetylglutamate synthase	-1.21	-1.71	-2.45	-0.82	-0.89	-0.86
102022	Ces6	carboxylesterase 6	-1.85	-8.11	-13.52	-0.81	-0.92	-0.86
67971	Tppp3	tubulin polymerization-promoting protein family member 3	1.90	-6.14	-10.34	-0.89	-0.77	-0.86
85308	Fam158a	family with sequence similarity 158, member A	-1.15	-2.03	-2.46	-0.84	-0.81	-0.87
12925	Crip1	cysteine-rich protein 1 (intestinal)	1.00	-4.06	-5.09	-0.86	-0.87	-0.87
56695	Pnkd	paroxysmal nonkinesinogenic dyskinesia	1.01	-1.28	-1.38	-0.85	-0.79	-0.87
22239	Ugt8a	UDP galactosyltransferase 8A	1.30	-2.55	-5.92	-0.84	-0.88	-0.87
58210	Sectm	secreted and transmembrane 1B	-1.19	-3.14	-5.17	-0.85	-0.89	-0.87
66353	2310007A19	RIKEN cDNA 2310007A19Rik	1.10	-2.26	-2.58	-0.84	-0.85	-0.87
68943	Pink1	PTEN induced putative kinase 1	1.01	-1.65	-2.38	-0.86	-0.90	-0.87
11409	Acads	acyl-Coenzyme A dehydrogenase, short chain	-1.12	-2.75	-2.90	-0.83	-0.91	-0.88
12522	Cd83	CD83 antigen	1.21	-1.14	-1.49	-0.85	-0.88	-0.88

Genes best correlated ($r_s > 0.8$) to histological score in Rag2^{-/-} x IL-10^{-/-} recipients

gene ID	gene name	description	gene expression (fold change of CTRL)			r_s : gene expression vs histo. score		
			CD25 ⁺ T cells	Wt CD25 ⁻ T cells	IL-10 ^{-/-} CD25 ⁻ T cells	Cecum	Colon	Cumulative
319176	Hist2h2ac	histone cluster 2, H2ac	-1.12	-2.32	-3.10	-0.83	-0.91	-0.88
20393	Sgk1	serum/glucocorticoid regulated kinase 1	1.12	-2.86	-6.80	-0.88	-0.84	-0.88
68047	Mpnd	MPN domain containing	1.15	-1.95	-1.55	-0.88	-0.85	-0.89
14915	Guca2a	guanylate cyclase activator 2a (guanylin)	1.07	-3.69	-6.39	-0.87	-0.91	-0.89
66859	Slc16a9	solute carrier family 16 (monocarboxylic acid transporters), member 9	-1.24	-2.93	-9.10	-0.85	-0.91	-0.89
104158	Ces3	carboxylesterase 3	1.24	-35.07	-62.28	-0.86	-0.90	-0.90
13614	Edn1	endothelin 1	-1.02	-1.91	-4.91	-0.89	-0.84	-0.90
22139	Ttr	transthyretin	1.65	-3.59	-5.01	-0.89	-0.85	-0.90
67758	Aadac	arylacetamide deacetylase (esterase)	1.39	-3.67	-5.20	-0.91	-0.80	-0.90
72082	Cyp2c55	cytochrome P450, family 2, subfamily c, polypeptide 55	-1.06	-41.26	-184.08	-0.89	-0.90	-0.91
20341	Selenbp1	selenium binding protein 1	1.11	-3.00	-4.31	-0.88	-0.91	-0.91
74134	Cyp2s1	cytochrome P450, family 2, subfamily s, polypeptide 1	1.01	-2.34	-2.97	-0.87	-0.90	-0.91
70337	lyd	iodotyrosine deiodinase	1.05	-2.73	-4.90	-0.90	-0.92	-0.93

Table A4. Genes best correlated (according to Spearman correlation coefficient, $r_s > 0.8$) to the presence of IL-10 and fold changes in gene expression after Wt CD4⁺ CD25⁺ T cell transfer to Rag2^{-/-} or Rag2^{-/-} x IL-10^{-/-} recipients vs non-reconstituted controls. The values assigned to the presence of IL-10 were: 0 for unreconstituted Rag2^{-/-} x IL-10^{-/-} mice; 1 for unreconstituted Rag2^{-/-} mice and 2 for Rag2^{-/-} x IL-10^{-/-} mice reconstituted with Wt CD4⁺ CD25⁺ T cells. The one-sided significance for r_s was $P < 0.001$ for all genes with $r_s > 0.8$.

Genes best correlated ($r_s > 0.8$) to the presence of IL-10

gene ID	gene name	description	gene expression: CD4 ⁺ CD25 ⁺ T cell transfer (fold change of CTRL)		r_s : IL-10 presence
			Rag2 ^{-/-} recipients	Rag2 ^{-/-} x IL10 ^{-/-} recipients	
209195	Clic6	chloride intracellular channel 6	-1.07	1.94	0.94
23882	Gadd45g	growth arrest and DNA-damage-inducible 45 γ	1.58	2.46	0.91
15433	Hoxd13	homeobox D13	1.80	3.63	0.87
20935	Surf6	surfeit gene 6	1.03	1.29	0.85
67441	Isoc2b	isochorismatase domain containing 2b	-1.08	2.02	0.85
102626	Mapkapk3	MAP kinase-activated protein kinase 3	1.22	2.15	0.85
23996	Psmc4	proteasome 26S subunit, ATPase, 4	1.01	1.29	0.83
235130	Adamts15	a disintegrin-like and metallopeptidase with thrombospondin type 1 motif, 15	1.11	1.78	0.83
240672	Dusp5	dual specificity phosphatase 5	1.57	2.30	0.83
13144	Dapk3	death-associated protein kinase 3	1.22	1.80	0.81
14645	Glul	glutamate-ammonia ligase (glut. synthetase)	1.11	1.53	0.81
19064	Ppy	pancreatic polypeptide	1.34	2.07	0.81
21991	Tpi1	triosephosphate isomerase 1	1.03	1.52	0.81
56473	Fads2	fatty acid desaturase 2	-1.01	1.97	0.81
67201	Glod4	glyoxalase domain containing 4	1.15	1.29	0.81
67963	Npc2	Niemann Pick type C2	1.07	1.59	0.81
110595	Timp4	tissue inhibitor of metalloproteinase 4	-1.15	2.18	0.81
380712	Tlcd2	TLC domain containing 2	1.05	1.75	0.81
16162	Il12rb2	interleukin 12 receptor, beta 2	-1.14	-1.22	-0.81
18127	Nos3	nitric oxide synthase 3, endothelial cell	-1.04	-1.29	-0.81
59043	Wsb2	WD repeat and SOCS box-containing 2	-1.11	-1.56	-0.81
66495	Ndufb3	NADH dehydrogenase 1 beta subcomplex 3	-1.06	-1.13	-0.81
67345	Herc4	hect domain and RLD 4	1.05	-1.22	-0.81
69802	Cox11	Cytochrome c oxidase assembly protein	-1.43	-1.39	-0.81
214639	4930486L24Rik	RIKEN cDNA 4930486L24 gene	1.06	-1.57	-0.81
432530	Adcy1	adenylate cyclase 1	-1.13	-1.50	-0.81
12577	Cdkn1c	cyclin-dependent kinase inhibitor 1C (P57)	1.14	-1.77	-0.83
15199	Hebp1	heme binding protein 1	-1.17	-1.63	-0.83
66845	Mrpl33	mitochondrial ribosomal protein L33	-1.02	-1.14	-0.83
73344	1700034J05Rik	RIKEN cDNA 1700034J05 gene	-1.01	-1.35	-0.83
83603	Elovl4	elongation of very long chain fatty acids-like 4	-1.31	-1.44	-0.83
14588	Gfra4	glial cell line derived neurotrophic factor family receptor alpha 4	-1.00	-1.21	-0.85
64011	Nrgn	neurogranin	-1.07	-1.66	-0.85
1000389	Gm1985	predicted gene 1985	1.10	-1.29	-0.85

Genes best correlated ($r_s > 0.8$) to the presence of IL-10

gene ID	gene name	description	gene expression: CD4 ⁺ CD25 ⁺ T cell transfer (fold change of CTRL)		r_s : IL-10 presence
			Rag2 ^{-/-} recipients	Rag2 ^{-/-} x IL10 ^{-/-} recipients	
14598	Ggt1	gamma-glutamyltransferase 1	1.06	-3.93	-0.87
56736	Rnf14	ring finger protein 14	-1.04	-1.20	-0.87
66358	2310004I24Rik	RIKEN cDNA 2310004I24 gene	-1.23	-1.73	-0.87
218977	Dlgap5	discs, large homolog-associated protein 5	1.08	-1.39	-0.87
227671	Gbgt1	globoside alpha-1,3-N- acetylgalactosaminyltransferase 1	1.10	-1.35	-0.87
235330	Ttc12	tetratricopeptide repeat domain 12	-1.06	-1.29	-0.87
78482	1700123L14Rik	nucleoporin 50 pseudogene	1.04	-1.45	-0.93
19226	Pth	parathyroid hormone	1.06	-1.26	-0.94

LIST OF FIGURES

Figure 1. Intestinal alterations in IBD cluster around IEC.	12
Figure 2. Schematic illustration of unfolded protein responses.	13
Figure 3. Endoplasmic reticulum unfolded protein response and associated signaling.	16
Figure 4. Mitochondrial unfolded protein response in <i>C elegans</i> and primate cells.	24
Figure 5. ER- mitochondrial network.	28
Figure 6. Inflammatory changes following CD4 ⁺ T cell transfer and purity of IEC isolation. .	46
Figure 7. Protein expression profiling links ER- and mitochondrial stress in intestinal inflammation.	48
Figure 8. ER chaperone GRP78, mitochondrial CPN60 and PKR are induced in primary IEC in response to colitogenic T cell transfer.	51
Figure 9. ER chaperone GRP78, mitochondrial CPN60 and PKR are induced in primary IEC in bacteria-induced colitis.	51
Figure 10. ER chaperone GRP78, mitochondrial CPN60 and PKR are induced in primary IEC from IBD patients.	53
Figure 11. Autophagy is induced in primary IEC following T cell transfer.	54
Figure 12. Truncated OTC induces mtUPR in Mode-K cells.	55
Figure 13. Mitochondrial UPR integrates into ER UPR-signaling via PKR and AP1.	57
Figure 14. Mitochondrial UPR does not induce ATF4 but Akt phosphorylation	58
Figure 15. Mitochondrial UPR-mediated PKR-induction is Ca ²⁺ and PACT independent.	60
Figure 16. Mitochondrial UPR signaling is dependent on PKR.	61
Figure 17. Tunicamycin-induced ER UPR signaling is not dependent on PKR	62
Figure 18. Mitochondrial UPR-signaling employs MEK and JNK2/3 and is dependent on ClpP	62
Figure 19. Mitochondrial UPR induces autophagy	63
Figure 20. <i>Pkr</i> ^{-/-} mice display enhanced colonic barrier function and increased mitochondrial markers	64
Figure 21. <i>Pkr</i> ^{-/-} mice show reduced sensitivity to DSS-induced colitis.	65
Figure 22. Mitochondrial abundance declines in <i>Pkr</i> ^{-/-} mice upon DSS-treatment.	66
Figure 23. Mitochondrial biogenesis is impaired in <i>Pkr</i> ^{-/-} mice upon DSS-treatment.	67
Figure 24. Histological changes in the large intestine of <i>Rag2</i> ^{-/-} and <i>Rag2</i> ^{-/-} x <i>IL-10</i> ^{-/-} recipients in response to regulatory or colitogenic T cell transfer.	70
Figure 25. Number and overlap of regulated genes in IEC of <i>Rag2</i> ^{-/-} and <i>Rag2</i> ^{-/-} x <i>IL-10</i> ^{-/-} recipients in response to CD4 ⁺ T cell transfer.	71
Figure 26. P21-activated kinase pathway.	85
Figure 27. Interleukin 6 pathway.	85
Figure 28. Genes best correlated to the histological score (cecum) in IEC of <i>Rag2</i> ^{-/-} recipients 4 weeks after CD4 ⁺ T cell transfer according to r_s and using gene intensities obtained by MADMAX software.	87

Figure 29. Genes best correlated to the histological score (cecum) in IEC of Rag2 ^{-/-} x IL-10 ^{-/-} recipients 4 weeks after CD4 ⁺ T cell transfer according to r _s and using gene intensities obtained by MADMAX software.	88
Figure 30. Genes best correlated to the histological score (colon) in IEC of Rag2 ^{-/-} recipients 4 weeks after CD4 ⁺ T cell transfer according to r _s and using gene intensities obtained by MADMAX software.	89
Figure 31. Genes best correlated to the histological score (colon) in IEC of Rag2 ^{-/-} x IL-10 ^{-/-} recipients 4 weeks after CD4 ⁺ T cell transfer according to r _s and using gene intensities obtained by MADMAX software.	90
Figure 32. Genes best correlated to the histological score (cumulative) in IEC of Rag2 ^{-/-} recipients 4 weeks after CD4 ⁺ T cell transfer according to r _s and using gene intensities obtained by MADMAX software.	91
Figure 33. Genes best correlated to histological score (cumulative) in IEC of Rag2 ^{-/-} x IL-10 ^{-/-} recipients 4 weeks after CD4 ⁺ T cell transfer according to r _s and using gene intensities obtained by MADMAX software.	92
Figure 34. Genes best correlated to the presence of non-T cell-/ T cell-derived IL-10 in IEC of recipients 4 weeks after non-colitogenic CD4 ⁺ CD25 ⁺ T cell transfer according to r _s and using gene intensities obtained by MADMAX software.	94
Figure 35. Schematic illustration of mitochondrial- and ER UPR integration.	96
Figure 36. Proposed mechanisms of mtUPR-induction.	97
Figure 37. Possible consequences of PKR-signaling under stress conditions.	98
Figure 38. Mitochondria as integrators of cellular danger signaling.	100
Figure 39. Involvement of Cyp2c55 and Ido1 in melatonin metabolism.	103
Figure 40. Cellular stress responses form a tightly interrelated network.	104

LIST OF TABLES

Table 1. Criteria for scoring the disease activity index (DAI)	35
Table 2. Primer sequences for real-time PCR	43
Table 3. Histological scores of Rag2 ^{-/-} and Rag2 ^{-/-} x IL-10 ^{-/-} recipients.	46
Table 4. Pkr ^{-/-} mice show reduced sensitivity to DSS-induced colitis.	65
Table 5. Number of regulated genes in Rag2 ^{-/-} and Rag2 ^{-/-} x IL-10 ^{-/-} recipients according to Genomatix ChipInspector or MADMAX software and number of genes found in both analyses.....	71
Table 6. Most highly regulated genes in IEC of Rag2 ^{-/-} recipients after CD4 ⁺ CD25 ⁺ T cell transfer according to Genomatix ChipInspector software	73
Table 7. Most highly regulated genes in IEC of Rag2 ^{-/-} recipients after CD4 ⁺ CD25 ⁺ T cell transfer according to MADMAX software.	73
Table 8. Most highly regulated genes in IEC of Rag2 ^{-/-} x IL-10 ^{-/-} recipients after CD4 ⁺ CD25 ⁺ T cell transfer according to Genomatix ChipInspector software	74
Table 9. Most highly regulated genes in IEC of Rag2 ^{-/-} x IL-10 ^{-/-} recipients after CD4 ⁺ CD25 ⁺ T cell transfer according to MADMAX software	74
Table 10. Most highly regulated genes in IEC of Rag2 ^{-/-} recipients after Wt CD4 ⁺ CD25 ⁻ T cell transfer according to Genomatix ChipInspector software	75
Table 11. Most highly regulated genes in IEC of Rag2 ^{-/-} recipients after Wt CD4 ⁺ CD25 ⁻ T cell transfer according to MADMAX software	75
Table 12. Most highly regulated genes in IEC of Rag2 ^{-/-} x IL-10 ^{-/-} recipients after Wt CD4 ⁺ CD25 ⁻ T cell transfer according to Genomatix ChipInspector software.....	76
Table 13. Most highly regulated genes in IEC of Rag2 ^{-/-} x IL-10 ^{-/-} recipients after Wt CD4 ⁺ CD25 ⁻ T cell transfer according to MADMAX software.....	76
Table 14. Most highly regulated genes in IEC of Rag2 ^{-/-} recipients after IL-10 ^{-/-} CD4 ⁺ CD25 ⁻ T cell transfer according to Genomatix ChipInspector software	77
Table 15. Most highly regulated genes in IEC of Rag2 ^{-/-} recipients after IL-10 ^{-/-} CD4 ⁺ CD25 ⁻ T cell transfer according to MADMAX software	77
Table 16. Most highly regulated genes in IEC of Rag2 ^{-/-} x IL-10 ^{-/-} recipients after IL-10 ^{-/-} CD4 ⁺ CD25 ⁻ T cell transfer according to Genomatix ChipInspector software.....	78
Table 17. Most highly regulated genes in IEC of Rag2 ^{-/-} x IL-10 ^{-/-} recipients after IL-10 ^{-/-} CD4 ⁺ CD25 ⁻ T cell transfer according to MADMAX software.....	78
Table 18. Z-scores of selected GO terms from the domain “cellular components” according to ChipInspector software.....	80
Table 19. Z-scores of selected GO terms from the domain “cellular components” according to MADMAX software.	80
Table 20. Z-scores of selected GO terms from the domain “biological process” according to ChipInspector software.....	81
Table 21. Z-scores of selected GO terms from the domain “biological process” according to MADMAX software.	81
Table 22. Signal transduction pathways with a significant enrichment of regulated genes in IEC from Rag2 ^{-/-} recipients reconstituted with Wt CD4 ⁺ CD25 ⁻ T cells according to ChipInspector (CI) or MADMAX (MM) software.....	82
Table 23. Signal transduction pathways with a significant enrichment of regulated genes in IEC from Rag2 ^{-/-} x IL-10 ^{-/-} recipients reconstituted with Wt CD4 ⁺ CD25 ⁻ T cells according to ChipInspector (CI) or MADMAX (MM) software.....	82

Table 24. Signal transduction pathways with a significant enrichment of regulated genes in IEC from Rag2 ^{-/-} recipients reconstituted with IL-10 ^{-/-} CD4 ⁺ CD25 ⁻ T cells according to ChiplInspector (CI) or MADMAX (MM) software.....	83
Table 25. Signal transduction pathways with a significant enrichment of regulated genes in IEC from Rag2 ^{-/-} x IL-10 ^{-/-} recipients reconstituted with IL-10 ^{-/-} CD4 ⁺ CD25 ⁻ T cells according to ChiplInspector (CI) or MADMAX (MM) software	84
Table 26. Genes best correlated to the histological score (cecum) in IEC of Rag2 ^{-/-} recipients after CD4 ⁺ T cell transfer using gene intensities obtained by MADMAX software	87
Table 27. Genes best correlated to the histological score (cecum) in IEC of Rag2 ^{-/-} x IL-10 ^{-/-} recipients CD4 ⁺ T cell transfer using gene intensities obtained by MADMAX software.....	88
Table 28. Genes best correlated to the histological score (colon) in IEC of Rag2 ^{-/-} recipients after CD4 ⁺ T cell transfer using gene intensities obtained by MADMAX software	89
Table 29. Genes best correlated to the histological score (colon) in IEC of Rag2 ^{-/-} x IL-10 ^{-/-} recipients after CD4 ⁺ T cell transfer using gene intensities obtained by MADMAX software	90
Table 30. Genes best correlated to the histological score (cumulative) in IEC of Rag2 ^{-/-} recipients after CD4 ⁺ T cell transfer using gene intensities obtained by MADMAX software	91
Table 31. Genes best correlated to the histological score (cumulative) in IEC of Rag2 ^{-/-} x IL-10 ^{-/-} recipients after CD4 ⁺ T cell transfer using gene intensities obtained by MADMAX software	92
Table 32. Genes best correlated to the presence of non-T cell-/ T cell-derived IL-10 in IEC of recipients after non-colitogenic CD4 ⁺ CD25 ⁺ T cell transfer using gene intensities obtained by MADMAX software.	94
Table A1. Differentially regulated proteins in primary large IEC identified by 2D SDS-PAGE and MALDI-TOF-MS analysis.....	107
Table A2. Genes best correlated to histological scores in Rag2 ^{-/-} recipients and fold changes in gene expression of the different CD4 ⁺ T cell reconstituted groups vs non-reconstituted controls.....	112
Table A3. Genes best correlated to histological scores in Rag2 ^{-/-} x IL-10 ^{-/-} recipients and fold changes in gene expression of the different CD4 ⁺ T cell reconstituted groups vs non-reconstituted controls	118
Table A4. Genes best correlated to the presence of IL-10 and fold changes in gene expression after Wt CD4 ⁺ CD25 ⁺ T cell transfer to Rag2 ^{-/-} or Rag2 ^{-/-} x IL-10 ^{-/-} recipients vs non-reconstituted controls	126

ABBREVIATIONS

Akt	thymoma viral proto-oncogene 1	MAVS	mitochondrial antiviral signaling
AMPK	AMP-activated protein kinase	MEF	murine embryonic fibroblasts
AP	activator protein	MEK	MAPK/ERK kinase
ATF	activating transcription factor	MIDAS	mitochondrial DNA absence sensitive factor
ATP	Adenosine triphosphate	MPTP	mitochondrial permeability transition pore
ARE	antioxidant-response element	mt	mitochondrial
Bcl	B cell lymphoma	Mtfn2	mitofusin 2
CaMK	calcium/calmodulin-dependent protein kinase	MURE	mtUPR elements
CD	Crohn's disease	NaF	Sodium fluoescine
ChIP	chromatin immuno-precipitation	NF- κ B	nuclear factor kappa-light-chain-enhancer of activated B cells
CHOP	CCAAT/enhancer-binding protein homologous protein	NLR	Nod-like receptor
ClpP	Clp protease (caseinolytic peptidase)	NO	nitric oxide
CNX	calnexin	Nrf2	Nuclear factor (erythroid-derived 2)-like 2
COX	cytochrome C oxidase	Opa	Optic atrophy protein
CPN	chaperonin	OTC	ornithine transcarbamyase
CREB	cAMP response element-binding	OXPHOS	oxidative phosphorylation
CRT	calreticulin	PACS	phosphofurin acidic cluster sorting protein
CRTC	CREB-regulated transcription coactivator	PDI	protein disulfide isomerase
DAI	disease activity index	PERK	PKR-like ER kinase
DSS	dextran sodium sulfate	PKR	double-stranded RNA-activated protein kinase
eIF	eukaryotic translation initiation factor	Rag	recombination activating gene
ER	endoplasmic reticulum	RIG	retinoic acid-inducible gene
ERAD	Endoplasmic Reticulum Associated Protein Degradation	ROS	reactive oxygen species
ERK	extracellular-signal-regulated kinase	S1P	site-1 protease
ERO1	ER oxidoreductin	S2P	site-2 protease
ERSE	ER stress response element	SDS-PAGE	sodium dodecyl sulfate polyacrylamide gel electrophoresis
GADD	growth arrest and DNA-damage inducible protein	SERCA	sarcoplasmic/endoplasmic reticulum calcium ATPase
GCN	general control of amino acid biosynthesis kinase	SPF	specific pathogen-free
GRP	glucose-regulated protein	SREBP	Sterol Regulatory Element-Binding Protein
HRI	hemin-regulated inhibitor	TAP	Transporter associated with antigen processing
HSP	heat shock protein	TCA	tricarboxylic acid cycle
IB	immunoblot	TER	transepithelial electrical resistance
IBD	inflammatory bowel diseases	TIM	transporter of the inner mitochondrial membrane
IEC	intestinal epithelial cell	TLR	toll-like receptor
IFN	interferon	Tm	tunicamycin
IHC	immunohistochemistry	TNF	Tumor necrosis factor
IKK	I κ B kinase	TOM	transporter of the outer mitochondrial membrane
IL	interleukin	TRAF	TNF receptor associated factor
IP	immune-precipitation	TSLP	Thymic Stromal Lymphopoietin
IP3R	inositol 1,4,5-triphosphate receptor	UC	ulcerative colitis
IRE	inositol requiring enzyme	UPR	unfolded protein response
IRF	interferon-regulatory factors	UPRE	UPR response element
JNK	cJUN NH ₂ -terminal kinase	VDAC	voltage-dependent anion channel
LC3	microtubule-associated protein 1A/1B-light chain 3	WB	Western blot
LPS	Lipopolysaccharide	Wt	Wild type
MALDI	matrix-assisted laser desorption/ionization		
MAM	mitochondria-associated membranes		
MAMP	microbial-associated molecular pattern		
MAPK	mitogen-activated protein kinase		

REFERENCES

1. Ogden CL, Lamb MM, Carroll MD, et al. Obesity and socioeconomic status in children and adolescents: United States, 2005-2008. *NCHS Data Brief* 2010;1-8.
2. Hossain P, Kawar B, El Nahas M. Obesity and diabetes in the developing world--a growing challenge. *N Engl J Med* 2007;356:213-215.
3. Sartor RB. Mechanisms of disease: pathogenesis of Crohn's disease and ulcerative colitis. *Nat Clin Pract Gastroenterol Hepatol* 2006;3:390-407.
4. Rodgers A, Ezzati M, Vander Hoorn S, et al. Distribution of major health risks: findings from the Global Burden of Disease study. *PLoS Med* 2004;1:e27.
5. Renz H, von Mutius E, Brandtzaeg P, et al. Gene-environment interactions in chronic inflammatory disease. *Nat Immunol* 2011;12:273-277.
6. Hotamisligil GS. Inflammation and metabolic disorders. *Nature* 2006;444:860-867.
7. Mayer L. Evolving paradigms in the pathogenesis of IBD. *J Gastroenterol* 2010;45:9-16.
8. Kaser A, Zeissig S, Blumberg RS. Inflammatory bowel disease. *Annu Rev Immunol* 2010;28:573-621.
9. Clavel T, Haller D. Bacteria- and host-derived mechanisms to control intestinal epithelial cell homeostasis: implications for chronic inflammation. *Inflamm Bowel Dis* 2007;13:1153-1164.
10. Kaser A, Lee AH, Franke A, et al. XBP1 links ER stress to intestinal inflammation and confers genetic risk for human inflammatory bowel disease. *Cell* 2008;134:743-756.
11. Blumberg RS, Li L, Nusrat A, et al. Recent insights into the integration of the intestinal epithelium within the mucosal environment in health and disease. *Mucosal Immunol* 2008;1:330-334.
12. Ma Y, Hendershot LM. The role of the unfolded protein response in tumour development: friend or foe? *Nat Rev Cancer* 2004;4:966-977.
13. Zhang K, Kaufman RJ. From endoplasmic-reticulum stress to the inflammatory response. *Nature* 2008;454:455-462.
14. Ozcan U, Cao Q, Yilmaz E, et al. Endoplasmic reticulum stress links obesity, insulin action, and type 2 diabetes. *Science* 2004;306:457-461.
15. Hood DA, Irrcher I, Ljubicic V, et al. Coordination of metabolic plasticity in skeletal muscle. *J Exp Biol* 2006;209:2265-2275.
16. Yoshida H. ER stress response, peroxisome proliferation, mitochondrial unfolded protein response and Golgi stress response. *IUBMB Life* 2009;61:871-879.
17. Bukau B, Weissman J, Horwich A. Molecular chaperones and protein quality control. *Cell* 2006;125:443-451.
18. Ron D, Walter P. Signal integration in the endoplasmic reticulum unfolded protein response. *Nat Rev Mol Cell Biol* 2007;8:519-529.
19. Hartl FU, Hayer-Hartl M. Molecular chaperones in the cytosol: from nascent chain to folded protein. *Science* 2002;295:1852-1858.
20. Yoneda T, Benedetti C, Urano F, et al. Compartment-specific perturbation of protein handling activates genes encoding mitochondrial chaperones. *J Cell Sci* 2004;117:4055-4066.
21. Zhao Q, Wang J, Levichkin IV, et al. A mitochondrial specific stress response in mammalian cells. *Embo J* 2002;21:4411-4419.
22. Martinus RD, Garth GP, Webster TL, et al. Selective induction of mitochondrial chaperones in response to loss of the mitochondrial genome. *Eur J Biochem* 1996;240:98-103.
23. Haynes CM, Petrova K, Benedetti C, et al. ClpP mediates activation of a mitochondrial unfolded protein response in *C. elegans*. *Dev Cell* 2007;13:467-480.
24. Horibe T, Hoogenraad NJ. The chop gene contains an element for the positive regulation of the mitochondrial unfolded protein response. *PLoS ONE* 2007;2:e835.
25. Aldridge JE, Horibe T, Hoogenraad NJ. Discovery of genes activated by the mitochondrial unfolded protein response (mtUPR) and cognate promoter elements. *PLoS ONE* 2007;2:e874.
26. Chen X, Shen J, Prywes R. The luminal domain of ATF6 senses endoplasmic reticulum (ER) stress and causes translocation of ATF6 from the ER to the Golgi. *J Biol Chem* 2002;277:13045-13052.
27. Rutkowski DT, Arnold SM, Miller CN, et al. Adaptation to ER stress is mediated by differential stabilities of pro-survival and pro-apoptotic mRNAs and proteins. *PLoS Biol* 2006;4:e374.
28. Szegezdi E, Logue SE, Gorman AM, et al. Mediators of endoplasmic reticulum stress-induced apoptosis. *EMBO Rep* 2006;7:880-885.
29. Calton M, Zeng H, Urano F, et al. IRE1 couples endoplasmic reticulum load to secretory capacity by processing the XBP-1 mRNA. *Nature* 2002;415:92-96.
30. Sidrauski C, Walter P. The transmembrane kinase Ire1p is a site-specific endonuclease that initiates mRNA splicing in the unfolded protein response. *Cell* 1997;90:1031-1039.
31. Lee AH, Iwakoshi NN, Glimcher LH. XBP-1 regulates a subset of endoplasmic reticulum resident chaperone genes in the unfolded protein response. *Mol Cell Biol* 2003;23:7448-7459.
32. Yamamoto K, Sato T, Matsui T, et al. Transcriptional induction of mammalian ER quality control proteins is mediated by single or combined action of ATF6alpha and XBP1. *Dev Cell* 2007;13:365-376.
33. Shaffer AL, Shapiro-Shelef M, Iwakoshi NN, et al. XBP1, downstream of Blimp-1, expands the secretory apparatus and other organelles, and increases protein synthesis in plasma cell differentiation. *Immunity* 2004;21:81-93.
34. Sriburi R, Jackowski S, Mori K, et al. XBP1: a link between the unfolded protein response, lipid biosynthesis, and biogenesis of the endoplasmic reticulum. *J Cell Biol* 2004;167:35-41.

35. Hollien J, Lin JH, Li H, et al. Regulated Ire1-dependent decay of messenger RNAs in mammalian cells. *J Cell Biol* 2009;186:323-331.
36. Nishitoh H, Matsuzawa A, Tobiume K, et al. ASK1 is essential for endoplasmic reticulum stress-induced neuronal cell death triggered by expanded polyglutamine repeats. *Genes Dev* 2002;16:1345-1355.
37. Urano F, Wang X, Bertolotti A, et al. Coupling of stress in the ER to activation of JNK protein kinases by transmembrane protein kinase IRE1. *Science* 2000;287:664-666.
38. Yoshida H, Haze K, Yanagi H, et al. Identification of the cis-acting endoplasmic reticulum stress response element responsible for transcriptional induction of mammalian glucose-regulated proteins. Involvement of basic leucine zipper transcription factors. *J Biol Chem* 1998;273:33741-33749.
39. Kokame K, Kato H, Miyata T. Identification of ERSE-II, a new cis-acting element responsible for the ATF6-dependent mammalian unfolded protein response. *J Biol Chem* 2001;276:9199-9205.
40. Bommasamy H, Back SH, Fagone P, et al. ATF6alpha induces XBP1-independent expansion of the endoplasmic reticulum. *J Cell Sci* 2009;122:1626-1636.
41. Bailey D, O'Hare P. Transmembrane bZIP transcription factors in ER stress signaling and the unfolded protein response. *Antioxid Redox Signal* 2007;9:2305-2321.
42. Murakami T, Saito A, Hino S, et al. Signalling mediated by the endoplasmic reticulum stress transducer OASIS is involved in bone formation. *Nat Cell Biol* 2009;11:1205-1211.
43. Zhang K, Shen X, Wu J, et al. Endoplasmic reticulum stress activates cleavage of CREBH to induce a systemic inflammatory response. *Cell* 2006;124:587-599.
44. Wu J, Rutkowski DT, Dubois M, et al. ATF6alpha optimizes long-term endoplasmic reticulum function to protect cells from chronic stress. *Dev Cell* 2007;13:351-364.
45. Harding HP, Zhang Y, Ron D. Protein translation and folding are coupled by an endoplasmic-reticulum-resident kinase. *Nature* 1999;397:271-274.
46. Harding HP, Zhang Y, Bertolotti A, et al. Perk is essential for translational regulation and cell survival during the unfolded protein response. *Mol Cell* 2000;5:897-904.
47. Ma Y, Brewer JW, Diehl JA, et al. Two distinct stress signaling pathways converge upon the CHOP promoter during the mammalian unfolded protein response. *J Mol Biol* 2002;318:1351-1365.
48. Connor JH, Weiser DC, Li S, et al. Growth arrest and DNA damage-inducible protein GADD34 assembles a novel signaling complex containing protein phosphatase 1 and inhibitor 1. *Mol Cell Biol* 2001;21:6841-6850.
49. Brush MH, Weiser DC, Shenolikar S. Growth arrest and DNA damage-inducible protein GADD34 targets protein phosphatase 1 alpha to the endoplasmic reticulum and promotes dephosphorylation of the alpha subunit of eukaryotic translation initiation factor 2. *Mol Cell Biol* 2003;23:1292-1303.
50. Cullinan SB, Diehl JA. Coordination of ER and oxidative stress signaling: the PERK/Nrf2 signaling pathway. *Int J Biochem Cell Biol* 2006;38:317-332.
51. Cullinan SB, Zhang D, Hannink M, et al. Nrf2 is a direct PERK substrate and effector of PERK-dependent cell survival. *Mol Cell Biol* 2003;23:7198-7209.
52. Garcia MA, Gil J, Ventoso I, et al. Impact of protein kinase PKR in cell biology: from antiviral to antiproliferative action. *Microbiol Mol Biol Rev* 2006;70:1032-1060.
53. Schroder M, Kaufman RJ. The mammalian unfolded protein response. *Annu Rev Biochem* 2005;74:739-789.
54. Nguyen DT, Kebache S, Fazel A, et al. Nck-dependent activation of extracellular signal-regulated kinase-1 and regulation of cell survival during endoplasmic reticulum stress. *Mol Biol Cell* 2004;15:4248-4260.
55. Hu P, Han Z, Couvillon AD, et al. Autocrine tumor necrosis factor alpha links endoplasmic reticulum stress to the membrane death receptor pathway through IRE1alpha-mediated NF-kappaB activation and down-regulation of TRAF2 expression. *Mol Cell Biol* 2006;26:3071-3084.
56. Iwakoshi NN, Lee AH, Vallabhajosyula P, et al. Plasma cell differentiation and the unfolded protein response intersect at the transcription factor XBP-1. *Nat Immunol* 2003;4:321-329.
57. Reimold AM, Iwakoshi NN, Manis J, et al. Plasma cell differentiation requires the transcription factor XBP-1. *Nature* 2001;412:300-307.
58. Yamazaki H, Hiramatsu N, Hayakawa K, et al. Activation of the Akt-NF-kappaB pathway by subtilase cytotoxin through the ATF6 branch of the unfolded protein response. *J Immunol* 2009;183:1480-1487.
59. Deng J, Lu PD, Zhang Y, et al. Translational repression mediates activation of nuclear factor kappa B by phosphorylated translation initiation factor 2. *Mol Cell Biol* 2004;24:10161-10168.
60. Jiang HY, Wek SA, McGrath BC, et al. Phosphorylation of the alpha subunit of eukaryotic initiation factor 2 is required for activation of NF-kappaB in response to diverse cellular stresses. *Mol Cell Biol* 2003;23:5651-5663.
61. Li Y, Schwabe RF, DeVries-Seimon T, et al. Free cholesterol-loaded macrophages are an abundant source of tumor necrosis factor-alpha and interleukin-6: model of NF-kappaB- and map kinase-dependent inflammation in advanced atherosclerosis. *J Biol Chem* 2005;280:21763-21772.
62. Zhang X, Zhang G, Zhang H, et al. Hypothalamic IKKbeta/NF-kappaB and ER stress link overnutrition to energy imbalance and obesity. *Cell* 2008;135:61-73.
63. Uehara T, Nakamura T, Yao D, et al. S-nitrosylated protein-disulphide isomerase links protein misfolding to neurodegeneration. *Nature* 2006;441:513-517.
64. Haynes CM, Titus EA, Cooper AA. Degradation of misfolded proteins prevents ER-derived oxidative stress and cell death. *Mol Cell* 2004;15:767-776.
65. Woo CW, Cui D, Arellano J, et al. Adaptive suppression of the ATF4-CHOP branch of the unfolded protein response by toll-like receptor signalling. *Nat Cell Biol* 2009;11:1473-1480.

66. Messlik A, Schmechel S, Kisling S, et al. Loss of Toll-like receptor 2 and 4 leads to differential induction of endoplasmic reticulum stress and proapoptotic responses in the intestinal epithelium under conditions of chronic inflammation. *J Proteome Res* 2009;8:4406-4417.
67. Martinon F, Chen X, Lee AH, et al. TLR activation of the transcription factor XBP1 regulates innate immune responses in macrophages. *Nat Immunol* 2010;11:411-418.
68. Aprahamian CJ, Lorenz RG, Harmon CM, et al. Toll-like receptor 2 is protective of ischemia-reperfusion-mediated small-bowel injury in a murine model. *Pediatr Crit Care Med* 2008;9:105-109.
69. Hoyer-Hansen M, Jaattela M. Connecting endoplasmic reticulum stress to autophagy by unfolded protein response and calcium. *Cell Death Differ* 2007;14:1576-1582.
70. Kroemer G, Jaattela M. Lysosomes and autophagy in cell death control. *Nat Rev Cancer* 2005;5:886-897.
71. Maiuri MC, Zalckvar E, Kimchi A, et al. Self-eating and self-killing: crosstalk between autophagy and apoptosis. *Nat Rev Mol Cell Biol* 2007;8:741-752.
72. Ogata M, Hino S, Saito A, et al. Autophagy is activated for cell survival after endoplasmic reticulum stress. *Mol Cell Biol* 2006;26:9220-9231.
73. Bernales S, McDonald KL, Walter P. Autophagy counterbalances endoplasmic reticulum expansion during the unfolded protein response. *PLoS Biol* 2006;4:e423.
74. Kouroku Y, Fujita E, Tanida I, et al. ER stress (PERK/eIF2alpha phosphorylation) mediates the polyglutamine-induced LC3 conversion, an essential step for autophagy formation. *Cell Death Differ* 2007;14:230-239.
75. Fujita E, Kouroku Y, Isoai A, et al. Two endoplasmic reticulum-associated degradation (ERAD) systems for the novel variant of the mutant dysferlin: ubiquitin/proteasome ERAD(I) and autophagy/lysosome ERAD(II). *Hum Mol Genet* 2007;16:618-629.
76. Scherz-Shouval R, Elazar Z. Regulation of autophagy by ROS: physiology and pathology. *Trends Biochem Sci* 2010;36:30-38.
77. Nakagawa T, Yuan J. Cross-talk between two cysteine protease families. Activation of caspase-12 by calpain in apoptosis. *J Cell Biol* 2000;150:887-894.
78. Nakagawa T, Zhu H, Morishima N, et al. Caspase-12 mediates endoplasmic-reticulum-specific apoptosis and cytotoxicity by amyloid-beta. *Nature* 2000;403:98-103.
79. Tan Y, Dourdin N, Wu C, et al. Ubiquitous calpains promote caspase-12 and JNK activation during endoplasmic reticulum stress-induced apoptosis. *J Biol Chem* 2006;281:16016-16024.
80. Morishima N, Nakanishi K, Takenouchi H, et al. An endoplasmic reticulum stress-specific caspase cascade in apoptosis. Cytochrome c-independent activation of caspase-9 by caspase-12. *J Biol Chem* 2002;277:34287-34294.
81. Rao RV, Castro-Obregon S, Frankowski H, et al. Coupling endoplasmic reticulum stress to the cell death program. An Apaf-1-independent intrinsic pathway. *J Biol Chem* 2002;277:21836-21842.
82. Fischer H, Koenig U, Eckhart L, et al. Human caspase 12 has acquired deleterious mutations. *Biochem Biophys Res Commun* 2002;293:722-726.
83. Hitomi J, Katayama T, Eguchi Y, et al. Involvement of caspase-4 in endoplasmic reticulum stress-induced apoptosis and Abeta-induced cell death. *J Cell Biol* 2004;165:347-356.
84. Fawcett TW, Martindale JL, Guyton KZ, et al. Complexes containing activating transcription factor (ATF)/cAMP-responsive-element-binding protein (CREB) interact with the CCAAT/enhancer-binding protein (C/EBP)-ATF composite site to regulate Gadd153 expression during the stress response. *Biochem J* 1999;339 (Pt 1):135-141.
85. Lin JH, Li H, Zhang Y, et al. Divergent effects of PERK and IRE1 signaling on cell viability. *PLoS One* 2009;4:e4170.
86. Harding HP, Novoa I, Zhang Y, et al. Regulated translation initiation controls stress-induced gene expression in mammalian cells. *Mol Cell* 2000;6:1099-1108.
87. Zinszner H, Kuroda M, Wang X, et al. CHOP is implicated in programmed cell death in response to impaired function of the endoplasmic reticulum. *Genes Dev* 1998;12:982-995.
88. McCullough KD, Martindale JL, Klotz LO, et al. Gadd153 sensitizes cells to endoplasmic reticulum stress by down-regulating Bcl2 and perturbing the cellular redox state. *Mol Cell Biol* 2001;21:1249-1259.
89. Puthalakath H, O'Reilly LA, Gunn P, et al. ER stress triggers apoptosis by activating BH3-only protein Bim. *Cell* 2007;129:1337-1349.
90. Marciniak SJ, Yun CY, Ouyang S, et al. CHOP induces death by promoting protein synthesis and oxidation in the stressed endoplasmic reticulum. *Genes Dev* 2004;18:3066-3077.
91. Chami M, Oules B, Szabadkai G, et al. Role of SERCA1 truncated isoform in the proapoptotic calcium transfer from ER to mitochondria during ER stress. *Mol Cell* 2008;32:641-651.
92. Lin JH, Li H, Yasumura D, et al. IRE1 signaling affects cell fate during the unfolded protein response. *Science* 2007;318:944-949.
93. Wei MC, Zong WX, Cheng EH, et al. Proapoptotic BAX and BAK: a requisite gateway to mitochondrial dysfunction and death. *Science* 2001;292:727-730.
94. Scorrano L, Oakes SA, Opferman JT, et al. BAX and BAK regulation of endoplasmic reticulum Ca²⁺: a control point for apoptosis. *Science* 2003;300:135-139.
95. Zong WX, Li C, Hatzivassiliou G, et al. Bax and Bak can localize to the endoplasmic reticulum to initiate apoptosis. *J Cell Biol* 2003;162:59-69.
96. Hetz C, Bernasconi P, Fisher J, et al. Proapoptotic BAX and BAK modulate the unfolded protein response by a direct interaction with IRE1alpha. *Science* 2006;312:572-576.
97. Acosta-Alvear D, Zhou Y, Blais A, et al. XBP1 controls diverse cell type- and condition-specific transcriptional regulatory networks. *Mol Cell* 2007;27:53-66.

REFERENCES

98. Wang Y, Vera L, Fischer WH, et al. The CREB coactivator CRTC2 links hepatic ER stress and fasting gluconeogenesis. *Nature* 2009;460:534-537.
99. Scheuner D, Song B, McEwen E, et al. Translational control is required for the unfolded protein response and in vivo glucose homeostasis. *Mol Cell* 2001;7:1165-1176.
100. Back SH, Scheuner D, Han J, et al. Translation attenuation through eIF2alpha phosphorylation prevents oxidative stress and maintains the differentiated state in beta cells. *Cell Metab* 2009;10:13-26.
101. Oyadomari S, Harding HP, Zhang Y, et al. Dephosphorylation of translation initiation factor 2alpha enhances glucose tolerance and attenuates hepatosteatosis in mice. *Cell Metab* 2008;7:520-532.
102. Gregor MG, Hotamisligil GS. Adipocyte stress: The endoplasmic reticulum and metabolic disease. *J Lipid Res* 2007.
103. Chen JC, Wu ML, Huang KC, et al. HMG-CoA reductase inhibitors activate the unfolded protein response and induce cytoprotective GRP78 expression. *Cardiovasc Res* 2008;80:138-150.
104. Wolins NE, Brasaemle DL, Bickel PE. A proposed model of fat packaging by exchangeable lipid droplet proteins. *FEBS Lett* 2006;580:5484-5491.
105. Lee AH, Scapa EF, Cohen DE, et al. Regulation of hepatic lipogenesis by the transcription factor XBP1. *Science* 2008;320:1492-1496.
106. Bobrovnikova-Marjon E, Hatzivassiliou G, Grigoriadou C, et al. PERK-dependent regulation of lipogenesis during mouse mammary gland development and adipocyte differentiation. *Proc Natl Acad Sci U S A* 2008;105:16314-16319.
107. Rutkowski DT, Wu J, Back SH, et al. UPR pathways combine to prevent hepatic steatosis caused by ER stress-mediated suppression of transcriptional master regulators. *Dev Cell* 2008;15:829-840.
108. Yang J, Croniger CM, Lekstrom-Himes J, et al. Metabolic response of mice to a postnatal ablation of CCAAT/enhancer-binding protein alpha. *J Biol Chem* 2005;280:38689-38699.
109. Flodby P, Barlow C, Kylefjord H, et al. Increased hepatic cell proliferation and lung abnormalities in mice deficient in CCAAT/enhancer binding protein alpha. *J Biol Chem* 1996;271:24753-24760.
110. Wang ND, Finegold MJ, Bradley A, et al. Impaired energy homeostasis in C/EBP alpha knockout mice. *Science* 1995;269:1108-1112.
111. Hotamisligil GS. Endoplasmic reticulum stress and the inflammatory basis of metabolic disease. *Cell* 2010;140:900-917.
112. Shkoda A, Ruiz PA, Daniel H, et al. Interleukin-10 blocked endoplasmic reticulum stress in intestinal epithelial cells: impact on chronic inflammation. *Gastroenterology* 2007;132:190-207.
113. Heazlewood CK, Cook MC, Eri R, et al. Aberrant mucin assembly in mice causes endoplasmic reticulum stress and spontaneous inflammation resembling ulcerative colitis. *PLoS Med* 2008;5:e54.
114. Bertolotti A, Wang X, Novoa I, et al. Increased sensitivity to dextran sodium sulfate colitis in IRE1beta-deficient mice. *J Clin Invest* 2001;107:585-593.
115. Hampe J, Franke A, Rosenstiel P, et al. A genome-wide association scan of nonsynonymous SNPs identifies a susceptibility variant for Crohn disease in ATG16L1. *Nat Genet* 2007;39:207-211.
116. Rioux JD, Xavier RJ, Taylor KD, et al. Genome-wide association study identifies new susceptibility loci for Crohn disease and implicates autophagy in disease pathogenesis. *Nat Genet* 2007;39:596-604.
117. Consortium TWTCC. Genome-wide association study of 14,000 cases of seven common diseases and 3,000 shared controls. *Nature* 2007;447:661-678.
118. Parkes M, Barrett JC, Prescott NJ, et al. Sequence variants in the autophagy gene IRGM and multiple other replicating loci contribute to Crohn's disease susceptibility. *Nat Genet* 2007;39:830-832.
119. Hayashi T, Su TP. Sigma-1 receptor chaperones at the ER-mitochondrion interface regulate Ca(2+) signaling and cell survival. *Cell* 2007;131:596-610.
120. Hugot JP, Chamaillard M, Zouali H, et al. Association of NOD2 leucine-rich repeat variants with susceptibility to Crohn's disease. *Nature* 2001;411:599-603.
121. Ogura Y, Bonen DK, Inohara N, et al. A frameshift mutation in NOD2 associated with susceptibility to Crohn's disease. *Nature* 2001;411:603-606.
122. Franchimont D, Vermeire S, El Housni H, et al. Deficient host-bacteria interactions in inflammatory bowel disease? The toll-like receptor (TLR)-4 Asp299gly polymorphism is associated with Crohn's disease and ulcerative colitis. *Gut* 2004;53:987-992.
123. Cadwell K, Liu JY, Brown SL, et al. A key role for autophagy and the autophagy gene Atg16l1 in mouse and human intestinal Paneth cells. *Nature* 2008;456:259-263.
124. Wehkamp J, Salzman NH, Porter E, et al. Reduced Paneth cell alpha-defensins in ileal Crohn's disease. *Proc Natl Acad Sci U S A* 2005;102:18129-18134.
125. Kaser A, Blumberg RS. Paneth cells and inflammation dance together in Crohn's disease. *Cell Res* 2008;18:1160-1162.
126. Werner T, Wagner SJ, Martinez I, et al. Depletion of luminal iron alters the gut microbiota and prevents Crohn's disease-like ileitis. *Gut* 2011;60:325-333.
127. Vecchi C, Montosi G, Zhang K, et al. ER stress controls iron metabolism through induction of hepcidin. *Science* 2009;325:877-880.
128. Ryan MT, Hoogenraad NJ. Mitochondrial-nuclear communications. *Annu Rev Biochem* 2007;76:701-722.
129. Arco AD, Satrustegui J. New mitochondrial carriers: an overview. *Cell Mol Life Sci* 2005;62:2204-2227.
130. Frey TG, Mannella CA. The internal structure of mitochondria. *Trends Biochem Sci* 2000;25:319-324.
131. Webb CT, Gorman MA, Lazarou M, et al. Crystal structure of the mitochondrial chaperone TIM9.10 reveals a six-bladed alpha-propeller. *Mol Cell* 2006;21:123-133.

132. Koehler CM, Beverly KN, Leverich EP. Redox pathways of the mitochondrion. *Antioxid Redox Signal* 2006;8:813-822.
133. Hoogenraad NJ, Ward LA, Ryan MT. Import and assembly of proteins into mitochondria of mammalian cells. *Biochim Biophys Acta* 2002;1592:97-105.
134. Ryan MT, Pfanner N. Hsp70 proteins in protein translocation. *Adv Protein Chem* 2001;59:223-242.
135. Wiedemann N, Frazier AE, Pfanner N. The protein import machinery of mitochondria. *J Biol Chem* 2004;279:14473-14476.
136. Martinus RD, Ryan MT, Naylor DJ, et al. Role of chaperones in the biogenesis and maintenance of the mitochondrion. *Faseb J* 1995;9:371-378.
137. Voos W, Rottgers K. Molecular chaperones as essential mediators of mitochondrial biogenesis. *Biochim Biophys Acta* 2002;1592:51-62.
138. Cocheme HM, Murphy MP. Complex I is the major site of mitochondrial superoxide production by paraquat. *J Biol Chem* 2008;283:1786-1798.
139. Broadley SA, Hartl FU. Mitochondrial stress signaling: a pathway unfolds. *Trends Cell Biol* 2008;18:1-4.
140. Benedetti C, Haynes CM, Yang Y, et al. Ubiquitin-like protein 5 positively regulates chaperone gene expression in the mitochondrial unfolded protein response. *Genetics* 2006;174:229-239.
141. Haynes CM, Yang Y, Blais SP, et al. The matrix peptide exporter HAF-1 signals a mitochondrial UPR by activating the transcription factor ZC376.7 in *C. elegans*. *Mol Cell* 2010;37:529-540.
142. Young L, Leonhard K, Tatsuta T, et al. Role of the ABC transporter Mdl1 in peptide export from mitochondria. *Science* 2001;291:2135-2138.
143. Haynes CM, Ron D. The mitochondrial UPR - protecting organelle protein homeostasis. *J Cell Sci* 2010;123:3849-3855.
144. Siegelin MD, Dohi T, Raskett CM, et al. Exploiting the mitochondrial unfolded protein response for cancer therapy in mice and human cells. *J Clin Invest* 2011.
145. Leary SC, Shoubridge EA. Mitochondrial biogenesis: which part of "NO" do we understand? *Bioessays* 2003;25:538-541.
146. Butow RA, Avadhani NG. Mitochondrial signaling: the retrograde response. *Mol Cell* 2004;14:1-15.
147. Wallace DC. A mitochondrial paradigm of metabolic and degenerative diseases, aging, and cancer: a dawn for evolutionary medicine. *Annu Rev Genet* 2005;39:359-407.
148. Ojuka EO, Jones TE, Han DH, et al. Raising Ca²⁺ in L6 myotubes mimics effects of exercise on mitochondrial biogenesis in muscle. *Faseb J* 2003;17:675-681.
149. Brookes PS, Levonen AL, Shiva S, et al. Mitochondria: regulators of signal transduction by reactive oxygen and nitrogen species. *Free Radic Biol Med* 2002;33:755-764.
150. Brookes PS, Kraus DW, Shiva S, et al. Control of mitochondrial respiration by NO^{*}, effects of low oxygen and respiratory state. *J Biol Chem* 2003;278:31603-31609.
151. Zong H, Ren JM, Young LH, et al. AMP kinase is required for mitochondrial biogenesis in skeletal muscle in response to chronic energy deprivation. *Proc Natl Acad Sci U S A* 2002;99:15983-15987.
152. Puigserver P, Spiegelman BM. Peroxisome proliferator-activated receptor-gamma coactivator 1 alpha (PGC-1 alpha): transcriptional coactivator and metabolic regulator. *Endocr Rev* 2003;24:78-90.
153. Lin J, Handschin C, Spiegelman BM. Metabolic control through the PGC-1 family of transcription coactivators. *Cell Metab* 2005;1:361-370.
154. Kelly DP, Scarpulla RC. Transcriptional regulatory circuits controlling mitochondrial biogenesis and function. *Genes Dev* 2004;18:357-368.
155. Nakashima-Kamimura N, Asoh S, Ishibashi Y, et al. MIDAS/GPP34, a nuclear gene product, regulates total mitochondrial mass in response to mitochondrial dysfunction. *J Cell Sci* 2005;118:5357-5367.
156. Chen H, Chomyn A, Chan DC. Disruption of fusion results in mitochondrial heterogeneity and dysfunction. *J Biol Chem* 2005;280:26185-26192.
157. Pich S, Bach D, Briones P, et al. The Charcot-Marie-Tooth type 2A gene product, Mfn2, up-regulates fuel oxidation through expression of OXPHOS system. *Hum Mol Genet* 2005;14:1405-1415.
158. Campello S, Lacalle RA, Bettella M, et al. Orchestration of lymphocyte chemotaxis by mitochondrial dynamics. *J Exp Med* 2006;203:2879-2886.
159. Amiri M, Hollenbeck PJ. Mitochondrial biogenesis in the axons of vertebrate peripheral neurons. *Dev Neurobiol* 2008;68:1348-1361.
160. Chen H, Detmer SA, Ewald AJ, et al. Mitofusins Mfn1 and Mfn2 coordinately regulate mitochondrial fusion and are essential for embryonic development. *J Cell Biol* 2003;160:189-200.
161. Chen H, Vermulst M, Wang YE, et al. Mitochondrial fusion is required for mtDNA stability in skeletal muscle and tolerance of mtDNA mutations. *Cell* 2010;141:280-289.
162. Twig G, Elorza A, Molina AJ, et al. Fission and selective fusion govern mitochondrial segregation and elimination by autophagy. *Embo J* 2008;27:433-446.
163. Gu Y, Wang C, Cohen A. Effect of IGF-1 on the balance between autophagy of dysfunctional mitochondria and apoptosis. *FEBS Lett* 2004;577:357-360.
164. Kanki T, Klionsky DJ. Mitophagy in yeast occurs through a selective mechanism. *J Biol Chem* 2008;283:32386-32393.
165. Narendra D, Tanaka A, Suen DF, et al. Parkin is recruited selectively to impaired mitochondria and promotes their autophagy. *J Cell Biol* 2008;183:795-803.
166. Bouman L, Schlierf A, Lutz AK, et al. Parkin is transcriptionally regulated by ATF4: evidence for an interconnection between mitochondrial stress and ER stress. *Cell Death Differ* 2010.

REFERENCES

167. Komatsu M, Waguri S, Ueno T, et al. Impairment of starvation-induced and constitutive autophagy in Atg7-deficient mice. *J Cell Biol* 2005;169:425-434.
168. Matsumoto N, Ezaki J, Komatsu M, et al. Comprehensive proteomics analysis of autophagy-deficient mouse liver. *Biochem Biophys Res Commun* 2008;368:643-649.
169. Nakahira K, Haspel JA, Rathinam VA, et al. Autophagy proteins regulate innate immune responses by inhibiting the release of mitochondrial DNA mediated by the NALP3 inflammasome. *Nat Immunol* 2011;12:222-230.
170. Zhou R, Yazdi AS, Menu P, et al. A role for mitochondria in NLRP3 inflammasome activation. *Nature* 2011;469:221-225.
171. Simmen T, Lynes EM, Gesson K, et al. Oxidative protein folding in the endoplasmic reticulum: tight links to the mitochondria-associated membrane (MAM). *Biochim Biophys Acta* 2010;1798:1465-1473.
172. Pizzo P, Pozzan T. Mitochondria-endoplasmic reticulum choreography: structure and signaling dynamics. *Trends Cell Biol* 2007;17:511-517.
173. Gilady SY, Bui M, Lynes EM, et al. Ero1alpha requires oxidizing and normoxic conditions to localize to the mitochondria-associated membrane (MAM). *Cell Stress Chaperones* 2010;15:619-629.
174. Myhill N, Lynes EM, Nanji JA, et al. The subcellular distribution of calnexin is mediated by PACS-2. *Mol Biol Cell* 2008;19:2777-2788.
175. Hayashi T, Rizzuto R, Hajnoczky G, et al. MAM: more than just a housekeeper. *Trends Cell Biol* 2009;19:81-88.
176. Princiotta MF, Finzi D, Qian SB, et al. Quantitating protein synthesis, degradation, and endogenous antigen processing. *Immunity* 2003;18:343-354.
177. Culic O, Gruwel ML, Schrader J. Energy turnover of vascular endothelial cells. *Am J Physiol* 1997;273:C205-213.
178. Csordas G, Thomas AP, Hajnoczky G. Quasi-synaptic calcium signal transmission between endoplasmic reticulum and mitochondria. *Embo J* 1999;18:96-108.
179. Hajnoczky G, Csordas G, Madesh M, et al. The machinery of local Ca²⁺ signalling between sarco-endoplasmic reticulum and mitochondria. *J Physiol* 2000;529 Pt 1:69-81.
180. Deniaud A, Sharaf el dein O, Maillier E, et al. Endoplasmic reticulum stress induces calcium-dependent permeability transition, mitochondrial outer membrane permeabilization and apoptosis. *Oncogene* 2008;27:285-299.
181. Gething MJ. Role and regulation of the ER chaperone BiP. *Semin Cell Dev Biol* 1999;10:465-472.
182. Griffiths EJ, Rutter GA. Mitochondrial calcium as a key regulator of mitochondrial ATP production in mammalian cells. *Biochim Biophys Acta* 2009;1787:1324-1333.
183. Tu BP, Weissman JS. The FAD- and O(2)-dependent reaction cycle of Ero1-mediated oxidative protein folding in the endoplasmic reticulum. *Mol Cell* 2002;10:983-994.
184. Pagani M, Fabbri M, Benedetti C, et al. Endoplasmic reticulum oxidoreductin 1-beta (ERO1-Lbeta), a human gene induced in the course of the unfolded protein response. *J Biol Chem* 2000;275:23685-23692.
185. Cabibbo A, Pagani M, Fabbri M, et al. ERO1-L, a human protein that favors disulfide bond formation in the endoplasmic reticulum. *J Biol Chem* 2000;275:4827-4833.
186. Manthey KC, Chew YC, Zempleni J. Riboflavin deficiency impairs oxidative folding and secretion of apolipoprotein B-100 in HepG2 cells, triggering stress response systems. *J Nutr* 2005;135:978-982.
187. Simmen T, Aslan JE, Blagoveshchenskaya AD, et al. PACS-2 controls endoplasmic reticulum-mitochondria communication and Bid-mediated apoptosis. *Embo J* 2005;24:717-729.
188. Szabadkai G, Bianchi K, Varnai P, et al. Chaperone-mediated coupling of endoplasmic reticulum and mitochondrial Ca²⁺ channels. *J Cell Biol* 2006;175:901-911.
189. de Brito OM, Scorrano L. Mitofusin 2 tethers endoplasmic reticulum to mitochondria. *Nature* 2008;456:605-610.
190. Hori O, Ichinoda F, Tamatani T, et al. Transmission of cell stress from endoplasmic reticulum to mitochondria: enhanced expression of Lon protease. *J Cell Biol* 2002;157:1151-1160.
191. Haga N, Saito S, Tsukumo Y, et al. Mitochondria regulate the unfolded protein response leading to cancer cell survival under glucose deprivation conditions. *Cancer Sci* 2010.
192. Arduino DM, Esteves AR, Domingues AF, et al. ER-mediated stress induces mitochondrial-dependent caspases activation in NT2 neuron-like cells. *BMB Rep* 2009;42:719-724.
193. Lim JH, Lee HJ, Ho Jung M, et al. Coupling mitochondrial dysfunction to endoplasmic reticulum stress response: a molecular mechanism leading to hepatic insulin resistance. *Cell Signal* 2009;21:169-177.
194. Nicholas SA, Coughlan K, Yasinska I, et al. Dysfunctional mitochondria contain endogenous high-affinity human Toll-like receptor 4 (TLR4) ligands and induce TLR4-mediated inflammatory reactions. *Int J Biochem Cell Biol* 2011.
195. Burkart A, Shi X, Chouinard M, et al. Adenylate kinase 2 links mitochondrial energy metabolism to the induction of the unfolded protein response. *J Biol Chem* 2010.
196. Maynard CL, Weaver CT. Diversity in the contribution of interleukin-10 to T-cell-mediated immune regulation. *Immunol Rev* 2008;226:219-233.
197. Autschbach F, Braunstein J, Helmke B, et al. In situ expression of interleukin-10 in noninflamed human gut and in inflammatory bowel disease. *Am J Pathol* 1998;153:121-130.
198. Kuhn R, Lohler J, Rennick D, et al. Interleukin-10-deficient mice develop chronic enterocolitis. *Cell* 1993;75:263-274.
199. Kim SC, Tonkonogy SL, Karrasch T, et al. Dual-association of gnotobiotic IL-10^{-/-} mice with 2 nonpathogenic commensal bacteria induces aggressive pancolitis. *Inflamm Bowel Dis* 2007;13:1457-1466.

200. Kim SC, Tonkonogy SL, Albright CA, et al. Variable phenotypes of enterocolitis in interleukin 10-deficient mice monoassociated with two different commensal bacteria. *Gastroenterology* 2005;128:891-906.
201. Abraham N, Stojdl DF, Duncan PI, et al. Characterization of transgenic mice with targeted disruption of the catalytic domain of the double-stranded RNA-dependent protein kinase, PKR. *J Biol Chem* 1999;274:5953-5962.
202. Okayasu I, Hatakeyama S, Yamada M, et al. A novel method in the induction of reliable experimental acute and chronic ulcerative colitis in mice. *Gastroenterology* 1990;98:694-702.
203. Schicho R, Krueger D, Zeller F, et al. Hydrogen sulfide is a novel prosecretory neuromodulator in the Guinea-pig and human colon. *Gastroenterology* 2006;131:1542-1552.
204. Katakura K, Lee J, Rachmilewitz D, et al. Toll-like receptor 9-induced type I IFN protects mice from experimental colitis. *J Clin Invest* 2005;115:695-702.
205. Rath HC, Herfarth HH, Ikeda JS, et al. Normal luminal bacteria, especially *Bacteroides* species, mediate chronic colitis, gastritis, and arthritis in HLA-B27/human beta2 microglobulin transgenic rats. *J Clin Invest* 1996;98:945-953.
206. Ruiz PA, Shkoda A, Kim SC, et al. IL-10 gene-deficient mice lack TGF-beta/Smad signaling and fail to inhibit proinflammatory gene expression in intestinal epithelial cells after the colonization with colitogenic *Enterococcus faecalis*. *J Immunol* 2005;174:2990-2999.
207. Grossmann J, Maxson JM, Whitacre CM, et al. New isolation technique to study apoptosis in human intestinal epithelial cells. *Am J Pathol* 1998;153:53-62.
208. Gehlenborg N, O'Donoghue SI, Baliga NS, et al. Visualization of omics data for systems biology. *Nat Methods* 2010;7:S56-68.
209. Gentleman RC, Carey VJ, Bates DM, et al. Bioconductor: open software development for computational biology and bioinformatics. *Genome Biol* 2004;5:R80.
210. R: A Language and Environment for Statistical Computing, R Foundation for Statistical Computing. 2007.
211. Saeed AI, Bhagabati NK, Braisted JC, et al. TM4 microarray software suite. *Methods Enzymol* 2006;411:134-193.
212. Vidal K, Grosjean I, evillard JP, et al. immortalization of mouse intestinal epithelial cells by the SV40-large T gene. Phenotypic and immune characterization of the MODE-K cell line. *J Immunol Methods* 1993;166:63-73.
213. Rowe TM, Rizzi M, Hirose K, et al. A role of the double-stranded RNA-binding protein PACT in mouse ear development and hearing. *Proc Natl Acad Sci U S A* 2006;103:5823-5828.
214. Mouritzen P, Noerholm, M., Nielsen, P. S., Jacobsen, N., Lomholt, C., Pfundheller, H.M. and Tolstrup, N. Probelibrary: A new method for faster design and execution of quantitative real-time PCR. *Nature Methods* 2005;2:313-317.
215. Asseman C, Read S, Powrie F. Colitogenic Th1 cells are present in the antigen-experienced T cell pool in normal mice: control by CD4+ regulatory T cells and IL-10. *J Immunol* 2003;171:971-978.
216. Koll H, Guiard B, Rassow J, et al. Antifolding activity of hsp60 couples protein import into the mitochondrial matrix with export to the intermembrane space. *Cell* 1992;68:1163-1175.
217. Lopez JL. Two-dimensional electrophoresis in proteome expression analysis. *J Chromatogr B Analyt Technol Biomed Life Sci* 2007;849:190-202.
218. Messlik A. Identifizierung zellulärer Stressantworten in intestinalen Epithelzellen mittels funktioneller Proteomanalyse - Bedeutung der Wechselwirkung zwischen Bakterien und Wirt. PhD Thesis 2010.
219. Kaser A, Blumberg RS. Endoplasmic reticulum stress in the intestinal epithelium and inflammatory bowel disease. *Semin Immunol* 2009;21:156-163.
220. Tanida I, Ueno T, Kominami E. LC3 conjugation system in mammalian autophagy. *Int J Biochem Cell Biol* 2004;36:2503-2518.
221. Clemens MJ. PKR--a protein kinase regulated by double-stranded RNA. *Int J Biochem Cell Biol* 1997;29:945-949.
222. Ito M, Onuki R, Bando Y, et al. Phosphorylated PKR contributes the induction of GRP94 under ER stress. *Biochem Biophys Res Commun* 2007;360:615-620.
223. Lee ES, Yoon CH, Kim YS, et al. The double-strand RNA-dependent protein kinase PKR plays a significant role in a sustained ER stress-induced apoptosis. *FEBS Lett* 2007;581:4325-4332.
224. Oyadomari S, Mori M. Roles of CHOP/GADD153 in endoplasmic reticulum stress. *Cell Death Differ* 2004;11:381-389.
225. Khan MT, Wagner L, 2nd, Yule DI, et al. Akt kinase phosphorylation of inositol 1,4,5-trisphosphate receptors. *J Biol Chem* 2006;281:3731-3737.
226. Aslan JE, You H, Williamson DM, et al. Akt and 14-3-3 control a PACS-2 homeostatic switch that integrates membrane traffic with TRAIL-induced apoptosis. *Mol Cell* 2009;34:497-509.
227. Gardner OS, Shiao CW, Chen CS, et al. Peroxisome proliferator-activated receptor gamma-independent activation of p38 MAPK by thiazolidinediones involves calcium/calmodulin-dependent protein kinase II and protein kinase R: correlation with endoplasmic reticulum stress. *J Biol Chem* 2005;280:10109-10118.
228. Bennett RL, Blalock WL, May WS. Serine 18 phosphorylation of RAX, the PKR activator, is required for PKR activation and consequent translation inhibition. *J Biol Chem* 2004;279:42687-42693.
229. Peters GA, Hartmann R, Qin J, et al. Modular structure of PACT: distinct domains for binding and activating PKR. *Mol Cell Biol* 2001;21:1908-1920.
230. Takada Y, Ichikawa H, Pataer A, et al. Genetic deletion of PKR abrogates TNF-induced activation of I κ B α kinase, JNK, Akt and cell proliferation but potentiates p44/p42 MAPK and p38 MAPK activation. *Oncogene* 2007;26:1201-1212.

REFERENCES

231. Thomis DC, Samuel CE. Mechanism of interferon action: autoregulation of RNA-dependent P1/eIF-2 alpha protein kinase (PKR) expression in transfected mammalian cells. *Proc Natl Acad Sci U S A* 1992;89:10837-10841.
232. Laukoetter MG, Nava P, Lee WY, et al. JAM-A regulates permeability and inflammation in the intestine in vivo. *J Exp Med* 2007;204:3067-3076.
233. Hoffmann M, Rath E, Holzwimmer G, et al. *Lactobacillus reuteri* 100-23 transiently activates intestinal epithelial cells of mice that have a complex microbiota during early stages of colonization. *J Nutr* 2008;138:1684-1691.
234. Genomatix. *ChipInspector 2 Manual*.
235. <http://www.genomatix.de/en/produkte/genomatix-software-suite.html>. 2011.
236. Bioinformatics W. <https://madmax.bioinformatics.nl>.
237. Manolakis AC, Kapsoritakis AN, Tiaka EK, et al. Calprotectin, Calgranulin C, and Other Members of the S100 Protein Family in Inflammatory Bowel Disease. *Dig Dis Sci* 2011.
238. Koblisch HK, Hansbury MJ, Bowman KJ, et al. Hydroxyamine inhibitors of indoleamine-2,3-dioxygenase potently suppress systemic tryptophan catabolism and the growth of IDO-expressing tumors. *Mol Cancer Ther* 2010;9:489-498.
239. Owen BM, Milona A, van Mil S, et al. Intestinal detoxification limits the activation of hepatic pregnane X receptor by lithocholic acid. *Drug Metab Dispos* 2010;38:143-149.
240. Norkina O, Dolganiuc A, Shapiro T, et al. Acute alcohol activates STAT3, AP-1, and Sp-1 transcription factors via the family of Src kinases to promote IL-10 production in human monocytes. *J Leukoc Biol* 2007;82:752-762.
241. Babeu JP, Darsigny M, Lussier CR, et al. Hepatocyte nuclear factor 4alpha contributes to an intestinal epithelial phenotype in vitro and plays a partial role in mouse intestinal epithelium differentiation. *Am J Physiol Gastrointest Liver Physiol* 2009;297:G124-134.
242. Luebke-Wheeler J, Zhang K, Battle M, et al. Hepatocyte nuclear factor 4alpha is implicated in endoplasmic reticulum stress-induced acute phase response by regulating expression of cyclic adenosine monophosphate responsive element binding protein H. *Hepatology* 2008;48:1242-1250.
243. Botella LM, Sanz-Rodriguez F, Komi Y, et al. TGF-beta regulates the expression of transcription factor KLF6 and its splice variants and promotes co-operative transactivation of common target genes through a Smad3-Sp1-KLF6 interaction. *Biochem J* 2009;419:485-495.
244. Ghaleb AM, Yang VW. The Pathobiology of Kruppel-like Factors in Colorectal Cancer. *Curr Colorectal Cancer Rep* 2008;4:59-64.
245. Scharl M, Weber A, Furst A, et al. Potential role for snail family transcription factors in the etiology of Crohn's disease-associated fistulae. *Inflamm Bowel Dis* 2010.
246. Rieder F, Fiocchi C. Intestinal fibrosis in inflammatory bowel disease - Current knowledge and future perspectives. *J Crohns Colitis* 2008;2:279-290.
247. Fukushima K, Fiocchi C. Paradoxical decrease of mitochondrial DNA deletions in epithelial cells of active ulcerative colitis patients. *Am J Physiol Gastrointest Liver Physiol* 2004;286:G804-813.
248. Nakamura T, Furuhashi M, Li P, et al. Double-stranded RNA-dependent protein kinase links pathogen sensing with stress and metabolic homeostasis. *Cell* 2010;140:338-348.
249. Shimazawa M, Ito Y, Inokuchi Y, et al. Involvement of double-stranded RNA-dependent protein kinase in ER stress-induced retinal neuron damage. *Invest Ophthalmol Vis Sci* 2007;48:3729-3736.
250. Hu S, Ciancio MJ, Lahav M, et al. Translational inhibition of colonic epithelial heat shock proteins by IFN-gamma and TNF-alpha in intestinal inflammation. *Gastroenterology* 2007;133:1893-1904.
251. Chakrabarti A, Sadler AJ, Kar N, et al. Protein kinase R-dependent regulation of interleukin-10 in response to double-stranded RNA. *J Biol Chem* 2008;283:25132-25139.
252. Shirihai OS, Gregory T, Yu C, et al. ABC-me: a novel mitochondrial transporter induced by GATA-1 during erythroid differentiation. *Embo J* 2000;19:2492-2502.
253. Passos JF, von Zglinicki T, Kirkwood TB. Mitochondria and ageing: winning and losing in the numbers game. *Bioessays* 2007;29:908-917.
254. Cakir Y, Ballinger SW. Reactive species-mediated regulation of cell signaling and the cell cycle: the role of MAPK. *Antioxid Redox Signal* 2005;7:726-740.
255. Sorbara MT, Girardin SE. Mitochondrial ROS fuel the inflammasome. *Cell Res* 2011.
256. Woo CH, Lim JH, Kim JH. Lipopolysaccharide induces matrix metalloproteinase-9 expression via a mitochondrial reactive oxygen species-p38 kinase-activator protein-1 pathway in Raw 264.7 cells. *J Immunol* 2004;173:6973-6980.
257. Jones RG, Plas DR, Kubek S, et al. AMP-activated protein kinase induces a p53-dependent metabolic checkpoint. *Mol Cell* 2005;18:283-293.
258. McBride HM, Neuspiel M, Wasiak S. Mitochondria: more than just a powerhouse. *Curr Biol* 2006;16:R551-560.
259. Seth RB, Sun L, Ea CK, et al. Identification and characterization of MAVS, a mitochondrial antiviral signaling protein that activates NF-kappaB and IRF 3. *Cell* 2005;122:669-682.
260. Kepp O, Galluzzi L, Kroemer G. Mitochondrial control of the NLRP3 inflammasome. *Nat Immunol* 2011;12:199-200.
261. Sen A, Pruijssers AJ, Dermody TS, et al. The early interferon response to rotavirus is regulated by PKR and depends on MAVS/IPS-1, RIG-I, MDA-5, and IRF3. *J Virol* 2011.
262. Schroder K, Tschopp J. The inflammasomes. *Cell* 2010;140:821-832.

263. Villani AC, Lemire M, Fortin G, et al. Common variants in the NLRP3 region contribute to Crohn's disease susceptibility. *Nat Genet* 2009;41:71-76.
264. Zhernakova A, Festen EM, Franke L, et al. Genetic analysis of innate immunity in Crohn's disease and ulcerative colitis identifies two susceptibility loci harboring CARD9 and IL18RAP. *Am J Hum Genet* 2008;82:1202-1210.
265. Monteleone G, Trapasso F, Parrello T, et al. Bioactive IL-18 expression is up-regulated in Crohn's disease. *J Immunol* 1999;163:143-147.
266. Pizarro TT, Michie MH, Bentz M, et al. IL-18, a novel immunoregulatory cytokine, is up-regulated in Crohn's disease: expression and localization in intestinal mucosal cells. *J Immunol* 1999;162:6829-6835.
267. Casini-Raggi V, Kam L, Chong YJ, et al. Mucosal imbalance of IL-1 and IL-1 receptor antagonist in inflammatory bowel disease. A novel mechanism of chronic intestinal inflammation. *J Immunol* 1995;154:2434-2440.
268. Siegmund B, Lehr HA, Fantuzzi G, et al. IL-1 beta -converting enzyme (caspase-1) in intestinal inflammation. *Proc Natl Acad Sci U S A* 2001;98:13249-13254.
269. Siegmund B, Fantuzzi G, Rieder F, et al. Neutralization of interleukin-18 reduces severity in murine colitis and intestinal IFN-gamma and TNF-alpha production. *Am J Physiol Regul Integr Comp Physiol* 2001;281:R1264-1273.
270. Ferretti M, Casini-Raggi V, Pizarro TT, et al. Neutralization of endogenous IL-1 receptor antagonist exacerbates and prolongs inflammation in rabbit immune colitis. *J Clin Invest* 1994;94:449-453.
271. Saitoh T, Fujita N, Jang MH, et al. Loss of the autophagy protein Atg16L1 enhances endotoxin-induced IL-1beta production. *Nature* 2008;456:264-268.
272. Beltran B, Nos P, Dasi F, et al. Mitochondrial dysfunction, persistent oxidative damage, and catalase inhibition in immune cells of naive and treated Crohn's disease. *Inflamm Bowel Dis* 2010;16:76-86.
273. Yu X, Wieczorek S, Franke A, et al. Association of UCP2 -866 G/A polymorphism with chronic inflammatory diseases. *Genes Immun* 2009;10:601-605.
274. Travassos LH, Carneiro LA, Ramjeet M, et al. Nod1 and Nod2 direct autophagy by recruiting ATG16L1 to the plasma membrane at the site of bacterial entry. *Nat Immunol* 2010;11:55-62.
275. Singh SB, Ornatowski W, Vergne I, et al. Human IRGM regulates autophagy and cell-autonomous immunity functions through mitochondria. *Nat Cell Biol* 2010;12:1154-1165.
276. Pecqueur C, Bui T, Gelly C, et al. Uncoupling protein-2 controls proliferation by promoting fatty acid oxidation and limiting glycolysis-derived pyruvate utilization. *Faseb J* 2008;22:9-18.
277. Brand MD, Esteves TC. Physiological functions of the mitochondrial uncoupling proteins UCP2 and UCP3. *Cell Metab* 2005;2:85-93.
278. Emre Y, Nubel T. Uncoupling protein UCP2: when mitochondrial activity meets immunity. *FEBS Lett* 2010;584:1437-1442.
279. Emre Y, Hurtaud C, Nubel T, et al. Mitochondria contribute to LPS-induced MAPK activation via uncoupling protein UCP2 in macrophages. *Biochem J* 2007;402:271-278.
280. Singh R, Kaushik S, Wang Y, et al. Autophagy regulates lipid metabolism. *Nature* 2009;458:1131-1135.
281. Barrett JC, Hansoul S, Nicolae DL, et al. Genome-wide association defines more than 30 distinct susceptibility loci for Crohn's disease. *Nat Genet* 2008;40:955-962.
282. Rinaldo P, Matern D, Bennett MJ. Fatty acid oxidation disorders. *Annu Rev Physiol* 2002;64:477-502.
283. Shekhawat PS, Srinivas SR, Matern D, et al. Spontaneous development of intestinal and colonic atrophy and inflammation in the carnitine-deficient *jvs* (OCTN2(-/-)) mice. *Mol Genet Metab* 2007;92:315-324.
284. Roediger WE, Nance S. Metabolic induction of experimental ulcerative colitis by inhibition of fatty acid oxidation. *Br J Exp Pathol* 1986;67:773-782.
285. He D, Sougioultzis S, Hagen S, et al. Clostridium difficile toxin A triggers human colonocyte IL-8 release via mitochondrial oxygen radical generation. *Gastroenterology* 2002;122:1048-1057.
286. Kamizato M, Nishida K, Masuda K, et al. Interleukin 10 inhibits interferon gamma- and tumor necrosis factor alpha-stimulated activation of NADPH oxidase 1 in human colonic epithelial cells and the mouse colon. *J Gastroenterol* 2009;44:1172-1184.
287. Lewis K, Lutgendorff F, Phan V, et al. Enhanced translocation of bacteria across metabolically stressed epithelia is reduced by butyrate. *Inflamm Bowel Dis* 2010;16:1138-1148.
288. Nazli A, Yang PC, Jury J, et al. Epithelia under metabolic stress perceive commensal bacteria as a threat. *Am J Pathol* 2004;164:947-957.
289. Soderholm JD, Olaison G, Peterson KH, et al. Augmented increase in tight junction permeability by luminal stimuli in the non-inflamed ileum of Crohn's disease. *Gut* 2002;50:307-313.
290. Schurmann G, Bruwer M, Klotz A, et al. Transepithelial transport processes at the intestinal mucosa in inflammatory bowel disease. *Int J Colorectal Dis* 1999;14:41-46.
291. Powrie F, Leach MW, Mauze S, et al. Inhibition of Th1 responses prevents inflammatory bowel disease in scid mice reconstituted with CD45RBhi CD4+ T cells. *Immunity* 1994;1:553-562.
292. Rutgeerts P, Vermeire S, Van Assche G. Biological therapies for inflammatory bowel diseases. *Gastroenterology* 2009;136:1182-1197.
293. Fedarovich A, Tomberg J, Nicholas RA, et al. Structure of the N-terminal domain of human CEACAM1: binding target of the opacity proteins during invasion of *Neisseria meningitidis* and *N. gonorrhoeae*. *Acta Crystallogr D Biol Crystallogr* 2006;62:971-979.
294. Barnich N, Carvalho FA, Glasser AL, et al. CEACAM6 acts as a receptor for adherent-invasive *E. coli*, supporting ileal mucosa colonization in Crohn disease. *J Clin Invest* 2007;117:1566-1574.

REFERENCES

295. van Waterschoot RA, Rooswinkel RW, Wagenaar E, et al. Intestinal cytochrome P450 3A plays an important role in the regulation of detoxifying systems in the liver. *Faseb J* 2009;23:224-231.
296. Wang H, Zhao Y, Bradbury JA, et al. Cloning, expression, and characterization of three new mouse cytochrome p450 enzymes and partial characterization of their fatty acid oxidation activities. *Mol Pharmacol* 2004;65:1148-1158.
297. Cipolla G, Crema F, Sacco S, et al. Nonsteroidal anti-inflammatory drugs and inflammatory bowel disease: current perspectives. *Pharmacol Res* 2002;46:1-6.
298. Morteau O, Morham SG, Sellon R, et al. Impaired mucosal defense to acute colonic injury in mice lacking cyclooxygenase-1 or cyclooxygenase-2. *J Clin Invest* 2000;105:469-478.
299. Levy BD, Clish CB, Schmidt B, et al. Lipid mediator class switching during acute inflammation: signals in resolution. *Nat Immunol* 2001;2:612-619.
300. Serhan CN, Chiang N, Van Dyke TE. Resolving inflammation: dual anti-inflammatory and pro-resolution lipid mediators. *Nat Rev Immunol* 2008;8:349-361.
301. Tahan G, Gramignoli R, Marongiu F, et al. Melatonin expresses powerful anti-inflammatory and antioxidant activities resulting in complete improvement of acetic-acid-induced colitis in rats. *Dig Dis Sci* 2011;56:715-720.
302. Mei Q, Diao L, Xu JM, et al. A protective effect of melatonin on intestinal permeability is induced by diclofenac via regulation of mitochondrial function in mice. *Acta Pharmacol Sin* 2011;32:495-502.
303. Onal C, Kayaselcuk F, Topkan E, et al. Protective effects of melatonin and octreotide against radiation-induced intestinal injury. *Dig Dis Sci* 2011;56:359-367.
304. Cadwell K, Patel KK, Maloney NS, et al. Virus-plus-susceptibility gene interaction determines Crohn's disease gene Atg16L1 phenotypes in intestine. *Cell* 2010;141:1135-1145.
305. Silva AM, Wang D, Komar AA, et al. Salicylates trigger protein synthesis inhibition in a protein kinase R-like endoplasmic reticulum kinase-dependent manner. *J Biol Chem* 2007;282:10164-10171.
306. Palakurthi SS, Aktas H, Grubisich LM, et al. Anticancer effects of thiazolidinediones are independent of peroxisome proliferator-activated receptor gamma and mediated by inhibition of translation initiation. *Cancer Res* 2001;61:6213-6218.
307. Ozcan U, Yilmaz E, Ozcan L, et al. Chemical chaperones reduce ER stress and restore glucose homeostasis in a mouse model of type 2 diabetes. *Science* 2006;313:1137-1140.
308. Ota T, Gayet C, Ginsberg HN. Inhibition of apolipoprotein B100 secretion by lipid-induced hepatic endoplasmic reticulum stress in rodents. *J Clin Invest* 2008;118:316-332.
309. Erbay E, Babaev VR, Mayers JR, et al. Reducing endoplasmic reticulum stress through a macrophage lipid chaperone alleviates atherosclerosis. *Nat Med* 2009;15:1383-1391.
310. Boyce M, Bryant KF, Jousse C, et al. A selective inhibitor of eIF2alpha dephosphorylation protects cells from ER stress. *Science* 2005;307:935-939.
311. Sokka AL, Putkonen N, Mudo G, et al. Endoplasmic reticulum stress inhibition protects against excitotoxic neuronal injury in the rat brain. *J Neurosci* 2007;27:901-908.
312. Palacios HH, Yendluri BB, Parvathaneni K, et al. Mitochondrion-specific antioxidants as drug treatments for Alzheimer disease. *CNS Neurol Disord Drug Targets* 2011;10:149-162.

PUBLICATIONS AND PRESENTATIONS**Peer-reviewed original manuscripts and reviews****Rath E**, Haller D

Mitochondria at the interface between danger signaling and metabolism: Role of unfolded protein responses in chronic inflammation.

Inflamm Bowel Dis. 2011 Dec 19. doi: 10.1002/ibd.21944. [Epub ahead of print]

Rath E, Berger E, Messlik A, Nunes T, Liu B, Kim SC, Hoogenraad N, Sans M, Sartor RB, Haller D

Induction of dsRNA-activated protein kinase links mitochondrial unfolded protein response to the pathogenesis of intestinal inflammation.

Gut. 2011 Oct 13. [Epub ahead of print]

Rath E, Haller D

Inflammation and cellular stress – a mechanistic link between immune-mediated and metabolically-driven pathologies

Eur J Nutr. 2011 Jun;50(4):219-33. Epub 2011 May 1. Review.

Hoffmann M*, **Rath E***, Hölzlwimmer G, Quintanilla-Martinez L, Loach D, Tannock G, Haller D.

Lactobacillus reuteri 100-23 transiently activates intestinal epithelial cells of mice that have a complex microbiota during early stages of colonization.

J Nutr. 2008 Sep;138(9):1684-91.

* these authors contributed equally to the manuscript

Published abstracts**Rath E**, Berger E, Messlik A, Fromme T, Klingenspor M, Hoogenraad N, Kim SC, Liu B, Sartor RB, Haller D.

Mitochondrial stress induction in the epithelium fuels endoplasmic reticulum unfolded protein responses via double-stranded RNA-activated protein kinase (PKR) under conditions of chronic intestinal inflammation

International Immunology Meeting Abstracts (2010) 22 (Suppl 1 Pt 3): iii137-iii142. doi: 10.1093/intimm/dxq245

Rath E, Liu B, Sartor RB and Haller D.

Microarray analysis of intestinal epithelial cells identifies novel interleukin 10-specific target genes in T cell-mediated colitis

Journal of Crohn's and Colitis Supplements (April 2010) Volume 4, Issue 1, Pages 1-48

Rath E, Berger E, Messlik A, Fromme T, Klingenspor M, Ensenauer R, Hoogenraad N, Kim SC, Liu B, Sartor RB, Haller D.

Mitochondrial stress induction in the epithelium fuels endoplasmic reticulum unfolded protein responses via double-stranded RNA-activated protein kinase (PKR) under conditions of chronic intestinal inflammation

Gastroenterology 2010 Vol. 138, Issue 5, Supplement 1, Page S-15

Messlik A*, **Rath E***, Berger E, Fromme T, Klingenspor M, Hoogenraad N, Kim SC, Liu B, Sartor RB, Haller D.

Signal integration of endoplasmic reticulum and mitochondrial unfolded protein stress responses in intestinal epithelial cells of patients with ulcerative colitis and murine models of immune-mediated colitis: inhibitory mechanisms of Interleukin 10.

Gastroenterology 2009 Vol. 136, Issue 5, Supplement 1, Page A-700

* these authors contributed equally to the work

Oral presentations

Rath E, Berger E, Waldschmitt N, Nunes T, Liu B, Kim SC, Hoogenraad N, Sans M, Sartor RB, Haller D

dsRNA-activated protein kinase links mitochondrial unfolded protein response to intestinal inflammation in humans and mice

8th NuGOweek 2011, September 6-9, 2011, Wageningen, Netherlands

Rath E, Berger E, Nunes T, Liu B, Hoogenraad N, Sans M, Sartor RB, Haller D

Mitochondrial Stress Mechanisms Fuel Chronic Intestinal Inflammation via PKR in Human IBD and Murine Models of Colitis

15th International Congress of Mucosal Immunology (ICMI), July 5-9, 2011, Paris, France

Berger E, **Rath E**, Nunes T, Hoogenraad N, Sans M, Haller D

Interrelated organelle stress responses via PKR: a central sensor and integrator of inflammatory and metabolic stress

48. Wissenschaftlicher Kongress der Deutschen Gesellschaft für Ernährung (German Nutrition Society), March 18-19, 2011, Potsdam, Germany

Rath E, invited lecture

Intestinal epithelial cells as targets and mediators of bacteria- and host derived signals

6th Annual Meeting of Japanese Association for Food Immunology (JAFI), June 1-2, 2010, Tokyo, Japan

Rath E, Berger E, Messlik A, Fromme T, Klingenspor M, Ensenaer R, Hoogenraad N, Kim SC, Liu B, Sartor RB, Haller D

Mitochondrial stress induction in the epithelium fuels endoplasmic reticulum unfolded protein responses via double-stranded RNA-activated protein kinase (PKR) under conditions of chronic intestinal inflammation

Digestive Disease Week (DDW) May 1-5, 2010, New Orleans, USA

Rath E, Berger E, Messlik A, Liu B, Kim SC, Sartor RB, Hoogenraad N, Haller D

Mitochondrial stress responses contribute to the pathogenesis of chronic intestinal inflammation

3rd Seeon Conference (German Society for Hygiene and Mikrobiology, DGHM), June 18-20, 2010, Kloster Seeon, Germany

Rath E, Berger E, Messlik A, Fromme T, Klingenspor M, Dunkel A, Hofmann T, Hoogenraad N, Haller D

Mitochondrial stress responses contribute to the pathogenesis of chronic intestinal inflammation

47. Wissenschaftlicher Kongress der Deutschen Gesellschaft für Ernährung (German Nutrition Society), March 11-12, 2010, Jena, Germany

Hoffmann M, **Rath E**, Hölzlwimmer G, Quintanilla-Martinez L, Loach D, Tannock G, Haller D

Lactobacillus reuteri 100-23 transiently activates intestinal epithelial cells of mice that have a complex microbiota during early stages of colonization.

Annual meeting of the German Society for Hygiene and Mikrobiology (DGHM), September 20-23, 2009, Göttingen, Germany

Steck N, Hoffmann M, **Rath E**, Hew CM, Kim SC, Liu B, Vogel RF, Sartor RB, Haller D.

Bacterial proteases contribute to the development of chronic intestinal inflammation by impairing epithelial barrier function

14th International Congress of Mucosal Immunology (ICMI), July 5-9, 2009, Boston, USA

Rath E, Messlik A, Kim SC, Liu B, Sartor RB, Haller D

Mitochondriale- und Endoplasmatisches Reticulum (ER)- Streßmechanismen in intestinalen Epithelzellen: Bedeutung für chronische Entzündung

46. Wissenschaftlicher Kongress der Deutschen Gesellschaft für Ernährung (German Nutrition Society), March 12-13, 2009, Gießen, Germany

Rath E, Messlik A, Liu B, Sartor RB, Haller D

Endoplasmic reticulum (ER) stress responses in intestinal epithelial cells in mouse models of T-cell mediated colitis

6th Meeting of the European Mucosal Immunology Group (EMIG), October 8-10, 2008, Milan, Italy

Poster presentations

Rath E, Berger E, Waldschmitt N, Nunes T, Liu B, Hoogenraad N, Sans M, Sartor RB, Haller D
dsRNA-activated protein kinase links mitochondrial unfolded protein response to intestinal inflammation in humans and mice

5th International Congress on Stress responses in Biology and Medicine, August 21-25, 2011, Quebec City, Canada

Berger E, **Rath E**, Nunes T, Liu B, Hoogenraad N, Sans M, Sartor RB, Haller D

Mitochondrial Stress Mechanisms Fuel Chronic Intestinal Inflammation via PKR in Human IBD and Murine Models of Colitis

EMBO Conference Series, The Biology of Molecular Chaperones, 2011, May 19-24, 2011, Grunglsee, Austria

Rath E, Berger E, Messlik A, Nunes T, Liu B, Kim SC, Hoogenraad N, Sans M, Sartor RB, Haller D

PKR links mitochondrial unfolded protein response in the epithelium to the pathogenesis of intestinal inflammation

4th Seeon Conference (German Society for Hygiene and Mikrobiology, DGHM), April 15-17, 2011, Kloster Seeon, Germany

Berger E, **Rath E**, Waldschmitt N, Schmöller I, Haller D

Mitochondrial stress is associated with altered mitochondrial creatine kinase expression in the intestinal epithelium

4th Seeon Conference (German Society for Hygiene and Mikrobiology, DGHM), April 15-17, 2011, Kloster Seeon, Germany

Rath E, Berger E, Messlik A, Fromme T, Klingenspor M, Hoogenraad N, Kim SC, Liu B, Sartor RB, Haller D

Mitochondrial stress induction in the epithelium fuels endoplasmic reticulum unfolded protein responses via double-stranded RNA-activated protein kinase (PKR) under conditions of chronic intestinal inflammation

14th International Congress of Immunology (ICI), August 22-27, 2010, Kobe, Japan

Rath E, Berger E, Messlik A, Fromme T, Klingenspor M, Ensenaer R, Hoogenraad N, Kim SC, Liu B, Sartor RB, Haller D

Mitochondrial stress fuels endoplasmic reticulum unfolded protein response via double-stranded RNA-activated protein kinase (PKR) under conditions of chronic intestinal inflammation

Annual meeting of the German Society for Hygiene and Mikrobiology (DGHM), March 28-31, 2010, Hannover, Germany

Messlik A*, **Rath E***, Berger E, Fromme T, Klingenspor M, Hoogenraad N, Kim SC, Liu B, Sartor RB, Haller D.

Signal integration of endoplasmic reticulum and mitochondrial unfolded protein stress responses in intestinal epithelial cells of patients with ulcerative colitis and murine models of immune-mediated colitis: inhibitory mechanisms of Interleukin 10.

* these authors contributed equally to the work

14th International Congress of Mucosal Immunology (ICMI), July 5-9, 2009, Boston, USA

Messlik A*, **Rath E***, Berger E, Fromme T, Klingenspor M, Hoogenraad N, Kim SC, Liu B, Sartor RB, Haller D.

Signal integration of endoplasmic reticulum and mitochondrial unfolded protein stress responses in intestinal epithelial cells of patients with ulcerative colitis and murine models of immune-mediated colitis: inhibitory mechanisms of Interleukin 10.

* these authors contributed equally to the work

Digestive Disease Week (DDW) 2009. May 30 - June 4, 2009; Chicago, USA

Rath E, Hoffmann M, Hölzlwimmer G, Quintanilla-Martinez L, Loach D, Tannock G, Haller D

Lactobacillus reuteri 100-23 transiently activates intestinal epithelial cells of mice that have a complex microbiota during early stages of colonization.

2nd Seeon Conference (German Society for Hygiene and Mikrobiology, DGHM), April 23-25, 2009, Kloster Seeon, Germany

Rath E, Hoffmann M, Tannock G and Haller D.

Intestinal epithelial cell activation in reconstituted lactobacillus-free mice after the colonization with *Lactobacillus reuteri*

44. Wissenschaftlicher Kongress der Deutschen Gesellschaft für Ernährung (German Nutrition Society), March 8-9, 2007, Halle, Germany

Rath E, Hoffmann M, Tannock G and Haller D.

Intestinal epithelial cell activation in reconstituted lactobacillus-free mice after the colonization with *Lactobacillus reuteri*

5th Meeting of the European Mucosal Immunology Group (EMIG), October 5-7 2006, Prague, Czech Republic

Grants

Travel Grant, Bund der Freunde der TUM e.V.
(5th International Congress on Stress responses in Biology and Medicine, August 21-25, 2011, Quebec City, Canada)

Travel Award, Organizing committee of the 15th International Congress of Mucosal Immunology (ICMI), July 5-9, 2011, Paris, France

Travel Grant, Institut Danone
Digestive Disease Week (DDW) May 1-5, 2010, New Orleans, USA

Travel Grant, Boehringer Ingelheim Fonds (2010)
(5th NuGO Hands on microarray data course, Maastricht, NL)

Travel Grant, GlaxoSmithKline foundation
(International Congress of Mucosal Immunology (ICMI) 2009, Boston, USA)

Travel Award, Organizing committee of the 6th Meeting of the European Mucosal Immunology Group 2008, Milano, Italy

General Travel Award, Anneliese Pfannenbergs-foundation (2008)

Travel Grant, Boehringer Ingelheim Fonds (2008)
(one-month research period at the University of North Carolina, Chapel Hill, USA)

Short-term scholarship of the German Academic Exchange Service, DAAD (2007)
(two-month research period at the University of North Carolina, Chapel Hill, USA)

Travel grant, Organizing committee of the 5th Meeting of the European Mucosal Immunology Group 2006, Prague, CZ

Awards

2011 Scientific Research Award, Institut Danone
"Ernährung (Nutrition) 2011", May 26-28, Graz, Austria

Poster award
4th Seeon Conference (German Society for Hygiene and Mikrobiology, DGHM), April 15-17, 2011, Kloster Seeon, Germany

ARPA-Bronzetti award for the best poster presentation
5th Meeting of the European Mucosal Immunology Group (EMIG), October 5-7 2006, Prague, Czech Republic

Award of the mayor of Freising "Preis des Oberbürgermeisters der Stadt Freising"
for the best Master's thesis of the Department of Nutrition in 2006

Jana Hemmerling
Alwin Rath Nadine Wald-
 schmitt Bernd Jankowski Sonja
 Böhm Volkmar "Eddi"
 Janicke A Christina
 Zhenchuk Philippo
 White Eric Plow
 Peidis Arsen
 Theresa Stewert
 Detlef Hoffmann
 Micha Jankowski
 Andrea Gebhardt
 Nico S e n
 Ganes Shkoda
 Anna Valérien
 René Wagner
 Stefan O cvirk
 Sören Patrick Carrena Irina Sava Diane
 Loach Doris Paechtner Andi
 Gabler Basti Altenberger

Vikto-
 Jürgen Sa-
Siewert-
 Katharina
 stetter Sylvia
 Theresa Falls
 Vogelmann Pia
 Tina Hallas
 Werner Anders
 Dana Kuntzsch
 Kislung
 Han-
 Bo Liu el David
 Dani- A ut o Vorstadt
 Meinem Barbara Lutz Der
 Cafe dung mit der
 Maus Marie-Anne von
 Schill- de Sophie Lili
 Carrena Jenny Berta
 G M S Pedro Ruiz
 Christi- an Schelb

Sandra
 Hennig
Dirk Haller
 Andrea Häd-
 rich KFZ Cha-
 ves Katrin Mair
 Jürgen Rieg-
 Werner Pa-
 wechtner Mark
 Boek- schoten
 Susan Chang
 Nata- lia Jörg
 Christian Blaich
 Karl Grim-
 minger Lena
 Deus Rubico Martin Milde Mei-
 nem Computer allen Mitgliedern
 des Kuratoriums für Prävention und
 Rehabilitation Martin Riesebrodt
 Thomas Mitsche-
 len Ben- jamin
 Tiemann Lise
 Baller Martin
 Klin- genspor

ría Doll
 Anker-
b i n e
R a t h
 Werk-
 Heinrich
 Roger
 Roger
 B a u r
 Tania
 Kielland
 Sigrid
 neiore
 Möhrle
 A ut o Vorstadt
 Barbara Lutz Der
 dung mit der
 Marie-Anne von
 de Sophie Lili
 Jenny Berta
 Pedro Ruiz
 an Schelb

Gabriele
 p e r g -
 Schieder
 S a r -
 Fromme
 Koromi-
 Riegler
 Emanuel
 Thomas
 via Pitari
Johannes Zang
 Lutz Anja Schwarz
 Zang Lisa Holt
 Katharina
 Spanier Anja
 Miquel
 Florian
 Ni c o
 Gerald
 Joachim
 Natalie
 Ni c k
 r a d

Hörmanns-
 er Arne
 Balfour
 tor Tobias
 Antonis
 las Daniel
 Sylvia
 Steininger
 Berger
 Clavel Sil-
 via Friedl
 Ulrike
Johannes Zang
 Thomas
 Barbara
 Britta
 Messlik
 R a n s
 S a n s
 R a n d o r f e r
 T a n n o c k
 Z a n g
 S t e c k
 Hoogen-
 N u s s i n i

Fré Pepping Nike Rath Tiago Nunes
 Andreas Krickl Job Mapesa Chris-
 toph Lammel Koji Hase Gerhard
 Zang all murine participants Lisa
 Gruber
 Brita
 Sturm
 A n d i
 K o c h
 John Bell
 Ingrid Schmöller Monika Weiher
Brigitte Jankowski Martina Eder
 Elisabeth Lippert Brigitte Ries-
 ebrodt
 Maria
 "Anna"
 Merkel
 Andrew
 Whitney-
 Steere
 Sibylle Schmitt Katharina Heil-
 er Gabriele Holzlwimmer Ben-
 jamin Erdmann Oktopussy

Curriculum Vitae

Personal information

Surname / First name **Rath, Eva Brigitte**
Date of birth 4 May 1979
Nationality German
E-mail eva.rath@wzw.tum.de
Telephone +49 172 8350630
Address Destouchesstrasse 14
80803 Munich

Work experience

since 06/2006 PhD Student
Department for Biofunctionality
Technische Universität München
Title of PhD thesis Mitochondrial unfolded protein response in the epithelium:
relevance to intestinal inflammation
01/2007 – 02/2007 two-month research period
University of North Carolina, Chapel Hill, USA

Education

09/2004 – 05/2006 **Master of Science** (Nutritional Sciences, focus: Biomedicine)
Title of Master thesis Influence of *Lactobacillus reuteri* 100-23 on primary intestinal epithelial
cells of reconstituted lactobacillus-free (RLF) mice
Technische Universität München
10/2001 - 08/2004 **Bachelor of Science** (Nutritional Sciences)
Title of Bachelor thesis Influence of flavonoids on pro-inflammatory cytokine production in
intestinal epithelial cell lines
Technische Universität München
09/1999 – 09/2001 Human Medicine
Ludwig Maximilians University, Munich
06/1999 German university entrance qualification
Willi – Graf – Gymnasium, Munich